UQAC
Université du Québec
à Chicoutimi

Seismic Microzonation Mapping Based on Nonlinear Site Response Analysis: Methodology Development and Application to Saguenay, Quebec

(Cartographie de la microzonation sismique basée sur l'analyse de la réponse non linéaire du site : développement d'une méthodologie et application à Saguenay, Québec)

By

A S M Fahad Hossain

Under the supervision of Dr. Ali Saeidi and the co-supervision of Dr. Miroslav Nastev

Thesis presented to the University of Quebec at Chicoutimi to obtain the degree of Doctor of Philosophy (PhD) in Engineering (Civil)

BOARD OF EXAMINERS:

Dr. Mathieu Fiset, Department of Applied Sciences at UQAC, President of the Board

Dr. Jamal Assaf, Geotechnical Engineer, AtkinsRéalis, External Member of the Board

Dr. Ripon Hore, Road Design Engineer, DOTD, Louisiana, USA, External Member of the Board

Dr. Ali Saeidi, Professor, Department of Applied Sciences at UQAC, Internal Member of the Board

Dr. Miroslav Nastev, Research Scientist, Geological Survey of Canada, Internal Member of the Board

Chicoutimi, QC, Canada

RÉSUMÉ
La compréhension des effets de site locaux constitue un élément fondamental pour une évaluation précise de l'aléa sismique en surface, notamment dans les régions présentant des conditions de subsurface complexes. Cette recherche porte sur la région du Saguenay, située dans l'Est du Canada, où la géologie de surface se caractérise par une forte hétérogénéité. Dans ce contexte, les schémas de classification sismique actuellement en vigueur ne permettent pas toujours de représenter de manière satisfaisante le comportement dynamique des sols. À travers une étude intégrée combinant des approches analytiques, numériques et empiriques, cette thèse propose un cadre méthodologique pour une microzonation sismique plus fine. Elle vise à identifier et à évaluer l'influence des paramètres géologiques et géotechniques dans le but d'améliorer la prévision de l'amplification sismique liée aux effets de site. L'analyse débute par une modélisation unidimensionnelle non linéaire de la réponse sismique de 50 profils géotechniques, en intégrant à la fois des enregistrements réels et des signaux synthétiques mis à l'échelle en fonction de différents niveaux d'aléa définis dans le Code national du bâtiment du Canada 2020 (CNB 2020). Les résultats révèlent que certains paramètres, tels que la vitesse des ondes de cisaillement, l'épaisseur totale des dépôts meubles, ainsi que la présence d'une couche de till à l'interface avec le substratum rocheux, ont une influence significative sur l'amplification de site — particulièrement sous des sollicitations fortes, où le comportement non linéaire des sols devient prédominant. Les périodes fondamentales ont été estimées à l'aide des méthodes de la couche équivalente et des couches multiples. Une période de site non linéaire a été introduite comme nouveau paramètre représentatif (proxy) dans les modèles empiriques d'amplification, spécifiquement adaptés aux conditions non linéaires induites par des mouvements sismiques intenses. À partir de la combinaison de sept paramètres potentiels, plusieurs modèles empiriques ont été élaborés, parmi lesquels le modèle optimal intègre les variables Vs_{30}, Vs_{avg}, T_{NL} et H_{till}. Ce modèle, combiné aux données issues d'études antérieures de microzonation, a permis de réaliser une microzonation sismique de niveau III pour la région du Saguenay.

Mots-clés : Aléa sismique, Microzonation sismique, accélérogrammes d'entrée, réponse non linéaire du sol, amplification de site, période fondamentale , vitesse des ondes de cisaillement

ABSTRACT

Understanding local site effects is essential for accurate seismic hazard assessment at the ground surface, particularly in regions with complex subsurface conditions. This research focuses on the Saguenay region of Eastern Canada, where surficial geology is highly variable, and standard seismic code classification schemes may not adequately capture soil dynamic behavior. Through an integrated study combining analytical, numerical, and empirical approaches, this thesis develops a framework for refined seismic microzonation. It identifies and investigates the effects of geological and geotechnical parameters to improve predictions of seismic site amplification. It begins with a comprehensive 1D nonlinear ground response analysis of 50 soil profiles, incorporating both real and synthetic ground motions scaled to multiple hazard levels defined in NBCC 2020. Results indicate that site parameters, such as shear-wave velocity, total soil thickness, and presence of till layer at the rock interface, exert a significant influence on site amplification, particularly under strong-motion scenarios where nonlinear behavior becomes dominant. Fundamental periods were estimated using both the Equivalent Single Layer and Multiple Layer methods. The nonlinear site period was introduced as a new proxy in the empirical site amplification models adapted to nonlinear conditions during strong earthquake motion. Empirical site amplification models were established using combinations of seven site amplification proxies. The optimal empirical site amplification model included Vs_{30}, Vs_{avg}, T_{NL}, and H_{till}. Together with existing data from previous microzonation studies, it was used for Level III seismic microzonation of the Saguenay region.

Keywords: Seismic hazard, Seismic microzonation, input time histories, nonlinear ground response, site amplification, fundamental site period, shear-wave velocity.

TABLE OF CONTENTS

LIST OF FIGURES

LIST OF TABLES

LIST OF SYMBOLS

Vs_{30}	: Average shear-wave velocity in the top 30 m
Vs_{avg}	: Average shear-wave velocity
Vs_{rock}	: Shear-wave velocity of rock
Vs_{soil}	: Shear-wave velocity of soil
Vs_f	: Shear wave velocity ratio of rock and soil
$H_{soi}l$	: Thickness of soil layer
H_{till}	: Thickness of till (glacial)
H_{PG}	: Total thickness of postglacial deposits
T_o	: Fundamental site period
T_{NL}	: Nonlinear site period
f_o	: Fundamental resonant frequency
S_a	: Spectral accelerations
F_s	: Sleeve friction
F_r	: Cone tip friction
Q_t	: Cone tip resistance
R_f	: Friction ratio
Q_{tn}	: Normalized cone resistance
N_r	: Effective stress friction angle
S_u	: Undrained shear strength
K_o	: Starting stress state (at-rest earth pressure coefficient)
ρ	: Density
ρ_{rock}	: Density of rock
E	: Young's modulus
G	: Shear modulus
G_{max}	: Maximum shear modulus
K	: Bulk modulus
ξ	: Damping ratio
R^2	: Coefficient of Determination

LIST OF ABBREVIATIONS

1D	: One-dimensional
2D	: Two dimensions
3D	: Three dimensions
AF	: Amplification Factor
ASCE	: American Society of Civil Engineers
CPT	: Cone Penetration Test
DR	: Damping ratio
ESL	: Equivalent single layer
FP	: Fundamental site period
GMM	: Ground motion prediction models
HVSR	: Horizontal-to-vertical spectral ratio
MASW	: Multichannel Analysis of Surface Waves
MSL	: Multiple layer
NBCC	: National Building Code of Canada
PEER	: Pacific Earthquake Engineering Research Center
PGA	: Peak ground acceleration
PGV	: Peak ground velocity
PI	: Plasticity Index
RMSE	: Root Mean Square Error
SASW	: Spectral Analysis of Surface Waves
SCPT	: Seismic Cone Penetration Test
SDMT	: Seismic dilatometer
SM	: Seismic microzonation
SM	: Modulus reduction
SPT	: Standard Penetration Test
UHS	: Uniform hazard spectrum
USGS	: United States Geological Survey

DEDICATION

To my parents, whose sacrifices, unwavering hopes, and countless prayers have been the foundation upon which this achievement rests, and whose love, guidance, and belief in me have illuminated every step of my journey.

ACKNOWLEDGMENTS

First and foremost, I would like to express my sincere gratitude to my supervisor, **Dr. Ali Saeidi**, for his unwavering trust and confidence in my abilities. His support and encouragement made it possible for me to pursue my PhD studies abroad. I have never had the privilege of working with someone more flexible and accommodating. Dr. Saeidi is not only academically accomplished but also a man of great integrity and kindness. His patience, humility, and genuine concern for his students have left a lasting impact on me, both professionally and personally.

I want to thank **Dr. Miroslav Nastev**, my co-supervisor, a kind and supportive mentor who was always available to offer suggestions and provide constant inspiration. His guidance and encouragement greatly contributed to making my PhD journey smoother and more fulfilling. I have learned a great deal from his vast knowledge and practical insights, which have enriched both my research and professional growth. His approachable nature and genuine interest in my work made every interaction productive and motivating.

I would also like to extend my heartfelt thanks to **Dr. Mohammad Salsabili**, my advisor, for providing timely and insightful guidance throughout my research. His expertise and steadfast support played a vital role in helping me navigate and resolve the challenges I encountered. The depth of his critical thinking and the thoughtfulness of his responses have significantly shaped my ability to approach fundamental questions effectively. His dedication, professionalism, and intellectual brilliance have been a continual source of motivation during every stage of my PhD.

My thanks also extend to **Dr. Naveel Islam**, who first informed me about the opportunity to work with Prof. Saeidi and encouraged me throughout the entire journey of my PhD. His motivation and guidance have been invaluable in helping me stay focused and determined in achieving my goals.

I am deeply grateful to my undergraduate and M.Sc. supervisor, **Dr. Mehedi Ahmed Ansary**, for offering me exceptional opportunities to work on geophysical investigations, laboratory-based seismic testing, and numerical analysis. These experiences not only broadened my technical knowledge but also provided hands-on exposure to industrial projects, which significantly enhanced my expertise and professional development. The skills and insights I gained during this time proved invaluable and directly contributed to the success of my PhD research.

My heartfelt gratitude goes to my beloved wife, **Faiza Faria Mirza**, and my dear daughter, **Alisha Tasni Farishta**, for their unwavering love, patience, and understanding throughout my PhD journey. Their constant encouragement and countless sacrifices have been the foundation upon which my achievements stand. They have endured my long hours of work, frequent absences, and moments of stress with remarkable grace, always offering me strength and comfort. Without their steadfast support, this accomplishment would not have been possible.

I would like to express my sincere gratitude to **Vineeth Reddy Karnati, Dr. Rama Vara Prasad Chavali, Akber Saeidi, Abdur Rahman, Zinan Ara Urmi, Asaduzzaman, Jashia Islam**, and all the other friends who made my time at UQAC truly memorable. Beyond studies and research, their friendship, laughter, and the many moments we shared brought joy and balance to my PhD journey. I am deeply thankful for the good times we spent, which added happiness and lightness to what would have been an otherwise demanding period of life.

FOREWORD

This thesis was prepared in accordance with the requirements for an article-based dissertation. It comprises four scientific articles that collectively address the research objectives of nonlinear seismic site amplification, the efficiency of geotechnical parameters and site proxies in predicting amplification, the evaluation of site periods through analytical and numerical simulations, and the development of seismic microzonation through site amplification modelling. The document includes a general introduction (Chapter 1), four article-based chapters (Chapters 2–5), and a concluding chapter (Chapter 6).

Chapter 1 provides the general introduction, presenting the scientific context, problem statement, objectives, and methodology of the thesis. Chapter 2 presents the first article and addresses the first research objective: offering a comprehensive review of the parameters and methods used in seismic site response analysis and establishing the methodological foundations of the work. Chapter 3 contains the second article and addresses the first two research objectives by evaluating nonlinear ground response and assessing the influence of geological and geotechnical parameters and site proxies on seismic amplification. Chapter 4 contains the third article and focuses on the third objective by analysing fundamental and nonlinear site periods using analytical and numerical approaches and by developing correlations and microzonation maps. Chapter 5 contains the fourth article and addresses the final objective by developing an empirical site amplification model and producing a seismic microzonation map based on multiple site proxies and nonlinear amplification modelling. Finally, Chapter 6 presents the general conclusions and recommendations for future research.

Author contributions for all four articles follow the same structure. A. S. M. Fahad Hossain performed the conceptualization, data curation, numerical analyses, interpretation of results, original drafting, and editing. Ali Saeidi provided supervision, methodology, resources, and revisions. Miroslav Nastev contributed supervision, scientific guidance, and revisions. Mohammad Salsabili contributed geological interpretation and revisions. Juliana Ruiz Suescun provided technical comments and revisions. Zeinab Bayati contributed to Article 1 only.

The publication status of the included articles is as follows. Article 1, A Review of Parameters and Methods for Seismic Site Response, published in Geosciences, appeared on 1 April 2025. Article 2, Effects of Complex Surficial Geology on Seismic Amplification in Quebec, Canada, published in Georisk, appeared on 24 November 2025. Article 3, Evaluation of Site Periods Derived from Analytical and Numerical Simulations for Seismic Microzonation in Saguenay, is not yet submitted and will be submitted to Earthquake Spectra. Article 4, Seismic Microzonation of a Region with Complex Surficial Geology Based on Comprehensive Nonlinear Site Amplification Modelling, was submitted to Soil Dynamics and Earthquake Engineering on 14 October 2025, and the first review was completed on 13 November 2025.

Each article chapter begins with the required elements, including the chapter and article titles, full authorship, author contributions, a complete French summary, and the full manuscript (abstract, keywords, main text, figures, tables, and references), ensuring full compliance with the regulations governing article-based theses.

AVANT-PROPOS

Cette thèse a été préparée conformément aux exigences relatives à la rédaction d'une thèse par articles. Elle comprend quatre articles scientifiques qui abordent collectivement les objectifs de recherche portant sur l'amplification sismique non linéaire, l'efficacité des paramètres géotechniques et des proxys de site pour prédire l'amplification, l'évaluation des périodes de site au moyen de simulations analytiques et numériques, ainsi que l'élaboration d'une microzonation sismique fondée sur la modélisation de l'amplification sismique. Le document comprend une introduction générale (Chapitre 1), quatre chapitres rédigés sous forme d'articles (Chapitres 2 à 5) et un chapitre de conclusion (Chapitre 6).

Le Chapitre 1 présente l'introduction générale, décrivant le contexte scientifique, la problématique, les objectifs et la méthodologie de la thèse. Le Chapitre 2 présente le premier article et répond au premier objectif de recherche en offrant une revue complète des paramètres et méthodes utilisés dans l'analyse de la réponse sismique des sols, établissant ainsi les fondements méthodologiques du travail. Le Chapitre 3 contient le deuxième article et répond aux deux premiers objectifs en évaluant la réponse sismique non linéaire et en analysant l'influence des paramètres géologiques et géotechniques ainsi que des proxys de site sur l'amplification sismique. Le Chapitre 4 présente le troisième article, qui se concentre sur le troisième objectif en analysant les périodes fondamentales et non linéaires du site au moyen d'approches analytiques et numériques, et en développant des corrélations et des cartes de microzonation. Le Chapitre 5 contient le quatrième article et aborde l'objectif final en développant un modèle empirique d'amplification du site et en produisant une carte de microzonation sismique basée sur plusieurs proxys de site et des modélisations non linéaires. Enfin, le Chapitre 6 présente les conclusions générales et des recommandations pour de futures recherches.

Les contributions des auteurs des quatre articles suivent la même structure. A S M Fahad Hossain a réalisé la conceptualisation, la préparation et la gestion des données, les analyses numériques, l'interprétation des résultats, la rédaction initiale et la révision du manuscrit. Ali Saeidi a assuré la supervision, la méthodologie, les ressources et les révisions. Miroslav Nastev a contribué à la supervision, à l'orientation scientifique et aux révisions. Mohammad Salsabili a fourni l'interprétation géologique et les révisions. Juliana Ruiz Suescun a apporté des commentaires techniques et des révisions. Zeinab Bayati a contribué uniquement au premier article.

Le statut de publication des articles inclus est le suivant. L'Article 1, A Review of Parameters and Methods for Seismic Site Response, publié dans Geosciences, est paru le 1er avril 2025. L'Article 2, Effects of Complex Surficial Geology on Seismic Amplification in Quebec, Canada, publié dans Georisk, est paru le 24 novembre 2025. L'Article 3, Evaluation of Site Periods Derived from Analytical and Numerical Simulations for Seismic Microzonation in Saguenay, n'est pas encore soumis et sera soumis à Earthquake Spectra. L'Article 4, Seismic Microzonation of a Region with Complex Surficial Geology Based on Comprehensive Nonlinear Site Amplification Modelling, a été soumis à Soil Dynamics and Earthquake Engineering le 14 octobre 2025, et la première révision a été complétée le 13 novembre 2025.

Chaque chapitre rédigé sous forme d'article commence par les éléments requis, dont le titre du chapitre et de l'article, la liste complète des auteurs, les contributions des auteurs, un résumé détaillé en français et le manuscrit complet (résumé, mots-clés, texte principal, figures, tableaux et références), assurant ainsi une conformité totale aux règlements encadrant les thèses par articles.

CHAPTER 1

INTRODUCTION

1.1 General

The increasing negative impacts of destructive earthquakes around the world, such as the 2010 M8.8 Chile, 2011 M9.0 Tohoku, 2015 M7.8 Nepal, and 2023 M7.8 Turkey-Syria events, have highlighted the critical importance of understanding site-specific ground response in mitigating seismic risk (Kramer, 1996). A significant lesson learned from past seismic disasters, notably the 1985 Mexico City earthquake, is that local site conditions, including soil type, layering, and stiffness, are critical for amplification of the ground motion intensity and its frequency content, often leading to spatially variable damage within short distances. This phenomenon, widely known as site effects, arises when the local mechanical and geometrical properties of near-surface materials modify seismic waves traveling from bedrock to the surface. Impedance contrast, soil column thickness, resonance phenomena, and topographic features often govern these effects (Hunter & Crow, 2015).

The Saguenay region, situated within the Charlevoix-Kamouraska seismic zone of Eastern Canada, is a geologically complex area prone to moderate to strong earthquakes (Foulon et al., 2018). Despite being an intraplate region with moderate seismicity, the 1988 M5.9 Saguenay earthquake, the largest in Eastern North America in over 50 years, demonstrated that substantial shaking and structural damage can still occur (Salsabili et al., 2021a). The region is covered by thick glacial and post-glacial sediments that exhibit strong impedance contrasts with the underlying bedrock, resulting in strong seismic amplifications and their variations across short distances. However, site effects in Saguenay remain under-investigated, particularly concerning nonlinear soil behavior and frequency-dependent amplification, which are crucial for seismic hazard modeling and land-use planning.

Traditional seismic hazard assessments and building codes, including the National Building Code of Canada (NBCC 2020), primarily use simplified proxies such as the average shear wave velocity over the top 30 meters (V_{S30}) and site class designations to account for local amplification effects (Atkinson & Adams, 2013; Boore & Atkinson, 2008; Kolaj et al., 2019). While V_{S30} provides a convenient and broadly applicable metric, it has well-known limitations, particularly in regions with complex stratigraphy or significant impedance contrasts, since it is unable to fully capture resonance effects or nonlinear site behavior (Harmon et al., 2019; Hashash et al., 2018; Hassani & Atkinson,

2016). Recent studies have highlighted that complementary proxies such as the fundamental site period (T_0) (Luzi et al., 2011; Zhu et al., 2020), average shear wave velocity over the entire soil column (V_{savg}) (Stambouli et al., 2017) , soil thickness (H_{soil}), and especially the nonlinear site period (T_{NL}) (Motazedian et al., 2011), provide improved estimates of amplification, particularly at medium to long spectral periods. These proxies capture the frequency-dependent behavior and reduce the variability of the seismic amplification (Derras et al., 2017; Ghofrani & Atkinson, 2014). Consequently, there is a growing trend in the seismological and geotechnical communities toward multi-proxy site characterization frameworks to inform seismic hazard assessments and microzonation efforts better (Zhu et al., 2020).

Moreover, the lack of strong earthquake events in Eastern Canada challenges traditional empirical methods based on field observations. As a result, advanced numerical simulations, such as 1D nonlinear ground response analysis using finite element or finite difference methods, have become essential tools for seismic microzonation in data-scarce regions. These models require the careful selection of input parameters, including site-specific geotechnical profiles, ground motions that are compatible with the regional seismic hazard, and accurate constitutive models that represent nonlinear soil behavior under cyclic loading.

In Eastern Canada, seismic microzonation has primarily focused on mapping spatial variations in site parameters such as V_{s30}, V_{savg}, and T_0 using geological and geophysical models. Studies have developed site-period- or Vs_{30}-based microzonation for cities such as Victoria, Ottawa, Québec City, and Montreal, while regional V_{s30} and T_0 maps have been created for the St. Lawrence Lowlands (Nastev et al., 2016). Similar approaches in Vancouver utilized geological proxies and seismic data, while in Saguenay, advanced probabilistic 3D V_s modeling and multi-parameter classification were employed to refine amplification hazard mapping (Salsaibili et al., 2013). Despite these efforts, most work targets site parameter microzonation, with limited emphasis on hazard-specific site amplification, which remains a critical area for further research in seismic hazard assessment.

This research is motivated by the need to bridge the gap between seismic microzonation, as currently practiced through simplified amplification modeling, and the complex soil-structure interactions observed in regions like Saguenay. A comprehensive nonlinear ground response analysis, incorporating site-specific properties of Saguenay, was employed to calculate seismic site

amplification, identify dynamic characteristics, and establish correlations between site amplification and specific parameters. By developing a refined amplification model that accounts for nonlinear effects, this study aims to enhance the predictive capabilities of seismic microzonation maps and contribute to the planning of earthquake-resilient infrastructure in Eastern Canada.

1.2. Problem statement

Despite advances in seismic hazard assessment, the current methodologies used in Eastern Canada remain inadequate for capturing the true nature of local site effects in geologically complex regions, such as the Saguenay. Widely used proxies such as Vs_{30} offer a generalized view of subsurface conditions but lack sensitivity to resonance effects, layered stratigraphy, and soil nonlinearity. Consequently, existing amplification models and seismic hazard maps may significantly overestimate or underestimate risk, leading to inconsistent design provisions and potentially unsafe infrastructure.

Furthermore, NBCC 2020 regional amplification factors are derived from empirical ground motion prediction models (GMMs) developed for broader regions. They may not reflect local geotechnical conditions in Saguenay, particularly in areas with thick, soft soils or multiple layers of contrasting stiffness. No comprehensive framework currently exists that integrates nonlinear site behavior, multiple amplification proxies, and region-specific geotechnical inputs into a unified micro-zonation model for Eastern Canada. This lack of localized understanding and methodological refinement constitutes a significant obstacle in developing reliable seismic hazard maps and urban planning tools for the Saguenay region.

1.3 Research objectives

This research aims to fill in the current gap in knowledge by developing a methodology for seismic microzonation mapping using site-specific numerical amplification models based on one-dimensional nonlinear soil dynamic responses in Saguenay, Quebec. The following specific objectives guide the study:

1. Determine the site amplification from nonlinear site response analysis
2. Assess the efficiency of soil geotechnical parameters and site proxies in seismic site amplification
3. Evaluate the site periods derived from analytical and numerical simulations

4. Develop seismic microzonation through site amplification modeling

1.4. Research methodology

The research methodology is divided into four main parts: site amplification from nonlinear ground response analysis; assessment of the efficiency of soil geotechnical parameters and site proxies in seismic site amplification; development of a correlation between amplification and site proxies; and development of a seismic micro-zonation map for amplification in Saguenay, eastern Canada. Each step is presented in Figure 1.

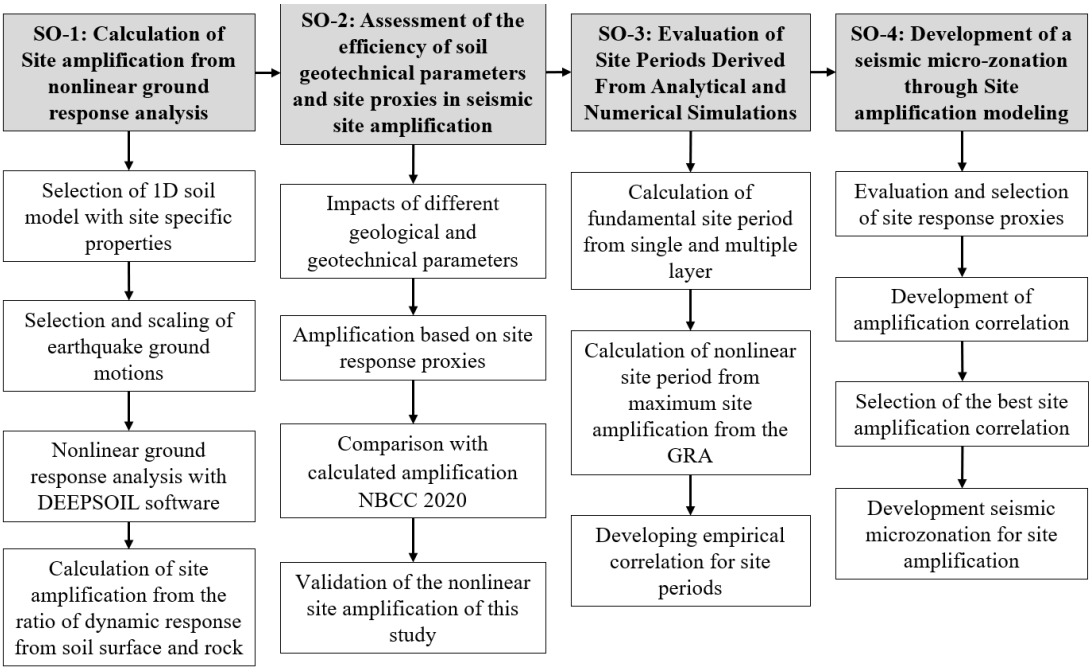

Figure 1. Applied methodology

1.4.1. Numerical site effect analysis

Fifty-one-dimensional (1D) cross-sectional soil profiles were selected to represent the study area and define the site-specific geotechnical engineering properties. Eastern Canadian earthquake ground motions were chosen and scaled to various hazard levels defined by NBCC 2020. 1D nonlinear ground response analysis was then performed using DEEPSOIL software to estimate the local site amplification. The calculated amplification values were subsequently validated by comparing the results with outputs from alternative software platforms to ensure reliability.

1.4.2. Assessment of the efficiency of soil geotechnical parameters and site proxies in seismic amplification

The influence of various geological and geotechnical parameters on seismic site amplification was evaluated. Parameters such as soil type, shear wave velocity profiles, and fundamental site period

were examined to determine their role in controlling amplification behavior. The effectiveness of site response proxies, including Vs_{30}, Vs_{avg}, T_0, and H_{soil}, was assessed based on the calculated site amplification. These findings were then benchmarked against the NBCC 2020 site amplification guidelines to evaluate their consistency and accuracy.

1.4.3. Evaluation of site periods derived from analytical and numerical simulations

The fundamental site period using both the equivalent single-layer and multi-layer methods was calculated, and the nonlinear site period for different hazard levels was determined through ground response analysis. We then developed correlations between the site periods and produced the corresponding seismic microzonation maps.

1.4.4. Development of seismic micro-zonation through site amplification modeling

In the final stage, various site amplification proxies were selected, and correlation equations were developed using both single and multiple proxies. The best-performing site amplification model was then identified. By integrating this model with both the existing and newly developed site proxy microzonation, we produced the seismic microzonation map for site amplification.

1.4.5. Validation of the study

The study's validation was conducted in two phases. In the first phase, the site amplification calculated using DEEPSOIL software was validated against the results obtained from RS2 software and previously recorded site amplification from real earthquake events. In the second phase, the site amplification estimated using the developed correlation equations was validated against the DEEPSOIL-calculated amplification for over 50 different soil profiles. The details of the validation part are given in the articles and the appendix.

1.5 Originality

This research makes several original contributions to advancing the understanding and prediction of amplification of earthquake-induced ground motions in regions with complex surficial geology, such as the Saguenay region in Eastern Canada:

- **Extensive nonlinear ground response database:** One of the most comprehensive regional datasets is assembled from >50 soil profiles exposed to real and synthetic ground motions scaled to NBCC hazard levels, offering robust validation for the proposed framework.

- **Introduction of the nonlinear site period (T_{NL}) as a proxy indicator for amplification:** T_{NL} is demonstrated to represent the frequency- and strain-dependent soil behavior better than the fundamental site period (T_0), improving predictive accuracy of amplification trends across medium to long period ranges. Empirical correlations are established between the fundamental site period at low strains and the nonlinear site periods.

- **Development of a nonlinear amplification framework:** A novel approach is introduced that correlates seismic amplification with multiple site proxies: T_{NL}, Vs_{30}, Vs_{avg}, H_{till}, addressing the limitations of single-parameter models incorporating nonlinear soil response, stratigraphy, and impedance contrasts.

- **Locally calibrated seismic microzonation maps:** Level III microzonation maps integrating geological, geotechnical, and modeled amplification data are generated, revealing some deficiencies in NBCC predictions and providing a practical tool enabling engineers to improve the accuracy of seismic hazard parameters needed for structural design.

1.7 Thesis outline

Four journal papers are the output of this thesis and are presented separately in Chapters 2 to 5. The general structure of the articles comprises the Abstract, Introduction, Numerical Framework, Constitutive Soil Model, Analysis, Discussion, and Conclusion.

Chapter 1. The chapter opens with an in-depth discussion of the research topic, outlining the central research questions. Building on this foundation, it presents the specific research objectives. It then offers a detailed explanation of the methodology adopted to address these objectives. The chapter concludes with a summary of the thesis structure, giving readers a clear roadmap of the content that follows.

Chapter 2. This chapter presents a comprehensive literature review on the key parameters and methods used in site response analysis for predicting earthquake-induced ground motions. It evaluates the effectiveness of common site effect proxies and highlights the importance of accurate dynamic soil characterization and modeling approaches for reliable amplification predictions.

Chapter 3. This chapter presents a nonlinear ground response analysis of 50 soil profiles from the Saguenay region, assessing the influence of shear-wave velocity, soil thickness, and till layers on

seismic amplification. It compares the performance of various site proxies and highlights the limitations of NBCC 2020, emphasizing the need for site-specific microzonation.

Chapter 4. This chapter evaluates fundamental and nonlinear site periods in Saguenay using analytical and numerical methods, highlighting the greater accuracy of the Multiple Layer System over the Equivalent Single Layer method. It develops empirical correlations between different period estimates and produces microzonation maps to support site-specific seismic assessments.

Chapter 5. This chapter presents a seismic microzonation study of Saguenay using 1D nonlinear ground response analyses to model site amplification. It introduces the nonlinear site period as a key proxy, develops correlation equations with optimal site parameters, and produces detailed geological, geotechnical, and amplification maps for regional hazard assessment.

Chapter 6. Summarizes the key findings of this study and outlines potential avenues for future research.

CHAPTER 2

ARTICLE 1: A REVIEW OF PARAMETERS AND METHODS FOR SEISMIC SITE RESPONSE

Authors

A S M Fahad Hossain, Ali Saeidi, Mohammad Salsabili, Miroslav Nastev, Juliana Ruiz Suescun and Zeinab Bayati

Author contributions

A S M Fahad Hossain: Conceptualization, Data curation, Formal analysis, Resources, Writing original draft, Writing review & editing. Ali Saeidi: Supervision, Methodology, Resources. Miroslav Nastev: Supervision, Writing – review & editing. Mohammad Salsabili: Writing – review & editing.

Status

Published in Geosciences on 1 April 2025 (Hossain, A. F., Saeidi, A., Salsabili, M., Nastev, M., Suescun, J. R., & Bayati, Z. (2025). A Review of Parameters and Methods for Seismic Site Response. Geosciences, 15(4), 128. https://doi.org/10.3390/geosciences15040128)

Declaration of competing interest

The authors declare the following financial interests/personal relationships, which may be considered potential competing interests: Ali Saeidi reports that financial support was provided by the Natural Sciences and Engineering Research Council of Canada and Hydro-Québec (CRDPJ 521771-17). Ali Saeidi reports financial support was provided by Natural Sciences and Engineering Research Council of Canada, Hydro-Quebec, Geostack, Rocscience and City of Saguenay (ALLRP 590081-23). If there are other authors, they declare that they have no known competing financial interests or personal relationships that could have appeared to influence the work reported in this paper.

Résumé

La prédiction de l'intensité des mouvements sismiques induits à la surface du sol suscite un vif intérêt au sein de la communauté des géosciences en raison des menaces importantes qu'ils représentent pour les populations et l'environnement bâti. Elle dépend de plusieurs facteurs, notamment la magnitude du séisme, la distance épicentrale et les conditions géologiques et géotechniques locales. Les effets de site, tels que l'amplification par résonance, la focalisation topographique et les interactions aux bordures de bassins, peuvent modifier de manière significative l'amplitude, le contenu fréquentiel et la durée des ondes sismiques incidentes. Ces effets sont généralement évalués à l'aide de proxies de site ou de modèles analytiques et numériques plus avancés intégrant des lois constitutives contrainte–déformation. Dans les simulations numériques, l'excitation sismique est représentée par un ensemble de mouvements sismiques d'entrée compatibles avec le contexte d'aléa sismique du site étudié et avec la probabilité de dépassement d'un niveau donné de secousses sur une période donnée ; ces mouvements sont appliqués à la base des profils de sol, et leur propagation verticale est simulée à l'aide d'approches équivalentes linéaires ou non linéaires, dans les domaines temporel ou fréquentiel. Cet article propose une revue bibliographique approfondie des principaux paramètres d'entrée des analyses de réponse de site, évalue l'efficacité des proxys de réponse de site et discute l'importance d'une modélisation précise pour la prédiction de l'amplification des mouvements sismiques au rocher, en mettant l'accent sur les paramètres dynamiques du sol tels que la vitesse des ondes de cisaillement, les courbes de réduction du module de cisaillement et d'amortissement, ainsi que sur la sélection et la mise à l'échelle des mouvements sismiques et les proxys de site couramment utilisés (V_{s30}, période fondamentale, vitesse moyenne des ondes de cisaillement, épaisseur du profil de sol, etc.).

2.1 Abstract

Prediction of the intensity of earthquake-induced motions at the ground surface attracts extensive attention from the geoscience community due to the significant threat it poses to humans and built environment. Several factors are involved, including earthquake magnitude, epicentral distance, and local soil conditions. Site effects, such as resonance amplification, topographic focusing, and basin edge interactions, can significantly influence the amplitude-frequency content and duration of the incoming seismic waves. They are commonly predicted using site effect proxies or applying more sophisticated analytical and numerical models with advanced constitutive stress-strain relationships.

The seismic excitation in numerical simulations consists of a set of ground input motions that are compatible with the seismic hazard settings at the studied location and the probability of exceeding a specific level of ground shaking over a given period. These motions are applied at the base of the considered soil profiles, and their vertical propagation is generally simulated using equivalent-linear and nonlinear approaches in time or frequency domains. This paper provides a comprehensive literature review of the major input parameters for site response analyses, evaluates the efficiency of site response proxies, and discusses the significance of accurate modeling approaches for predicting bedrock motion amplification. Discussed are the important dynamic soil parameters: shear wave velocity, shear modulus reduction, and damping ratio curves together with the selection and scaling of earthquake ground motion and the widely accepted site proxies: shear-wave velocity of the top 30m, fundamental vibration period, average shear-wave velocity, the thickness of the soil profile, etc.
Keywords: Shear-wave velocity, shear modulus, damping ratio, earthquake ground motions, site amplification, soil fundamental period, ground response analysis, site effect.

2.2 Introduction

Recent strong earthquakes have demonstrated their destructive potential, causing damage to structures and disrupting human activities, e.g., the 2010 M8.8 Chile, 2011 M9.0 Tohoku, 2013 M7.7 Pakistan, 2015 M7.8 Nepal, 2018 M7.5 Sulawesi, Indonesia, 2021 M7.2 Haiti, and 2023 M7.8 Turkey-Syria earthquakes. Since the 1985 M8.0 Mexico City earthquake, it has been widely recognized that near-surface geological and geotechnical conditions can significantly impact the amplitude-frequency content and duration of bedrock ground motion (Kramer, 1996; Hossain et al., 2023). Namely, when vertically propagating seismic shear waves encounter a low-stiffness medium, their propagation velocity decreases rapidly, whereas the amplitude increases, thus conserving their energy (Hunter & Crow, 2015). This phenomenon is commonly referred to as the "site effect".

In case of a relatively uniform infinite soil layer on top of considerably stiffer bedrock, the site effect is characterized by a well-defined single amplification peak at the soil fundamental vibration period. Multiple-peak amplification corresponds to the presence of multiple heterogeneous surficial layers. In contrast, broadband amplification occurs when a relatively gradual decrease in the shear-wave velocity (V_S) takes place towards the ground surface (Naggar El, 2010). In addition to impedance contrasts between surficial layers, ground shaking may also be amplified due to topographical conditions and basin effects. Typically, soft soils with low shear-wave velocity (strength) tend to

amplify low-frequency bedrock motions from distant earthquakes. In contrast, stiff shallow soils amplify the high-frequency content from nearby earthquakes (Nastev et al., 2016). It was also confirmed that the dynamic response of structures built on soft soils differs from that of structures on stiff soils and rock outcrops, which can lead to increased damage (Kwon & Elnashai, 2017). Whatever the cause of local amplification, it may contribute to significant variations in the ground motion intensity at relatively short distances.

The development of sophisticated analytical and numerical models for predicting potential seismic shaking at the ground surface and its subsequent negative impacts on the built environment is rapidly advancing. Among these, the finite element and finite difference methods are the most frequently used. They apply advanced constitutive stress-strain models to simulate the soil's nonlinear dynamic behavior during cyclic loading induced by the ground motion input. Accounting for site effects typically involves developing design ground motions through experimental and numerical methods. Numerical techniques include linear and/or nonlinear seismic response analyses in 1D, 2D, or 3D, which require representative geotechnical properties and ground motions as input. To this end, one of the objectives of geotechnical earthquake engineering is to understand, measure, and quantitatively model important soil properties and ground motion parameters (Dobry, 1987).

Important soil geotechnical properties include soil density (ρ), small-strain shear modulus (G_{max}), and the associated Vs, shear modulus reduction curve (SM), material damping ratio curve (DR), and Poisson's ratio. The soil mechanical properties and dynamic response vary with cyclic loading and strain levels and therefore necessitate representative field and laboratory measurements (Clayton, 2011). Various techniques exist for their assessment, each with its pros and cons concerning different parameters and soil types (Luna & Jadi, 2000). The advantage of laboratory tests is that they allow control of important settings, such as confining pressure and dynamic strain. In contrast, field investigations provide measurements under undisturbed conditions and are representative of larger soil volumes. Also of interest are the local site parameters, such as the time-averaged shear-wave velocity of the soil deposits, the shear-wave velocity of the top 30 meters (Vs_{30}), and the fundamental vibration period (T_0), which are commonly used as proxies for predicting the potential amplification of bedrock motion.

The intensity of the seismic hazard is typically calculated for reference soil conditions, usually the interface between surficial sediments and bedrock, with V_S values ranging from 760 m/s to 3000 m/s

(Adams, John et al., 2015). The seismic hazard can be represented through probability of exceedance (return period) curves for various ground motion parameters, such as spectral accelerations (S_a), peak ground acceleration (PGA), peak ground velocity (PGV), or with a uniform hazard response spectrum across the entire period range of interest. What-if earthquake scenarios can also be used to simulate the seismic hazard. To ensure the reliability of the time-domain simulations, a suite of hazard-consistent acceleration time histories is needed in this case (Tremblay et al., 2015). This requirement, however, may pose a problem in low-to-moderate-seismicity intraplate regions, characterized by less frequent earthquake events and an insufficient number of strong-motion records. In such cases, alternative approaches must be applied, including the upscaling of existing accelerograms, such as ground motions recorded in other regions with similar site conditions, and/or the use of synthetic ground motions (Motazedian & Atkinson, 2005).

The objective of this paper is to provide a comprehensive review of the parameters and methods used for evaluating seismic site responses. This includes: i) determination of essential soil parameters, ii) evaluation of potential site effects, site effect parameters, and their relationship to amplification of the ground motion, iii) assessment of the seismic hazard and selection of representative ground motions, and iv) discussion on numerical methods for modelling of the site response. The conclusions provide a critical summary of the present review and highlight the procedures that must be followed to ensure an accurate assessment of the dynamic soil response.

2.3 Site effects

The local geological and geotechnical properties of soils can impact the amplitude-frequency content and duration of incoming seismic waves (Seed and Idriss, 1982). This phenomenon, referred to as site effect, may lead to significant variation in seismic shaking intensity and associated damage potential at short distances (Foulon et al., 2018). The most frequent site effects are schematically presented in Figure 2.

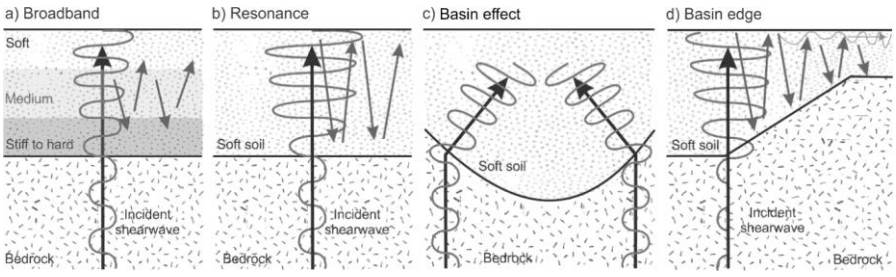

Figure 2. Schematic representations of the main amplifying effects in soft soil: a) Broad band amplification, b) resonance effect, c) buried valley focusing effect, and d) Basin edge effect.

As can be observed in Figure 1, the seismic site effect is a complex phenomenon involving a variety of factors, such as impedance contrast at the interface between geological layers (Figure 1a and b), focusing effects due to irregularities in bedrock and terrain topography (Figure 1c), basin edge effects (Figure 1d), etc. Seismic site effects and soil amplification have been widely studied in the aftermath of past strong earthquakes. The 1985 M8.0 Mexico City earthquake was likely the event that taught the engineering community the most important lessons to date. The epicentral distance was about 350 km, the distance travelled by seismic waves through the rock before entering the Mexico City basin. The simplified stratigraphy of the lake zone beneath the downtown area consists of approximately (from the ground surface): 30 m of extremely soft clayey lake sediments, 60 m of stiff clays, and on top of well-compacted and dense sandy silt (Stone et al., 1987). The estimated PGA amplification on soft soil was up to 5 times higher than the PGA measured on rock outcrops. The highest amplification, approximately 8 times, occurred in spectral accelerations around 2.0 s, corresponding to the fundamental vibration period of approximately 40 m thick, soft lake sediments. The high damage observed in buildings with a vibration period of approximately 2.0 s (12-20 stories) was attributed to the resonance effect in the soft lake sediments exposed to a distant earthquake with an energy content within the same period range. The strong motion duration of the seismic waves trapped in soft lake sediments was elongated to about 60-100 s, comparatively longer than on rocky sites, which translates into an increased number of cyclic loadings that would occur otherwise (Mayoral et al., 2019). Likewise, the city of Victoria in British Columbia experienced significant soil amplification during the 2001 M6.8 Nisqually earthquake. The strong impedance contrast between the Victoria clay (Vs=164~262 m/s) and bedrock (Vs=2000~3500 m/s) resulted in peak spectral accelerations at a period range of 0.2~0.5 s up to six times higher at soil sites compared to bedrock sites (Molnar & Cassidy, 2006).

As well, topographical effects were observed during the 1987 Whittier Narrows earthquake, California, contributing to as much as ten times higher amplitudes in a hilly region than in the nearby plains, whereas during the M6.7 Northridge earthquake in 1994, an unexpectedly high PGA=1.78 was recorded on the same Tarzana hill, 60-meter-tall feature 44 km from the epicenter, which is among the highest PGAs ever recorded (Bouchon & Barker, 1996; Spudich et al., 1996). The effects of forward directivity at the edge of the epicentral zone were first documented during the Mw 7.3 1992 Landers earthquake and Mw 6.7 1994 Northridge earthquake (Abrahamson & Somerville,

1996). The high damage concentration observed along the sediment-to-rock boundaries during the M6.7 1994 Northridge and M6.9 1995 Kobe earthquakes demonstrate the significance of the basin edge effect on ground motion amplification (Graves et al., 1998; Molnar et al., 2022).

Where possible, the prediction and evaluation of the site effects are based on recorded strong earthquake motions and field observations. The most frequent alternative is to conduct numerical site response analyses using specific dynamic soil parameters and ground motions. This type of analysis evaluates the distribution of soil dynamic stresses and strains exerted by the propagation of the seismic waves and the resulting surface ground motion.

2.3.1 Resonance amplification

The amplification of the bedrock motion can be characterized with a single amplification peak at the fundamental vibration period T_0 (resonance) of a relatively uniform soft layer with relatively poor mechanical properties on top of stiff soil or bedrock with negligible contribution of other surficial layers; multiple amplification peaks corresponding to a few well-defined surficial layers; and a broadband amplification in case of gradual decrease of Vs towards the ground surface (Naggar El, 2010). The resonance amplification is linked to a well-defined strong impedance contrast, defined as the ratio between the products of Vs and density in both soft and stiff units, approximately $\rho_{rock}Vs_{rock}^2/\rho_{soil}Vs_{soil}^2$. It governs the process of seismic wave reflection and transmission. In this case, as the Vs decreases, the amplitude of the vertically propagating horizontal shear waves increases. They become trapped within the low Vs layer, reflecting back and forth between the ground surface and the soil-bedrock interface at the fundamental vibration period of the soft soil unit. This phenomenon is common in Central and Eastern North America (ENA), where bedrock is firmer and less fragmented than in the Western United States. Equation 2.1 (Kramer, 1996) provides the fundamental resonant period (f0) and its harmonics (f1, f2, ...). The fundamental resonance frequency, f0, is often linked to the most significant spectral peak of the resonance transfer function; the amplitude of this peak varies directly as in equation 2.2.

$$f_n = (V_{savg}/4H) * (1+2n) \text{ for } n = 0,1,2,3,4\ldots\ldots \quad (2.1)$$

$$A_{res} \sim (\rho_{rock}*V_{srock})/(\rho_{avsoil}*V_{savsoil}) \quad (2.2)$$

Here, Vs_{avg}, H, ρ_{avsoil} and Vs_{avsoil} are the average shear-wave velocity of the soil (m/s), thickness of the soil column (m), average density of the soil column and travel-time-weighted average shear-wave velocity of the soil column respectively.

T_0 is an important property and depends on geometrical and mechanical soil properties, $T_0 \approx 4H/V_{Ssoil}$, where H is the thickness of the soil layer (Kramer, 1996). The effects of T_0 and H have been evaluated and shown to be significant in low-strain linear site amplification (Hossain et al., 2023, 2024). Figure 3 depicts the linear amplification of soil with varying natural periods in the Saguenay region of eastern Canada, as derived from a 1D ground response simulation. It reveals that resonance amplification occurs near the natural period of the soil. Recent earthquakes, like the M 5.8 Mineral Virginia earthquake in 2011, highlighted the seismic hazards in the region, with V_{Ssoil}~150-200 m/s and V_{Srock}~2700 m/s, leading to a significant impedance ratio, resulting in a linear amplitude increase of roughly ≥12.

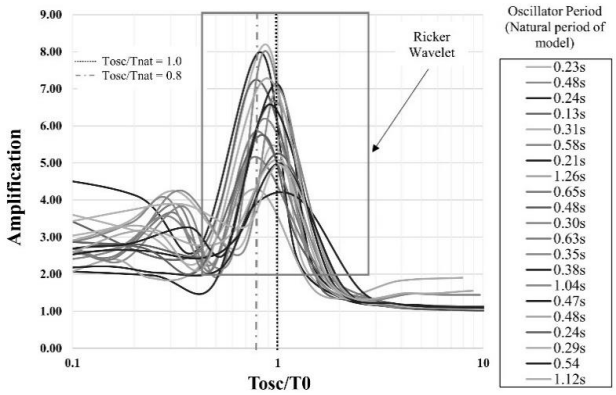

Figure 3. Natural period residuals of soil models for periods 0.001 to 10 s as a function of T_{osc} and T_0 (Hossain et al., 2024).

2.3.2 Broad-band amplification

Broad-band amplification often occurs in flat or gently sloping terrains due to a gradual decrease of soil Vs towards the ground surface. Since there is no explicit strong impedance contrast between surficial soil layers overlying the bedrock, these sites' amplification tends to be broadband (Figure 4a). In cases where there is minimal attenuation within the soil, the calculation of the broadband amplification effect is based on equation 2.3. This phenomenon is common in Western North America (WNA), where bedrock is weathered and fragmented close to the ground surface. The Mexico City and the 2001 M6.8 Nisqually earthquakes exemplify soil amplification in locations with soft clay with significant impedance variations at the bedrock contact (Pischiutta et al., 2020). The significant impedance differential between cemented sand and gravel (V_S ~500–900 m/s) and lake deposits (Vs ~75 m/s) beneath it contributed to damage in Mexico City, with amplification ratios reaching 10 at intervals of approximately 2 seconds. Victoria, British Columbia, experienced

significant soil amplification after the Nisqually earthquake in 2001 due to impedance in V_S profiles and the brown Victoria clay has lower shear-wave velocity values (~164–262 m/s) than bedrock (~2000–3500 m/s), resulting in peak accelerations up to six times higher at soil sites during intervals of 0.2–0.5 seconds compared to bedrock sites (Molnar & Cassidy, 2006).

Significant amplification around the 4–6 Hz range has been noted in both locations with thick sediment and along the northern boundary of the Fraser delta of Vancouver Island during the 2015 M 4.7 Vancouver Island Earthquake, as documented by Jackson et al. (2017). Figure 4 illustrates a cross-section of the Fraser delta, highlighting the widespread broadband amplification observed in that area due to soft, thick sediments.

$$A \sim (\rho_{rock} * Vs_{rock})/(\rho_{soil} * Vs_{soil})^{1/2} \quad (2.3)$$

Here, ρ_{rock}, ρ_{soil}, Vs_{rock} and Vs_{soil} are, in order, the average bedrock density, the average soil density, the shear-wave velocity of the bedrock at the interface between the overburden and the bedrock, and the shear-wave velocity of the soil at the ground surface.

a)

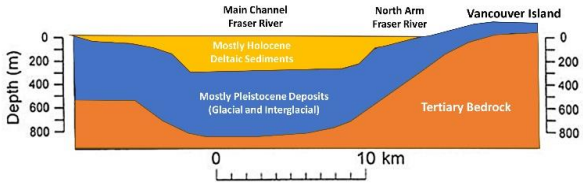

b)

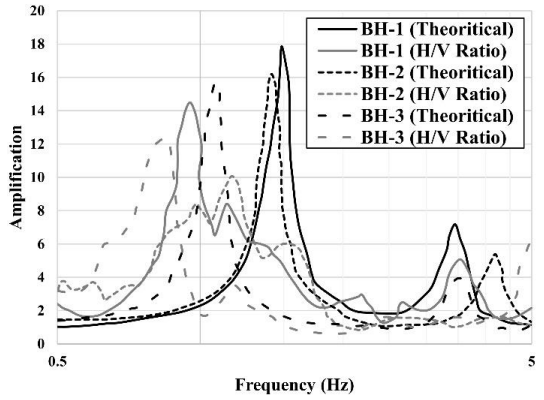

Figure 4. Fraser Delta in Vancouver a) Cross section of the Fraser delta (Modified from Jackson et al., 2017) b) amplification in three boreholes near Port Mann Bridge, Vancouver from H/V ratio and 1D analysis (Jamal Assaf et al., 2018)

2.3.3 Topographic effect

The topographic heights (hills, ridges, etc.) can contribute to a focusing effect on seismic waves, resulting in an increase in amplitude compared to leveled terrains (Assimaki, 2005). The

phenomenon of increased ground accelerations on topographic highs is caused by seismic waves that enter the base of the topographic ridge, partially reflect into the rock mass, and diffract along the free surface, progressively focusing upward. As one approaches the ridge crest, the constructive interference of these reflections and the corresponding diffractions rises (Meunier et al., 2008). Topographic lows, such as buried bedrock valleys with a relatively narrow topographic profile filled with thick, soft sediment, can focus or even diffract seismic waves (Bard & Bouchon, 1985). The crest of Tarzana Hill, a 60-meter-tall feature 44 kilometers from the epicenter, recorded seismic waves during the 1987 Whittier Narrows, California earthquake with an amplitude ten times higher than in the nearby plains (Spudich et al., 1996). One of the strongest recorded earthquake accelerations, PGA = 1.78 g, was detected on the same hill during the Northridge earthquake in 1994 (Bouchon & Barker, 1996). Topographic irregularities amplify the acceleration at 2-3 times the slope height (H) from the slope crest (Shabani et al., 2022). Seismic motion magnifies by up to 70% at the slope's crest compared to the free field behind the crest (Sitar & Clough, 1983). The angle and height of the slope additionally have a significant role in amplification (Bararpour et al., 2016). Slope edge curvature also affects acceleration amplification (Zhang et al., 2018). The acceleration amplification factor along the surface for a slope with various curvatures is shown in Figure 5.

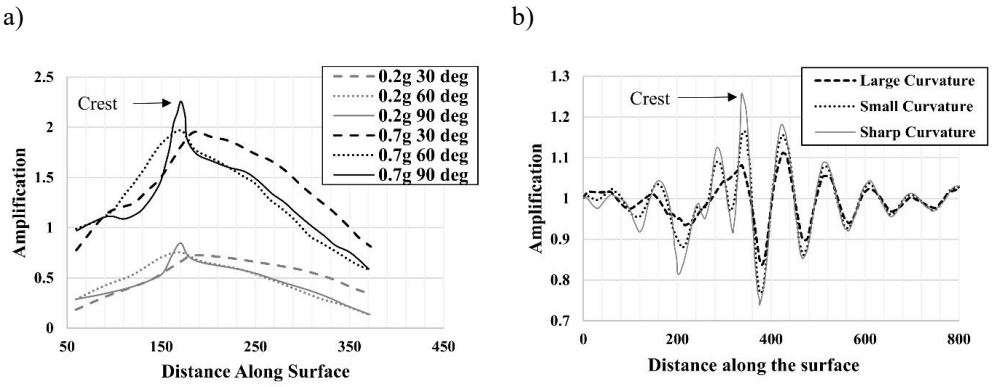

Figure 5. Topographic amplification effect on a gentle slope: a) Effect of slope angle (modified from Bararpour et al., 2016) b) Effect of slope curvature (modified from Zhang et al., 2018)

2.3.4 Basin effect

The term "basin edge effect" describes the reverberation of seismic energy at the wedge-shaped margins, where soft sediments pinch out, as well as seismic waves trapped in soft sediments deposited in bedrock depressions. As demonstrated in 1909 in Lambesc, France, 1980 in Irpinia, Italy, and 1983 in Liège, Belgium, these diffraction effects are characterized by notable increases in damage intensity that may occur in narrow, stiff zones (a few tens of meters) surrounded by softer

material (Bard & Riepl-Thomas, 2000). The most significant damage, however, was concentrated within an extended zone, parallel to both the causative fault and the sediment-to-rock boundary along the Western side of the Osaka basin, when the M6.9 Kobe earthquake struck in 1995. The other basin effect considers the impacts of deep sedimentary basins on long-duration ground motions studied in a variety of geographical locations through both numerical simulations (Molnar et al., 2014a; Molnar et al., 2014b; Marafi et al., 2019; Kakoty et al., 2021) and recorded motions (Graves et al., 1998; Rekoske et al., 2022). Basin effects have now been incorporated into the building code for periods T>1 s, ASCE 7-22, and the USGS National Seismic Hazard Model 2018 (Petersen et al., 2020). Recently, Kakoty et al. (2023) have assessed the basin effects of the Georgia sedimentary basin beneath Metro Vancouver. The average basin amplification factors in the deepest locations can reach values of 2.24 to 6.29 at 2-second intervals when compared to reference locations at the basin edge and outside the basin. Pratt et al., (2003) has investigated on the Seattle Basin, Washington State and illustrated that Initial body wave arrivals are mainly amplified by 1D basin effects, increasing direct arrivals by 4-6 times at basin sites, while topographic effects contribute only 2-3 times, indicating the dominance of 1D effects beneath the Seattle basin as shown in Figure 6. It was shown that the amplification was highest at the basin edge.

a) b)

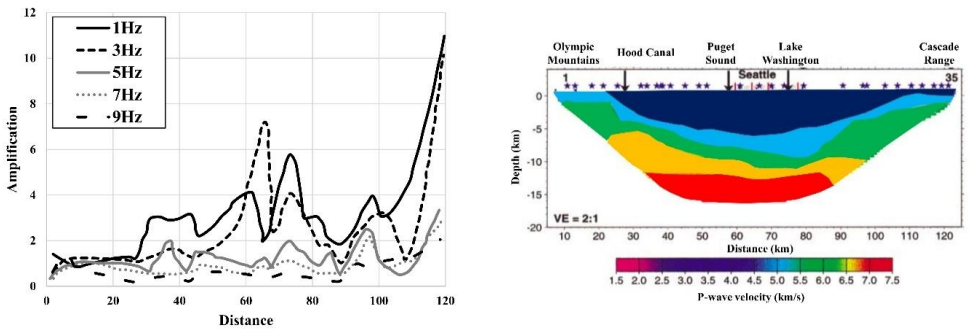

Figure 6. Amplification of local Seismic events by the Seattle Basin, Washington State a) amplification for waves of different frequencies along horizontal distance b) geological cross section of the basin (Modified from Pratt et al., 2003)

2.4 Soil parameters

2.4.1 Shear-wave velocity (V_S)

The V_s (shear-wave velocity) is a key strength parameter directly linked to the elastic shear modulus (G_{max}) and is commonly used for calculating soil dynamic response. Vs can be measured or inferred

under both field and laboratory conditions. Field tests are categorized into two types: invasive and non-invasive, both of which are also referred to as geophysical tests. The following section provides a general overview of these methods, along with their respective advantages and disadvantages.

2.4.1.1 In-situ measurements

Active, non-invasive in-situ methods, including seismic reflection and seismic refraction tests, are used to measure the compression wave (V_P) from the reflected or refracted wave generated by a mechanical hammer. Vs is then converted using an empirical correlation from V_p and other soil properties. However, the seismic refraction test is more applicable to thinner subsurface stratigraphy. Other geophysical methods like Multichannel Analysis of Surface Waves (MASW) or Spectral Analysis of Surface Waves (SASW), rely on generating and measuring surface waves and operate at low strain levels, typically less than 0.001% (Pelekis & Athanasopoulos, 2011). Both methods estimate Vs by analyzing the dispersion of surface (Rayleigh) waves, which travel along the Earth's surface. In MASW, multiple geophones arranged in a linear array record surface wave propagation across various offsets, creating a dispersion curve that relates phase velocity to frequency. SASW utilizes only two sensors to measure phase differences at different frequencies, thereby deriving the dispersion curve. Vs is calculated by inverting the dispersion curve, fitting observed phase velocities to theoretical models of subsurface properties, while considering factors such as layer thickness and Poisson's ratio. MASW can probe deeper depths and offers better resolution at greater scales, while SASW is more straightforward and effective for shallow investigations. MASW's key advantage is its robustness for large-scale surveys and high depth range, but it requires more equipment and computational resources. SASW is cost-effective and easy to deploy but has limited depth penetration and lower resolution for deeper layers.

Invasive in-situ tests, such as the Seismic Cone Penetration Test (SCPT) and Suspension Logging Tests, involve generating seismic waves (P-waves or S-waves) using methods like sledgehammer strikes, weight drops, or explosives. Suspension logging tests can be further categorized into seismic downhole, seismic up-hole, and seismic cross-hole tests. Figure 7 shows a schematic diagram of a field Vs measurement using a suspension logging test, which consists of a geophone receiver and a seismic source to generate waves. To produce a P-wave, a direct vertical impulse is applied to a wooden or steel plank using a hammer. In contrast, for S-wave generation, a horizontal blow is applied, and the wave is generated from friction between the soil and the plate. The geophone

receiver records the waves in three directions, and the V_P and V_S are calculated based on the travel time and travel distance of the waves. These tests provide accurate estimations of wave velocities but can be expensive and somewhat challenging, depending on site conditions.

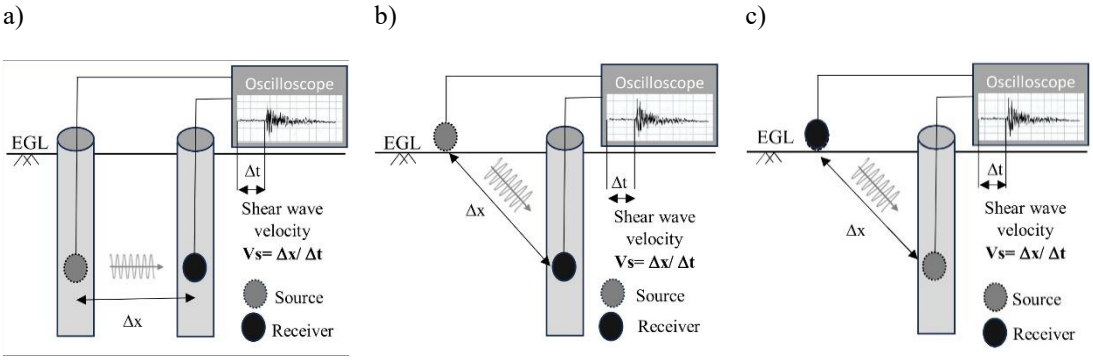

Figure 7. Suspension Logging Test a) cross-hole test b) down-hole test c) up-hole test (modified from Kamalb and Alama, 2013)

In SCPT, the seismic downhole test is conducted in conjunction with the CPT. The SCPT enables persistent subsurface assessment and facilitates the development of a precise empirical relationship between soil strength properties and V_s (Salsabili et al., 2022). The interpretations of the encountered soil stratigraphy can be based on standard CPTu properties, such as sleeve friction (f_s), cone tip friction (F_r), resistance (qt), friction ratio ($R_f = f_s/q_t$), and normalized cone resistance (Q_{tn}). Additional parameters, such as the stress exponent and normalized pore pressure B_q, are used in determining the soil behavior type index I_c. Additionally, correlations between CPT data and SPT N-values are often used to relate most field parameters to the SPT N-values. The V_s values are typically inferred from directly measured field parameters, enabling the development of several Vs correlations for various soil types and depths. Such correlations can be of a regional or site-specific nature, requiring caution when applied to other regions (Nastev, Parent, Benoit, et al., 2016). An extensive list of Vs correlations with CPT parameters is given in Table 1. Table 2 provides the advantages and disadvantages of each method.

Table 1. Empirical correlations of Vs with CPT parameters (after Salsabili et al., 2022)

Correlation	Soil Type	Reference
$Vs = [10^{0.55 I_c} + 1.68(\frac{q_t - \sigma_{vo}}{P_a})]^{0.5}$	All Soils	Robertson (2009)
$Vs = 1.75 q_c^{0.627}$	Clayey Soil	Mayne and Rix (1995)
$Vs = 155 q_c^{0.29} f_s^{-0.10}$	Clayey Soil	Madiai and Simono (2004)

$Vs = 224 q_c^{0.26} f_s^{-0.01}$	Sandy Soil	
$Vs = 0.0831 Q_{tn} e^{1.786 Ic} (\frac{\sigma_a'}{P_a})$	All Soils	Hegazy and Mayne (2006)
$Vs = 2.27 q_t^{0.412} I_c^{0.098} Z^{0.033}$	All Soils	Andrus et al. (2007)
$Vs = 2.934 q_t^{0.395} I_c^{0.912} Z^{0.124}$	All Soils	
$Vs = 1.961\ q_t^{0.579}\ (1+B_q)^{1.202}$	Marine Clay Soil	Long and Donohue (2010)
$Vs = 10^{(0.8 I_c - 1.17)} Q_{tn}$	Silty Soil	Tonni and Simonini (2013)
$Vs = 18.4 q_c^{0.144} I_c^{0.0832} Z^{0.278}$	Sandy Soil	Mcgann et al. (2015)
$Vs = 39 q_t^{0.164} Z^{0.137}$	Sandy Soil	Perret et al. (2016)
$Vs = 8.35(q_t - \sigma_{vo})^{0.22}\ \sigma_{vo}'^{0.357}$	Marine Clay	L'Heureux and Long (2017)
$Vs = 43.7(\frac{Q_{tn}^{0.25}}{D_{50}^{0.215}})$	Clayey Soil	Karray and Hussien (2017)
$Vs = 71(\frac{Q_{tn}^{0.25}}{D_{50}^{0.1}})$	Sandy Soil	
$Vs = 35.1\ q_t^{0.188} f_s^{0.102} Z^{0.139}$	Silt and Sand mixtures	Tong et al. (2018)

Where V_s is shear-wave velocity, I_c is soil behavior type index, σ_{vo} is overburdening stress, q_c is raw cone tip resistance, q_t is corrected cone tip resistance, Z is depth, B_q is normalized pore pressure, Q_{tn} is normalized cone resistance, D_{50} is effective mean diameter, and f_s is sleeve friction resistance.

Table 2. Advantages and Disadvantages of In Situ Methods of Measuring Shear-Wave Velocity

Method	Advantages	Disadvantages
Seismic Reflection	Provides detailed imaging of subsurface layers. Can explore deeper depths. Cost effective and easy to use Non-invasive.	Not a direct calculation method of Vs Requires advanced processing and interpretation skills.
Seismic Refraction	Cost-effective for thinner stratigraphy. Easy to deploy in suitable conditions. Non-invasive.	Not a direct calculation method of Vs Limited to increasing velocity layers. Less effective for complex

		subsurface or thin layers.
MASW	Probes deeper depths with good resolution. Suitable for large-scale surveys. Provides detailed imaging of Vs along the array. Cost effective and easy to use Non-invasive.	Not a direct calculation method of Vs Requires more equipment and computational effort. Sensitive to noise and ground coupling issues.
SASW	Simple setup and cost-effective. Effective for shallow investigations. Non-invasive.	Not a direct calculation method of Vs Limited depth penetration. Lower resolution compared to MASW for deeper layers.
Suspension Logging	Accurate measurements of Vs along the depth	Invasive and costly. Challenging weather and other site conditions Requires suitable borehole conditions.
Seismic Cone Penetration Test (SCPT)	Provides both geotechnical and dynamic properties. High accuracy for Vs measurement. Reliable in soft soils.	Invasive and site-dependent. More expensive than non-invasive methods. Requires skilled operation.

2.4.1.2 Laboratory measurements

Non-invasive laboratory tests determine Vs from undisturbed soil samples, categorized into (i) low-strain methods such as Resonant column, Ultrasonic pulse test, Piezoelectric bender element test, and (ii) high-strain tests like cyclic triaxial test, Cyclic direct simple shear test, and Cyclic torsional test. In these tests, a seismic pulse is applied to the soil sample, and G_{max} is estimated as $G_{max} = \rho Vs^2$, where ρ represents the soil density. The direct use of G_{max} for deformation analysis is not

recommended; instead, SM and DR curves are applied as functions of the attained strain (Fernandes et al., 2023). Shaking table tests (Zayed et al., 2021) and Centrifuge modeling tests (Lee et al., 2012) are two types of model tests conducted under controlled laboratory conditions, which measure seismic behavior and wave propagation in soil samples. Model tests typically involve cyclic loading on a small-scale physical model, aiding in better seismic simulation and validation of prediction hypotheses. Due to the need for sophisticated equipment and highly trained operators, model testing is usually conducted by academic and governmental organizations.

Low-strain methods, including the Resonant Column Test, Ultrasonic Pulse Test, and Piezoelectric Bender Element Test, are effective for measuring soil properties such as shear modulus and shear-wave velocity at low strains. These tests are accurate, cost-effective, and non-destructive but are limited to small strain ranges and require high-quality samples with careful calibration. High-strain tests, such as the Cyclic Triaxial Test, Cyclic Direct Simple Shear Test, and Cyclic Torsional Shear Test, provide insights into soil strength, deformation, and liquefaction potential under cyclic loading, simulating real-world stress conditions. The use of normalized stiffness degradation curves from different laboratory tests is shown in Figure 8. However, these tests are time-intensive, require sophisticated equipment, and are constrained by boundary effects and sample limitations. Model tests, such as Shaking Table Tests and Centrifuge Modeling, offer realistic simulations of earthquake loading and full-scale stress conditions, respectively, making them valuable for studying soil-structure interactions and failure mechanisms. Despite their accuracy, these tests are costly, infrastructure-dependent, and require careful scaling to ensure applicability.

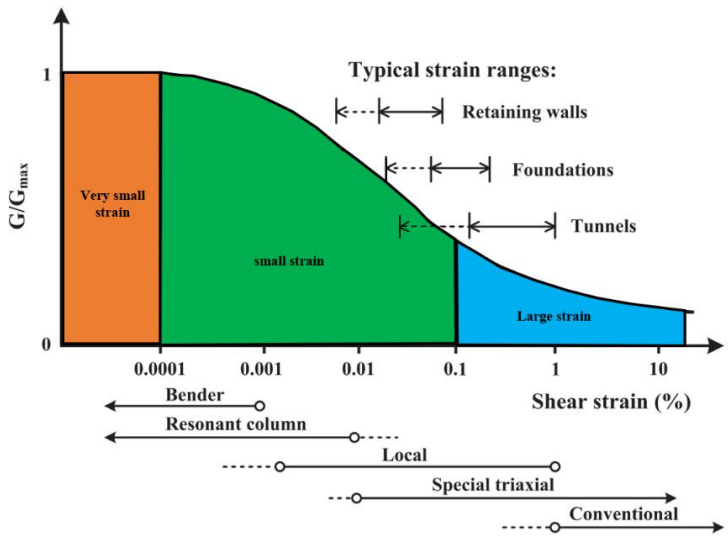

Figure 8. Normalized stiffness degradation curve (modified from Likitlersuang et al., 2013)

2.4.2 Shear Modulus and damping ratio

Soft soils typically exhibit nonlinear behavior during close strong earthquakes, where an increase in the shear strain leads to a rapid decrease of the shear modulus (SM) and an increase in the material damping ratio (DR) (Idriss & Seed, 1968). Such nonlinear behavior is implemented in dynamic soil analysis of ground response or slope stability studies. Seismological evidence from Port Island, following the 1995 M6.9 Kobe earthquake, highlights significant nonlinearities, particularly the near-perfect filtering of high-frequency motion in a liquefied sand layer (Mohammadioun, 1997). So, it is necessary to determine the nonlinear behavior of soil through the SM and DR curves. The following sections describe the measurements and the factors affecting the SM and DR.

2.4.2.1 Measurement of SM and DR

The shear modulus (SM) and damping ratio (DR) vs. strain curves (G–γ and ξ–γ) are commonly obtained with standard laboratory tests, such as Bender element, Resonant column, Cyclic triaxial test, Torsional shear tests, or Monotonic triaxial tests (Kramer, 1996). In those laboratory tests, soil behavior remains nonlinear across a broad range of strain amplitudes, forming a distinct stress-strain route known as the hysteresis loop. A complete stress reversal occurs during cycles between equal positive and negative values in the stress-strain relationship loop, described by the hysteresis damping ratio (DR) and the shear modulus (G), which is determined as the slope of a line connecting the end points (Figure 9).

a) b)

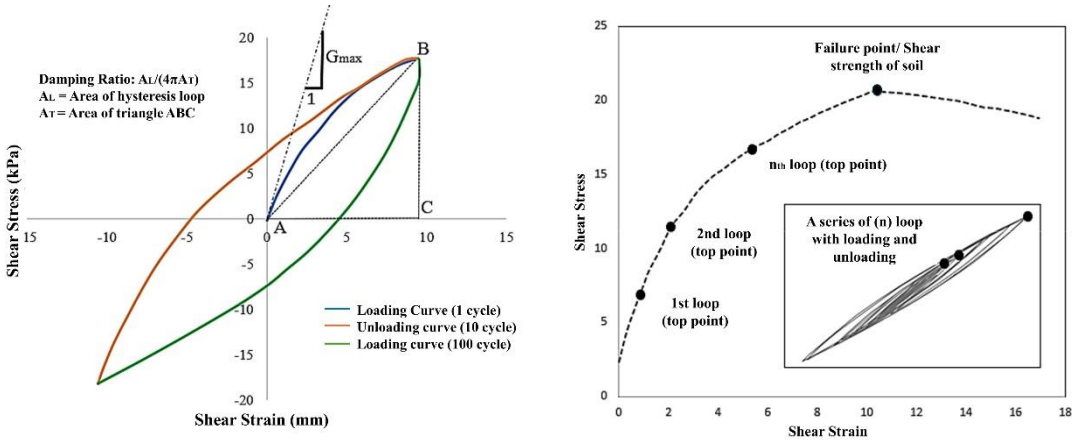

Figure 9. Stress-strain behavior in dynamic loading a) complete hysteresis loop with loading and unloading, b) loading curve only with failure stage (Modified from Dobry, 1987)

The area covered by the loop serves as a measure of the soil's internal damping, representing the energy absorbed during deformation. The soil exhibits the characteristics of a linear elastic material

at small strain amplitudes (<0.0001%), with minimal energy loss and a maximum shear modulus (G_{max}). However, as strength amplitude starts to increase, the shear modulus (G) decreases, accompanied by an increase in the hysteretic damping. Poisson's ratio correlates the shear modulus with elastic moduli, such as Young's modulus (E) and Bulk modulus (K). Among the factors influencing the strain modulus, damping ratio, and strain amplitude are the number of strain reversal cycles, loading frequency and history, void ratio, relative density, and plasticity index. Grain size distribution and particle surface texture have a lesser impact on the outcomes (Dobry, 1987).

While hysteresis damping (D) can be measured accurately in the laboratory, accurately assessing it in the field poses a significant challenge. The seismic piezocone SCPTu and seismic dilatometer SDMT measure two different points on the stress-strain curve, capturing failure states aligned with material strength characteristics and non-destructive attributes related to elastic wave propagation and soil stiffness, E or G (Mayne, 2001). SCPTu and SDMT tests assess stiffness across stress-strain-strength responses utilizing a modified hyperbola (Fahey & Carter, 1993) to degrade initial stiffness (E_0) with increasing load levels and obtain nonlinear load-displacement-capacity (Figure 10). Standard procedures for clean sands involve drained penetration with assumed zero effective cohesion intercept (cr = 0) and with focus on the effective stress friction angle (Nr). In contrast, typical assumptions for clayey soil are total stress assessments with no volume change and penetration data that provide undrained shear strength (c_u or s_u). Various factors, including starting stress state (K_o), anisotropy, boundary conditions, strain rate, loading direction, degree of disturbance, etc., have significant impact on the undrained strength.

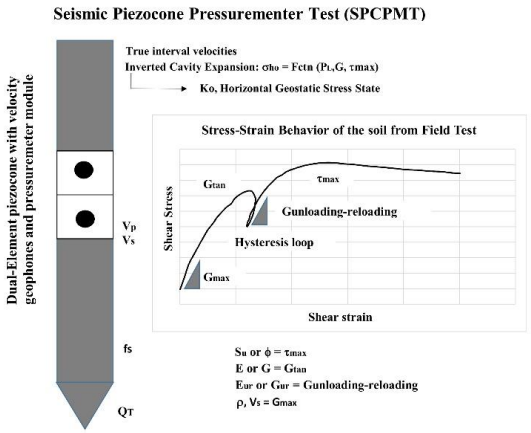

Figure 10. Concept for the use of seismic piezocone pressure meter test with dissipation phase for site exploration (modified from Mayne, 2001)

2.4.2.2 Factors affecting shear modulus reduction and damping ratio curves

The multiple factors that affect nonlinear soil behavior are discussed below.

Cohesionless soil

Numerous studies have confirmed the significant impact of particle grain size, shape, and fine particle percentage on the structure of SM and DR curves in coarse-grained soils. Baghbani et al. (2023) demonstrated that the roundness, sphericity, and regularity of sand particles during cyclic loading affect the DR, leading to increased DR as particles become more rounded. Saathoff and Achmus (2023) highlighted that grain size distribution and shape influence soil behavior, where smaller grains display higher shear strain thresholds and stress-dependent behavior. Parameters such as density, effective stress, percentage of fine particles, confining stress, and moisture content were identified as important, with cyclic shear strain and effective stress being the most critical (Seed et al., 1986). Figure 11 illustrates the non-linear SM and DR relationships with increasing shear strain. At the same time, the increasing vertical stress has the opposite impact on SM and DR, i.e., SM increases while DR decreases (Seed, 1970*; EPRI, 1993;* Assimaki et al., 2000).

In cohesionless soils, density and confining stress are also important factors affecting SM and DR curves. Rollins et al. (1998) and Rohilla and Sebastian (2023) highlighted trends related to relative density, effective stress, and loading frequency, indicating that higher strain levels reduce the influence of relative density. Confining pressure exhibits an increasing trend in SM and a decreasing trend in DR. Bozyigit and Altun (2023) identified that relative density and void ratio control the dynamic SM of non-plastic sand and low-plastic silts, with confining pressure and mean effective stress impacting the dynamic shear modulus. For sand-gravel mixtures, Bayat and Ghalandarzadeh (2018) reported changes in both parameters with an increase in confining pressure, showing an increase in SM and a decrease in DR.

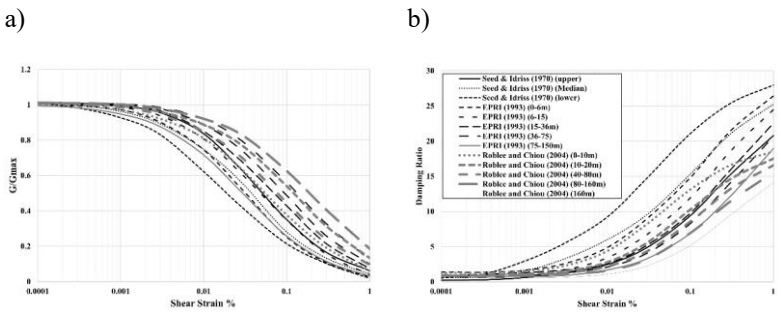

Figure 11. Cyclic relations for a) shear modulus (SM), and b) damping ratio (DR) curves for sandy soils (after Assimaki et al., 2000)

Cohesive soil

Among the parameters identified as impacting SM and DR in cohesive soils are geological age, confining pressure, void ratio, cementation, plasticity index (PI), and confining pressure (Dobry, 1987; Ishihara, 1996). Vucetic and Dobry (1991) identified the plasticity index (PI) as the primary factor, and their SM and DR models, developed for various PI scenarios, are frequently used to assess the dynamic behavior of cohesive soils, as shown in Figure 12. It was also demonstrated that in cases with decreasing SM, the effective vertical stress and over-consolidation ratio (OCR) have a greater influence than PI (Lanzo et al., 1997). As an update to earlier work by Seed et al., (1986) and Vucetic and Dobry, (1991), Darendeli, (2001) developed SM and DR versus shear strain relations running uncertainty analysis based on PI and effective vertical stress and obtained similar effects of soil type and loading conditions.

Sensitive clay

Sensitive clays represent a special category of fine glaciomarine sediments where the original sea pore water was wholly or partially replaced by infiltration of fresh atmospheric or ground water (Rankka et al., 2004). They are characterized by sensitivity, determined by the ratio of the undisturbed shear strength to the disturbed (remolded) strength, of >30. Areas with sensitive clays are frequently found in eastern Canada and Scandinavian countries. The SM and DR curves in sensitive clays appear to be influenced by similar factors as for standard clays. For example, Abdellaziz et al. (2021) developed SM and DR versus shear strain relationships for typical eastern Canadian sensitive clays. They compared them with SM and DR of Vucetic & Dobry (1991) and Darendeli (2001). The results indicate that the SM and DR versus shear strain relations for sensitive clays initially follow the trend of conventional clay curves up to a particular strain level, ranging from 0.2% to 0.3%, before deviating at

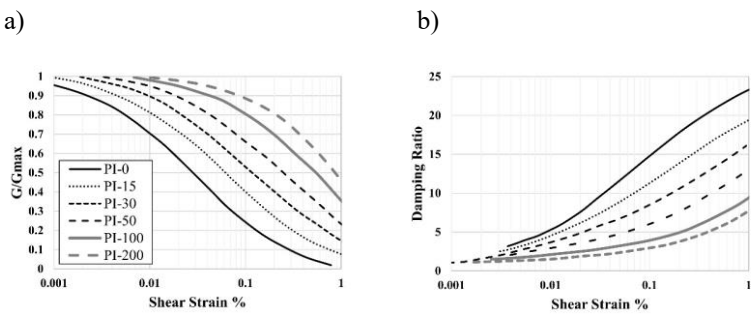

Figure 12. Cyclic relations for a) shear modulus (SM), and b) damping ratio (DR) curves for clayey soil (OCR 1-15) (after Vucetic and Dobry, 1991)

higher strains. Figure 13 illustrates the SM and DR curves for sensitive clays in eastern Canada.

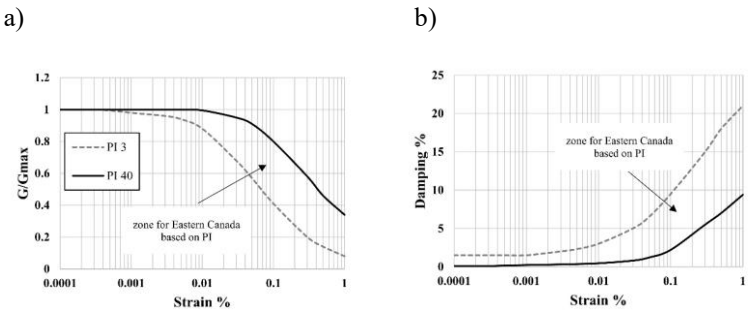

Figure 13. Cyclic relations for a) shear modulus (SM), and b) damping ratio (DR) curves for eastern Canadian sensitive clay (after Abdellaziz et al., 2021)

2.4.2.3 Nonlinear effects in dynamic loading

Soft soils generally experience higher amplification under seismic loading due to their low Vs values, where an increase in motion amplitude results in a reduction in shear strength and an increase in shear strain. At the same time, due to the non-linear effect, material damping increases, absorbing more energy and decreasing the motion amplitude. Consequently, the relative amplification may become lower in the case of strong earthquake shaking, a phenomenon addressed by Seed and Idriss (1982), as shown in Figure 14, and supported by numerical simulations by Mohammadioun and Pecker (1984). Stiff-soil sites exhibit quasi-linear behavior for PGA ranging from 0.006 g to 0.43 g (Darragh & Shakal, 1991). Field observations and calculations suggest that significant nonlinear effects in soft sandy soils may occur when the PGA at the rock interface exceeds a threshold level of around 0.1 to 0.2 g (Bard & Riepl-Thomas, 2000).

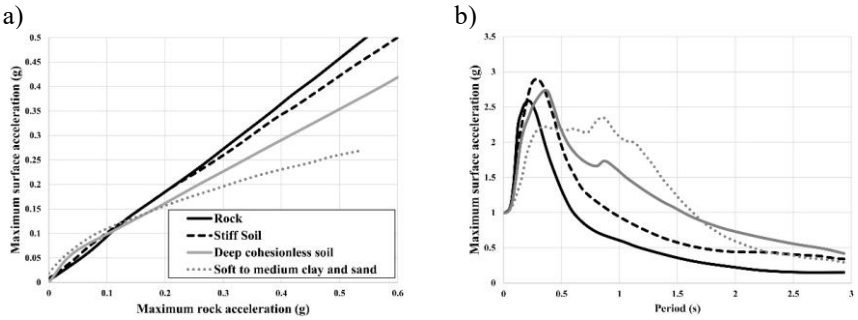

Figure 14. Nonlinear effect in dynamic loading for different types of soil: a) reduction of PGA on soft soils for destructive earthquakes (modified from (Seed and Idriss, 1982) b) Spectral acceleration at surface vs the vibration period from a statistical analysis of 104 strong-motion records (modified from (Seed et al., 1976).

2.5 Site parameters

To account for site effects, building codes rely mainly on simplified site response proxies and amplification factors. Among them, the shear-wave velocity of the top 30 meters, VS30, and the fundamental site period, T0, are the most frequently used. They correlate the local site conditions with the potential amplification of the bedrock motion, whereas V_{Savg} and H are considered as secondary site parameters.

2.5.1 Average shear-wave velocity in top 30m (V_{S30})

Figure 15 illustrates ground motion models developed by recent researchers based on V_{s30} for vibration periods of 0.2 seconds and 1.0 seconds. However, building codes simplify and propose a soil categorization, known as $V_{S30.}$ Typically, a standard site classification scheme includes categories such as hard rock, moderately fractured and weathered rock, stiff and dense soil, loose sandy soil, and soft clayey soil. Table 3 presents the VS30-based classification used for seismic hazard assessment in the design of new buildings and structures, as outlined in the NBCC (NRC, 2015) and Eurocode 8 (CEN, 2004). V_{S30} was first introduced by Borcherdt (1992) as a parameter that delineates site categories with similar amplification potential. It was developed based on site amplification studies in California, where soft surficial soils gradually transform to regolith and rock without any distinct impedance contrast. The V_{S30} concept, therefore, is not always well correlated to the observed amplification, particularly in regions with high impedance contrast at the bedrock interface, such as eastern Canada.

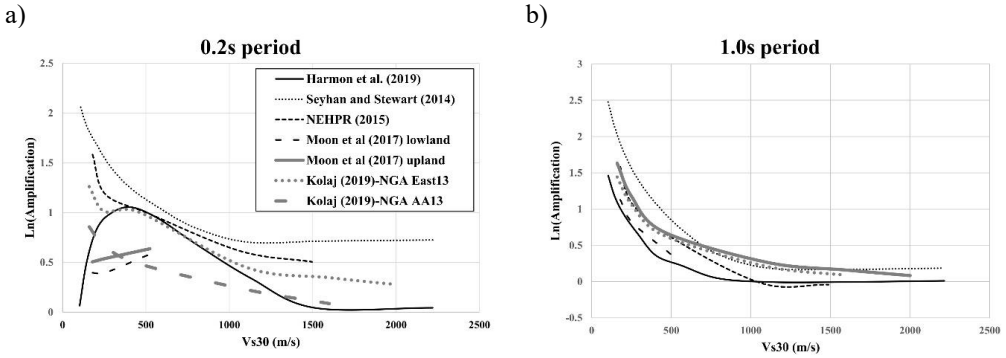

Figure 15. Site amplification empirical models as a function of V_{S30} a) for 0.2s period b) for 1.0s period (Modified from Harmon et al., 2019)

Table 3. Standard site classification schemes according to the NBCC and Eurocode 8

Code	Site Class and V_{s30} (m/s)				
	A	B	C	D	E
NBCC (NEHRP)	>1500(*)	760-1500(*)	360-760	180-360	<180
Eurocode 8	>800(**)	360-800	180-360	<180	(***)

*Soft Soil must be <3m in thickness

**Surface weak materials must be <5m

***V_{savg} < 360m/s and thickness 5 <H <20m

2.5.2 Fundamental site period

The fundamental site period (FP) or T_0 represents the most extended period at which the soil column preferably vibrates under natural loading. At the same time, it corresponds to the period when the highest soil amplification can be expected. It can therefore be used as a proxy for site amplification (Hossain et al., 2023a, 2024). T_0 is a function of soil thickness, density, and the low-strain stiffness properties. It can be measured using field microtremor measurements and the horizontal-to-vertical spectral ratio, as well as the standard spectral ratio from ground motions recorded on the soil surface and nearby rock outcrops, and with approximate analytical solutions.

2.5.2.1 Field measurements

The fundamental site period, T_0, is related to the local geological settings, including the individual thickness of the soft soil layers, depth to bedrock, and their stiffness. It can be relatively easily obtained from field measurements of natural vibrations (microtremors) over time. The soil column naturally vibrates at T_0, excited by natural and/or anthropogenic disturbances (wind, sea tides, traffic, machinery operation, etc.). Due to their small energy content, microtremors are typically recorded with high-sensitivity seismometers, such as the Tromino. The horizontal-to-vertical spectral ratio (HVSR) is then computed from the Fourier spectra of the three orthogonal vibration components—two horizontal and one vertical—and used to determine T_0 as the period with the highest HVSR (Kobayashi, 1980; Nakamura, 1989). The recording duration must be sufficiently long to show a statistically stable HVSR, usually ≥200 T_0 (Molnar et al., 2022). On the other hand, the reference site method, developed by Borcherdt (1970), is based on the comparison of acceleration response spectra of earthquake ground motions recorded on the ground surface and those recorded nearby on rock outcrops. Since both records share the exact source mechanisms and source-to-site propagation path,

the differences can be attributed to local site conditions. In this case, T_0 is obtained as the maximum of the ratio between the response spectral acceleration at the two locations, i.e., maximum amplification is anticipated at T_0.

2.5.2.2 Analytical approach

Previous studies have explored both approximate and analytical solutions for determining the fundamental period (FP) in layered soil profiles and continuous-variation models. Widely used approximate methods involve a weighted average of shear-wave velocities in layered soil profiles (Vijayendra et al., 2015). Idriss and Seed (1968) illustrated the relationship between the power of depth and rising Vs, while Ambraseys (1959) and Urzua A. (1974) assessed the fundamental period for specific soil situations, considering linear variations in shear modulus with depth. Madera G. (1970) provided FP for a two-layer system, extendable to multi-layered soil deposits. Urzua A. (1974) also determined the essential time for over-consolidated crust over ordinary conditions. All these methods are demonstrated in Wang et al. (2018), which introduces the π times the travel time of the shear-wave velocity method, applicable to both single- and multiple-layered soils. Table 4 provides an overview of the most popular techniques for calculating the FP of soil.

Table 4. Representative Techniques for Determining the Fundamental Period from Soil Profiles (modified from Wang et al., 2018)

Number	Equation	Velocity Model	Method name	Reference
1	$T = 4\frac{H}{Vs}$	Single Layer	Constant Distribution of Shear-Wave Velocity with Depth	(Urzua A., 1974) and (Dobry et al., 1976)
2	$T = 4\sum_{i=1}^{n}(\frac{h_i}{V_i})$	Multiple Layer		
3	$T = \pi\sum_{i=1}^{n}(\frac{h_i}{V_i})$	Single Layer	π times the V_S travel time method (Wang et al., 2018)	(Wang et al., 2018)

4	$a_1 = \frac{2z_1^2 \ln\left(\frac{H}{z_1}-1\right)}{(H-2z_1)T_t(H)}$; $b_1 = \frac{2\ln\left(\frac{H}{z_1}-1\right)}{T_t(H)}$ $\mu = \frac{V(H)}{V(0)} = 1 + b_1\frac{H}{a_1}$ $T = \frac{4H}{a_1}\frac{1}{0.206+0.798\mu_1^{0.853}}$ For $\mu_1 > 1$ $T = \frac{4H}{a_1}\frac{1}{0.0715+0.928\mu_1^{0.750}}$ For $\mu_1 \leq 1$	Single Layer	Linear Distribution of Shear-Wave Velocity with Depth (Deposit with $V = a_1 + b_1 z$)	Zhao (1996) and (Vijayendra et al., 2015)
5	$a_2 = \frac{\ln\left(\frac{H}{z_1}\right)H^{\frac{\ln 2}{\ln\left(\frac{H}{z_2}\right)}}}{T_t(H)}$; $b_2 = \frac{\ln\left(\frac{H}{2z_1}\right)}{\ln\left(\frac{H}{z_1}\right)}$ $T = \frac{4H}{a_2H^{b2}}\frac{1}{-0.25b_2^2-0.34b_2+1}$ for $0 \leq b_2 < 0.875$ $T = \frac{4H}{a_2H^{b2}}\frac{1}{-4.1b_2^2+6.4b_2+1.958}$ for $0.875 \leq b_2 < 0$	Single Layer	Power-Law Distribution of Shear-Wave Velocity with Depth (Deposit with $V = a_2 z^{b2}$)	(Idriss and Seed, 1968) and (Dobry et al., 1976)
6	$a_3 = \left(\frac{4z_2-H}{T_t(H)}\right)^2$; $b_3 = \frac{8(H-2z_1)}{T_t(H)^2}$ $\mu 3 = \frac{V(H)}{V(0)} = \sqrt{1+b_3H/a_3}$ $T = \frac{4H}{a_3^{0.5}}\frac{1}{0.280+0.719\mu_3^{0.960}}$ for $0 \leq \mu_3 < 1$ $T = \frac{4H}{a_3^{0.5}}\frac{1}{0.303+0.691\mu_3^{1.031}}$ for $0 \mu_3 > 1$	Single Layer	Linear Distribution of Shear Modulus with Depth (Deposit with $V = (a_3 + b_2 z)^{0.5}$)	(Ambraseys, 1959), (Urzua A., 1974)
7	$T_{a\text{-}b} = T_a\sqrt{\frac{\pi^2}{8}\left[0.75+\left(\frac{T_b}{T_a}\right)^2\left(1+2\frac{h_a}{h_b}\right)\right]}$ for $T_b/T_a > 0.1$, $h_a > h_b$ $T_a\left[1+\beta\left(\frac{T_b}{T_a}\right)^k\left(1+\frac{h_a}{h_b}\right)^k\right]^{1/k}$ for $T_b/T_a > 0.1$, $h_a \leq h_b$		Approximate Madera model	(Madera G., 1970)

	$T_a\,[1+\frac{h_a}{h_b}\left(\frac{T_b}{T_a}\right)^2]$ for $T_b/T_a \leq 0.1$ Here, $\beta = 1\text{-}0.2(h_a/h_b)^2$ and $k = 4\text{-}1.8(h_a/h_b)$			
8	$T_a = \frac{4d_a}{V_{sa}}; T_b = \frac{4d_b}{V_{sb}}$ $\tan(\frac{\pi}{2}\frac{T_a}{T_{a-b}})\tan(\frac{\pi}{2}\frac{T_b}{T_{a-b}}) =$	Multiple Layer	Successive application of two layer	(Madera G., 1970)
9	$X_i = 0; X_{i+1} + (H\text{-}H_{mi})\frac{h_i}{V_i^2}$ $T = \pi\sqrt{\frac{\sum_{i=1}^{n}(X_i+X_{i+1})^2 h_i}{\sum_{i=1}^{n}\frac{(X_i+X_{i+1})^2}{h_i}v_i^2}}$	Multiple Layer	Simplified Rayleigh method	(Dobry et al., 1976)
10	$T = 2\pi\sqrt{\frac{D^3}{3\sum_{i=1}^{N}V_{si}^2 d_i}}$	Multiple Layer	Linear fundamental Mode Shape	(Dobry et al., 1976)
11	$T = \sqrt{\sum_{i=1}^{n}(\frac{4h_i}{V_i})^2}\frac{2H_{mi}}{h_i}$	Multiple Layer	Japanese seismic design code (BCJ) method	Building Center of Japan (BCJ), 2005

where, μ_1 =bottom-to-surface velocity ratio, H= soil depth, T_t = the travel time from surface to bedrock z_1 = depth corresponding to half of the travel time H_{mi} = depth of midpoint of the i^{th} soil layer, $4h_i/V_i$ = the fundamental period of the i^{th} layer and $2H_{mi}/h_i$ = weight value determined by the depth and thickness of the i^{th} layer

As a comparative example, the fundamental period of soil columns with thicknesses ranging from 10 m to 1500 m is evaluated, assuming average shear-wave velocities between 150 m/s and 500 m/s. The FP was first determined using the Constant Distribution of Shear-Wave method, method #1in Table 4 (Dobry et al., 1976; Urzua A., 1974) as a single-layer approach, widely used in many studies. Five additional methods, #2 to #6, are compared against method #1, revealing significant deviations. Since method #1 tends to overestimate T_0 due to its assumption of constant properties throughout the soil depth as shown in Figure 16.

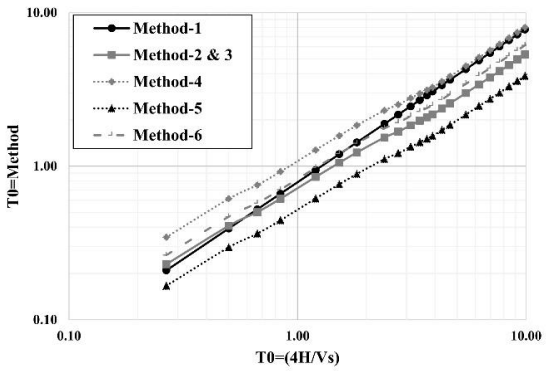

Figure 16. Comparison of the FP of soil in different methods

Methods #2 and #3 account for soil property variations, while method #4 considers two layers with different shear-wave velocities. Methods #5 and #6 consider the mode shape from bedrock to the surface, considering multiple layers, and require actual data for accuracy. It is essential to note that the computations use presumptive data, and current data may alter the observed trends (see detailed computations in Table A2 in the appendix).

To improve the site response in deeper sediments, Salsabili et al. (2021, 2023) included V_{Savg} and T_0 as secondary parameters. Alternative classification schemes incorporate the fundamental site period T_0 (Zhao et al., 2006) as shown in Table 5, and the hybrid classification method (Pitilakis et al., 2019), which combines soil thickness and stiffness properties based on V_{savg}, V_{s30}, T_0, and the thickness of the soil deposit, Figure 17. These approaches allow for a more comprehensive consideration of the impact of stiffness and thickness of surficial sediments.

Table 5. Site classification based on fundamental site period and corresponding NEHRP site classes.

(After Zhao et al., 2006)

Site Class	Description	Site Period	NEHRP site Class
Hard Rock			A
SC I	Rock	To < 0.2s	A+B
SC II	Hard Soil	0.2 ≤ To < 0.4s	C
SC III	Medium Soil	0.4 ≤ To < 0.6s	D
SC IV	Soft Soil	To ≥ 0.6s	E+F

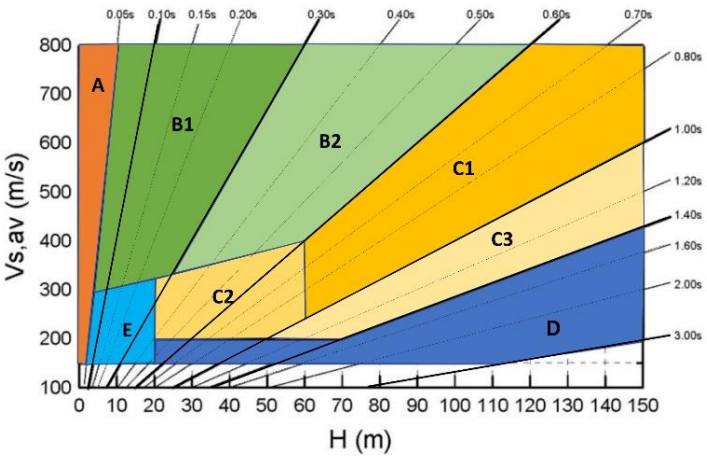

Figure 17. Correlation of H with V_{savg} and T_0 for the site classes A through E (Pitilakis et al., 2019)

2.5.2.3 Experimental evaluation

The standard experimental approaches for quantitative prediction of potential amplification of the earthquake ground motion rely on (i) assessment of the H/V ratio from microtremor measurements, and (ii) comparison of recorded accelerograms on soft soils and reference rock conditions. Ambient noise is generated by natural disturbances such as wind gusts and sea tides, and by human activities (traffic, machinery, building vibrations, etc.). Field acquisition of ambient noise is relatively easy and can be conducted rapidly with high-sensitivity seismometers. They have been used for assessment of soil dynamic characteristics since the 1950s (Aki K, 1957). Nakamura (1989) proposed the H/V technique, based on single station microtremor measurements, for assessment of the site response to vertically propagating shear waves. It compares Fourier amplitude spectra derived from recorded horizontal and vertical components, assuming that the site amplification effects on the vertical component are negligible compared to the horizontal component. In this way, the H/V ratio closely mimics the transfer function for the 1D shear wave. Ever since, numerous studies have shown that the H/V ratio can be used to effectively evaluate the site resonant frequency and the linear viscoelastic amplification generated by multiply refracted horizontal shear-waves (Costanzo & Caserta, 2019; Paolucci et al., 1999). When a sufficiently strong impedance contrast exists at sites with soft soils on top of high Vs bedrock, the H/V ratio identifies the dominant frequency with a distinct and stable peak. Gallipoli and Mucciarelli (2009); Ghofrani et al. (2013); Ghofrani and Atkinson (2014); Molnar et al. (2022) used peak amplitude (A_{peak}) and peak frequency (f_{peak}) to evaluate site amplifications. Figure 18 illustrates average H/V ratios based on site classes and V_{s30} ranges.

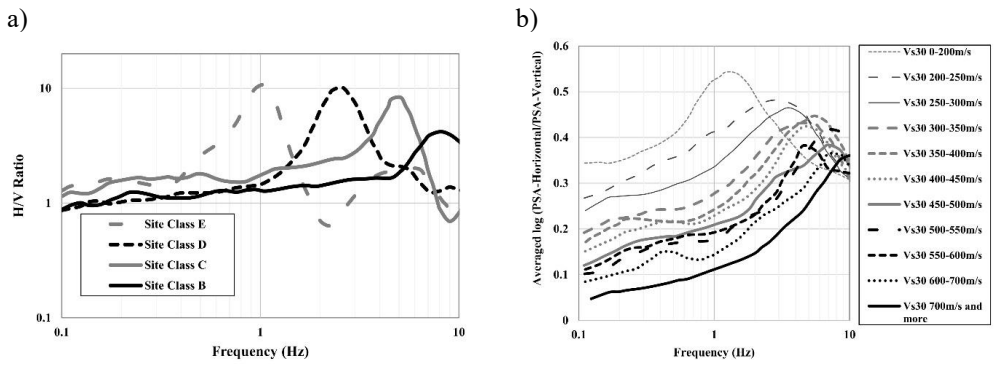

Figure 18. Comparison of H/V ratio a) based on site class from NEHRP, b) based on V_{s30} (modified from Ghofrani and Atkinson, 2014)

The standard spectral ratio method (SSR), developed by Borcherdt (1970), involves calculating the ratio between the response spectra of strong motion accelerograms recorded at the site of interest and a nearby reference site, typically a rock outcrop. SSR is a reliable method for estimating site effects as it practically measures the site amplification at the site of interest. The reference site must be close enough and free of almost any local site effects so that the differences in source and propagation path effects are negligible for both records. The setback of this technique is that it involves logistical challenges, well-characterized reference sites, and requires relatively dense seismic arrays. The HVSR method, on the other hand, represents a cost-effective and straightforward approach for determining the resonant frequency, assuming that vertical motion is unaffected by site conditions. HVSR results for site amplification assessment can only be considered preliminary, as they are based on ambient noise records at low strain levels. Such conditions are considerably different from those that occur during strong earthquake shaking, when the soil response is in the high-strain, nonlinear domain.

2.6 Seismic parameters

In contrast to static analyses, seismic excitation in dynamic analyses is specified in terms of real or synthetic acceleration time histories. The selection of representative ground motions is a crucial step, relying on criteria such as seismic settings, scaling, and the number of ground motions required for meaningful analysis. The ground motions are typically selected based on seismic settings and hazard evaluation for reference site conditions, primarily engineering bedrock with a shear wave velocity (Vs) of≥ 760 m/s. The preferred technique for scaling the selected accelerograms is to match approximately a corresponding target response spectrum, or to satisfy a specified design level, usually for PGA and/or a spectral acceleration for a given period, Sa(T).

2.6.1 Seismic Hazard

Seismic hazard represents the likelihood that a potential earthquake with a given intensity will occur in a particular area in the future. There are two basic types of seismic hazard analysis: probabilistic (PSHA) and deterministic (DSHA) seismic hazard analysis. PSHA aims to establish the 'ground motion hazard curve,' indicating the probability of exceeding a specific intensity measure (IM) in the study area. The first step involves identifying active seismic sources and determining their distances from the study area, utilizing point, fault, and areal sources in the source model (Figure 18a). The second step assesses the annual probability of earthquake magnitudes occurring on nearby sources, employing the Gutenberg-Richter relationship (Figure 18b). The third step predicts the intensity of shaking through regression analysis and ground motion models, represented by ground motion prediction equations (GMPEs) (Atkinson & Adams, 2013*;* Goulet et al., 2017) (Figure 18c). Due to the complexity of seismic waves and local site amplification, the observed data exhibit variation around the median line. The ground motion hazard curve combines the frequency-magnitude model with GMPEs, yielding one point on the elastic spectrum for a given return period (Figure 18d). The process continues for different vibration periods, forming a uniform hazard spectrum (UHS), where each point shares the same probability of exceedance. Typically, the focus is on high-intensity (low-frequency) earthquakes, with the UHS's high-frequency content influenced by small nearby earthquakes and more extended periods by large distant earthquakes.

The DSHA, on the other hand, provides a relatively straightforward and trackable method for computing the seismic hazard. It calculates the likelihood of an earthquake occurring, not its probability. It combines steps a) and c) in Figure 19 to generate a single maximum credible earthquake scenario. This is the most severe earthquake scenario expected at a site that gives the most significant predicted ground motion without explicitly considering the likelihood. For less important projects, the seismic hazard in terms of UHS with a return period of 2475 years (0.000404 p.a.) is prescribed in the seismic design provisions of NBCC 2020 (NRC, 2020). UHS for return periods ranging from 98 to 2475 years with local site conditions as a continuous function of the time-average shear-wave velocity of the top 30 meters (Vs_{30}) can be downloaded from the earthquakescanada.nrcan.gc.ca website. The latest 6_{th}-generation seismic hazard model of Canada, developed within the OpenQuake engine, can also be obtained through the same website. It

incorporates regional seismic sources with respective maximum magnitudes, earthquake rate data and epistemic uncertainty in median hazard estimates (Adams John et al., 2015).

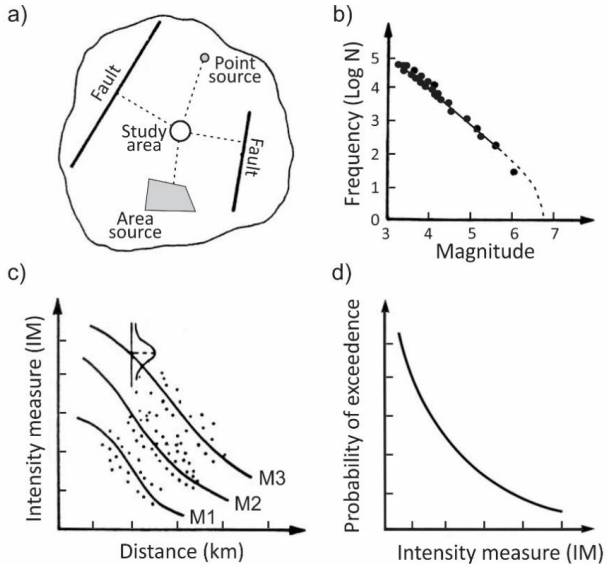

Figure 19. Probabilistic seismic hazard analysis (PSHA): a) study area with nearby sources, b) earthquake occurrence (Gutenberg–Richter relation), c) ground motion prediction equations (GMPE), d) ground motion hazard curve that describes the probability of exceedance of a given level of the selected shaking intensity measure.

2.6.2 Input ground motions

2.6.2.1 Selection of real accelerogram

Representative ground motion records play a crucial role in time domain dynamic analyses. Representative ground motion records play a crucial role in time domain dynamic analyses. Various regional databases, including the USGS Earthquake Catalog, the British Geological Survey database, COSMOS, K-NET, KiK-net, NIED, and PEER, store diverse data on earthquakes that have occurred. The ground motion selection process considers parameters such as earthquake magnitude, source-site distance, local site conditions, and rupture mechanism (J. W. Baker and Lee, 2018; Bommer & Acevedo, 2004). Additionally, the selected records must meet design spectral accelerations with a reasonable scaling factor while maintaining the strong motion duration and waveforms.

The above selection process, based on several criteria, reduces the pool of candidate records, impacting on the reliability of the dynamic analyses (Bommer & Acevedo, 2004; Tarbali & Bradley, 2016). Selecting an acceptable number of earthquakes is particularly challenging. Dynamic analyses necessitate acceptable ground motion records, often characterized by the highest response among three input accelerograms or the mean of seven (BSSC 2001; ASCE, 2005a; NERHP 2011). In

NBCC 2005, eleven ground motion time histories were proposed, whereas Tremblay et al. (2015) suggested two suites of at least five to six motions for two magnitude-distance (M-R) scenarios. On the other hand, to obtain an average response at a site, Talukder et al. (2021) recommend seven records. As can be seen, the minimum number of samples varies between three and eleven; however, all the above references recommend an increased number of acceleration time histories, particularly when evaluating the statistical significance of the uncertainty. When the initial selection criteria cannot be satisfied, which is often the case in intraplate regions due to fewer strong earthquakes compared to interplate boundaries, the remaining option is to use increased scaling factors or synthetic ground motions (Atkinson, 2009). An exhaustive review of ground motion selection has been illustrated in (Iervolino et al., 2010; Pagliaroli & Lanzo, 2008; Smerzini et al., 2014).

2.6.2.2 Synthetic accelerograms

Synthetic acceleration time histories can be generated by simulating the fault rupture mechanism, the source-to-site seismic wave propagation, and local site amplification. In this way, a variety of earthquake-magnitude-distance-site conditions scenarios can be considered, offering a viable alternative to the available real records. Stochastic simulation methods, such as SMSIM (Boore, 2003) and EXSIM (Motazedian & Atkinson GM, 2005), utilize deterministic ground motion amplitude and random phase spectra. SMSIM randomly distributes fault radiation over a time interval determined by earthquake magnitude and source-to-site distance. EXSIM considers finite-fault effects by subdividing the fault surface into sub-faults, each treated as a small point source. Ground motions from activated sub-faults are successively summed up at the observation point. For example, to compensate for the insufficient number of earthquake records, Atkinson (2009) used EXSIM to generate suites of synthetic earthquake accelerograms that are compatible with the provisions of NBCC 2005 (*www.seismotoolbox.ca*).

2.6.2.3 Spectral matching in the time domain

Spectral matching techniques in both the time and frequency domains enhance the compatibility of the selected ground motions with the target spectra typically proposed in building codes. The most straightforward technique for scaling ground motion records involves linear scaling with a constant factor to minimize the difference between the record and target spectrum accelerations (Kiani & Khanmohammadi, 2015). This method shifts the record's response spectrum proportionally, preserving frequency content and original phasing (Figure 20a). To prevent bias, scaling factors must

be limited due to the strong correlation between earthquake magnitude and strong-motion duration. Alternatively, in other words, accelerograms of low magnitude earthquakes that occur relatively frequently cannot be scaled to match target spectrum with long return period. Recommended maximum scaling factors vary, with generally safe ranges from 0.3-0.5 to 2-3 (Shome et al., 1998), 0.5-2.0 (Vanmarcke, 1979), 0.25-4.0 (Krinitzsky & Marcuson, 1983), and 0.2-0.3 to 3-5 for NGA database records (Goulet et al., 2017). Target spectra include UHS from building codes usually with probability of exceedance of 2%/50 years (e.g., NBCC 2015, ASCE 2010), conditional mean spectrum (Figure 20b; J. Baker, 2005; J. W. Baker and Allin Cornell, 2006), conditional spectrum (Lin, 2012; Lin et al., 2013), or matching a single Sa(T) value from a ground motion prediction equation (J. W. Baker and Allin Cornell, 2006).

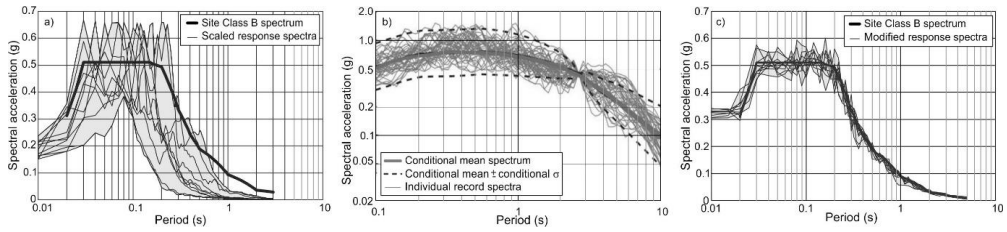

Figure 20. 5% damped response spectra of selected ground motions matching the target spectrum with different techniques: (a) scaled linearly with a constant factor, (b) conditional mean spectrum (CMS), and (c) modified in the frequency domain (modified from Lin, 2012; Nastev et al., 2008)

The target spectra in Figure 20 connect the seismic hazard information with the ground motion selection process. The widely used uniform hazard spectrum (UHS) from PSHA represents an envelope of spectral accelerations at all periods, often leading to overdesigned structures and high costs (Figure 20a). The conditional mean spectrum (CMS) represents a more realistic and less conservative technique, which correlates the spectral accelerations of the selected ground motions, Sa(T), to the expected Sa(T) at all periods given the target Sa(T*) value (Baker & Lee, 2018). CMS incorporates ground motion models for scaling, allowing records from an active region to be scaled to target periods for intraplate earthquakes in the study area (García de Quevedo Iñarritu et al., 2023).

2.6.2.4 Spectral matching in the frequency domain

Matching the response spectra of the selected accelerograms to the target spectrum in the frequency domain involves adjusting the Fourier amplitudes, while the phases remain unchanged. Early software like SIMQKE (Gasparini & Vanmarcke, 1976) and RASCAL (Silva & Lee, 1987) employed this method. Likewise, Naumoski (2001) introduced an iterative procedure that matches

the NBCC target acceleration spectra, involving both forward and inverse Fourier transforms. To accelerate the selection and scaling process, Kottke & Rathje (2008) developed a semi-automated procedure scaling real ground motions from a database to match target spectrum by modifying amplitudes and frequency content.

The frequency domain target spectrum matching technique represents a powerful tool that modifies the amplitude and frequency content of the initial accelerograms. However, the usual UHS target spectra cover a wide range of periods. Although it is well known that earthquakes close to the recording stations have their energy content primarily in high frequencies. In contrast, the energy content of distant earthquakes is concentrated at longer periods. Therefore, any single time-history matching closely the target spectrum at all periods of interest is physically unrealistic and exaggerated. In other words, it is doubtful that both nearby and faraway frequency-amplitude scenarios occur in a single earthquake event simultaneously. In this respect, matching the CSM is a better option for designing new structures and for conducting realistic seismic risk analyses of existing structures.

2.7. Numerical analysis

Site effects can be evaluated through ground response analysis using numerical methods, such as the finite element method, the distinct element method, and the finite differences method, which can be highly accurate when validated. However, their application at a specific site depends greatly on the available data about the local geomechanical properties. Various numerical techniques are employed to predict the dynamic soil response to earthquake loading, each involving different steps. They can be categorized as linear (L), equivalent linear (EL), and non-linear (NL) analyses in one dimension (1D), two dimensions (2D), and three dimensions (3D). 1D analyses rely on two major assumptions: all considered soil layers are horizontal and infinite, and the dynamic response considers the vertical propagation of horizontal shear waves. For more complex soil stratigraphy, 2D and 3D site response analyses are preferred. Equivalent linear programs, such as SHAKE code, QUAD-4, and QUAD4M, operate in both the frequency and time domains. DEEPSOIL and D-MOD2000 are widely used for 1D analyses, with DEEPSOIL enabling both frequency and time-domain analyses. Structures like earth dams, tunnels, and retaining walls benefit from 2D GRA, while 3D GRA is essential for soil-structure interaction (SSI) problems. These analyses can be conducted in the frequency or time domain using methods like spectral element, boundary element, and finite element. Advanced

numerical techniques have significantly enhanced adaptability, contributing substantially to our understanding of site impacts over the past two decades. The linear, equivalent linear, and nonlinear analysis is described with a comparison below. In the following section, ground response analysis methods, including linear (L), equivalent linear (EL), and non-linear (NL) approaches, are described.

2.7.1 Linear site response (L)

Linear analyses assume linear elastic soil with constant shear modulus (G) and damping ratio (ξ) in each considered soil layer (Kramer, 1996) (Kramer, 1996). It is performed in the time or frequency domain and is described with the following steps: conduct forward Fourier transformation of the input ground motion set at the base of the soil model in time domain, compute the transfer function of the soil model which correlates the output motion at the ground surface to the input motion in the frequency domain, multiply the Fourier series of the input motion with the transfer function, and conduct backward Fourier transformation to obtain the output motion in time domain. The key step in the linear response analysis is the computation of the frequency-dependent transfer function, since it determines the amplification of the frequency components of the input motion by the soil column. Site effects predicted using the L method are adequate only for linear viscoelastic behavior of soils, such as low-strain levels and stiff soil conditions.

2.7.2 Equivalent linear site response (EL)

Equivalent linear is also a linear method that runs in the frequency domain. It solves the equation of motion for a constant G and during seismic loading. The difference from the linear method is that it applies a procedure to determine the non-linear soil stress-strain behavior with equivalent linear properties: G as the secant shear modulus, and the damping ratio corresponding to the energy loss of the actual hysteretic loop. An iterative process is applied to determine G and ensure it is compatible with the adequate strain level reached in each layer. The effective strain is determined empirically within the range of 50-70% of the maximum strain (Kramer, 1996). The procedure starts with assigning the initial G and values corresponding to zero (low) strains. Once the effective shear strains are determined for each layer, updated G values are applied in the following iteration. Iterations are conducted until differences in G and ξ between two successive iterations are lower than the assigned threshold levels.

2.7.3 Non-linear site response (NL)

The non-linear approach provides site response simulations applying direct numerical integration of the equation of motion in the time domain, which requires a complete nonlinear shear modulus and damping curves. The integration with small time steps, Δt, allows the application of any nonlinear stress-strain model and rigorous consideration of loading-unloading cycles. The computation starts with assigning the acceleration time history at the base of the model. The soil properties for each time step and each layer are obtained from the stress-strain curve at the beginning of the time step. Several integration techniques can be used to solve the wave equation.

2.7.4 Comparison between the numerical methods

The 1994 Northridge earthquake in California provided a basis for studying soil nonlinearity (Field et al., 1998). Previous research suggests that the EL method approximates the soil's accurate nonlinear behavior under cyclical loading, but it fails to adequately account for the strong strain dependence observed in shear modulus and damping ratio experimentally ((Schnabel PB et al., 1972); (Idriss IM & Sun JI, 1992); (Kramer, 1996)). Although EL analyses provide significant results for shear strains between 1% and 2%, practitioners tend to prefer NL analyses for strains exceeding 1%, despite the threshold being considered too high (Matasovic & Hashash, 2012). (Kim and Hashash, 2013) found significant distinctions between the NL and EL approaches, for stations where site response assessments show maximum shear stress greater than 0.3%.

Disparities between the NL and EL approaches extend to ground motion frequency or period ranges. (Stewart et al., 2008) conducted a comparison between EL and NL analyses and found a good agreement over most frequencies (0.1 Hz to 100 Hz) for stiff soils and weak motions (PGA < 0.4 g). However, for more vigorous motions (PGA ≥ 0.4 g) and frequencies above 10 Hz, NL responses exceed EL responses. Peak spectral accelerations and amplifications are higher using EL for lower and medium periods, but both approaches yield similar estimates for higher periods (Huang et al., 2005; Arslan & Siyahi, 2006; Mir Mohammad Hosseini and Asadollahi Pajouh, 2012; Adampira et al., 2015). At basic periods, differences in spectral behavior are around 20% for short periods, decreasing at medium to high periods (Civelekler et al., 2024).

Additional disparities exist between EL and NL analyses. NL methods require more analysis time compared to EL methods (Basu D and Dey A, 2016; Johari & Heidari, 2020). When soil with extra pore water pressure building is modeled using the equivalent linear technique, the findings obtained

in the time domain are significantly different from those obtained in the frequency domain (Adampira et al., 2015). Assimaki and Li, (2012) discovered that the gap between EL and NL analyses is more prominent and dependent on factors such as peak ground acceleration and the time-averaged V_s in the top 30 meters of the soil profile (V_{S30}). The response is nearly identical in sufficiently stiff soil; conversely, in soft soils, the distinctions between EL and NL become more apparent (Stewart et al., 2008; Kumar et al., 2014). Nonlinear ground response, which accounts for the hysteretic stress-strain relationship of the ground (damping-shear modulus), is often considered more practical than the corresponding linear method. Both methods of soil behavior analysis perform adequately in low-stress conditions (such as weak bedrock movement and/or hard soil). However, nonlinear analyses are conventionally preferred for high-stress levels over equivalent linear methods. The distinctions L, EL, and NL are summarized in Table 6 below.

Table 6. Advantages and shortcomings of linear, equivalent linear, and nonlinear analyses

	Advantages	Limitations
Linear	Requires less time Requires fewer input parameters. Simple methodology Produces satisfactory results for stiff soil and low-frequency ground motion. No need for nonlinear soil curves.	Unable to capture nonlinear soil behavior or provide hysteresis curves due to earthquake motion Unsatisfactory results for soft soil and high-frequency ground motion Analysis confined to specific strain ranges
Equivalent linear	Requires less time Simple methodology Yields comparable results to nonlinear analysis within specific frequency ranges	Unable to capture nonlinear soil behavior or provide hysteresis curves during earthquake motion Results may vary compared to nonlinear analysis for high-frequency ranges Analysis is restricted to specific strain ranges
Nonlinear	Captures nonlinear soil behavior and provides hysteresis curves during earthquake motion	Requires more time Requires more input parameters Demands precise and in-situ nonlinear

	Offers real stress-strain curves and information on pore pressure buildup Analysis feasible for any strain range Suitable for all types of soil and ground motion intensity	soil curves (shear modulus and damping ratio)

2.8 Conclusion and discussion

The prediction of surface ground motion is an important step in quantifying seismic hazards and understanding the damaging effects of strong earthquake motion. It is well-established that local site conditions significantly influence the amplitude-frequency content and duration of bedrock earthquake motions. The primary challenge in evaluating these impacts consists in determining representative and site-specific soil properties, evaluating the intensity of seismic shaking at reference site conditions, applying appropriate site effect proxies, and conducting numerical site response analyses. The latter is particularly relevant in cases where there are insufficient strong earthquake records, preferably simultaneous records on soft surficial soils and nearby rock outcrops, a common concern in regions of low to moderate seismicity. This paper addresses the four major components of the site response analysis, as outlined above, through a comprehensive review of an extensive list of references. The following are the key points of the review:

i) Site effects

Site effects can significantly impact incoming seismic waves and vary depending on the local geological and geotechnical conditions. The most frequent site effects are the resonance amplification, which occurs in a relatively uniform soft soil layer over bedrock with a sharp impedance contrast. This results in a single well-defined peak at the fundamental vibration period. Multiple peak amplification corresponds to the presence of distinct heterogeneous surficial layers, and broadband amplification develops when soil stiffness gradually increases with depth, generating a broad range of amplified frequencies rather than a single peak. On the other hand, topographic amplification is induced by the focusing effect of seismic waves in elevated features, such as hills and ridges, leading to increased wave amplitudes. Basin edge effects occur when seismic waves propagate in soft sediments with a gradually decreasing depth at the edges of sedimentary basins, resulting in an increasing amplitude to conserve energy. Similarly, the basin effect involves the trapping and reverberation of seismic waves within a concave rock basin filled with soft sediments,

amplifying ground motion and prolonging shaking. All these potential effects require attention during the evaluation of the seismic hazard for structural design and risk assessment.

ii) Soil Parameters

Soil parameters important for evaluating the seismic site response include the shear-wave velocity, density, shear modulus reduction, and damping ratio curves. They collectively help to determine how seismic waves are amplified or attenuated as they travel through the soil layers.

Among the existing field tests, the seismic cone penetration test (SCPT) or suspension logging yields highly accurate results for the shear-wave velocity (V_S). However, it is often costly and challenging to perform in gravelly soil. Non-invasive geophysical methods, on the other hand, are more applicable in various soil conditions and can provide a broader range of V_S profiles. The setback is that to ensure accuracy, they must be validated against results from at least one invasive investigation at similar/nearby sites. In addition, empirical correlations developed between different measured parameters from SCPT can be used in combination with more numerous CPT results, when they are readily available for the study area.

Shear modulus and damping ratio curves are critical for characterizing the nonlinear behavior of soil during earthquake motions. They define how the soil stiffness (shear modulus) and energy dissipation (damping ratio) vary with strain levels. These parameters are essential for realistic seismic site response analyses, as they directly influence ground motion amplification and deformation. These curves are obtained through laboratory tests such as resonant column tests, cyclic triaxial tests, or cyclic direct simple shear tests, tailored to the specific application and soil type. The factors influencing these parameters must be carefully considered for both cohesive and cohesionless soils. For example, in cohesive soils, properties such as plasticity, water content, and over-consolidation ratio significantly impact the modulus reduction and damping behavior. In contrast, more critical factors in cohesionless soils are the particle size distribution, relative density, and adequate confining pressure. Proper evaluation of these factors ensures reliable selection or development of shear modulus and damping ratio curves for dynamic analyses.

iii) Site parameters

Site effects can be accounted for using simple amplification factors defined as the ratio of the response spectral accelerations at the ground surface to those at the bedrock level. The amplification factors are typically provided in national hazard maps. They are commonly applied in ground motion

models (GMMs) to correlate spectral accelerations at reference site conditions with earthquake parameters, such as magnitude and distance. GMMs rely on various proxies to represent site conditions, including the average shear-wave velocity over the top 30 meters (V_{s30}), soil fundamental period (T_0), soil thickness, and others. However, relying solely on a single proxy, such as V_{s30}, may introduce bias and/or uncertainty, as it may not fully capture the complex nature of the site effects. Incorporating multiple proxies can improve the reliability and accuracy of GMMs by providing a more comprehensive representation of the site conditions.

V_{S30} is undoubtedly the most frequently used proxy recommended in the building codes. A standard site classification scheme according to V_{S30} ranges includes site categories with similar amplification potential, such as hard rock, moderately fractured and weathered rock, stiff and dense soil, loose sandy soil, and soft clayey soil. For each site category, a respective amplification factor is provided. More recent building codes provide an amplification factor concerning V_{S30} as a continuous function. However, the V_{S30} concept was developed primarily based on studies in California, where soft surficial soils gradually transform into regolith and rock without a distinct impedance contrast. As such, it is not always correlated to the amplification observed in regions with high impedance contrast at the bedrock interface.

On the other hand, T_0 reflects the vibration period at which the seismic waves are expected to be most amplified. It is measured relatively easily using horizontal-to-vertical spectral ratio (HVSR) field measurements, which provide direct and practical insights into the site's resonance characteristics. However, since the ambient noise does not induce significant strain, HVSR cannot account for the nonlinear behavior of soil during strong ground motion, thus overestimating the actual amplification. Alternatively, T_0 can be calculated analytically if the soil thickness and in-depth shear-wave velocity are known. While the commonly used quarter-wavelength equation ($T = 4H/V_s$) is simple and widely applied, it appears to be limited to relatively shallow soil layers. To improve accuracy, other analytical approaches that account for complex soil stratification, varying velocity profiles, and impedance contrasts should be considered, offering more precise estimations of the fundamental site period depending on site-specific conditions.

iv) Seismic parameters

The selection of representative ground motions considers the seismic settings in the study area, the amplitude-frequency content, and the duration of the ground motions. To ensure consistency with the

seismic hazard at the site, the selected ground motions can be matched to the target response spectrum at periods of interest. Herein, a detailed summary of reference rock conditions, seismic hazard assessment, and the selection and scaling of earthquake motions is provided.

The impacts of the complex medium through which seismic waves propagate from the source fault can be divided into two parts: the source-to-site propagation part, commonly determined with the ground motions from semi-empirical ground motion prediction equations, GMPEs, and the amplification part, approximated with horizontal shear-waves propagating vertically from the reference rock conditions. For engineering purposes, this interface is commonly defined as V_{S30} = 760~800 m/s (B/C boundary) and measured using geophysical surveys or geotechnical investigations.

The seismic hazard at reference rock conditions is determined based on the seismic sources affecting the studied location, respective magnitude–frequency relationships, and applicable GMPEs. Probabilistic seismic hazard analysis yields the uniform hazard spectrum (UHS) with spectral acceleration (Sa) as the common ground motion output having the same probability of exceedance. In each period, UHS consists of the maximum possible Sa value generated from different earthquake events. A less conservative option is the conditional mean response spectrum (CMS) and conditional response spectrum (CS), which consider the correlations between Sa at different periods.

To evaluate the potential amplification with numerical analyses, a suite of at least seven acceleration representative time histories is commonly recommended. When the number of strong earthquake records collected is not sufficient, synthetic or ground motions from other regions with similar seismotectonic settings (magnitude, fault rupture mechanisms, source-to-site distance, and reference site conditions) may be used. In terms of the amplitude-frequency content, time histories are typically scaled to match the hazard spectrum at periods of interest in the time domain. Frequency-matching techniques can reproduce spectral accelerations across all periods; however, it would be highly unlikely to expect a single earthquake event to reach the maximum Sa values of the UHS.

v) Numerical modelling

Several methods for predicting the site response were considered. The simple site amplification factors recommended in building codes are commonly adjusted in relation to the bedrock interface or according to the local V_{S30} value. The standard spectral ratio method is based on at least two ground motions recorded on the soil surface and a nearby rock outcrop. It compares the response spectral

accelerations of both records and provides a more realistic estimation of the potential site amplification in that area. The soil dynamic response can also be simulated numerically in 1D, 2D, or 3D, adopting linear, equivalent linear, or nonlinear approaches. In 1D analysis, the horizontal seismic shear waves are assumed to propagate vertically through the infinite horizontal soil layers, making it suitable for sites with simple stratigraphy. For more complex soil conditions or irregular geometries, 2D and 3D site response analyses are preferred, as they account for lateral variations and interactions. The linear analysis assumes that soil behavior can be modeled as a linear elastic material with a constant minimum damping ratio and maximum shear modulus assigned to each soil unit. In this way, it simplifies the analysis at the expense of soil nonlinearity. The equivalent linear analysis approximates nonlinearity iteratively by assigning updated linear properties to each layer at the beginning of each step based on the shear modulus and damping ratio curves, as well as the adequate strain levels attained. In contrast, nonlinear analysis directly integrates the equation of motion in the time domain, utilizing stress-strain relationships to calculate soil properties dynamically at each time step. Nonlinear analysis is most accurate, as it fully considers the total nonlinearity of soil under earthquake loading and is particularly suitable for high-strain conditions. However, the challenge is getting appropriate nonlinear curves for the soil units in the study area that reliably capture the actual response during intense earthquake shaking.

CHAPTER 3

ARTICLE 2: EFFECTS OF COMPLEX SURFICIAL GEOLOGY ON SEISMIC AMPLIFICATION IN QUEBEC, CANADA

Authors

A S M Fahad Hossain, Mohammad Salsabili, Ali Saeidi, Miroslav Nastev, and Juliana Ruiz Suescun

Author contributions

A S M Fahad Hossain: Conceptualization, Data curation, Formal analysis, Resources, Writing original draft, Writing review & editing. Ali Saeidi: Supervision, Methodology, Resources. Miroslav Nastev: Supervision, Writing – review & editing. Mohammad Salsabili: Writing – review & editing.

Status

Published in Geosciences on 24 November 2025 (Hossain, A. S. M. F., Salsabili, M., Saeidi, A., Nastev, M., & Suescun, J. R. (2025). Effects of complex surficial geology on seismic amplification in Quebec, Canada. Georisk: Assessment and Management of Risk for Engineered Systems and Geohazards, 1–21. https://doi.org/10.1080/17499518.2025.2591757)

Declaration of competing interest

The authors declare the following financial interests/personal relationships, which may be considered potential competing interests: Ali Saeidi reports that financial support was provided by the Natural Sciences and Engineering Research Council of Canada and Hydro-Québec (CRDPJ 521771-17). Ali Saeidi reports financial support was provided by Natural Sciences and Engineering Research Council of Canada, Hydro-Quebec, Geostack, Rocscience and City of Saguenay (ALLRP 590081-23). If there are other authors, they declare that they have no known competing financial interests or personal relationships that could have appeared to influence the work reported in this paper.

Résumé

Les conditions géologiques et géotechniques locales jouent un rôle essentiel dans la modification de l'intensité et du contenu fréquentiel des mouvements sismiques du sol. Les codes sismiques utilisent souvent un facteur d'amplification (AF) pour ajuster le spectre de réponse au rocher en fonction de paramètres du sous-sol reflétant les conditions de site locales ; toutefois, le recours à un seul paramètre, tel que V_{s30}, ou à des classes de site larges peut négliger la variabilité régionale et introduire des biais dans l'évaluation de l'aléa sismique. Dans cette étude, une analyse détaillée de la réponse sismique non linéaire a été réalisée sur 52 profils de sol de la région du Saguenay, au Québec (Canada), en utilisant six mouvements sismiques de l'Est du Canada mis à l'échelle selon cinq niveaux d'aléa du NBCC 2020. L'influence de la vitesse des ondes de cisaillement dans les sols et le rocher, de l'épaisseur totale du sol et des couches intermédiaires de till sur l'amplification non linéaire a été examinée. L'efficacité de différents proxys de site — V_{s30}, la vitesse moyenne des ondes de cisaillement V_s,avg, l'épaisseur du sol Hsoil et la période fondamentale du site T_0 — à représenter le comportement d'amplification a également été évaluée. Les résultats montrent que la vitesse des ondes de cisaillement, l'épaisseur du sol et la présence de couches de till influencent significativement la réponse de site ; le comportement non linéaire des sols réduit l'amplification aux niveaux élevés de secousses, en particulier pour les profils rigides et peu épais, tout en entraînant un décalage des périodes dominantes. Alors que V_{s30} représente efficacement la réponse aux périodes courtes à intermédiaires, T_0 s'avère plus pertinent pour caractériser l'amplification aux longues périodes. La comparaison avec le NBCC 2020 indique une surestimation fréquente de l'amplification et souligne la nécessité d'une microzonation sismique spécifique au site reposant sur des proxys de site optimaux.

3.1 Abstract

Local geological and geotechnical conditions play an important role in modifying the intensity and frequency content of seismic ground shaking. Seismic codes often use an amplification factor (AF) to adjust the rock-level response spectrum based on subsurface parameters that reflect local site conditions. However, using a single parameter such as V_{s30} or broad site classes may overlook regional variability, introducing bias in hazard assessments. In this study, we conducted a detailed nonlinear ground response analysis on 52 soil profiles from the Saguenay region of Quebec, Canada, using six eastern Canadian ground motions scaled to five NBCC 2020 hazard levels. We examined

how shear-wave velocity in soil and rock, total soil thickness, and intermediate till layers affect nonlinear amplification. We also evaluated the effectiveness of different site proxies—V_{s30}, average shear-wave velocity (V_{savg}), soil thickness (H_{soil}), and fundamental site period (T_0)—in capturing amplification behavior. Our results show that shear-wave velocity, soil thickness, and till layers significantly influence site response. Nonlinear soil behavior reduces amplification at high shaking levels, especially in stiff and shallow profiles, and shifts the predominant periods. While V_{s30} effectively captures short-to-medium period responses, T_0 better represents long-period amplification. A comparison with our findings reveals that NBCC 2020 often overestimates amplification and underscores the need for site-specific micro-zonation using optimal site proxies.

Keywords: Site amplification, Ground response analyses, average shear wave velocity, soil fundamental period.

3.2 Introduction

Local geological and geotechnical conditions play a critical role in altering seismic ground motion, affecting both its amplitude and frequency content. These significant short-distance spatial variations in the intensity of ground shaking can lead to associated structural damage, as exemplified by Goto & Morikawa, (2012). Since the 1985 M8.0 Mexico City earthquake, a classic example of various local site effects, its investigation has become an essential subject of research, as stated by Seed et al. (1988) and Stone et al. (1987). To support risk reduction, urban planning, and building code development, local site effects must be thoroughly analyzed and mapped, with seismic micro-zonation serving as a fundamental tool in this process (Falcone et al., 2020). Efforts have been made to simplify the quantification of seismic site effects and approximate respective amplitude- and frequency-dependent site amplifications (Hossain et al. 2025). Site effects are generally accounted for through the amplification factor (AF), defined as the ratio between the response spectral accelerations at the ground surface and at reference rock spectral accelerations (Raja et al., 2025; Harmon et al., 2019 and Hashash et al., 2018). Building on these principles, recent contributions by Ansal (2025); Pagliaroli (2018) highlight probabilistic site response analyses, subsoil modeling, and interdisciplinary zoning approaches as key components of modern seismic microzonation.

Various geotechnical and geological parameters, such as the shear wave velocity of soil and rock, and the total thickness of the soil deposit, contribute to local site effects. The change in soil layer thickness and shear wave velocity strongly influences the fundamental vibration period of the soil,

thereby affecting amplification and its dominant period (Hossain et al., 2023, 2025; Mercado et al., 2023; Ghofrani & Atkinson, 2014). To derive site proxies representing the amplification factor of a region these geotechnical and geological parameters are often used as demonstrated by Rosset et al., (2025), Nikellis et al., (2018) and Stambouli et al., (2017). V_{s30}, the time-average shear-wave velocity of the top 30 meters, was first introduced by Borcherdt (1970), emerged as the standard site parameter and a widely adopted proxy for local site response, gaining global recognition. In the National Building Code of Canada 2020 (NBCC 2020), regionalized AFs were implemented through NGA-East and NGA-West Ground Motion Models (GMMs) (Bozorgnia et al., 2014; Goulet et al., 2017) and used to generate Canadian seismic hazard maps (Kolaj et al., 2019; Petersen et al., 2024). V_{s30}'s effectiveness as a site parameter for central and eastern North America has been questioned due to its inability to account for site-specific resonance effects, which can be significant depending on the deposit depths and average shear wave velocity, particularly in regions with heterogeneous geology (Hossain et al., 2024; Harmon et al., 2019; Hashash et al., 2018; Hassani & Atkinson, 2016). Consequently, there is a growing interest in using complementary site amplification proxies, such as the fundamental site period (T_0), the predominant vibration period at strong motion, the average shear-wave velocity of soil (V_{savg}), or the sediment thickness (H_{Soil}) (Hosseinpour et al., 2024; Zhu et al., 2020; Nastev et al., 2016 and Luzi et al., 2011).

To address the limitations of V_{s30}-based site amplification and to develop a detailed site amplification micro-zonation map, we performed nonlinear site response analyses on 52 geotechnical profiles from the Saguenay region, part of the Charlevoix-Kamouraska seismic zone in eastern Canada, an area exposed to earthquake magnitude of up to 7 (Earthquakes Canada). The 1988 M5.9 Saguenay earthquake remains the largest recorded in Eastern North America in the past 56 years. We performed 1,560 1D nonlinear simulations in DEEPSOIL, applying six eastern Canadian ground motions scaled to five NBCC 2020 hazard levels (NBCC 2020). The geometric mean amplification from the six ground motions at each hazard level was considered as the final amplification factor for each profile. First, we examined how bedrock shear wave velocity, soil thickness, and intermediate till layers affect amplification. Then, we evaluated the performance of site proxies—V_{s30}, V_{savg}, H_{soil}, and T_0—in capturing site response. Our results are compared against NBCC 2020 amplification factors and provide a solid foundation for developing a region-specific amplification micro-zonation map.

3.3 Geology of Saguenay

The City of Saguenay, located in southern Québec about 200 km north of Québec City, has a population of 147,100 and serves as a regional hub for commerce and administration (Foulon et al., 2018). The area, characterized by a flat-bottomed valley surrounded by hills, is located within the seismically active Saguenay graben and affected by the Charlevoix-Kamouraska seismic zone. The strong earthquake records include the 1663 M7+ and 1988 M5.9 earthquakes (Salsabili et al., 2021a). The bedrock primarily consists of Precambrian rocks from the Grenville province cropping out in the highlands, whereas postglacial and glacial sediments cover the lowlands. The Quaternary succession of deposits is from bottom to top: glacial deposit (till), covered by glaciofluvial sediments (gravel), fine glaciomarine clays and silts (clay), with coarse deltaic and alluvial sediments (sand) on top. The relatively compact up to 10 m thick glacial till at the base is a transitional unit between the stiff bedrock and the soft post-glacial sediments, highlighting the region's complex geological history. Figure 21 provides a simplified illustration of the surficial geology in the Saguenay region.

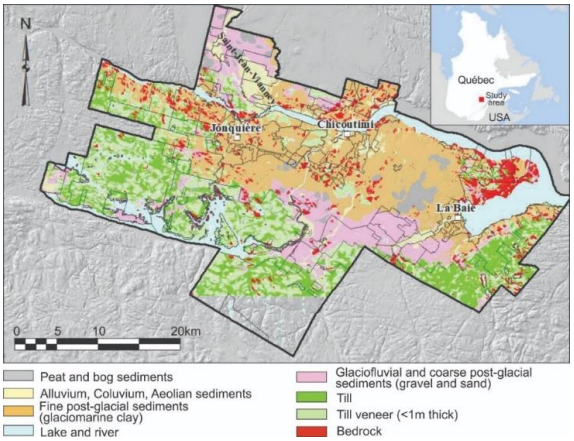

Figure 21. Simplified surficial geology in the Saguenay region (modified from CERM-PACES, 2013; Salsabili et al. 2021b).

3.4 Materials and methods

3.4.1 Soil Model and Geotechnical Properties

A set of 52 characteristic 1D soil profiles was selected for numerical analyses considering the lateral and vertical presence of the four main surficial units (till, gravel, clay and sand). Figure 22a is a map of the thickness of surface deposits, including the cross sections shown in Figure 22b. As can be seen, two relatively deep basins, filled with soft sediments, are located in the northwestern and southeastern parts of the study area, coinciding with the watersheds of two tributaries of the Saguenay River. The cross-sections from which about 10 to 15 soil profiles were selected are shown

in Figure 22b. The 52 selected 1D soil profiles are shown in Figure 22c. In addition, representative shear-wave velocity, density, shear modulus reduction, and damping ratio curves were assigned to each unit as shown in Table 1. The shear wave velocity was calculated using the mentioned empirical correlation, which was developed using 991 CPTu-V_s measurements at 40 sites by Salsabili et al., (2021b, 2022, 2023). The nonlinear curve was selected from a similar site in the Quebec region. The bedrock in the simulations was considered as an elastic half-space with its shear-wave velocity and density as shown in Table 7, and the input ground motions were assigned at the rock layer.

Table 7. Geotechnical and dynamic properties of soil and rock, and associated bibliographical reference. Data indicated with `*` are from studies in other regions.

	Unit Weight (kN/m^3)	Shear-wave Velocity vs. Depth (m/s)	Shear Modulus Reduction and Damping Ratio curves
Clay	18.7 (Sanou et al., 2022)	$V_s = 114.5 + 9.4 \times D^{0.76}$ (Salsabili et al., 2023)	(Abdellaziz et al., 2023)
Sand	17.5 (Sanou et al., 2022)	$V_s = 144.9 + 2.55 \times D$ (Salsabili et al., 2023)	(EPRI, 1993)*
Gravel	18.3 (Rollins et al., 1998)*	$V_s = 46.861 + 61.55 \times D^{0.5}$ (Salsabili et al., 2023)	(Seed et al., 1986)*
Till	21.0 (Urgeles et al., 2002)	$V_{Still} = 582$, $\sigma=\pm174$ (Motazedian et al., 2011)*	Hydro Quebec (internal communication)
Rock	28.0 (Saeidi et al., 2021)	$V_{Srock} = 1875$, $\sigma=\pm781$ (Ladak et al., 2021) *	N/A

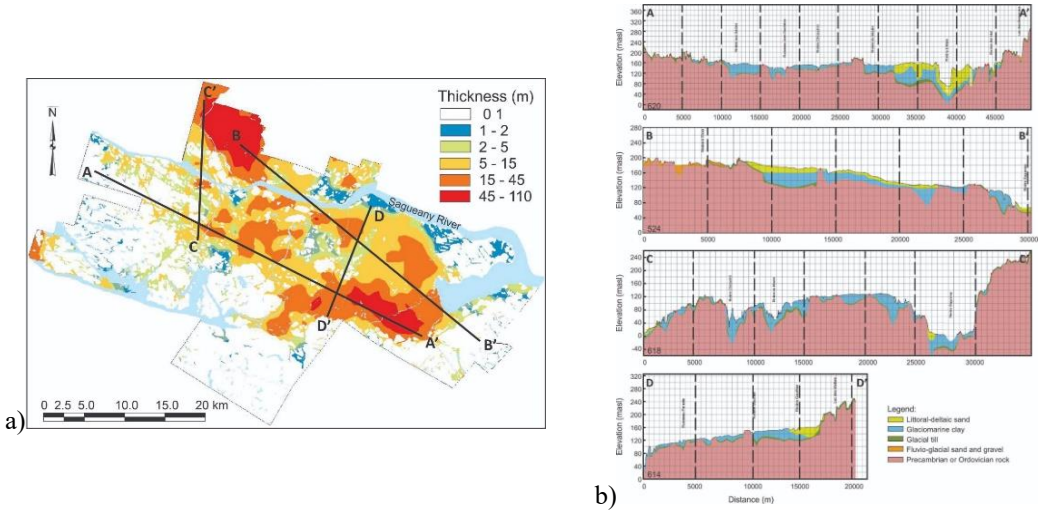

c)

M1	M2	M3	M4	M5	M6	M7	M8	M9	M10	M11	M12	M13	M14	M15	M16	M17	M18
8m	10m	30m	10m	2m	4m	16m	4m	14m	30m	4m	10m	24m	6m	14m	16m	6m	80m
Rock	Rock	Rock	2m	Rock	Rock	Rock	4m	4m	4m	4m	4m	48m	22m	6m	66m	6m	20m
			Rock				Rock	Rock	Rock	Rock	Rock	Rock	4m	2m	10m	Rock	6m
													Rock	Rock	Rock		Rock

M19	M20	M21	M22	M23	M24	M25	M26	M27	M28	M29	M30	M31	M32	M33	M34	M35	M36
4m	16m	28m	4m	8m	12m	4m	30m	26m	12m	86m	106m	12m	6m	6m	20m	6m	8m
Rock	Rock	Rock	2m	4m	4m	14m	3m	8m	32m	2m	2m	40m	14m	Rock	Rock	2m	2m
			Rock	Rock	Rock	Rock	Rock	4m	4m	Rock	Rock	4m	Rock			Rock	Rock
								Rock	Rock			Rock					

M37	M38	M39	M40	M41	M42	M43	M44	M45	M46	M47	M48	M49	M50	M51	M52	
10m	16m	22m	48m	2m	3m	5m	8m	10m	20m	22m	24m	150m	120m	80m	80m	Gravel
2m	2m	2m	2m	Rock	Rock	Rock	Rock	Rock	18m	23m	36m	Rock	15m	70m	40m	Sand
Rock	Rock	Rock	Rock						Rock	Rock	Rock		Rock	Rock	15m	Clay
															Rock	Till
																Rock

Figure 22. Typical cross sections in the Saguenay region used for selection of soil profiles in the site response analyses: a) thickness of surficial deposits, b) Cross-sections depicted in Figure 2a (Salsabili et al., 2021b and CERM-PACES, 2013) and c) selected 52 1D soil profiles for numerical analyses.

3.4.2 Ground motion data

For this study, two seismic scenarios were considered with moment magnitudes M6 and M7 and average source-to-site distances of about 40 to 60 km. They represent the seismic hazard for the Saguenay region with probabilities of exceedance of approximately 1/1000 and 1/2500 years, respectively (https://www.seismotoolbox.ca/index.html). Accordingly, four synthetic ground motions were selected (Atkinson, 2009) in addition to two real accelerograms from the 2010 M5.1 Val des Bois earthquake, recorded at an epicentral distance of 22 km, and the 1988 M5.9 Saguenay earthquake, recorded in downtown Saguenay with an epicentral distance of 35 km. Original acceleration time histories for these ground motions are shown in Figure 23a with NBCC 2020 response spectra for the Saguenay region and five different probabilities of exceedance assumed as

target spectra (Figure 23b). The ground motions were then scaled to match approximately the NBCC 2020 spectra using the SeismoMatch program (SeismoSoft, 2022). As noted by Pagliaroli & Lanzo, (2008), scaling factors above 4 are inappropriate; most motions were well scaled using spectral matching, except Val-des-Bois, which was limited by its low magnitude.

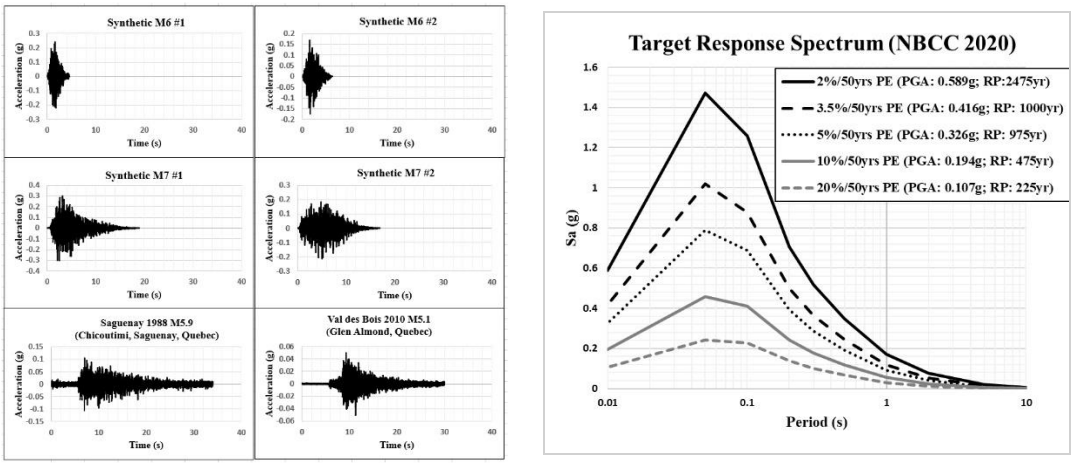

Figure 23. a) Acceleration time histories of the unscaled input ground motions, and b) NBCC 2020 target response spectra for selected seismic hazard levels with Peak Ground Acceleration (PGA) values and return period (RP).

3.4.3 Ground response analysis

To assess the site amplification characteristics for the geological and geotechnical settings of the Saguenay region, 1D analyses were run, assigning site-specific soil properties to 52 typical soil profiles exposed to a seismic input consisting of a suite of 6 time-histories scaled to NBCC 2020 response spectra for five return periods. Nonlinear analyses were carried out in 1D for 1560 site responses to incident shear-waves in the time domain using implicit integration of the equation of motion. In the DEEPSOIL framework, the pressure-dependent modified Konder–Zelasko hyperbolic model was used to represent the modulus reduction and the respective shear stress backbone curves, as it better captures the nonlinear soil behavior due to some additional parameters as suggested by the program manual. The program handbook provides a brief description of each approach for calculating the response of single-degree-of-freedom systems and solving the dynamic equilibrium equation.

Seismic amplification AF was defined as the ratio between the computed response spectral accelerations on the soil surface, Sa(T)s, and the input response accelerations at the bedrock level, Sa(T)b. The final amplification values for each soil profile were calculated from the geometric mean

of the amplification values obtained from the six ground motions. Figure 24 illustrates the simplified flowchart of the methodology. The comparison of the DEEPSOIL simulation with another software is demonstrated in Appendix A.

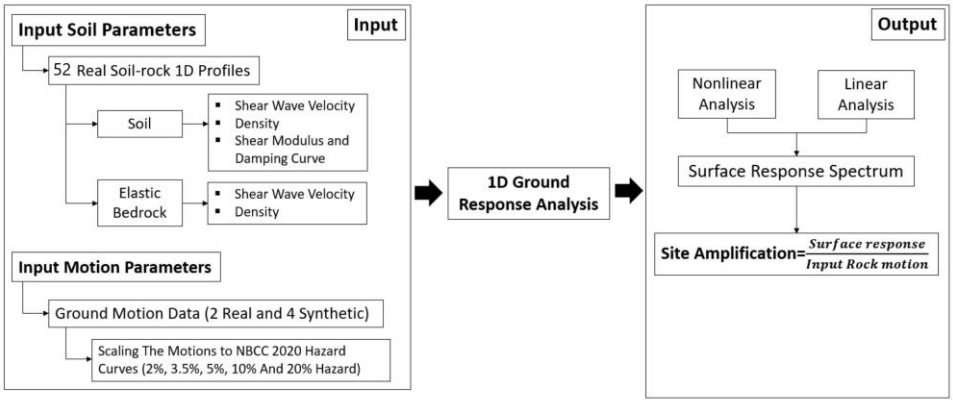

Figure 24. Flowchart of the ground response analysis in DEEPSOIL.

3.5 Impacts of different geological and geotechnical parameters

In this section, the impacts of geological and geotechnical soil properties, such as the thickness of soil units, soil and rock shear-wave velocities, and the presence of a till layer, on the seismic site response are examined by assessing surficial amplification. The nonlinear behavior of soil under earthquake loading is characterized through hysteretic stress-strain behavior. Since the focus was on quantifying the importance of individual parameters, site-specific soil profiles were utilized for this exercise.

3.5.1 Thickness and shear-wave velocity of soils

We compared the surface amplification for five uniform soil profiles with thicknesses of 10, 20, 30, 50, and 100 meters, each profile having an average shear wave velocity of 200 m/s. Figure 25 illustrates the surface acceleration and the amplification for the mentioned soil model. With the increase in soil deposit thickness, the surface acceleration decreases. As expected, it can be observed that the predominant amplification period shifts gradually towards longer periods with an increase in soil thickness, as the fundamental period of the soil is higher for thicker soils.

Similarly, a 30 m soil profile with varying average shear-wave velocities: 150, 200, and 250 m/s was considered, and the surface acceleration and amplification values are plotted in Figure 26. The spectral acceleration is higher for soil columns with higher average V_s up to 1 second, after which the trend is reversed. Additionally, increasing the average shear-wave velocity of soil columns decreases the predominant vibration period, which is inversely proportional to the soil column's thickness, as

the soil's fundamental period is lower for soil with higher shear-wave velocity. The rate of increase of the predominant period was observed to be 0.33 seconds for a 10 m increment in soil thickness and 0.30 seconds for a 50 m/s decrement. As the shear-wave velocity is a depth-dependent parameter, the soil thickness is more important.

As stated earlier, the bedrock in the simulations was considered as an elastic half-space with dynamic properties. To examine the effect of rock shear-wave velocity on the soil response results for a soil column with a thickness of 30m, the average shear-wave velocity of 250 m/s was compared for two rock shear-wave velocities, 760 and 2500 m/s. The results are shown in Figure 27. Comparatively, amplification, the maximum effects are observed at the predominant vibration period of the soil column, $T_0 \approx 0.6$-0.7 s, with approximately 50% higher amplification in the case of $V_{srock} = 2500$ m/s, which the comparatively higher impedance contrast can explain. The black bold line in Figure 27 is the amplification line.

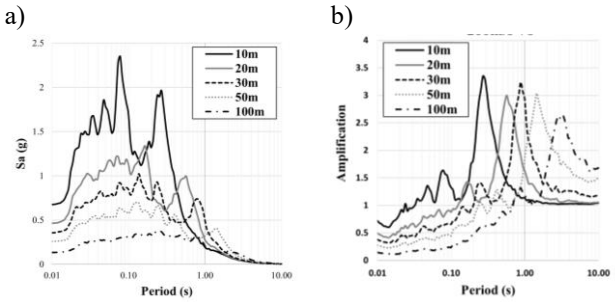

Figure 25. Dynamic response of soil columns with a shear wave velocity of 200m/s and different thicknesses of 10, 20, 30, 50, and 100 m: a) Spectral acceleration at the surface (in g), b) Amplification factor at the surface.

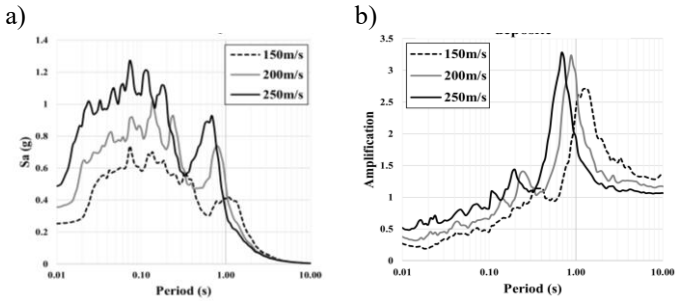

Figure 26. Dynamic response of a 30 m soil column with different shear wave velocities of 150, 200, and 250 m/s: a) Spectral acceleration at the surface (in g), b) Amplification factor at the surface.

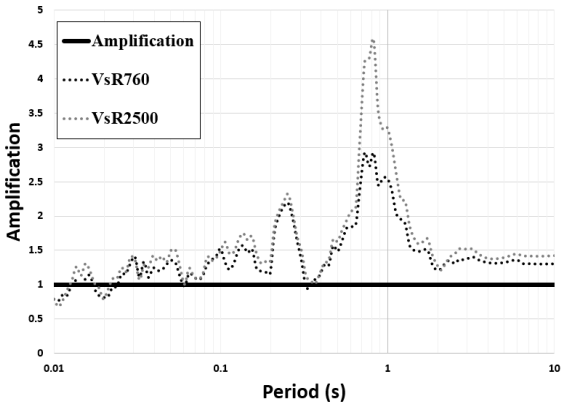

Figure 27. Amplification factor at the surface for rock shear-wave velocity of 760 and 2500 m/s.

3.5.2 Effect of glacial till on surficial amplification

A till layer is a heterogeneous mixture of clay, silt, sand, gravel, and boulders, directly deposited by glacial ice or meltwater after the peak of the last glaciation. It can influence seismic wave propagation and the site response to earthquakes. In this study, we examined the effect of the till layer on surficial amplification due to earthquake motion. A 30 m clay deposit overlying till layers of varying thicknesses (0, 5, 10, 20, and 30 m) was considered. For the till, three shear wave velocities (V_s) 309, 400, and 580 m/s were selected from the reference of Hydroquebec, Nastev et al., (2016), and Motazedian et al., (2011) respectively. As mentioned before, six earthquake motions were scaled to the NBCC 2% probability of exceedance in 50 years. The geometric mean of the amplification values from the six surface responses was considered for each case.

Figure 28 presents the surficial amplification values for the 30 m clay layer over different till thicknesses. It is observed that for till with V_s = 309 m/s, increasing the thickness of the till layer beneath the clay reduces the amplification and shifts the dominant vibration period to a longer value. This effect becomes less pronounced for till with V_s = 400 m/s. When the till V_s reaches 582 m/s, the maximum amplification and dominant period changes become almost negligible, indicating that the dynamic response of the soil profile becomes increasingly stable as the underlying till approaches bedrock-like stiffness. Figure 29 illustrates the effect of the shear wave velocity of the glacial till layer on the maximum amplification, indicating that with increasing till thickness, the maximum amplification decreases. This effect is more pronounced for till with lower shear wave velocity (V_s).

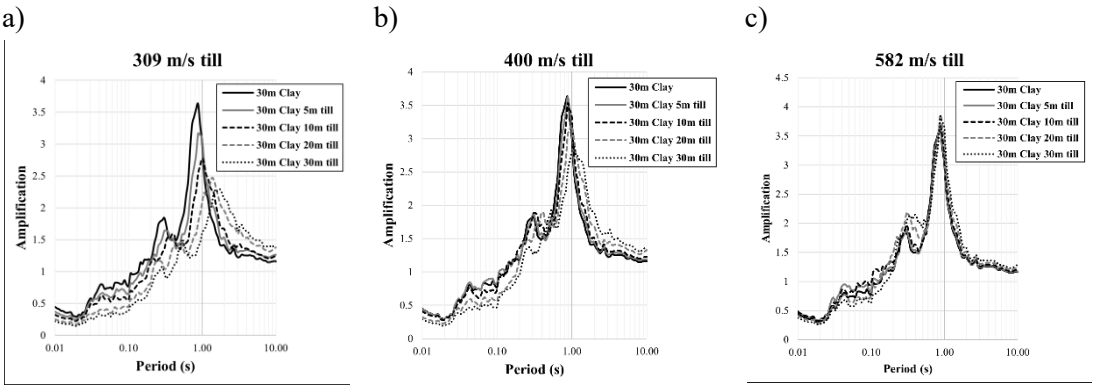

Figure 28. Effect of glacial till layer on surficial amplification for a 30m clay deposit over a till layer with shear wave velocity of a) 309m/s, b) 400m/s, c) 582m/s

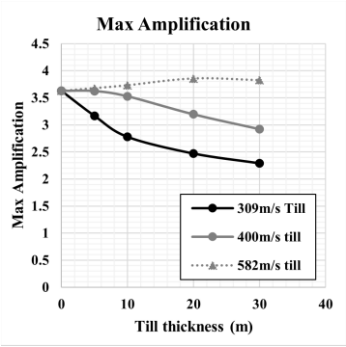

Figure 29 Effect of shear wave velocity of the glacial till layer on maximum amplification

3.5.3 Nonlinear soil behavior

We examined the effect of soil nonlinear behavior on site amplification due to earthquake ground motion. Maximum amplification values were calculated for all 52 soil profiles under five earthquake hazard levels, corresponding to PGA values of 0.59 g, 0.41 g, 0.32 g, 0.19 g, and 0.10 g, respectively. As previously mentioned, each of the six ground motions was scaled to match the five hazard levels defined by NBCC 2020, and the geometric mean amplification was computed based on the surface responses from the six motions for each hazard level. A scatter plot was created with PGA values on the x-axis and maximum amplification on the y-axis. The legend shows that different colors represent various natural periods and V_{s30} values of the 52 soil profiles, as illustrated in Figure 30.

As seen in Figure 30a, the maximum amplification values exhibit a decreasing trend as the PGA increases. This pattern reflects the influence of nonlinear soil behavior during strong ground motions. Specifically, as seismic shaking intensifies, the induced strain within the soil increases, resulting in a corresponding increase in the soil's damping ratio, which effectively reduces its capacity to amplify seismic waves. Consequently, the maximum amplification values tend to diminish at higher PGA levels. Furthermore, the dataset reveals that this nonlinear attenuation effect is more pronounced in

soil profiles with higher V_{s30} values (i.e., stiffer or denser soils). These stiffer profiles tend to show a steeper reduction in amplification with increasing PGA.

Figure 30b illustrates the maximum amplification values at different PGA levels for soil columns with varying fundamental periods (T_0). The T_0 was calculated using the constant distribution of shear wave velocity method ($4H/V_{savg}$). The maximum amplification generally decreases as PGA increases, indicating the influence of nonlinear soil behavior. However, in this case, the effect of nonlinearity is more prominent in soil columns with lower T_0 values, which typically correspond to shallower or thinner soil layers. These soils exhibit greater sensitivity to increasing ground motion intensity, resulting in a more substantial reduction in amplification. In contrast, soil columns with higher T_0 values, associated with deeper or thicker profiles, show comparatively less reduction in amplification, indicating weaker nonlinear effects.

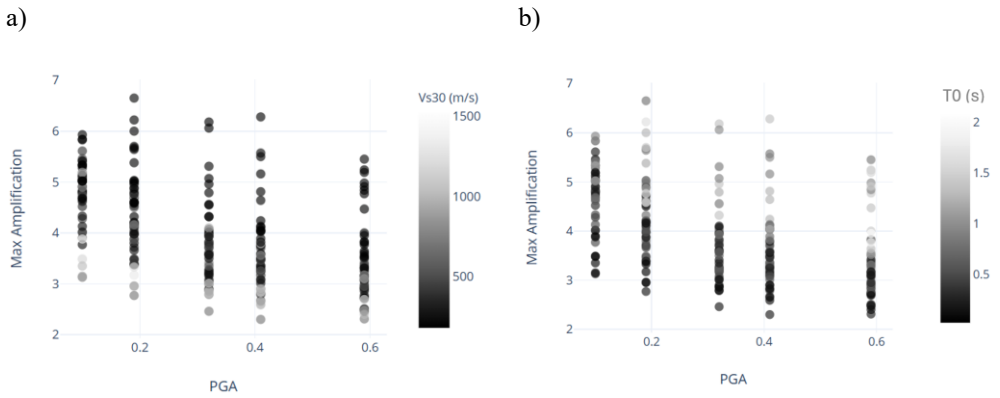

Figure 30 Maximum amplification values across five hazard levels, corresponding to five PGA values for soil profiles a) with different V_{s30} values and b) with different T_0 values

To describe the non-linear amplification, a 30m clayey soil layer over a 3m thick glacial till on top of rock is considered. The linear and non-linear amplification for hazards with probabilities of exceedance of 2, 5, 10, and 20% in 50 years are shown in Figure 31. As demonstrated, the linear amplification for various probabilities of exceedance shows no significant differences, as the maximum stiffness and minimum damping are used in the analysis at every strain level, as shown in Figure 31a. However, it becomes evident in the case of nonlinear analyses, depicted in Figure 31b, that for smaller probabilities of exceedance (higher input accelerations), the amplification decreases. This is a consequence of the high input motion amplitudes, which generate higher strains and, in turn, contribute to reduced stiffness and increased damping.

As more motion energy is absorbed throughout the oscillations due to increased damping, the response amplitudes and the amplification decrease. At the same time, the nonlinear soil response is accompanied by a gradual shift of the dominant vibration period towards longer period ranges due to higher motion intensities, which lowers the soil stiffness and lengthens the fundamental period of the vibrating soil column. At the 20%/50yrs probability of exceedance, the maximum observed amplification is 5.3. The maximum amplifications are lower, at 5.0, 4.1, and 3.9, when compared to 10%, 5%, and 2%/50-year probability of exceedance, showing decreases of 6%, 24%, and 28%, respectively. On the other hand, at the 20%/50yrs hazard level, the predominant vibration period is 0.64 s. In comparison, the probabilities of exceedance is 0.68 s, 0.73 s, and 0.82 s for the probabilities of 10%, 5%, and 2%/50 years, respectively, reflecting increases of 6%, 14%, and 28%.

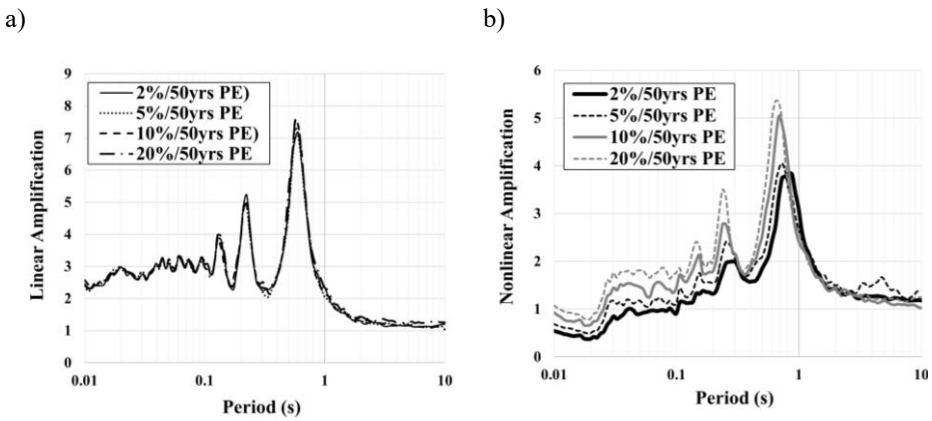

Figure 31 Amplification for a 30m soil column over a 3m glacial till on rock for 2%, 5%, 10% and 20% hazards a) Linear amplifications b) Nonlinear amplifications.

3.6. Amplification based on site response proxies

The effectiveness of different site response parameters in predicting seismic site response was assessed through the shear-wave velocity of the top 30 meters (V_{s30}), the fundamental vibration period (T_0), the time-averaged shear-wave velocity of the soil column (V_{savg}), and the thickness of the soil column (H_{soil}). The amplification of the ground motion is calculated as a function of each of these site response parameters for input PGA, which corresponds to the probability of exceedance of 10%/50 years and 2%/50 years, and for two spectral periods of 0.2 s and 1.0 s of interest for seismic risk assessment, as they approximately correspond to vibration periods of low- and high-rise buildings. At the end of the article, a comparison is given between the simulated amplification and the amplification predicted in NBCC 2020.

3.6.1 Shear-wave velocity of top 30 m (V_{s30})

V_{s30} is commonly used as a site response parameter due to its correspondence to the ratio of shear stress to shear strain, which measures the stiffness of surficial sediments and is recognized for its correlation with site response amplification. Figure 32 shows the nonlinear amplification at different vibration periods: 0.2 s, 0.5 s, 1.0 s, and 5.0 s for both considered seismic hazard levels, 2%/50 years Probability of Exceedance (PE) and 10%/50 years PE.

At short to medium vibration periods, amplification increased with rising V_{s30} values up to a threshold value, after which it began to decrease. At a period of 0.2 seconds, the maximum amplification value is approximately 3.1 and 3.6, at V_{s30} values of around 600 m/s and 500 m/s, and hazard levels of 2%/50 years and 10%/50 years probability of exceedance (PE), respectively. The amplification factor is close to 1 for V_{s30} values higher than 1300 m/s. At a vibration period of 0.5 seconds, amplification values of 3.2 and 4.2 were observed at a V_{s30} of 180 m/s for both hazard levels. After a V_{s30} value of approximately 926 m/s, amplification again approached 1. For 1.0 seconds, the maximum amplification values were 5.2 and 5.6 for the 2%/50 years and 10%/50 years hazard levels, respectively. Amplification decreased with increasing V_{s30} values up to around 500 m/s, beyond which it stabilized close to 1.

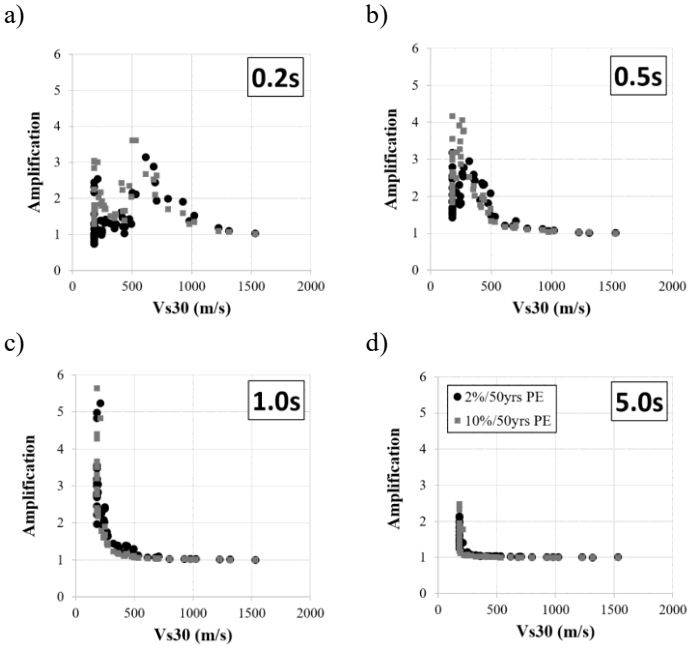

Figure 32 Nonlinear amplification as functions of V_{s30} for 2%/50yrs PE and 10%/50yrs PE: a) 0.2s, b) 0.5s, c) 1.0s, and d) 5.0s vibration period.

At a longer period of 5.0 seconds, amplification was only notable at significantly low V_{s30} values (approximately 180 m/s), with maximum amplification values of 2.5 and 2.3 for the 2%/50-year and 10%/50-year hazard levels, respectively. Beyond a V_{s30} of 190 m/s, the amplification dropped to nearly 1. Overall, the amplification trend suggests that V_{s30} is a reliable proxy for amplification at short to medium periods; however, its effectiveness diminishes at medium to long periods as shown by Derras et al., (2017). Notably, a very shallow till cover (2–4 m, $V_s \approx 582$ m/s) above bedrock yields V_{s30} values of ~1500 m/s.

3.6.2 Fundamental site period (T_0)

The fundamental site period (T_0) is increasingly used in conjunction with V_{s30} to characterize site amplification behavior, as it incorporates the soil column's thickness and the average shear wave velocity to approximate site-specific vibration response (Zhu et al., 2020 and Stambouli et al., 2017). Figure 33 presents the ground motion amplification as a function of T_0 for nonlinear simulations at vibration periods of 0.2 s, 0.5 s, 1.0 s, and 5.0 s for both seismic hazard levels: 2%/50 years and 10%/50 years probability of exceedance (PE). At short to medium vibration periods, amplification generally increases with rising T_0 values up to a peak, after which it begins to decrease. However, amplification increases again beyond a certain T_0 threshold at long vibration periods.

At 0.2 s, the maximum amplification values were approximately 3.14 and 3.6, corresponding to T_0 values of around 0.14 s and 0.19 s for the 2%/50yrs and 10%/50yrs hazard levels, respectively. Beyond these T_0 values, a declining trend in amplification was observed. At a vibration period of 0.5 s, amplification increased with T_0 up to 0.34 s and 0.43 s, reaching maximum values of 2.9 and 4.0 for the 2%/50yrs and 10%/50yrs hazard levels, respectively. Amplification decreased until $T_0 \approx 0.62$ s, followed by another increase, peaking at 3.6 and 4.2 at $T_0 \approx 1.57$ s for both hazard levels, before decreasing again. For the 1.0s period, amplification rose after $T_0 \approx 0.17$s, reaching peak values of 5.2 and 5.6 at $T_0 \approx 1.0$s for the 2%/50yrs and 10%/50yrs hazard levels, respectively, and then decreased.

At the longer period of 5.0 s, significant amplification occurred only at higher T_0 values, increasing gradually beyond $T_0 \approx 0.57$ s, with maximum amplification values of 2.5 and 2.3 for the 2%/50yrs and 10%/50yrs hazard levels, respectively. Overall, the amplification trend indicates that T_0 is a reliable proxy for capturing site response across all vibration periods, including long-period ground motions.

It is well known that resonance occurs when the system vibrations coincide with the fundamental period of a soil column, leading to high-amplitude oscillations (Ilhan et al., 2024). The vibration periods were divided by the fundamental period of all soil columns, and the respective linear amplification was correlated with each (vibration period / fundamental period) T/T_0 ratio as shown in Figure 34 (a). In each soil column, the highest response amplification to a Ricker wavelet pattern occurred approximately at the fundamental period T_0. Figure 34 (b) demonstrates the nonlinear amplification with the T/T0 ratios of the soil column, where it is shown that the peak amplification values shift from 1 towards longer values, representing the extension of the fundamental vibration of the soil column in earthquake motion. The dominant vibration period can be used as an alternative proxy for the site's fundamental period in cases of nonlinear amplification.

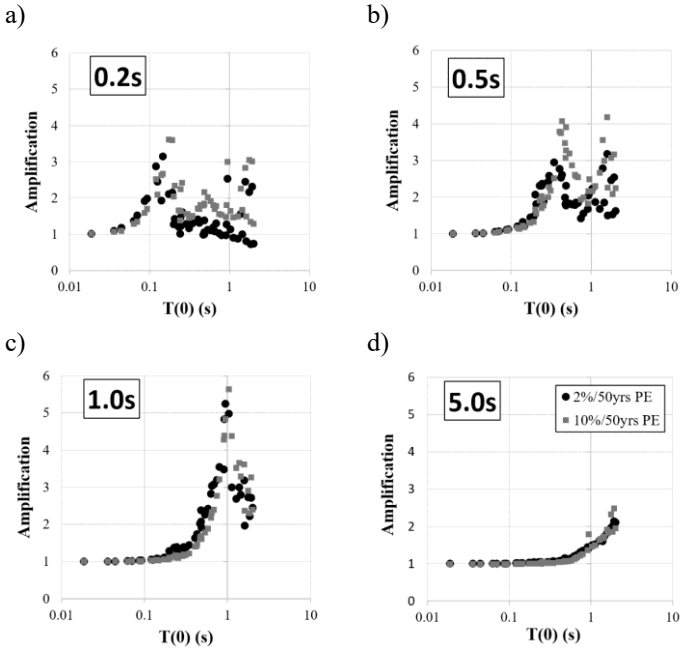

Figure 33. Nonlinear amplification as a function of fundamental vibration period (T_0) for 2%/50yrs PE and 10%/50yrs PE: a) 0.2s, b) 0.5s, c) 1.0s, and d) 5.0s vibration period.

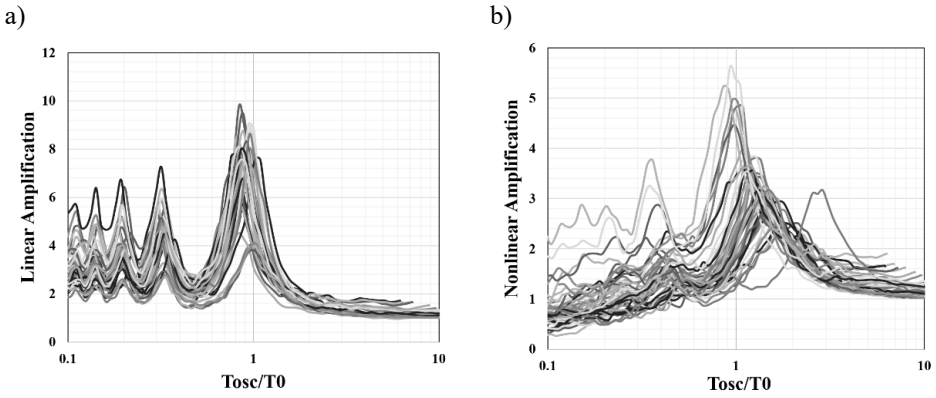

Figure 34. Amplification as a function of vibration period/ site fundamental period (T_{osc}/T_0) for 2%/50yrs PE motion for different soil profiles: a) Linear amplification and b) Nonlinear amplification

3.6.3 Soil thickness (H_{soil})

Soil column thickness (H_{soil}) is another important proxy for site amplification. In general, greater thickness corresponds to a higher fundamental site period and average shear wave velocity, while lower thickness values are typically associated with shorter fundamental periods and lower velocities. In this study, nonlinear amplification values were plotted as a function of soil column thickness for two seismic hazard levels: 2%/50 yrs and 10%/50 yrs probability of exceedance (PE) across vibration periods of 0.2 s, 0.5 s, 1.0 s, and 5.0 s, as shown in Figure 35.

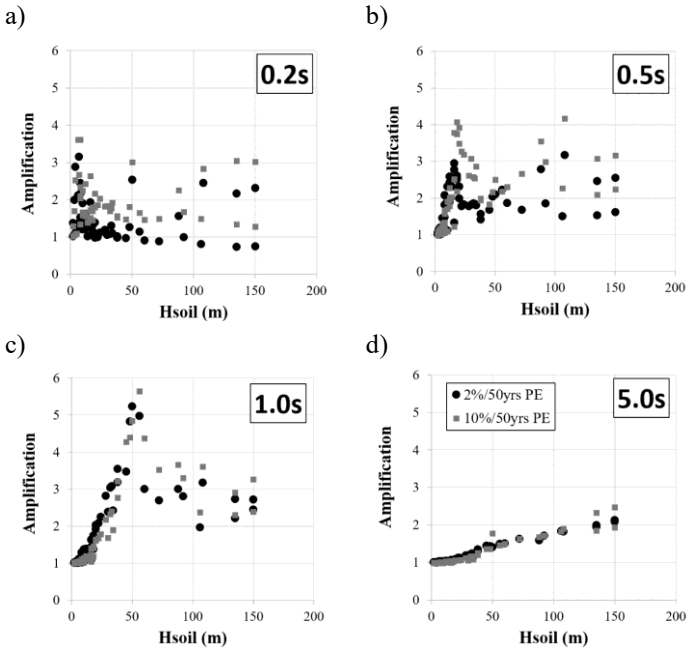

Figure 35. Nonlinear amplification as a function of soil column thickness H_{soil} for 2%/50yrs PE and 10%/50yrs PE: a) 0.2s, b) 0.5s, c) 1.0s, and d) 5.0s vibration period.

At short to medium periods (0.2 s and 0.5 s), amplification values appeared scattered across different soil thicknesses, indicating a weak relationship. However, at the medium period of 1.0 s, amplification increased with increasing soil thickness, reaching peak values of 5.2 and 5.6 for soil thicknesses of 50 m and 56 m under 2%/50yrs PE and 10%/50yrs PE motions, respectively, before decreasing again. Over the long period of 5.0 s, amplification values also increased with soil thickness, peaking at 2.1 and 2.5 for the highest thickness values considered under the two hazard levels. These observations suggest that soil thickness is a relatively poor proxy for site amplification at short to medium periods but becomes more reliable at medium to long periods.

3.6.4 Time-averaged soil shear-wave velocity (V_{Savg})

The last proxy parameter considered in this study is the time-averaged shear-wave velocity over the total thickness of the soil column (V_{Savg}), which indicates the overall stiffness of a soil model. Figure 36 presents the nonlinear amplification values as a function of V_{Savg} for input ground motions scaled to two seismic hazard levels: 2%/50 years and 10%/50 years probability of exceedance (PE): across vibration periods of 0.2 s, 0.5 s, 1.0 s, and 5.0 s.

The correlation between the site amplification and V_{savg} was weak across most of the vibration period. A positive trend was observed at the long period of 5.0 s, where amplification generally increases with V_{Savg}, reaching maximum values of 1.9 and 2.5 at 300 m/s for the 2%/50yrs and 10%/50 yrs hazard levels, respectively. For the shorter periods of 0.2 s, 0.5 s, and 1.0 s, the maximum amplification values were 3.1, 3.2, and 5.2 at V_{Savg} values of 192 m/s, 274 m/s, and 181 m/s under the 2%/50yrs PE level, and 3.6, 4.2, and 5.6 at 166 m/s, 274 m/s, and 216 m/s for the 10%/50yrs PE level. The above finding suggests that the proxy V_{savg} provides a minimal prediction of site amplification, except at longer periods, and represents an inadequate proxy for assessing site amplification.

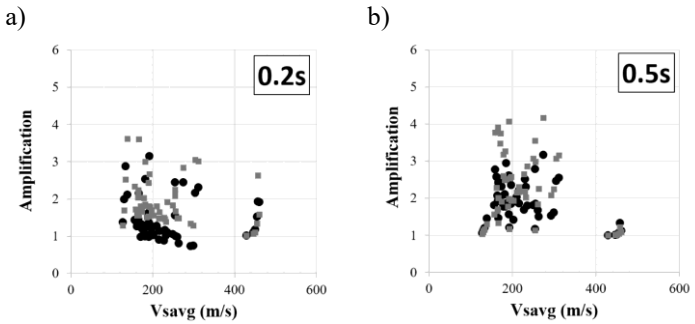

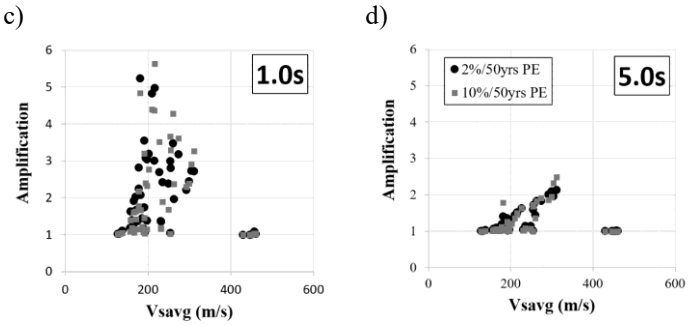

Figure 36. Nonlinear amplification as a function of time-averaged shear wave velocity (V_{Savg}) for 2%/50yrs PE and 10%/50yrs PE: a) 0.2s, b) 0.5s, c) 1.0s, and d) 5.0s vibration period.

3.6.5 Comparison with NBCC 2020

To verify the applicability of the obtained nonlinear amplification results from the comprehensive 1D ground response analysis, a comparison is made with the respective NBCC 2020 amplification factors obtained for four specific locations within the Saguenay study area. Four soil profiles, each characterized by its own V_{s30} and T_0 values corresponding to three NBCC site classes, were selected for this comparison. The design code amplification factors were calculated for each soil column using the seismic hazard calculator on the NBCC 2020 website, based on the ratio of the V_{s30} of the soil site and the Rock V_{s30} value for the specific locations (www.earthquakescanada.nrcan.gc.ca/hazard-alea/interpolat/nbc2020-cnb2020-en.php), as illustrated in Figure 37. Nonlinear analyses reveal peak amplification near the fundamental site period, indicating resonance effects that the NBCC 2020 broadband amplification factors do not capture. Notable differences were observed between NBCC 2020 and the present amplification values across all soil classes B, C, and D, particularly at short to medium periods (up to the predominant vibration period). Specifically, NBCC 2020 underestimates amplification for site classes B and D, while overestimating it for site class C.

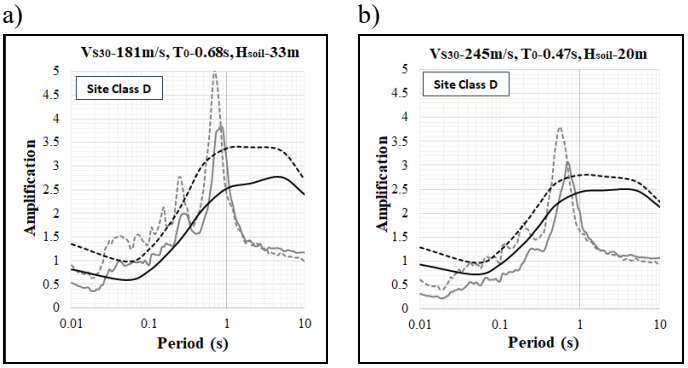

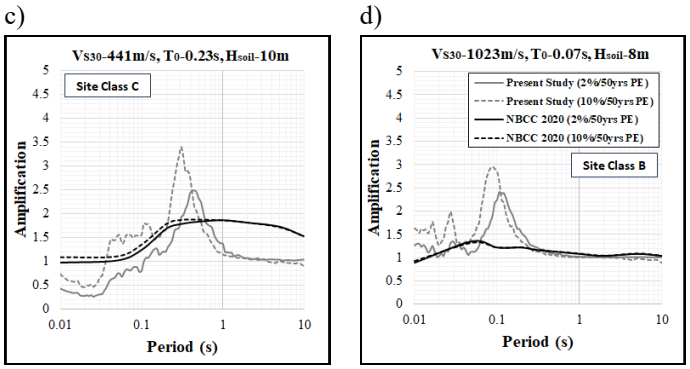

Figure 37. Comparison between amplifications from this study and NBCC 2020 amplification factors for four soil profiles in the Saguenay region with: a) V_{S30}=181m/s, T_0=0.68s, b) V_{S30}=245m/s, T_0=0.47s, c) V_{S30}=441m/s. T_0=0.23s and d) V_{S30}=1023m/s, T_0=0.07s

At medium to long periods, NBCC 2020 generally predicts higher amplification values for site classes C and D than those calculated in this study. In contrast, differences remain minimal for the stiffer soil profiles associated with site class B. It is important to note that NBCC amplification factors are derived from linear and equivalent-linear analyses, based on empirical correlations between amplification and Vs_{30}, which only considers the average shear-wave velocity in the upper 30 meters of soil. NBCC 2020 tends to underestimate amplification at short to medium periods and overestimate it at medium to long periods. Therefore, a more detailed amplification model incorporating additional site-specific parameters beyond V_{s30} is recommended to characterize site response more accurately.

3.7. Discussion

The following findings, specifically for the Saguenay Region, can be drawn from the numerical modeling of seismic site response conducted using DEEPSOIL software and the resulting data.

3.7.1 Impact of various geological and geotechnical properties on seismic site effects

The study highlights the significant impact that geological and geotechnical properties have on the seismic site effects. The Saguenay region has sediment thicknesses up to 150 m and average shear-wave velocities between 130 and 480 m/s. Both are decisive for the stiffness and fundamental period of the soil deposits, as well as for the amplification of vertically propagating horizontal seismic shear waves. Stiffer soils amplify the high-frequency content of the ground motions, whereas softer soils exhibit a response at longer periods, as demonstrated by Kramer (1996).

- The study confirms that increased soil thickness leads to longer fundamental periods. The predominant period increases by approximately 0.3 seconds per 10 meters of thickness.

Lower shear-wave velocities V_s resulted in longer vibration periods. A 50 m/s decrease in V_s led to a 0.3 s increase in the fundamental period.

- Introducing a glacial till layer beneath a 30 m clay deposit reduces surface amplification and shifts the predominant vibration period, particularly when the till has a lower shear wave velocity. This reduction in amplification and the increase in vibration period become more pronounced as the till thickness increases, especially for softer tills (V_s = 309 m/s). In contrast, tills with higher V_s (580 m/s) produce minimal changes in amplification and period, indicating a transition toward bedrock-like stability in the site response.
- High bedrock stiffness (V_s = 2500 m/s) results in up to 50% greater amplification at the dominant vibration period compared to softer rock (V_s = 760 m/s), due to a larger impedance contrast with the overlying soil.
- Nonlinear soil behavior plays a key role in reducing seismic amplification with increasing earthquake intensity. Analysis of 52 soil profiles under varying PGA levels showed a consistent decrease in maximum amplification as PGA increased, due to enhanced damping and reduced stiffness under stronger shaking. This effect was more significant in stiffer soils (higher V_{s30}) and profiles with lower fundamental periods (T_0), highlighting that shallower or denser soils exhibit more substantial nonlinear attenuation compared to deeper, softer profiles. Nonlinear analysis of a 30 m clayey soil layer over 3 m of glacial till revealed that as seismic intensity increases, amplification decreases due to strain-induced damping and stiffness reduction. Amplification factor decreases 28%, from 5.4 to the 20%/50yrs level, to 3.9 to the 2%/50yrs level. Concurrently, the dominant vibration period shifted from 0.64 s to 0.82 s—a 28% increase—highlighting the dual impact of nonlinearity: reduced amplification and elongated periods under stronger motions.

3.7.2 Effectiveness of site proxies in predicting surface amplification

This study evaluated the effectiveness of site proxies—V_{s30}, T_0, H_{soil}, and V_{savg}—for 52 soil profiles, with values ranging from 181 m/s to 1531 m/s for V_{s30}, 0.02 to 1.85 s for T_0, 2 to 150 m for H_{soil}, and 127 to 460 m/s for V_{savg}, to characterize nonlinear site amplification. The following findings were observed:

- V_{s30} is a reliable proxy for amplification at short to medium vibration periods. Amplification increased with V_{s30} values up to 600–700 m/s, beyond which it decreased or stabilized. The

amplification peak was observed for the soil profiles having V_{s30} = 500–600 m/s at a vibration period of 0.2 s. At longer periods (1.0–5.0 s), peak amplification was seen at lower V_{s30} values (≈approximately 180–300 m/s) and decreased significantly beyond 300 m/s, indicating a reduced sensitivity of V_{s30} at long periods. Amplification values approached 1 for V_{s30} values greater than 900 m/s.

- T_0 is shown to be a good predictor of amplification, especially at medium to long periods. Amplification generally increased with T_0 up to a resonance point, after which it declined. For example, at a 1.0 s vibration period, peak amplification of 5.6 was observed near T_0 = 1.0–1.1 s. A secondary peak in amplification was noted at long T_0 values for long vibration periods, confirming the effectiveness of T_0 in capturing resonance behavior. Nonlinear amplification showed a systematic shift of peak response towards longer T_0 values due to strain-induced period elongation.
- Resonance effects are observed when the vibration period matches the fundamental period ($T_{osc}/T_0 \approx 1$). Linear amplification peaked at this ratio, while nonlinear amplification shifted slightly beyond 1.0, reflecting the period lengthening under strong motion.
- Soil thickness (H) showed a weaker correlation with amplification at short to medium periods. However, amplification increased with H at 1.0s and 5.0s periods, peaking at 50–60m before declining, suggesting a stronger relationship at longer periods. The variability in amplification at short periods across different soil thicknesses implies that H is a less consistent proxy at those frequencies. However, it becomes more reliable over longer periods due to its correlation with T_0.
- Time-averaged shear-wave velocity (V_{Savg}) was found to be a poor predictor of amplification across most periods. While weak trends were observed at very long periods (e.g., 5.0s), amplification values showed no consistent correlation with V_{Savg} elsewhere. For periods ≤1.0 s, amplification peaked at low V_{Savg} values (≈approximately 180–220 m/s), but no clear pattern emerged beyond this range, limiting the practical use of V_{Savg} as a site response proxy.
- A comparison shows that NBCC 2020 underestimated amplification for soft and stiff soils (site classes D and B) at short to medium periods, while overestimating for medium soils (site class C). This highlights the limitations of using V_{s30} alone for seismic site

classification. Peak amplification from the nonlinear analyses consistently occurred near the soil's fundamental period, reflecting resonance effects not captured by the smoother NBCC curves. This suggests a need for site-specific, frequency-dependent amplification models in seismic hazard assessments.

3.8. Conclusion and recommendation

A comprehensive site-specific 1D ground response analysis was conducted to evaluate the dynamic soil behavior in the Saguenay region. Different geological and geotechnical parameters, as well as site response proxies, were considered to predict site amplification. They were evaluated using the dynamic characteristics of the local soils and ground motion respective for the Saguenay study area. The findings indicate that geological and geotechnical characteristics substantially impact the seismic site effects, with soil nonlinearity being a key factor across different levels of ground motion hazards. The study demonstrates that soil thickness, shear-wave velocity, and layering have a significant influence on seismic site amplification through their effects on the fundamental period and impedance contrast. Among the site proxies evaluated, T_0 emerged as the most robust predictor across all periods, while V_{s30} was effective mainly at short to medium periods; H_{soil} and V_{Savg} showed weaker and less consistent correlations, especially under nonlinear conditions. The disparities observed between the V_{s30}-based NBCC 2020 broadband amplification and the results presented in this study emphasize the need for a site-specific ground motion model and a comprehensive set of site amplification proxies. Therefore, it is recommended that a detailed amplification model be formulated that will incorporate multiple site response proxies. Since V_{savg} and layer thickness are essential to determining the fundamental soil period, incorporating both V_{s30} and T_0 proxies into the model will undoubtedly increase its accuracy. Given the current seismic activity in the Saguenay region, the focus must be put on the regional geological and geotechnical mapping that will provide appropriate knowledge of these critical parameters.

Although this study provides valuable insights into the seismic site effects of the Saguenay region, several limitations must be acknowledged. Due to the scarcity of strong-motion records in Eastern Canada, synthetic ground motions were used in conjunction with available real accelerograms. Additionally, the nonlinear soil curves were not explicitly developed for the investigated sites; instead, curves from similar soil types within the Québec region were adopted. A major limitation of the study is the reliance on one-dimensional analysis, as conducting a large number of nonlinear

dynamic simulations in a two-dimensional framework remains computationally challenging, and an example of site amplification from 2D analysis for this site has been demonstrated in Hossain et al. (2025). These limitations may introduce uncertainties in the site amplification results. Further uncertainties also arise from the assumption of uniform thicknesses for specific sedimentary layers, such as glacial deposits and post-glacial till.

.

CHAPTER 4

ARTICLE 3: EVALUATION OF SITE PERIODS DERIVED FROM ANALYTICAL AND NUMERICAL SIMULATIONS FOR SEISMIC MICROZONATION IN SAGUENAY, EASTERN CANADA

Authors

A S M Fahad Hossain, Ali Saeidi, Mohammad Salsabili, Miroslav Nastev, and Juliana Ruiz Suescun

Author contributions

A S M Fahad Hossain: Conceptualization, Data curation, Formal analysis, Resources, Writing original draft, Writing review & editing. Ali Saeidi: Supervision, Methodology, Resources. Miroslav Nastev: Supervision, Writing – review & editing. Mohammad Salsabili: Writing – review & editing.

Status

Manuscript is ready to be submitted

Declaration of Competing Interest

The authors declare the following financial interests/personal relationships, which may be considered potential competing interests: Ali Saeidi reports that financial support was provided by the Natural Sciences and Engineering Research Council of Canada and Hydro-Québec (CRDPJ 521771-17). Ali Saeidi reports financial support was provided by Natural Sciences and Engineering Research Council of Canada, Hydro-Quebec, Geostack, Rocscience and City of Saguenay (ALLRP 590081-23). If there are other authors, they declare that they have no known competing financial interests or personal relationships that could have appeared to influence the work reported in this paper.

Résumé

La période de vibration du site constitue l'un des principaux proxys pour prédire l'amplification des ondes sismiques incidentes due aux conditions locales de site. Les périodes de site ont été évaluées dans le cadre d'une étude de microzonation sismique de la ville de Saguenay, dans l'Est du Canada. Des solutions analytiques simples fondées sur les méthodes de la couche équivalente unique (Equivalent Single Layer, ESL) et des couches multiples (Multiple Layer, ML) ont été appliquées afin de quantifier la période fondamentale du site (T_0) à partir de modèles géologiques et géotechniques tridimensionnels (3D) de la zone d'étude. Les périodes de site non linéaires (TNL) ont été déterminées à l'aide d'analyses de réponse sismique non linéaire unidimensionnelles (1D), en utilisant des mouvements sismiques d'entrée mis à l'échelle selon des niveaux d'aléa correspondant à des probabilités de dépassement de 10 % et 2 % en 50 ans. Les résultats indiquent que T_0-ESL tend à surestimer la période de site, tandis que TML présente une meilleure concordance avec la période fondamentale T_0 issue des analyses de réponse sismique linéaires. Des corrélations empiriques ont été établies entre T_{esl} et TML, ainsi qu'entre T_{esl} et TNL. Enfin, des cartes de microzonation illustrant la distribution spatiale des périodes de site T_{esl} et TNL ont été produites en tant que proxys de l'amplification sismique locale.

4.1 Abstract

The site vibration period is one of the key proxies for predicting the amplification of incoming seismic waves caused by local site conditions. Site periods were evaluated in the scope of a seismic microzonation study of the Saguenay city, Eastern Canada. Simple analytical solutions with the Equivalent Single Layer (ESL) and the Multiple Layer (ML) methods were applied to quantify the fundamental site period (T_0) based on 3D geological and geotechnical models of the study area. Nonlinear site periods (T_{NL}) were determined using one-dimensional (1D) nonlinear ground response analysis with input ground motions scaled to seismic hazard of 10% and 2% probability of exceedance in 50 years. Results indicate that $T_{0\text{-}ESL}$ tends to overestimate, whereas the T_{ML} shows a better match to T_0 from linear ground response. Empirical correlations were developed between T_{ESL} and T_{ML} and between T_{ESL} and T_{NL}. Microzonation maps of the spatial distribution of the site periods T_{ESL} and T_{NL} were generated as a proxy for seismic site amplification.

Keywords: nonlinear ground response analysis, site amplification, fundamental site period, nonlinear site period.

4.2. Introduction

Seismic site effects play a significant role in the ground motion characteristics. They can contribute to substantial variations in the shaking intensity and damage potential over relatively short distances (Kramer, 1996). The best practice to mitigate impacts from seismic hazards is to conduct seismic microzonation of potential site amplification (Salsabili et al., 2023). Site effects are commonly accounted for with simple proxies that reflect local site conditions. The time-averaged shear-wave velocity of the top 30 m (V_{S30}) is considered the standard site parameter (Hossain et al., 2025). Less frequently, the fundamental vibration period T_0 is also used to improve surface ground motion prediction. It can be readily measured with field techniques such as the Horizontal-to-Vertical Spectral Ratio (HVSR) (Zhao et al., 2006). Additionally, analytical and empirical solutions are employed for the quantification of T_0. Since the soil's nonlinear behavior during strong ground motion modifies the dominant site period, it is essential to accurately measure the site period in both weak and strong ground motions (Motazedian et al., 2011).

Analytical methods are commonly applied when adequate field information is available. Wang et al. (2018) reviewed several analytical techniques for estimating T_0 based on the shear-wave velocity (V_S). The quarter-wavelength relation, $T_{0\text{-ESL}} = 4H/V_{savg}$, is typically applied when the average shear-wave velocity and soil layer thickness are known (Hossain et al., 2023). This ESL approach, however, often results in overestimation of T_0 as the interlayer impedance is not accounted for. Moreover, the assumption of uniform V_S fails to reflect the most typical scenario of increasing V_S with depth (Motazedian et al., 2011, 2020). To address these limitations, Hadjian (2002) introduced the ML method, building upon studies by Madera (1970) and Dobry et al. (1976). This approach accounts for V_S variation between unconsolidated stratigraphic layers. Therefore, evaluation and comparison of T_0 across different methods is important, particularly since ESL remains widely used as a secondary site parameter (proxy) in site amplification models.

During strong earthquake shaking, soil exhibits nonlinear behavior, which causes the fundamental period to shift to longer values, a phenomenon referred to as the nonlinear site period (T_{NL}). This behavior has been observed in strong-motion records from the 1985 Michoacán and 1989 Loma Prieta earthquakes (Steidl, 2000). Several studies (e.g., Zhao et al.; 2006; Fukushima et al., 2007; Di Alessandro et al., 2012) have focused on fundamental site period measurements with microtremor HVSR for enhanced classification across diverse geological settings. More recent work (e.g.,

Ghofrani et al., 2013; Ghofrani & Atkinson, 2014; Hassani et al., 2019; Livaoğlu et al., 2021; Aydın et al., 2022) further refined these methods by integrating HVSR with strong-motion and geotechnical data, reducing uncertainties through combined analyses with borehole velocity profiles, validating site periods using numerical site-response modeling, and extending applications to regional classification and building response. Motazedian et al. (2020, 2011) employed nonlinear ground response analyses to evaluate the impact of soil nonlinearity on site periods, highlighting the importance of incorporating T_{NL} for improved quantification of seismic amplification.

The present study is part of an ongoing seismic microzonation of the Saguenay region, Eastern Canada (Foulon et al., 2018; Hosseinpour et al., 2024; Salsabili et al., 2023). Located near the Charlevoix-Kamouraska seismic zone, the Saguenay region is exposed to significant seismic hazard, as highlighted by the 1988 M5.9 earthquake. The objective of the study is to propose practical methods for quantifying local site periods. Fifty-one-dimensional (1D) soil profiles were selected from various locations, incorporating site-specific geological and geotechnical parameters. The fundamental site period T_0 was estimated to be using both ESL and ML analytical methods. In parallel, T_{NL} was quantified through 1D nonlinear ground response analyses using the DEEPSOIL v7.0 software (Hashash et al., 2020). The seismic input consisted in six recorded and synthetic acceleration time histories representative of the seismotectonic settings in the study area. The bedrock ground motions were scaled to the NBCC 2020 hazard levels with probability of exceedance of 10%/50 years (return period of 475 years) and 2%/50 years (return period of 2475 years). In both cases, empirical correlations and respective microzonation maps were developed.

4.3. Study area and input parameters

The study area encompasses densely populated regions of Eastern Quebec, along the Saguenay River, including municipalities of Saguenay, Jonquiere, and La Baie. The region is underlain by post-glacial sediments of the Late Pleistocene and Holocene periods deposited by the Laflamme Sea waters. These sediments originated from glacial erosion of the source rock from three geological provinces: the Canadian Shield to the north (Precambrian crystalline rocks), the St. Lawrence Platform (Palaeozoic sandstones and limestones), and the Appalachians to the south (Palaeozoic shales, sandstones, and volcanic rocks) (Salsabili et al., 2021b). The Saguenay region was selected as a study area due to its complex stratigraphy, characterized by the presence of thick and soft silty-clay deposits, and its proximity to the seismically active Charlevoix zone (Du Berger et al., 1991;

Lamontagne, 2002). The standard stratigraphic sequence comprises (from bottom up) compact glacial till, glaciofluvial sands and gravels, fine glaciomarine sediments, and heterogeneous post-glacial deposits, including alluvium and landslide colluvium (Foulon et al., 2018; Salsabili et al., 2021a). The silty-clay unit can reach over 100 m in thickness in lowland areas and is susceptible to seismic-induced failure (Salsabili et al., 2021b). Table 8 and Figure 38 give the coverage, thickness, and spatial distribution of the individual Quaternary units within the study area.

Table 8. Major Quaternary units and respective coverage of the study area (Modified from Salsabili et al., 2021).

Geological Unit	**Area (km²)**	**% of Total Area**
Alluvial deposits	30	2.8
Wind-blown (eolian) sediments	2	0.2
Landslide-related deposits	28	2.6
Organic-rich peat and bog materials	41	3.8
Coarse post-glacial deposits (primarily sand and gravel)	149	13.9
Fine post-glacial deposits (glaciomarine clay)	317	29.6
Glaciofluvial materials (gravel and sand from meltwater streams)	16	1.5
Glacial till	407	38.0
Rock outcrop	81	7.6
Total	**1071**	**100.0**

Initially, fifty 1D typical soil profiles, along with site-specific geotechnical properties, were selected. 1D nonlinear site response analyses were then conducted using six real and synthetic ground motion records, each scaled to match approximately five seismic hazard levels defined in NBCC 2020 with 20%, 10%, 5%, 3.5%, and 2% probability of exceedance in 50 years. The time-domain simulations were conducted using the open-source software DEEPSOIL v7.0 (Hashash et al., 2020), renowned for its accuracy and reliability in site response modeling. The modified Kondner-Zelasko hyperbolic model (MKZ), which incorporates pressure-dependent behavior, was applied to represent the modulus reduction and shear stress responses. The input time histories and site-specific geotechnical properties are presented in Figure 39.

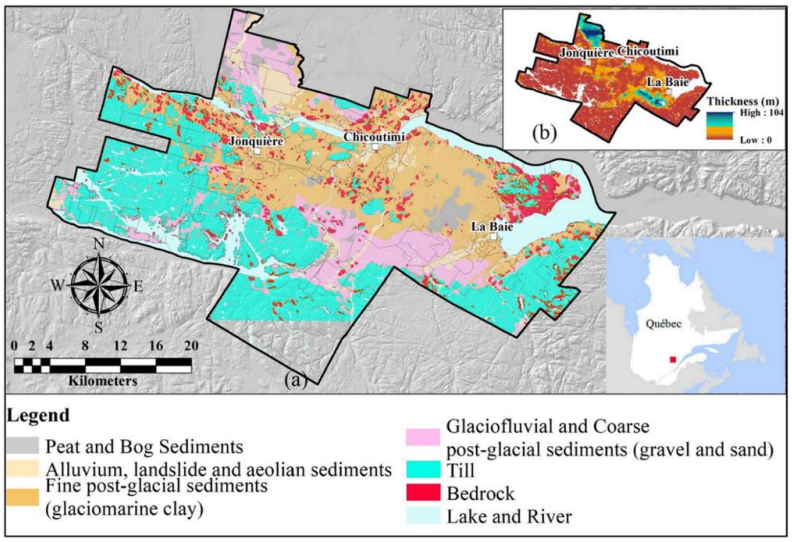

Figure 38. Study area: a) simplified surface geology; b) thickness of surficial deposits (modified from Salsabili et al., 2021b).

a) b)

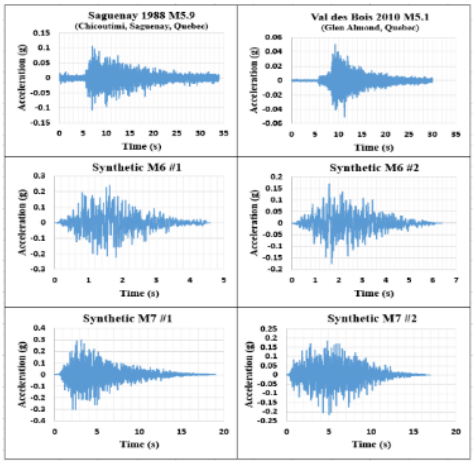

Unit	Vs (m/s)	γ (kN/m³)	G_{max} and ξ curves
Clay	$114.5+9.4xD^{0.76}$	18.7	Abdellaziz 2023
Sand	144.9+2.55xD	17.5	EPRI, 1993
Gravel	$46.861+61.55xD^{0.5}$	18.3	Seed et al., 1986
Till	580, σ=±174	21.0	Hydro Quebec
Rock	1875, σ=±781	28.0	N/A

Figure 39. a) Unscaled input time histories, and b) Geotechnical properties of soil and rock (modified from Hossain et al., (2024, 2025).

A flowchart of the applied methodology is presented in Figure 40. For each soil profile, the fundamental site period was first evaluated using the ESL and ML methods, T_{ESL} and T_{ML}, respectively. In parallel, for each soil profile and input ground motion time history, the seismic amplification was calculated as the ratio of the response spectrum at the ground surface to that at the bedrock. The final amplification factor (AF) for each soil profile was then determined as the geometric mean of the amplification factors obtained from the six input ground motions. This procedure was repeated for each of the five seismic hazard levels. The AF, as defined, is not only dependent on seismic intensity but also varies with frequency and is influenced by the geotechnical

properties of the soil units present in the profile. The nonlinear site period, T_{NL}, was now calculated as the period at which the maximum site amplification occurs.

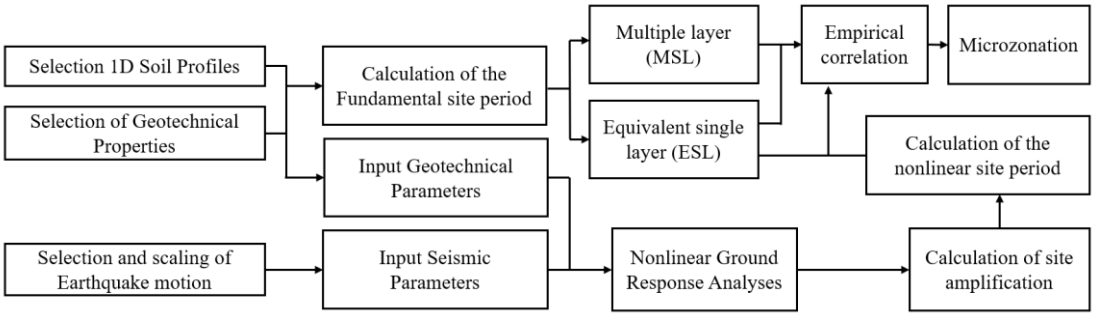

Figure 40. Flowchart of the applied methodology

Following the calculations of the different site periods, correlation equations were developed between (i) T_{ESL} and T_{ML}, and (ii) T_{ESL} and T_{NL}. The final step consists of the development of seismic microzonation maps for T_{ML} and T_{NL}.

4.4. Fundamental site period

4.4.1 Calculation

The fundamental site period, T_0, is the principal natural vibration period of a site, representing the time required for the soil profile to complete a full cycle of back-and-forth motion. It is representative of linear response under low-intensity seismic excitation (microtremors). Herein, two methods for assessment of T_0 are applied: (i) equivalent single-layer approach ESL (Equation 4.1) and (ii) multiple soil layer approach ML (Equations 4.2 through 4.4). As outlined by Hadjian, (2002). The ML computation process begins by considering the upper two layers, corresponding to periods T_1 and T_2, and calculating the aggregate period using Equation 4.1. The combined period (T) for these two layers is calculated using Equations 4.2 to 4.4. In the subsequent stage, these two layers constitute a single layer and are considered as T_1, and the underlying third layer is considered as T_2. Again, using Equations 4.2 to 4.4, the combined T for these two layers is considered. The technique is iteratively repeated over all layers until the final layer at the bottom, which is the final T_{ML} for the soil profile. The number of iterations equals the number of layers considered, minus one.

$$T_{ESL} = \frac{4H}{Vs_{avg}} \quad (4.1)$$

$$\frac{T}{T_1} = \sqrt{\frac{\pi^2}{8}[0.75 + \left(\frac{T_2}{T_1}\right)^2 \left(1 + 2\frac{H_1}{H_2}\right)]}; [\text{for } \frac{T_2}{T_1} > 0.1, H_1 > H_2] \quad (4.2)$$

$$\frac{T}{T_1} = [1 + \beta\left(\frac{T_2}{T_1}\right)^n \left(1 + 2\frac{H_1}{H_2}\right)^n]^{\frac{1}{n}}; [\text{for } \frac{T_2}{T_1} > 0.1, H_1 \leq H_2] \quad (4.3)$$

$$\frac{T}{T_1} = [1 + \frac{H_1}{H_2}(\frac{T_2}{T_1})^2]; [\text{for } \frac{T_2}{T_1} \leq 0.1] \quad (4.4)$$

$$\text{where, } \beta = 1\text{-}0.2(\frac{H_1}{H_2})^2; \text{ and } n = 4 - 1.8\frac{H_1}{H_2}$$

Once T_{ESL} and T_{ML} are computed for all 50 soil profiles, an empirical correlation was developed between these two parameters. The objective was to enable the conversion of the fundamental site period TESL to TML, as shown in Equation 4.5. The calculated and empirical fundamental site periods in multiple soil-layered methods are shown against T_{ESL}, as shown in Figure 4.5 with a coefficient of determination of 0.99 and standard deviation of 0.018. This figure shows that T_{ML} is lower than T_{ESL}, and that the discrepancy increases with longer fundamental periods in soil columns.

$$T_{ML} = 0.87 * T_{ESL}^{0.93}; R^2 = 0.99; \sigma = 0.018 \quad (4.5)$$

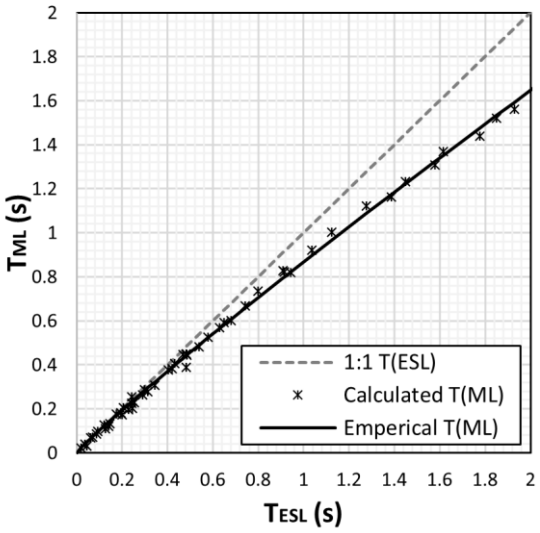

Figure 41. Comparisons between the fundamental site periods obtained using the equivalent single layer, T_{ESL}, and the multiple soil layer T_{ML} approaches.

To better understand the variation between the two methods with respect to site parameters, Figure 42 shows the difference between T_{ESL} and T_{ML} as a function of site proxies: V_{s30}, V_{savg}, and H_{soil}. It can be observed that the difference decreases rapidly with increasing V_{s30}, whereas it shows a strong linear correlation with V_{savg} and H_{soil}.

a) b) c)

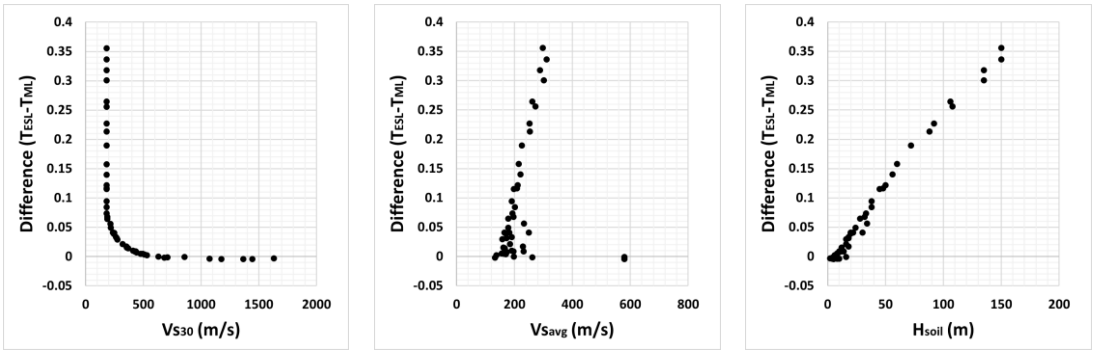

Figure 42. Difference between T_{ESL} and T_{ML} as a function of Site Proxies: a) V_{s30}, b) V_{savg}, and c) H_{soil}.

4.4.2 Spatial distribution of fundamental site periods

The spatial distribution map for T_{ESL} for the Saguenay region was previously developed by Salsabili et al., (2021, 2023). Combining this T_{ESL} map with the T_{ML}-T_{ESL} empirical correlation given with Equation 4.5, it is now possible to develop the T_{ML} site period map. Figure 43 shows the T_{ESL} and T_{ML} maps along with the difference between T_{ESL} and T_{ML}. Both maps show similar overall patterns, with higher site periods (>0.54 s) concentrated mainly in the northwestern part near Jonquière and the southeastern part near La Baie, while lower periods (<0.20 s) dominate the central and peripheral areas. The difference map indicates that the two methods are generally consistent, as most areas exhibit minimal discrepancies, though localized variations are observed where ESL tends to predict slightly higher values than ML, particularly in parts of Jonquière and La Baie.

a) b)

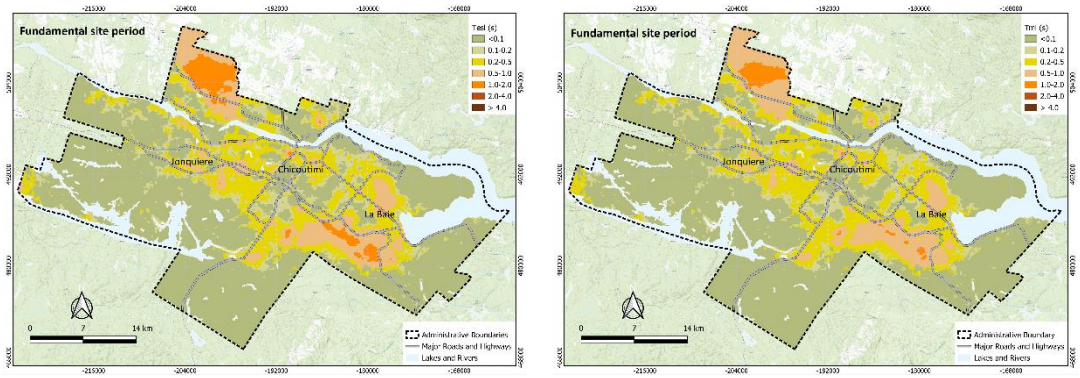

c)

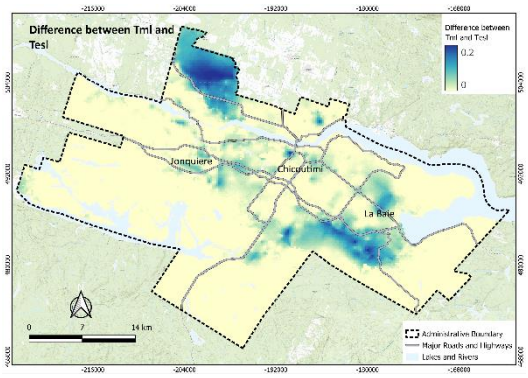

Figure 43. The micro-zonation map for Saguenay shows the spatial distribution of the fundamental site period: a) the equivalent single T_{ESL}, b) multiple-layer T_{ML} methods, and c) T_{ESL}–T_{ML} discrepancies.

4.5 Nonlinear site period

4.5.1 Shift of site period due to nonlinear behavior

During strong cyclic motion induced by seismic waves, shear strains in soil can increase significantly. This nonlinear behavior is typically accompanied by a reduction in shear stiffness (i.e., softening of the soil profile) and an increase in material damping, leading to greater energy dissipation. As a result, the amplitude of ground motion may be reduced, and amplification decreases, potentially even becoming negative, resulting in de-amplification of seismic waves. Consequently, the fundamental site period shifts toward longer values. In Figure 44, the computed spectral amplifications for 50 soil profiles are plotted against the ratio of the oscillation period (T_{osc}) to the site fundamental period (T_{ESL}).

a) b)

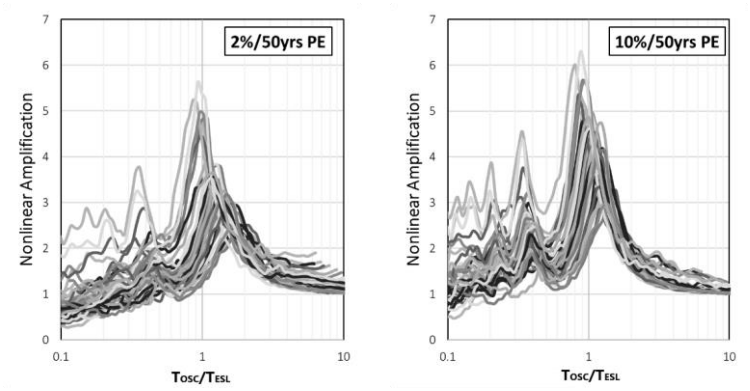

Figure 44. Nonlinear amplification for 50 soil profiles against the ratio between oscillation period and site fundamental period by T_{ESL}: a) 10%/50yrs PE and b) 2%/50yrs PE

Figures 8 show a clear shift of the maximum nonlinear amplification from a ratio of 1 toward higher values. In general, for linear site response, the peak amplification occurs at a ratio of about 1, corresponding to resonance under low levels of excitation. In this study, however, a fully nonlinear analysis was conducted using nonlinear soil shear modulus and damping reduction curves. A similar trend has been observed in other studies, e.g., Harmon et al., (2019) and Hashash et al., (2018).

4.5.2 Calculation of nonlinear site period

The nonlinear site period (T_{NL}) was identified as the period corresponding to the maximum spectral amplification. The soil profiles were exposed to input motions scaled to the NBCC 2020 seismic hazard with 10%/50 yrs and 2%/50 yrs probability of exceedance (PE). Empirical correlations for T_{NL} and T_{ESL} were developed using Equations 4.6 and 4.7, respectively. Figure 45 shows the computed site periods values together with the regression correlations, exhibiting a good match (R^2 and σ of 0.99 and 0.05 for 10%/50yrs PE and 0.97 and 0.09 for 2%/50yrs PE, respectively).

$$T_{NL\text{-}10\%/50yrs\ PE} = 0.98 * T_{ESL}^{0.86}; \quad R^2 = 0.99; \quad \sigma = 0.05 \tag{4.6}$$

$$T_{NL\text{-}2\%/50yrs\ PE} = 1.13 * T_{ESL}^{0.82}; \quad R^2 = 0.97; \quad \sigma = 0.09 \tag{4.7}$$

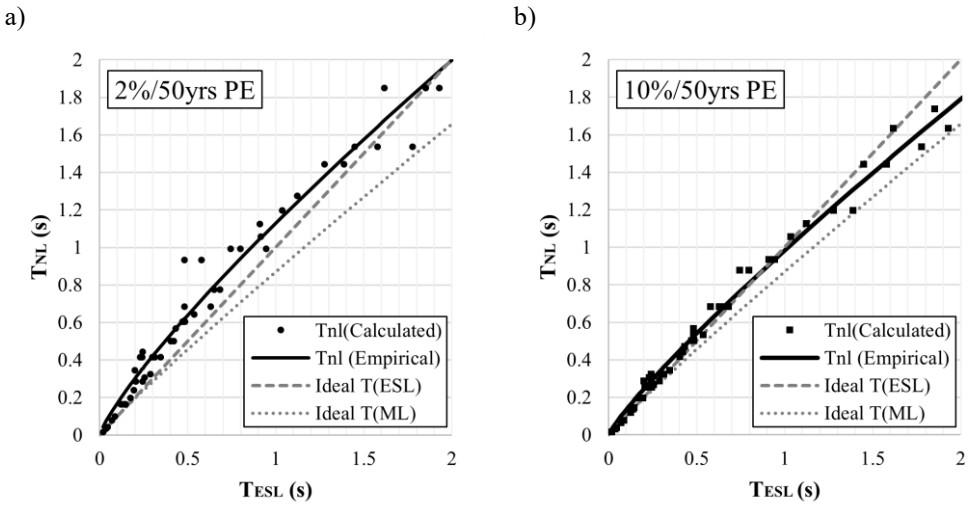

Figure 45. Nonlinear site period of soil for ground motion with a) 2%/50 years PE and b) 10%/50 years PE.

Figure 45 shows that, in the short- to medium-period range, T_{NL} exceeds T_{ESL} for both hazard levels. However, at longer periods, T_{NL} becomes lower than T_{ESL}. Such behavior can be explained by the conventional ESL method, which tends to overestimate T_0, especially in thicker soil columns. In contrast, the ML method provides more accurate estimates and is steadily lower than T_{NL}. Although not explicitly shown, it is observed that stiffer soil columns with a higher V_{savg} exhibit a smaller shift

in T_0 than those with softer profiles. For a better understanding of the shifting period, Figure 46 presents the empirical correlations of T_{NL} for 10%/50 years and 2%/50 years hazard levels, along with the ideal (1:1) T_{ML} and T_{ESL}. It can be concluded that T_{ML} is a better indicator than T_{ESL} for the natural (linear) vibration period.

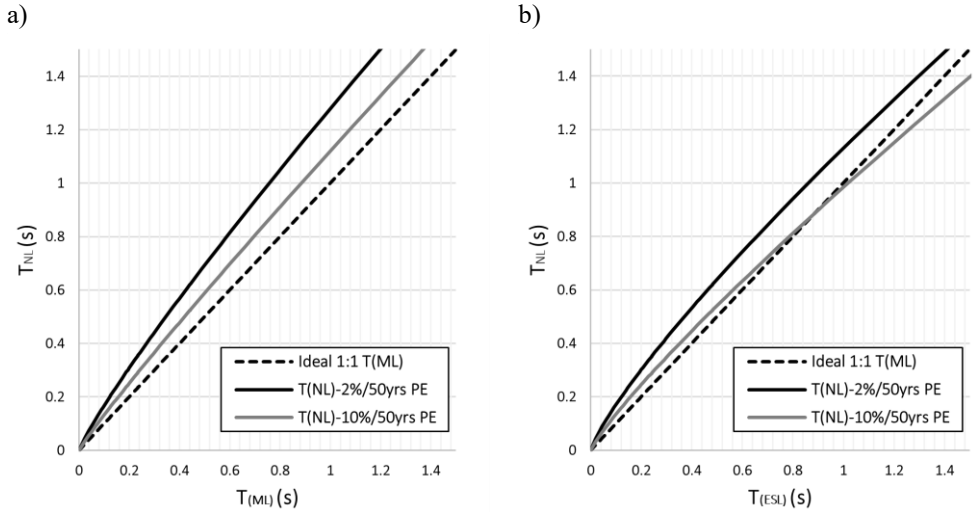

Figure 46. Empirical correlations between a) T_{NL} and T_{ML}, and b) T_{NL} and T_{ESL}

It is now of interest to develop a relationship between the nonlinear site period T_{NL}, on one hand, and the peak ground acceleration (PGA) and the fundamental site period (T_{ESL}), on the other. Information on PGA for the Saguenay region for five hazard levels with probability of exceedance of 2% (PGA=0.589g), 3.5% (PGA=0.44g), 5% (PGA=0.35g), 10% (PGA=0.20g), and 20% (PGA=0.11g) in 50 years is provided by NBCC 2020 (Equation 4.8). The nonlinear site period at different hazards and the T_{ML} for 50 soil profiles are plotted as a function of the T_{ESL} as scatter plots in Figure 47. It is observed that, with increasing the motion amplitude (increasing the hazard), the scatter plots shift toward longer values, and the shift is observed as more organized compared to the T_{ML} line rather than the T_{ESL} line. At lower levels of hazards (e.g., 10% and 20%/50 years PE), the points remain close to the 1:1 reference, indicating limited nonlinearity. In contrast, at higher hazard levels (e.g., 2%/50 years PE), the nonlinear effects are evident, with an upward deviation from the T_{ESL} line. Overall, the comparison demonstrates that the multilinear approach better captures the trend of site-period elongation due to nonlinear effects than the equivalent single-layer approximation.

$$T_{NL} = 1.28 * PGA^{0.14} * T_{ESL}^{0.92}\ ; \quad R^2 = 0.98\ ; \quad \sigma = 0.086 \qquad (4.8)$$

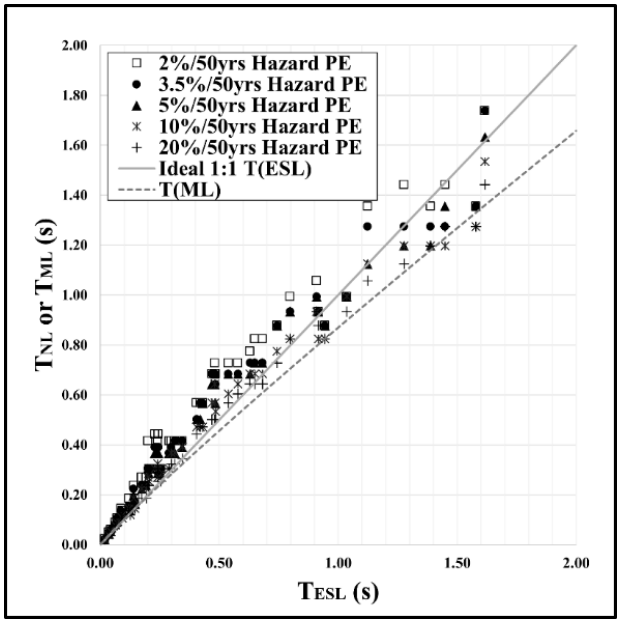

Figure 47. The variability of nonlinear site periods T_{NL} from various soil models across all five hazard levels, as well as T_{MSL}, is compared against the fundamental site periods T_{ESL}. The black dashed line represents a 1:1 relationship, indicating where T_{NL} or T_{ML} equals T_{ESL}.

4.5.3 Assessment of T_{ESL}–T_{ML} discrepancies as a function of site proxies and site amplification

To evaluate the discrepancies between the T_{ESL} and T_{NL}, it was demonstrated that the difference in fundamental site period calculations between the two methods is illustrated in Figure 48 as a frequency distribution histogram and a pie chart for 50 soil profiles. The comparison of frequency distributions shows that for the 2%/50 yrs PE case, the differences are more widely spread, with notable contributions up to 0.35. In contrast, the 10%/50 yrs PE case is more concentrated within the 0.04–0.15 range. The proportional distributions confirm this trend: about 78% of the 10%/50 yrs PE differences fall below 0.15, while the 2%/50 yrs PE scenario exhibits a broader spread, with nearly half of the values exceeding 0.15. This highlights more substantial variability under the higher intensity motion condition at higher hazard.

The scatter plots compare the difference (T_{NL} – T_{ESL}) for 2% and 10%/50 yrs PE against V_{s30}, V_{savg}, and $H_{soil,}$ as shown in Figure 48. Differences decrease rapidly with increasing V_{s30}, becoming negligible beyond ~500 m/s, while for V_{savg}, most variations cluster between 150–300 m/s. A clear increasing trend with H_{soil} is observed, where the 2%/50 yrs PE case shows larger differences than the 10%/50 yrs PE, emphasizing the influence of soil thickness and hazard level on period estimates. Overall, the results highlight that softer sites (low V_{s30}, low V_{savg}, and thick soil) exhibit the highest sensitivity, while stiffer sites show minimal differences regardless of return period.

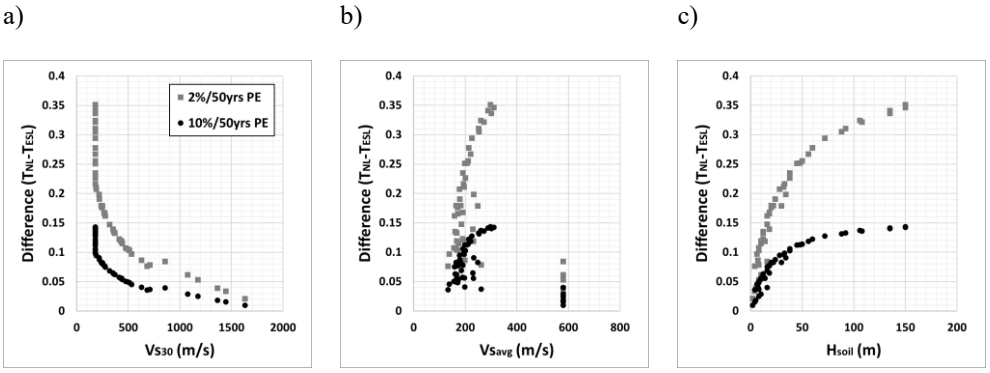

Figure 48. TESL–TNL Discrepancies as a Function of Site Proxies: a) V_{s30}, b) V_{savg}, and c) H_{soil}.

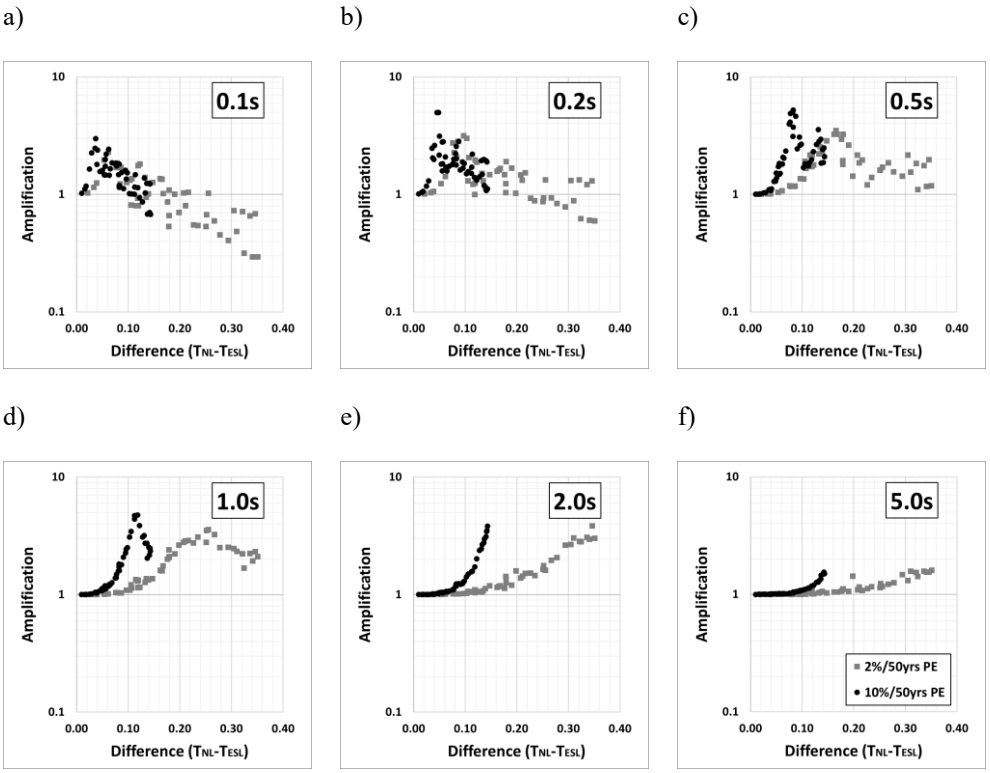

Figure 49. T_{ESL}–T_{NL} Discrepancies as a Function of Nonlinear Site Amplification at: a) 0.1s, b) 0.2s, c) 0.5s, d) 1.0s, e) 2.0s, and f) 5.0s.

The amplification vs the difference ($T_{NL} - T_{ESL}$) plots are shown in Figure 49 for two hazard levels: 2% and 10%/50-year PE for six vibration periods. At shorter periods (0.1–0.2 s), amplification is generally higher for minor differences, gradually reducing with increasing difference values. With medium periods (0.5–1.0 s), distinct divergence is observed: the 10%/50 yrs PE case exhibits peak amplifications at lower differences, whereas the 2%/50 yrs PE case shows increasing amplification with larger differences. At longer periods (2.0–5.0 s), both scenarios converge near unity, indicating that amplification increases with the difference value, and the difference between the 2% and 10%/50-year PE hazards becomes minimal.

4.5.4 Microzonation map for fundamental site period

Combining the spatial distribution of T_{ESL} (Salsabili et al., (2021, 2023) and empirical correlations given with equations 4.6 and 4.7, the spatial distribution of the nonlinear site period for the Saguenay region was developed. Figure 50 shows the microzonation maps of the nonlinear site period (T_{NL}) for both hazard levels (2%/50 yrs and 10%/50 yrs), highlighting significant spatial variability across the Saguenay urban area. Higher T_{NL} values (>0.51 s) are concentrated in river valleys and low-lying depositional environments around Chicoutimi and La Baie, indicating thicker sediments and greater amplification potential. Moderate values (0.37–0.51 s) occur as transitional belts surrounding these areas. In contrast, lower values (<0.37 s) predominate in upland and till-covered regions. Despite slight variations between hazard levels, both maps consistently demonstrate that site response in the region is strongly influenced by local geology, with higher amplification potential in densely populated urban centers.

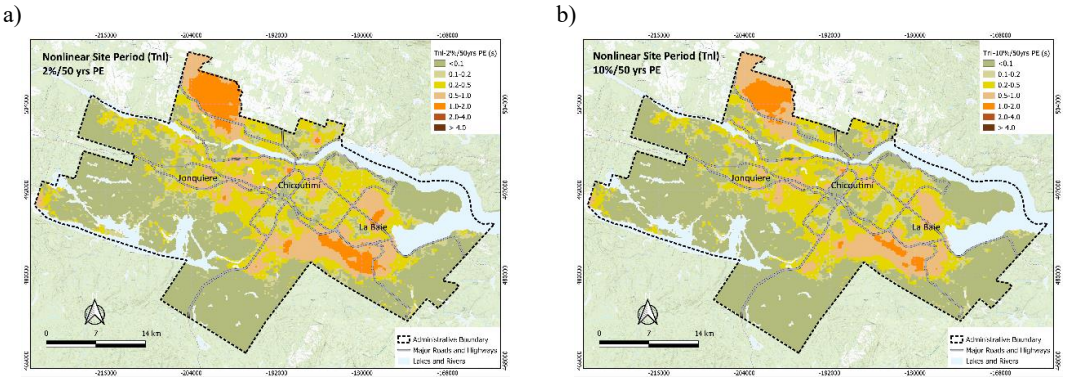

Figure 50. Spatial distribution of nonlinear site period T_{NL} for: a) 10%/50yrs PE and b) 2%/50yrs PE.

Figure 51 illustrates the spatial discrepancy between the nonlinear site period (T_{NL}) and the equivalent–linear site period (T_{ESL}) for both hazard levels. The maps show that the differences are generally minor across much of the study area, with values clustering at the lower end of the scale. However, localized zones—particularly around Chicoutimi and La Baie—exhibit relatively higher discrepancies, reflecting the stronger nonlinear soil behavior in thick sedimentary deposits. These differences are less pronounced in upland and till-covered regions, where stiff soils minimize nonlinear effects. Overall, the comparison highlights that while T_{NL} and T_{ESL} estimates are broadly consistent, the discrepancy is more pronounced under the 2%/50 yrs hazard level, underscoring the increasing importance of nonlinear soil response in higher shaking intensity scenarios.

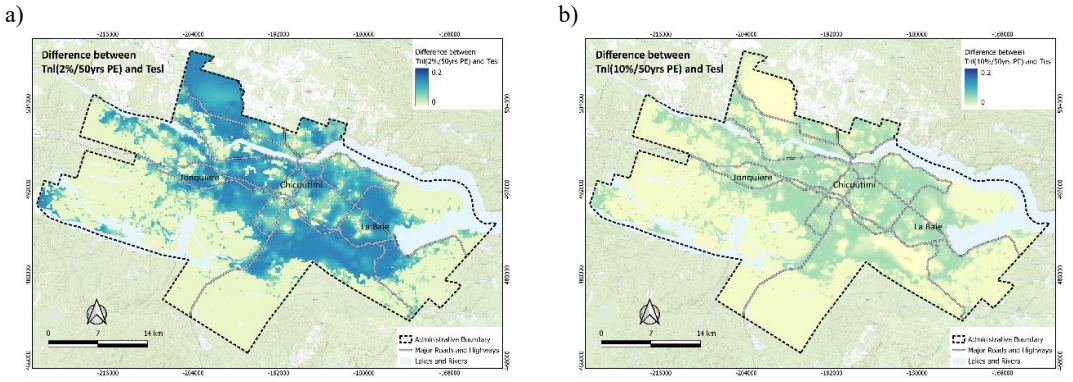

Figure 51. Spatial distribution of the difference between T_{ESL} and T_{NL} for: a) 10%/50yrs PE and b) 2%/50yrs PE.

4.5.5 Site amplification vs nonlinear site period

The site amplification values of 50 soil profiles across six vibration periods: 0.1s, 0.2s, 0.5s, 1.0s, 2.0s, 5.0s, and for hazard level 10%/50yrs and for 2%/50yrs PE are plotted as a function of site parameters T_{NL} in Figure 52. Amplification decreases rapidly over a short period of 0.01 s as T_{NL} values increase, with de-amplification beginning after 0.20 s for both 2%/50yrs PE and 10%/50yrs PE. As expected, amplification is higher for 10%/50yrs PE than for 2%/50yrs PE, where stronger nonlinearity occurs. Over 0.2 seconds, amplification values increased with T_{NL}, reaching a peak of approximately 5, at around 0.15 seconds for 2%/50 years PE and 0.19 seconds for 10%/50 years PE. Beyond this peak, amplification fluctuates as T_{NL} continues to increase. At 0.5s, a similar trend is observed, with peak amplification of 3 at 0.50s for the 2%/50yrs PE and 5 at 0.6s for the 10%/50yrs PE. At 1.0 s, amplification rises with T_{NL}, peaking at 3 and 4.5 for 2%/50yrs PE and 10%/50yrs PE, respectively, around 1.0 s; after this peak, amplification decreases as T_{NL} increases. Over 5.0 seconds, where motion energy is low, amplification increases with T_{NL} beyond 0.5 seconds, with similar values for both hazard levels.

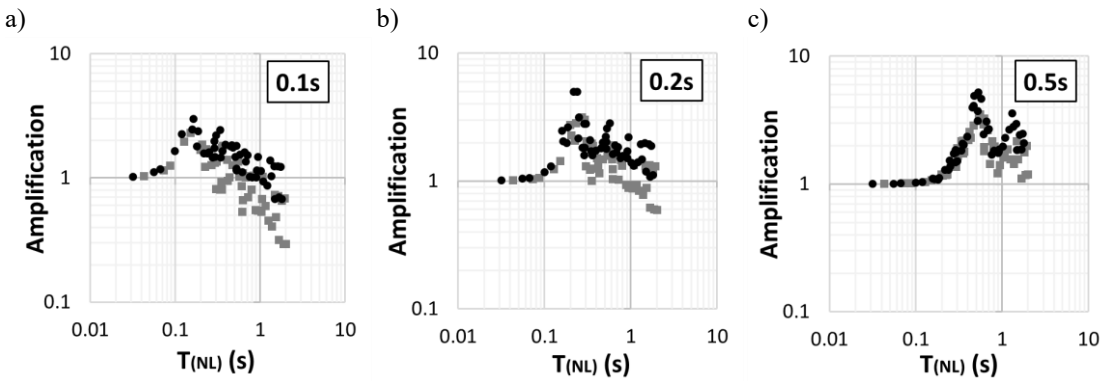

d) e)

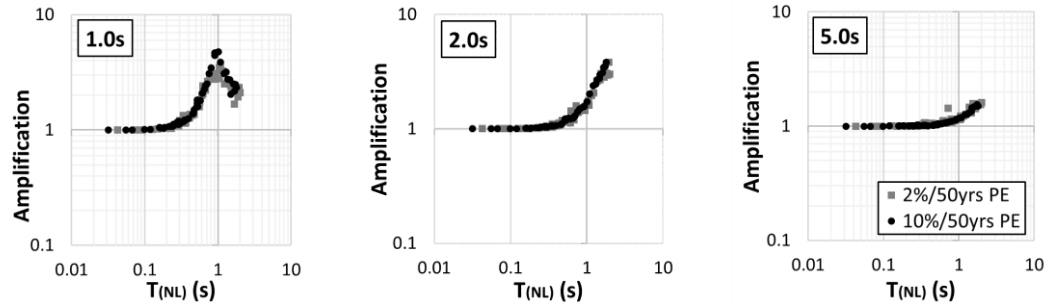

Figure 52. Seismic amplification vs. T_{NL} for two hazard levels 10%/50yrs PE and 2%/50yrs PE and vibration period of a) 0.1s, b) 0.2s, c) 0.5s, d) 1.0s, e) 2.0s, and f) 5.0s

4.6. Conclusion and recommendation

The site period is a critical geotechnical parameter. It is widely used in modeling surface ground motion and evaluating site amplification, essential components of seismic hazard prediction. Despite its importance, proper evaluation of the site period is often overlooked. This study contributes to the development of seismic microzonation for the Saguenay region in Eastern Canada, with a focus on site amplification. The fundamental site period was estimated using both the conventional equivalent single-layer method ESL and the multi-layer ML approaches. Additionally, nonlinear site periods were derived from a comprehensive one-dimensional (1D) nonlinear ground response analysis. Empirical correlations were established between the fundamental site periods obtained from the conventional method T_{ESL}, the multi-layer method T_{ML}, and the nonlinear analysis T_{NL}. Based on these analyses, spatial distribution maps were developed for all three site periods (T_{ESL}, $T_{ML,}$ and T_{NL}). The key findings and recommendations are as follows:

- The equivalent single-layer method (T_{ESL}) systematically overestimates the fundamental site period, while the multi-layer method (T_{ML}) provides a more accurate estimation. An empirical correlation was developed to derive the fundamental site period (T_{ML}) from T_{ESL}, offering a practical tool to refine site period estimations in future studies.

- Nonlinear soil behavior during earthquake loading causes the site period to shift toward longer values, referred to as the nonlinear site period (T_{NL}). This shift is particularly significant at higher seismic hazard levels due to deep nonlinear soil response.

- Additional empirical correlations were established to estimate T_{NL} directly from T_{ESL}, thereby enabling its application in engineering practice without extensive numerical modeling.

CHAPTER 5

ARTICLE 4: SEISMIC MICROZONATION OF A REGION WITH COMPLEX SURFICIAL GEOLOGY BASED ON COMPREHENSIVE NONLINEAR SITE AMPLIFICATION MODELLING

Authors

A S M Fahad Hossain, Mohammad Salsabili, Ali Saeidi, Miroslav Nastev, and Juliana Ruiz Suescun

Author contributions

A S M Fahad Hossain: Conceptualization, Data curation, Formal analysis, Resources, Writing original draft, Writing review & editing. Ali Saeidi: Supervision, Methodology, Resources. Miroslav Nastev: Supervision, Writing – review & editing. Mohammad Salsabili: Writing – review & editing.

Status

Submitted to Soil Dynamics and Earthquake Engineering on 14 October 2025, and the first review was completed on 13 November 2025

Declaration of Competing Interest

The authors declare the following financial interests/personal relationships, which may be considered potential competing interests: Ali Saeidi reports that financial support was provided by the Natural Sciences and Engineering Research Council of Canada and Hydro-Québec (CRDPJ 521771-17). Ali Saeidi reports financial support was provided by Natural Sciences and Engineering Research Council of Canada, Hydro-Quebec, Geostack, Rocscience and City of Saguenay (ALLRP 590081-23). If there are other authors, they declare that they have no known competing financial interests or personal relationships that could have appeared to influence the work reported in this paper.

Résumé

La microzonation sismique permet de quantifier les impacts imprévisibles de l'aléa sismique à l'aide de modèles d'amplification de site visant à prédire l'intensité des secousses sismiques. Une méthodologie novatrice de microzonation sismique régionale est appliquée à la région du Saguenay, dans l'Est du Canada, caractérisée par une géologie superficielle fortement hétérogène. Le contraste d'impédance élevé entre le substratum rocheux et les dépôts superficiels, combiné à une forte résonance de site à certaines périodes, peut contribuer à une amplification sismique relativement élevée. Des cartes d'amplification de site ont été élaborées à partir d'un modèle robuste fondé sur des analyses de réponse sismique non linéaire unidimensionnelles (1D) de cinquante profils de sol, utilisant des mouvements sismiques réels et synthétiques mis à l'échelle selon deux niveaux d'aléa du Code national du bâtiment du Canada (CNBC 2020), correspondant à des probabilités de dépassement de 2 % et 10 % en 50 ans. La période de site non linéaire (T_{NL}), calculée à partir des analyses de réponse sismique non linéaires, s'avère plus représentative des conditions non linéaires que la période naturelle du site (T_0) et est utilisée pour modéliser l'amplification sismique non linéaire. Des équations de corrélation ont été établies entre l'amplification de site et plusieurs proxys, notamment la vitesse moyenne des ondes de cisaillement dans les 30 premiers mètres (V_{s30}), la vitesse moyenne des ondes de cisaillement de la colonne de sol (V_{savg}), le rapport des vitesses des ondes de cisaillement du rocher et du sol (V_f), la période non linéaire T_{NL}, l'épaisseur totale du sol (H_{soil}), l'épaisseur totale des sols postglaciaires (H_{pg}) et l'épaisseur totale des sols glaciaires (H_{till}). La combinaison optimale de proxys a été identifiée comme étant V_{s30}, V_{savg}, T_{NL} et H_{till}, permettant ainsi l'élaboration d'une microzonation sismique de l'amplification de site pour la région du Saguenay.

5.1 Abstract

Seismic microzonation helps quantify the unpredictable impacts of seismic hazards through site amplification models that predict the ground shaking intensity. A novel methodology for regional seismic microzonation is applied to Saguenay, Eastern Canada, a region with highly heterogeneous surficial geology. The high impedance contrast between bedrock and surficial sediments, combined with strong site resonance at specific periods, may contribute to relatively high seismic amplification. Site amplification maps were developed using a robust site amplification model based on 1D nonlinear ground response analyses of fifty soil profiles, with real and synthetic input motions scaled to two National Building Code of Canada (NBCC) 2020 hazard levels: 2%/50yrs and 10%/50yrs

probability of exceedance. The nonlinear site period (T_{NL}), computed from nonlinear ground response analyses, is a more effective parameter under nonlinear conditions than the natural site period (T_0) and is used to model the nonlinear site amplification. Correlation equations were developed between site amplification and proxies such as average shear wave velocity over the top 30 m (V_{s30}), average shear wave velocity for the soil column (V_{savg}), shear wave velocity ratio of rock and soil (V_f), T_{NL}, total soil thickness (H_{soil}), total thickness of postglacial soils (H_{pg}), and total thickness of glacial soils (H_{till}). The optimal combination was found using V_{s30}, V_{savg}, T_{NL}, and H_{till}, which enabled the development of seismic microzonation for site amplification in the Saguenay region.

Keywords: Microzonation, nonlinear ground response, site amplification, soil thickness, shear wave velocity, fundamental site period, nonlinear site period.

5.2 Introduction

Seismic microzonation (SM) is widely recognized as one of the most important tools for assessing seismic hazard and risk. SM provides a structured framework for subdividing a big region into small zones of differing seismic hazard by integrating geological, geotechnical, and geophysical information to evaluate local site effects. Globally, a wide range of approaches have been adopted, spanning from qualitative geological assessments to fully quantitative numerical simulations. These approaches differ in scale, data requirements, and the degree of standardization adopted by each country. Seismic microzonation is commonly carried out in three levels: Level I uses existing regional geological and geophysical data, Level II applies empirical site parameters such as V_{s30} and T_0 from in-situ measurements, and Level III conducts detailed numerical or experimental analyses (Mihalić et al., 2011; Moscatelli et al., 2020; Yamin et al., 2018). Global SM studies—including those by Panzera et al., (2019), Regnier et al., (2000), Talhaoui et al. (2004), and Yamin et al. (2018)—show that combining HVSR, Vs-profiling, geological modelling, and numerical amplification analysis enables increasingly refined hazard assessment consistent with Levels I, II, and III of seismic microzonation.

SM involves mapping of spatial variations in the seismic site response, local geological, geotechnical, and morphological features can significantly alter the intensity and frequency content of the ground shaking (Kramer, 1996). This results in notable variations in seismic intensity and damage even over short distances (Hossain et al., 2025). Such localized amplification patterns are

directly linked to seismic risk, because site effects control the spatial distribution of ground-motion levels while the exposure and vulnerability of the built environment determine how these amplified motions translate into actual damage. Several studies have demonstrated that realistic representation of site effects, soil conditions, and building inventory characteristics substantially modifies estimated seismic losses and risk patterns (Fayjaloun et al., 2021; Hashimoto & Miyajima, 2002; Mori et al., 2020; Panzera et al., 2018; Sabetta et al., 2023). Characteristics of eastern North America are the substantial impedance contrast at the bedrock interface, which causes amplified motion, and resonance in the lower-impedance surficial units (Nastev, et al., 2016).

To assess site-specific seismic amplification, SM is performed using a combination of field-based techniques (e.g., ambient noise measurements with HVSR and Multichannel Analysis of Surface Waves (MASW) methods), laboratory analyses (e.g., resonant column or cyclic triaxial tests, which provide small strain shear modulus and damping that control the soil's spectral and frequency response), ground response analysis (GRA), and empirical modeling based on site proxies such as average shear wave velocity over the top 30 m (V_{s30}), average shear wave velocity for the soil column (V_{savg}), fundamental site period (T_0) etc. V_{s30} has been widely used as a simple response metric for sites since the late 1990s (Borcherdt, 1994). While it effectively captures broadband amplification, it does not account for frequency-specific resonance, impedance contrast, and three-dimensional effects (Molnar et al., 2020). Despite these limitations, V_{s30} remains the standard for mapping site effects and is adopted in Canada's building and bridge design codes (Natural Resources Canada, 2020).

Seismic microzonation studies in Eastern Canada applied geological and geophysical models to characterize the spatial variability in site parameters, including V_{s30}, $V_{savg,}$ and T_0. Most research focuses primarily on microzonation of site parameters. For example, V_{s30}-based map was developed by Motazedian et al. (2011) in Ottawa; Leboeuf et al. (2013) in Québec City and Rosset et al. (2015) in Montreal. (Mihaylov, 2011; Nastev et al., 2016) created regional V_{s30} and T_0 maps across the St. Lawrence Lowlands. In Saguenay, advanced methods integrating probabilistic 3D V_s modeling and multi-parameter site classification were applied by Salsabili et al., (2021, 2023) to improve amplification hazard mapping. As a result, the seismic microzonation of hazard-specific site amplification, derived from these site parameters, remains limited and requires further investigation to support advanced seismic hazard assessment.

The objective of the present study is to develop a detailed level III seismic microzonation map of site amplification, enhancing the current seismic hazard model for Saguenay, Canada. The region is characterized by its complex Quaternary stratigraphy, featuring varying glacial and post-glacial sediments, as well as uneven bedrock topography. The strong impedance contrast between bedrock and surficial deposits makes the area particularly susceptible to seismic amplification (Hossain et al., 2023, 2024). We first conducted a comprehensive 1D ground response analysis on 50 soil profiles, utilizing site-specific geotechnical properties and ground motion records. Next, we quantified the seven key site response proxies as V_{s30}, V_{savg}, shear wave velocity ratio of rock and soil (V_f), nonlinear sit period (T_{NL}), total soil thickness (H_{soil}), total thickness of postglacial soils (H_{pg}), and total thickness of glacial soils (H_{till}) that capture amplification patterns derived from the GRA. We then developed 7 site amplification correlations using individual single proxies and 120 site amplification correlations using proxy combinations to predict future amplification in the region. Finally, to produce a detailed seismic microzonation based on site amplification, we applied the best correlations into the site classification framework proposed by Salsabili et al., (2021, 2023) where he developed site parameter maps.

5.3 Seismic microzonation process

In general, the SM process follows a multi-level approach, progressing through increasingly detailed and comprehensive investigations (ISSMGE, 1993). Level I is a preparatory level where broad-scale geological, geophysical, and geotechnical subsoil modeling is conducted using existing data, typically at a scale of 1:1,000,000. This is followed by Level II, which incorporates empirical evaluations based on national codes and site-specific parameters, such as V_{s30} and T_0, derived from in-situ geophysical measurements at a finer scale of 1:50,000. Level III involves a detailed experimental or numerical evaluation, focusing on microzonation based on hazard amplification, with scales ranging from 1:25,000 to as fine as 1:5,000. Figure 53 illustrates the general methodology employed in seismic microzonation studies. This stepwise framework ensures increasingly accurate and location-specific seismic microzonation through progressively detailed data and analysis.

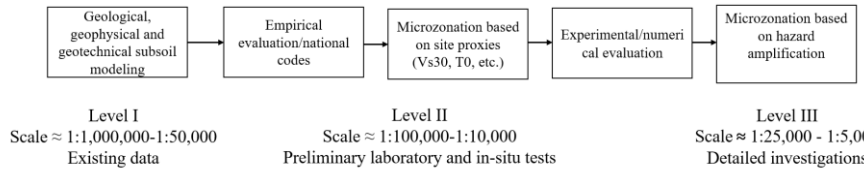

Figure 53. General Methodology for Seismic Microzonation Mapping (ISSMGE, 1999)

Recently, the Saguenay region underwent seismic microzonation analyses. Level 1 (geological, geophysical, and geotechnical subsoil modeling) was conducted by Foulon et al., (2018); Salsabili et al., (2021, 2022); Sanou et al., (2022). Level II (empirical evaluation and microzonation based on national codes and site proxies) was conducted by Salsabili et al., (2021, 2023). The present study focuses on Level III (experimental/ numerical hazard evaluation and microzonation), which involves detailed microzonation based on hazard-specific amplification. In this phase, representative subsoil profiles and input ground motions were selected and employed in 1D nonlinear ground response analyses to simulate seismic behavior under strong seismic bedrock shaking. Site amplification factors (the ratio of the surface response to bedrock motion) were computed for the different soil profiles. To generalize amplification behavior across the entire study area, the effectiveness of the seven site proxies was evaluated for amplification modeling. Based on computed amplification values, empirical correlation equations for both single- and multiple-proxy cases were developed in the form Amp = f (Site Proxy) and the optimal correlation was selected. This equation enabled the extrapolation of amplification values across the region using the spatial distribution of the proxy data and the generation of amplification-based seismic microzonation that reflects site-specific seismic responses. The methodology employed in this study is illustrated in Figure 54.

Results compared site amplification from GRA with the results from nearby regions, and also using different software applied to the same area, as explicitly illustrated in (Hossain et al., 2025). The predicted site amplification from the empirical model was compared with the actual GRA results and the NBCC amplification factors. A detailed comparison across a 20 km cross-section is also presented in Section 7 of the present article.

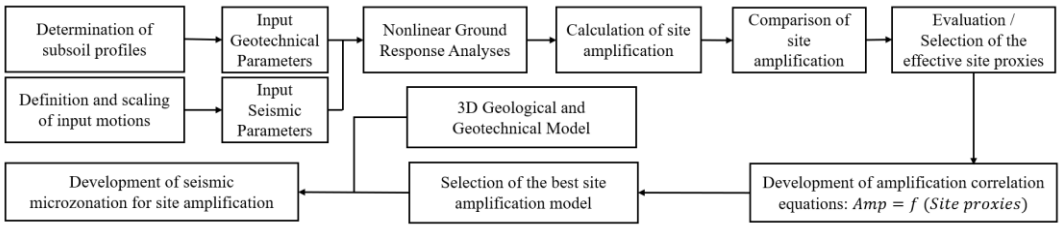

Figure 54. Flowchart of the proposed methodology for seismic microzonation mapping based on hazard amplification

5.4 Seismicity of Saguenay

Saguenay is situated approximately 200 km north of Québec City. It serves as a regional commercial and administrative center, with a population of around 147,100 (Foulon et al., 2018). Most of the

region lies within the seismically active Saguenay graben, considered as a part of the broader Charlevoix-Kamouraska Seismic Zone (CSZ). CSZ is seismically the most active region in eastern Canada, located about 50 km southeast of Saguenay along the St. Lawrence River (Foulon et al., 2018). Several historic earthquakes have been generated there, exceeding magnitude 6, including the 1663 (M 7), 1791 (M 6), and 1925 (M 6.2) events. Figure 55a illustrates historical earthquake data, color-coded by magnitude in the CSZ region. The 1988 Saguenay earthquake (M 5.9), one of the strongest recent earthquakes in eastern North America (Figure 55b), underscores the importance of accurately evaluating seismic hazard, including local amplification due to the complex geology of the Saguenay region [34]. As illustrated in Figure 55b, the entire region falls under the red-marked zone of the MMI scale: VI-VII.

The urban area is situated mainly on the south shore of the Saguenay River on a relatively flat terrain bordered by a hilly relief that descends sharply towards the river. It is underlain by Precambrian bedrock of the Grenville Province, with a complex sequence of glacial and postglacial sediments on top, including glacial till, glaciomarine clays, deltaic sands, and alluvial deposits. At the base of the Quaternary sequence, up to 10 m thick till sediments are ubiquitous across the study area. They are covered by relatively soft postglacial sediments: fine Laflamme sea sediments, silty clays, and recent sandy alluvial sediments. Such a stratigraphic sequence contributes to the region's strong impedance contrast at the rock interface and a weaker one at the interface between glacial and postglacial sediments.

a) b)

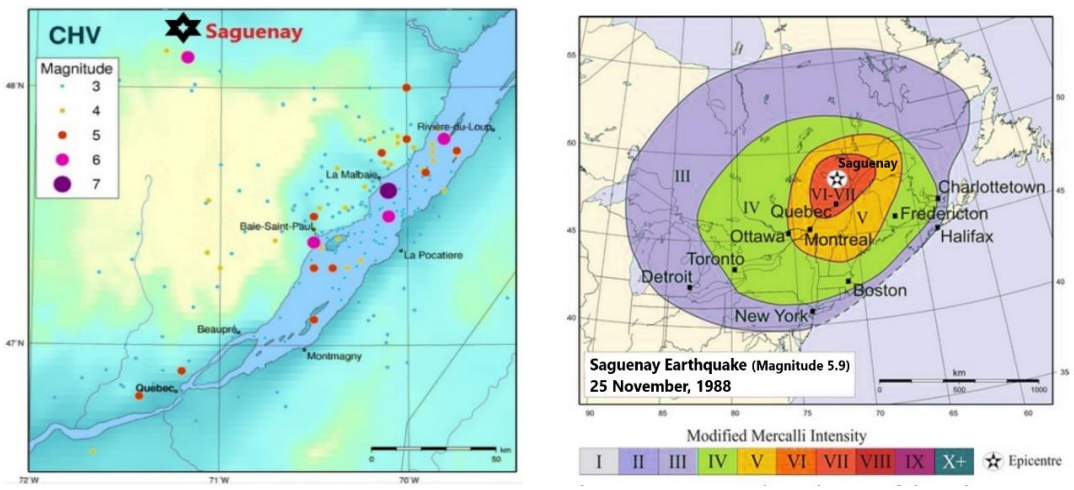

Figure 55. Seismicity of Saguenay a) Historical earthquakes in the zone of CSZ b) MMI during the Saguenay 1988 earthquake (Modified from Natural Resources Canada, 2024)

5.5. Nonlinear ground response analysis

Based on the previous work by Salsabili et al. (2023), where 3D geological and geotechnical V_s models for Saguenay were generated, 50 typical 1D soil profiles were selected. The soil profiles were selected from the four cross-sections, shown in Figure 53, based on the vertical distribution and thickness of the four surficial components considered: sand, gravel, clay, and till. In Figure 56a, the thickness refers to the depth of the crystalline Precambrian bedrock, and the map covers the entire Saguenay area. A total of 50 stratigraphic soil profiles were retrieved, equivalent to approximately 10-15 profiles per cross-section. These 50 profiles were chosen to span the full range of surficial thicknesses and geological conditions present across the Saguenay region, ensuring representative coverage of the area's stratigraphic variability. Ground response analyses were conducted using six ground motions, each scaled to two seismic hazard levels. The nonlinear time domain simulations were carried out using the open-source software DEEPSOIL v7.0 (Hashash et al., 2020). The soil model for each simulation was prepared by discretizing the total depth to bedrock into 1-meter intervals and assigning density, V_s, shear modulus reduction, and damping ratio curves to each depth interval. The Modified Hyperbolic (MKZ) model was adopted to represent the nonlinear stress–strain relationship (Konder & Zelasko, 1963; Matasović & Vucetic, 1993). The Modular reduction and damping (MRD) procedure proposed by Hashash et al. (2010) was selected to achieve the best simultaneous fit for both the modulus reduction and damping curves, and the Flexible time-step option with a maximum strain increment of 0.005 (%) was used. The small-strain damping was defined using the formulation proposed by Hashash & Park, (2001), and the hysteretic (unload–reload) behavior was modeled following the Masing Rules.

a)

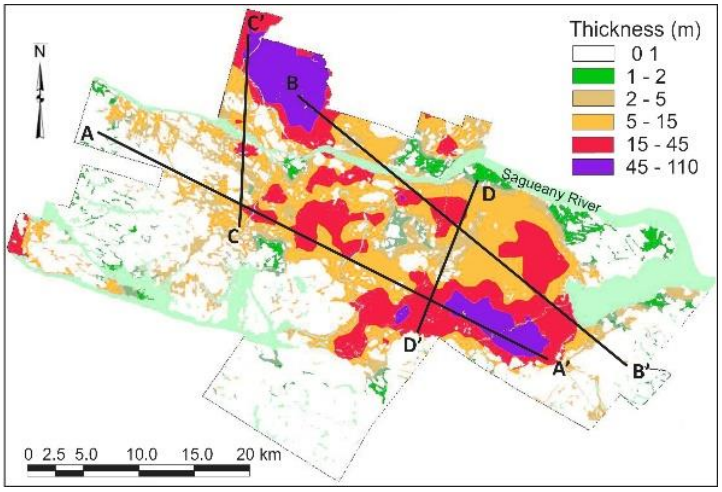

b)

M1	M2	M3	M4	M5	M6	M7	M8	M9	M10	M11	M12	M13	M14	M15	M16	M17	M18
8m	10m	30m	10m	2m	4m	16m	4m	14m	30m	4m	10m	24m	6m	14m	16m	6m	80m
Rock	Rock	Rock	2m	Rock	Rock	Rock	4m	4m	4m	4m	4m	48m	22m	6m	66m	6m	20m
			Rock				Rock	Rock	Rock	Rock	Rock	Rock	4m	2m	10m	Rock	6m
													Rock	Rock	Rock		Rock

M19	M20	M21	M22	M23	M24	M25	M26	M27	M28	M29	M30	M31	M32	M33	M34	M35	M36
4m	16m	28m	4m	8m	12m	4m	30m	26m	12m	86m	106m	12m	6m	6m	20m	6m	8m
Rock	Rock	Rock	2m	4m	4m	14m	3m	8m	32m	2m	2m	40m	14m	Rock	Rock	2m	2m
			Rock	Rock	Rock	Rock	Rock	4m	4m	Rock	Rock	4m	Rock			Rock	Rock
								Rock	Rock			Rock					

M37	M38	M39	M40	M41	M42	M43	M44	M45	M46	M47	M48	M49	M50
10m	16m	22m	48m	5m	8m	10m	20m	22m	24m	150m	120m	80m	80m
2m	2m	2m	2m	Rock	Rock	Rock	18m	23m	36m	Rock	15m	70m	40m
Rock	Rock	Rock	Rock				Rock	Rock	Rock		Rock	Rock	15m
													Rock

Gravel
Sand
Clay
Till
Rock

c)

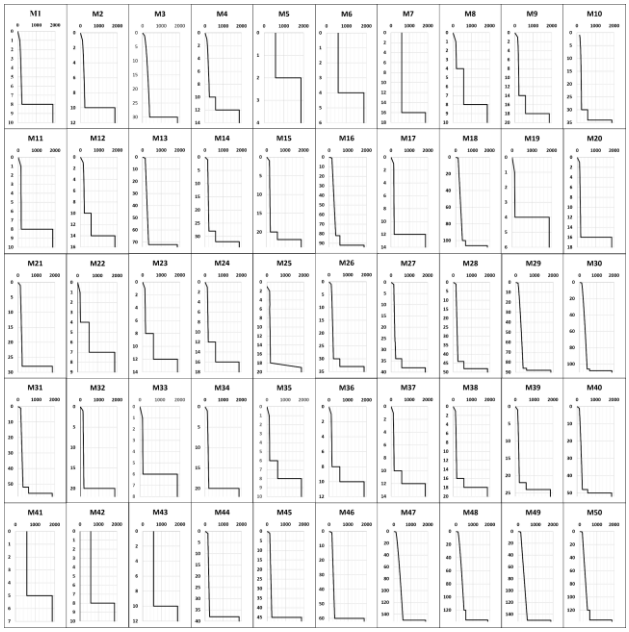

Figure 56. Thickness of surficial deposits with four cross-sections used for selection of soil profiles in the site response analyses (modified from Salsabili et al., 2022), b) Selected 50-1D soil profiles, and c) V_s profiles of selected soil models.

The resulting seismic amplification (SA) in each simulation was defined as the ratio between the computed response spectral accelerations (S_a) at the soil surface and those of the input ground motions at the bedrock level ($S_a(T)_{soil}/S_a(T)_{rock}$) (Harmon et al., 2019; Hashash et al., 2018; Ilhan et al., 2024; Talukder et al., 2021). The final amplification for each model was determined as the geometric mean of the results obtained from six input motions at each hazard level.

In Table 9, representative input parameters are given for each geologic unit. The reference shear modulus and damping ratio curves are shown in Figure 57. In the simulations, bedrock was considered an elastic half-space with a specified density and shear wave velocity. The analysis considers two earthquake scenarios with moment magnitudes of M6 and M7. They represent the

seismic hazard scenarios for the Saguenay area, with corresponding 475-year (10%/50yrs PE) and 2475-year (2%/50yrs PE) return periods. As a result, four synthetic ground motions were selected for a source-to-site distance of approximately 30–60 km (Atkinson, 2009). In addition, two real earthquake records from eastern Canada were included: the 1988 M5.9 Saguenay earthquake recorded in downtown Saguenay at an epicentral distance of 35 km and 29 km below the ground surface (Lefebvre et al., 1992), and the 2010 M5.1 Val-des-Bois earthquake recorded at 22 km below the epicenter located near Val-des-Bois, Québec (Atkinson & Assatourians, 2010). Figure 58 (a) displays the initial acceleration time histories. The ground motions were then scaled to match the National Building Code of Canada (NBCC) 2020 target spectra using the SeismoMatch program following the period band of 0.05s to 10.0s. The matched response spectra are shown in Figure 58(b). According to Pagliaroli and Lanzo (2008), scaling factors exceeding 4 are not recommended. While spectral matching allowed proper scaling for most motions, the Val-des-Bois record was restricted by its inherently low magnitude.

Table 9. Geotechnical and dynamic properties of soil and rock.

	Density (kN/m^3)	Shear Wave Velocity vs. Depth (m/s)	Shear Modulus Reduction and Damping Ratio curves
Clay	18.7 (Sanou et al., 2022)	$V_s = 114.5 + 9.4 \times D^{0.76}$ (Salsabili et al., 2023)	(Abdellaziz et al., 2023) (PI 15)
Sand	17.5 (Sanou et al., 2022)	$V_s = 144.9 + 2.55 \times D$ (Salsabili et al., 2023)	(EPRI, 1993)* (Mean of 0 to 78m)
Gravel	18.3 (Rollins et al., 1998)*	$V_s = 46.861 + 61.55 \times D^{0.5}$ (Salsabili et al., 2023)	(Seed et al., 1986)*
Till	21.0 (Urgeles et al., 2002)	$V_{Still} = 580$, $\sigma = \pm 174$ (Motazedian et al., 2011)*	Hydro Quebec (internal communication)
Rock	28.0 (Saeidi et al., 2021)	$V_{Srock} = 1875$, $\sigma = \pm 781$ (Ladak et al., 2021) *	N/A

Data indicated with `*` are from studies in other regions. The G/G_{max} and Damping Ratio (DR) curves are well described in Hossain et al. (Hossain et al., 2025)

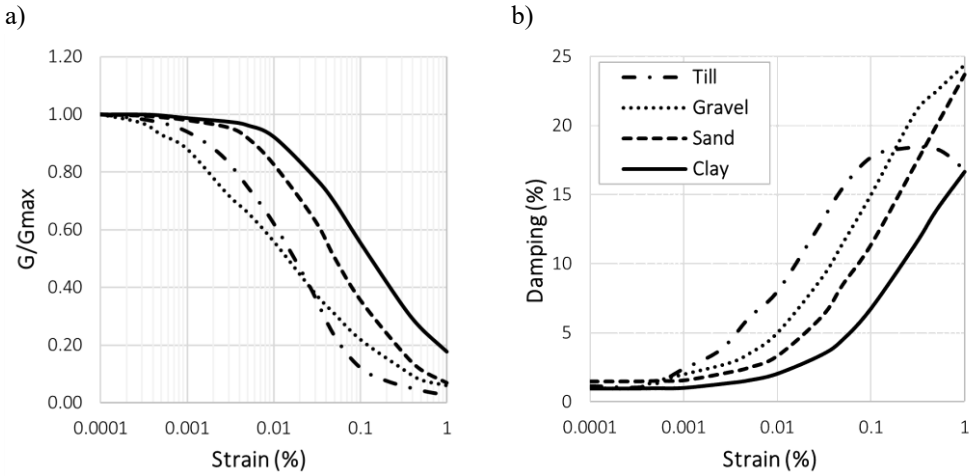

Figure 57. Soil nonlinear reference curves used in the ground response analysis: a) Shear modulus reduction (G/G_{max}) versus shear strain, and b) Damping ratio versus shear strain

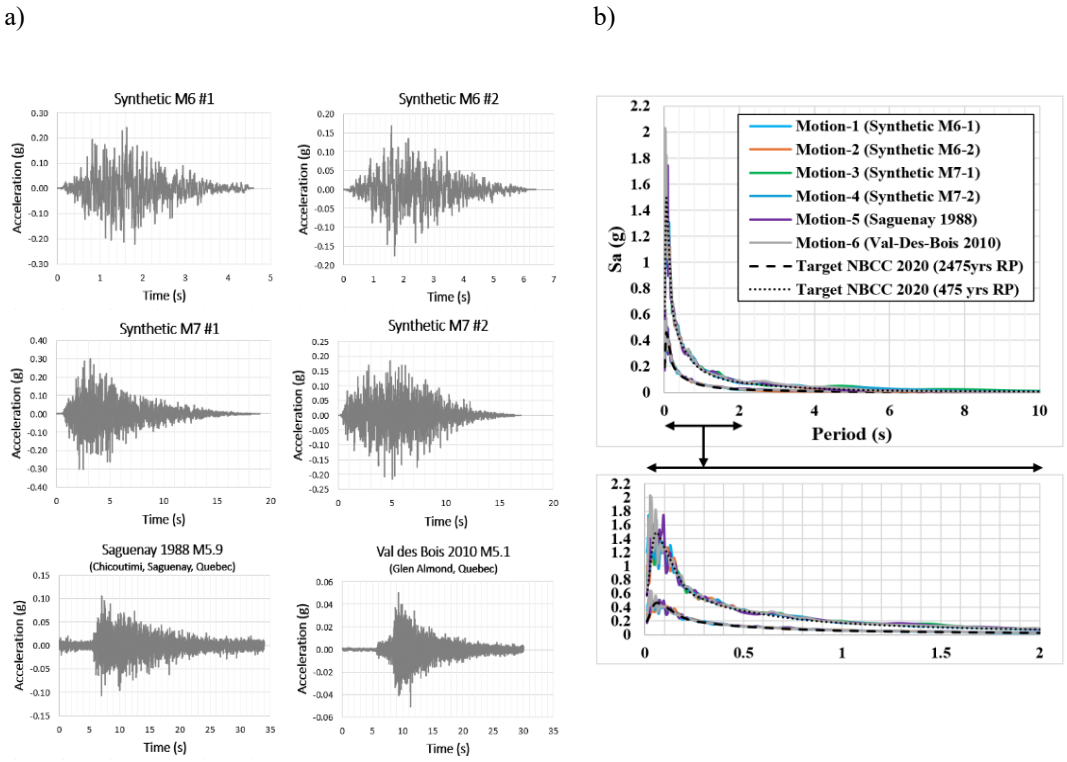

Figure 58. a) Time histories of the unscaled input ground motions b) Spectral acceleration of the scaled motion and NBCC 2020 target hazard

The resulting seismic amplification values (SA) across a range of periods for 50 soil profiles, for both 2%/50-yrs PE and 10%/50-yrs PE scenarios, are illustrated in Figure 59. The gray lines represent the geometric mean amplification from six surface responses of soil profiles, while the black line shows the mean value across the 50 soil models. It was observed that amplification values are higher for the 10%/50-year PE scenario than for the 2%/50-year PE, due to increased damping resulting from higher motion amplitudes at higher hazard levels. As shown in Figure 59, de-

amplification occurs at short periods for both hazard levels, but shifts depending on shaking intensity. Under the less severe hazard (10%/50 yr), de-amplification is limited to shorter periods (≈0.03 s). In contrast, for the more severe hazard (2%/50 yr), stronger nonlinearity causes de-amplification to extend toward prolonged periods (≈0.1 s). The maximum amplification values in the nonlinear analysis were approximately 4 for the 2%/50-year PE and around 5 for the 10%/50-year PE. Soil profiles with lower thickness and lower average shear wave velocity have shorter fundamental periods, which leads them to amplify low-period motions. In contrast, soils with higher fundamental periods amplify high-period (low-frequency) motions. The objective of this paper was to derive amplification values based on site parameters; therefore, a detailed evaluation of amplification for different soil profile types is not included, beyond the general overview provided above. As can be seen in Figure 59, the shape of the amplification curves remains similar for both hazard levels; what changes are the amplification amplitudes. The soil response in Figure 59a is in deep nonlinearity due to the higher input accelerations, where larger strains induce higher damping ratios resulting in lower SAs. SAs shown in Figure 59b are larger since the lower input accelerations induce more minor strains and damping ratios.

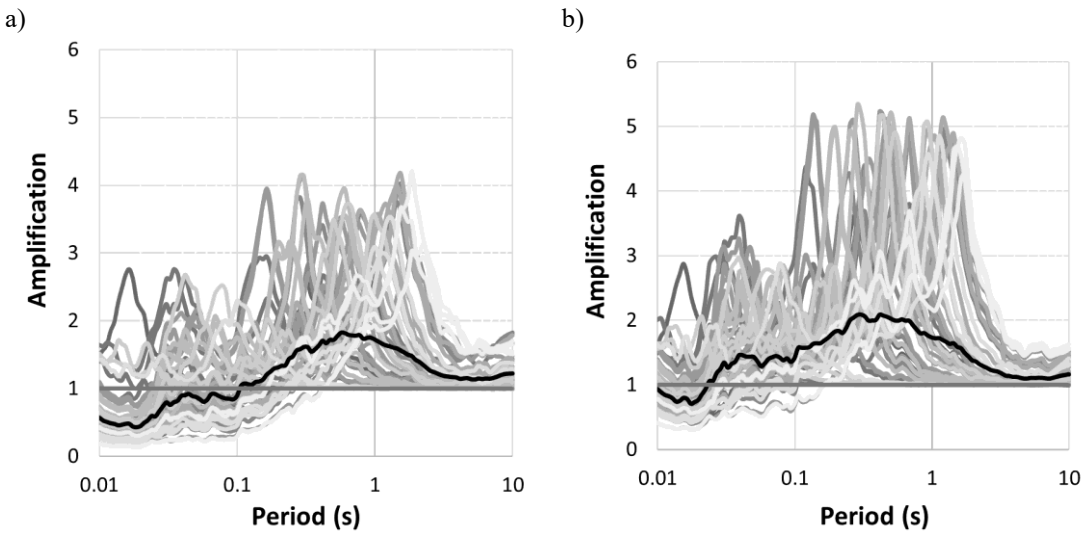

Figure 59. Nonlinear Seismic Amplification (SA) for 50 1D soil profiles of Saguenay for hazard levels with a)2%/50 yrs PE, b) 10%/50 yrs PE. (The black bold line is the mean amplification of the 50 soil profiles).

5.6 Site parameters considered

The next step, following the determination of the seismic amplifications for a range of spectral periods between 0.01 and 10 s, consisted of selecting site parameters that would correlate best with

SAs. A site parameter (proxy) refers to a measurable or derived parameter from the local site conditions that captures soil profile behavior during seismic shaking and can be used to represent the amplification model. The commonly used primary site parameters that can be directly correlated to the site amplification as proxies include V_{s30}, V_{savg}, $T_{0,}$ and H_{soil} (Stambouli et al., 2017). T_0 is the most accessible parameter in field measurements and has a vital role in linear analysis. However, a fully nonlinear site response analysis was performed to accurately capture the soil's dynamic behavior, which exhibits a distinct period shift toward longer values corresponding to the maximum amplification. This shifted fundamental period, defined as the nonlinear site period (T_{NL}), represents the effective period of the soil under nonlinear deformation conditions, replacing the small-strain fundamental period (T_0). The empirical relationship for T_{NL}, developed by Hossain et al., (2025), is presented in Equations 5.1 and 5.2. Their frequency distribution histograms for 50 soil profiles are shown in Figure 60. Since a relatively thin and stiff glacial till layer exists between the post-glacial sediments and bedrock, as shown in Figures 60b and 60c, which necessarily impacts site amplification as shown by Hossain et al., (2025), separate thicknesses of the post-glacial soils (H_{pg}) and glacial soils (H_{till}) were considered as secondary parameters. The presence of this thin, stiff layer over the bedrock can shift the impedance contrast and alter the fundamental resonance characteristics, thereby influencing the overall amplification response (Hossain et al., 2025). In this study, H_{till} typically varies between 2m and 8m. This means that they are correlated to the seismic amplification in combination with primary parameters. In addition, the rock-to-soil ratio (V_{srock} to soil V_{savg}, V_f) was included among the secondary site parameters. The final list of 7 site parameters considered to represent the site amplification is given in Table 10.

$$T_{NL}\text{-}2\%/50\text{yrs PE} = 1.13 * T_0^{0.82} \quad (5.1)$$

$$T_{NL}\text{-}10\%/50\text{yrs PE} = 0.98 * T_0^{0.86} \quad (5.2)$$

a) b) c)

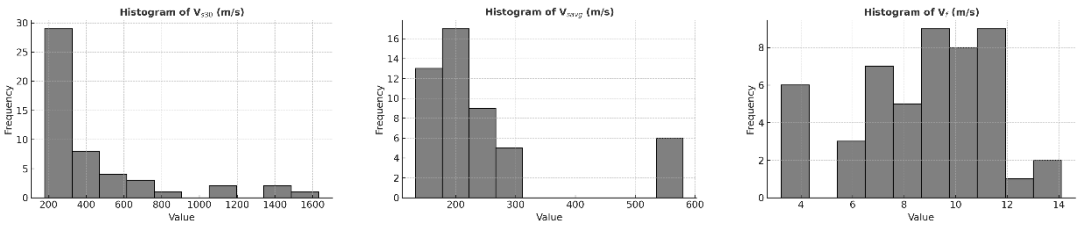

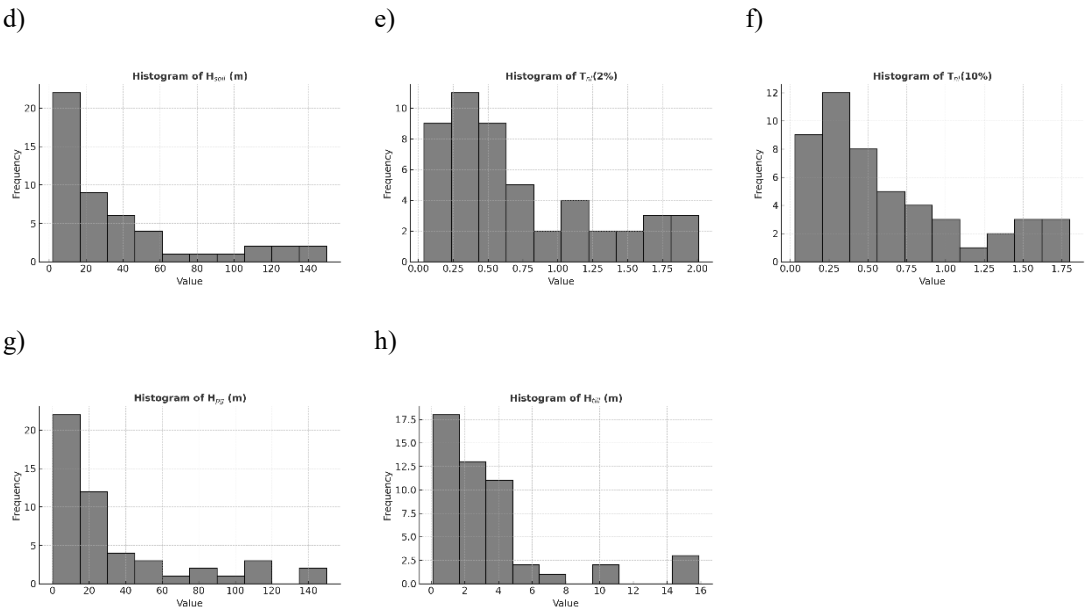

Figure 60. Frequency distribution histograms: a) shear wave velocity of top 30 m V_{s30}, b) average shear wave velocity of soil sediments on top of bedrock V_{savg}, c) V_{Srock} to V_{Savg} ratio V_f, d) total soil thickness H_{soil}, e) nonlinear site period T_{nl} (2%/50yrs), f)nonlinear site period T_{Nl} (10%/50yrs), g) thickness of post-glacial soils H_{pg} and h) thickness of glacial soils H_{till}.

Table 10. Selected site parameters for modeling site amplification

Sl No.	Site parameter		Symbol
1	Average shear wave velocity over the top 30 m	primary	(V_{s30})
2	Average shear wave velocity	primary	(V_{savg})
3	Nonlinear site period	primary	(T_{NL})
4	Total soil thickness	primary	(H_{soil})
3	The ratio of rock and soil shear wave velocity	secondary	(V_f)
6	Thickness of post-glacial soils	secondary	(H_{pg})
7	Thickness of glacial soils	secondary	(H_{till})

5.7 Empirical correlations between site parameters and SA

In our previous study by Hossain et al. Hossain et al., (2025), we have shown that the linear relationship between site amplification and single-site proxies is not well at all periods. So, develop the empirical correlation between selected site parameters and SA, firstly, we determined the nonlinear logarithmic correlation between amplification and all seven individual proxies: V_{s30}, V_{savg}, V_f, T_{NL}, and H_{soil}, H_{pg}, and H_{till} as a single proxy at both hazard levels for vibration periods of: 0.01s, 0.1s, 0.2s, 0.5s, 1.0s, 5.0s, and 10.0s, and the R^2 values are presented in Figure 61. It is observed that V_{s30} serves as a good proxy for very short periods, with an R^2 value of more than 0.8, whereas T_{NL} and H_{soil} surveys are more effective beyond 2.0s, where the R^2 is within 0.6-0.8. T_{NL}, H_{pg}, and H_{soil} have better R^2 values like V_{S30} at very short periods. Even using logarithmic regression rather than linear regression, no single proxy is suitable across all vibration periods, so we have decided to use multiple proxies together in site amplification modeling to capture site amplification more accurately across all periods.

a)

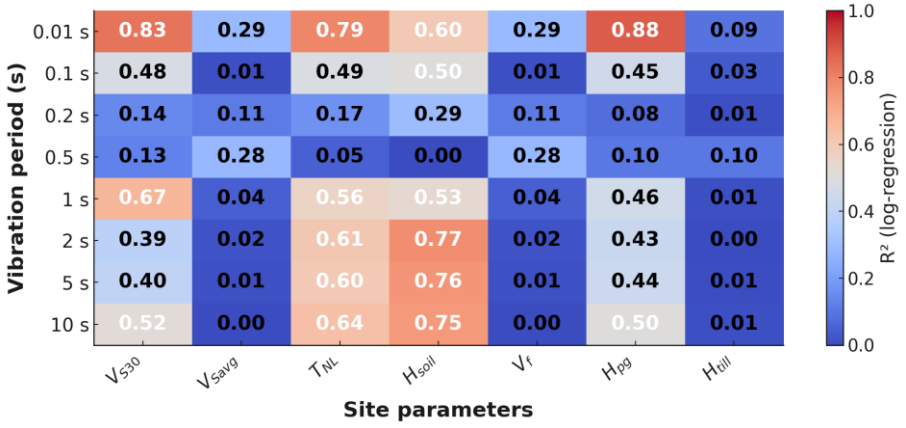

b)

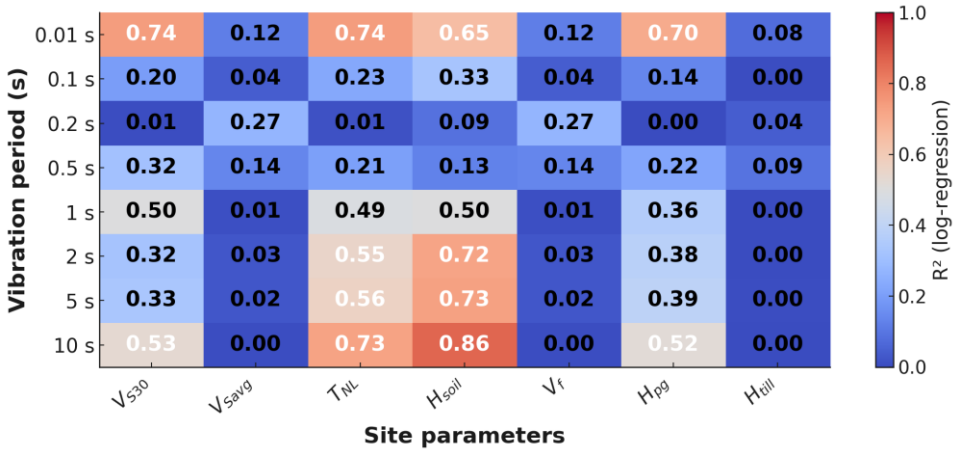

Figure 61. R^2 value of linear correlation between site amplification and different proxies at different vibration periods: a) 2%/50yrs PE, b) 10%/50yrs PE

As the first step of using multiple proxies for modelling site amplification, we checked the multicollinearity between each proxy pair for 50 profiles. The R^2 values between each proxy pair are given in Figure 62. We selected a threshold value of R^2 = 0.8 for assessing collinearity status to ensure minimal multicollinearity among the predictor variables. The collinearity status table is shown in Table 3. From the table, we can see that: Each proxy cannot be used twice in a regression model, and T_{NL}, H_{soil} and H_{pg} cannot be used together in a regression model.

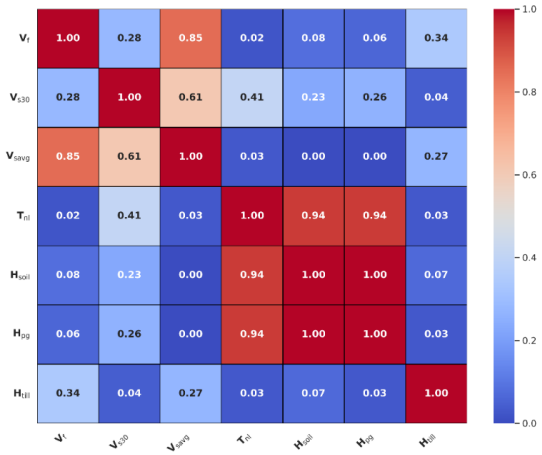

Figure 62. R^2 values between each proxy pair

Table 11. Collinearity status table (✕ indicates collinearity above the threshold R^2 value of 0.9)

	V_f	V_{S30}	V_{Savg}	T_{NL}	H_{soil}	H_{pg}	H_{till}
V_f	✕	✓	✓	✓	✓	✓	✓
V_{S30}	✓	✕	✓	✓	✓	✓	✓
V_{Savg}	✓	✓	✕	✓	✓	✓	✓
T_{NL}	✓	✓	✓	✕	✕	✕	✓
H_{soil}	✓	✓	✓	✕	✕	✕	✓
H_{pg}	✓	✓	✓	✕	✕	✕	✓
H_{till}	✓	✓	✓	✓	✓	✓	✕

As opposed to the standard correlation with a single proxy for SA (e.g., V_{S30}), modern site amplification models express the natural logarithm of amplification, ln(SA), as the sum of linear and nonlinear components (Hashash et al., 2018). The linear component reflects intensity-independent behavior under weak motions, while the nonlinear component captures reductions due to nonlinear soil effects during strong seismic shaking. This study focuses on two specific hazard levels:

2%/50yrs PE and 10%/50yrs PE motions. Therefore, only nonlinear analysis results were considered, and the peak ground acceleration (PGA) was not treated separately, as the hazard level was fixed. The type of nonlinear regression was conducted with logarithmic transformations as shown in Equation 5.3.

$$\ln(Y) = \ln(\beta_0) + \beta_1 \ln(X_1) + \beta_2 \ln(X_2) + \beta_3 \ln(X_3) + \beta_4 \ln(X_4) \quad (5.3)$$

where, Y is site amplification; X_1, X_2, X_3 and X_4 are site parameters (variables); β_1, β_2, β_3 and β_4 are coefficients and β_0 is intercept.

The correlations were developed using regressions that started with two site parameters, V_{s30} and T_{NL}, to which the remaining site parameters were added, for a maximum of seven site parameters. The regression analysis was performed using Python, with libraries such as Pandas, NumPy, StatsModels, and scikit-learn. The correlation equations using multiple site parameters were ranked for each vibration period for both hazards. Overall, the combination of V_{s30}, T_{NL}, $V_{savg,}$ and H_{till} showed the highest R^2 and lowest RMSE values for all periods. The best correlation equation type is given in Equation 5.4. The respective R^2 and RMSE values are presented in Figure 63. At short periods (<0.1 s), R^2 values remain moderate (≈0.6–0.7) with relatively higher RMSE (≈0.25–0.30), indicating greater dispersion between observed and predicted amplifications. In the intermediate range (0.1–1 s), model fit decreases slightly due to increased complexity in soil response, while at longer periods (>1 s), R^2 increases (>0.85) and RMSE decreases (<0.1), reflecting improved agreement. The standard errors and P values of different regression parameters are given as Appendix A.

$$\ln(Amp) = \ln(\beta_0) + \beta_1 \ln(Vs30) + \beta_2 \ln(Tnl) + \beta_3 \ln(Vsavg) + \beta_4 \ln(Htill) \quad (5.4)$$

(Here, V_{s30} and V_{savg} are in m/s, T_{NL} is in s, and H_{till} is in m.)

The values of the coefficients with the best correlation are given in Table 4. The period-dependent behavior of the regression coefficients provides insight into the role of each site proxy in controlling ground motion amplification. The intercept term ln(β_0) peaks around 1 s and dips at more extended periods, reflecting shifts in the baseline amplification level. V_{s30} (β_1) exhibits a strong negative peak at approximately 1 s, indicating its dominant influence on site response at intermediate periods. T_{NL} (β_2) becomes increasingly positive beyond 2.0s, highlighting its role in capturing nonlinear effects at longer periods. V_{savg} (β_3) is negatively correlated at short periods but grows positively after 0.5 s, emphasizing its contribution to medium- and long-period motions. In contrast, H_{till} (β_4) remains

relatively small and stable across all periods, suggesting a consistent but minor effect on amplification behavior.

a) b)

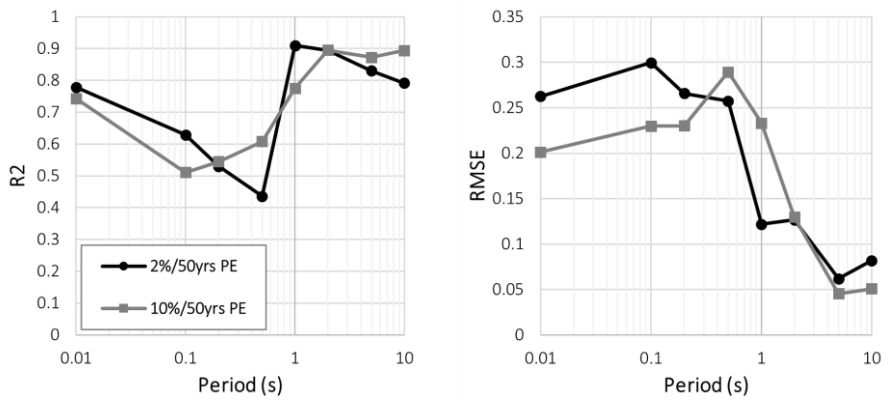

Figure 63. R^2 and RMSE values for the best model (V_{s30}, T_{NL}, V_{savg} and H_{till} combination): a) R2 and b) RMSE

Table 12. Coefficient value for 2% and 10%/50yrs PE

Period (s)	2%/50yrs PE					10%/50yrs PE				
	Parameters					Parameters				
	$\ln(\beta_0)$	β_1	β_2	β_3	β_4	$\ln(\beta_0)$	β_1	β_2	β_3	β_4
0.01	-0.90	0.12	-0.48	-0.12	0.05	-0.18	0.21	-0.24	-0.25	0.05
0.1	0.94	0.32	-0.25	-0.57	0.06	1.42	0.39	0.01	-0.62	0.05
0.2	0.93	0.67	0.15	-0.81	0.03	1.97	0.62	0.27	-0.87	0.02
0.5	5.43	-0.64	-0.38	-0.26	-0.01	6.76	-1.30	-0.54	0.19	-0.04
1	5.58	-1.42	-0.54	0.52	-0.02	3.57	-1.10	-0.22	0.58	-0.02
2	-3.33	0.38	0.69	0.35	-0.02	-4.53	0.65	0.82	0.32	-0.02
5	-1.32	0.16	0.27	0.12	0.00	-1.60	0.25	0.28	0.09	0.00
10	-0.06	-0.09	0.13	0.16	0.01	-0.91	0.07	0.22	0.15	-0.01

An uncertainty analysis was conducted using residual plots (actual vs. predicted) and the bandwidth (upper 95% prediction interval minus the lower 95% prediction interval). Uncertainty was considered as low, medium, and high for the values of: ≤ 0.45, 0.45 to 0.9, and > 0.9. Bandwidth values are shown in Figure 64 for the best model. The scatter plots for the difference between actual and predicted values at various vibration periods are shown in Figure 65. Amplification prediction uncertainty is most pronounced at periods of 0.2 s, 0.5 s, and 1.0 s, particularly for the 10% probability of exceedance (PE) scenario, which consistently shows higher uncertainty than the 2%/50yrs PE case. For instance, at 0.2 seconds (10%/50yrs PE), the model underestimates amplification for sites with approximately 6 meters of soil. At 0.5 s, underestimation occurs around

16–24 m (2% & 10%/50yrs PE), while overestimation is evident at depths of 38–50 m (10%/50yrs PE) as shown in Figure 65d. At 1.0 s under 10%/50yrs PE, the underestimation shifts toward sites with 40–60 m of soil. These uncertainties are reflected in the bandwidth values derived from the residual distribution: at 0.2 s, the bandwidth reaches 1.49 (2%/50yrs PE) and 2.24 (10%/50yrs PE), and peaks at 0.5 s with 2.05 and 3.38, both of which are classified as high uncertainty levels. Even at 1.0 s, bandwidths remain high (1.09 for 2% PE and 2.63 for 10% PE), confirming that the most significant modeling challenges lie within the 0.2–1.0 s range and are more significant under the 10%/50yrs PE condition.

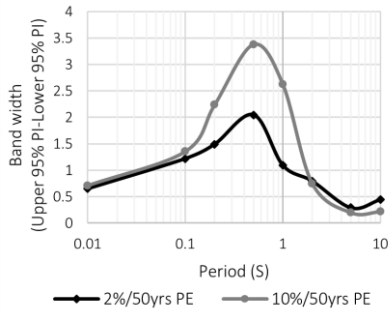

Figure 64. Bandwidth (upper 95% prediction interval - lower 95% prediction interval) for the best site amplification correlation.

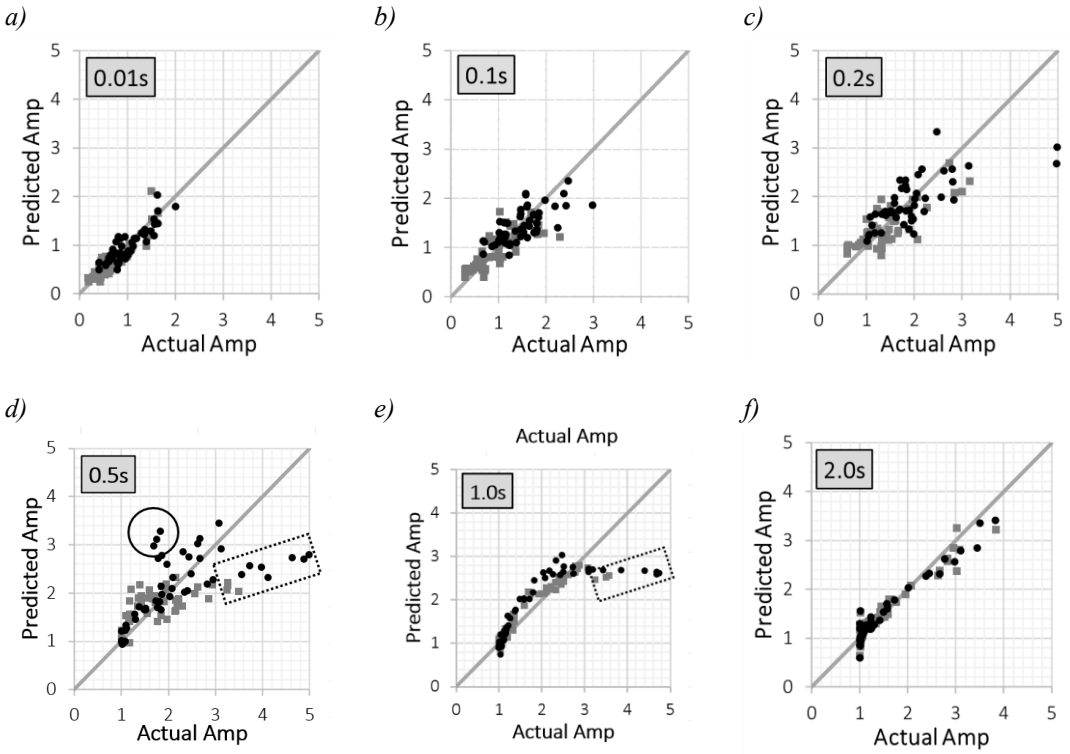

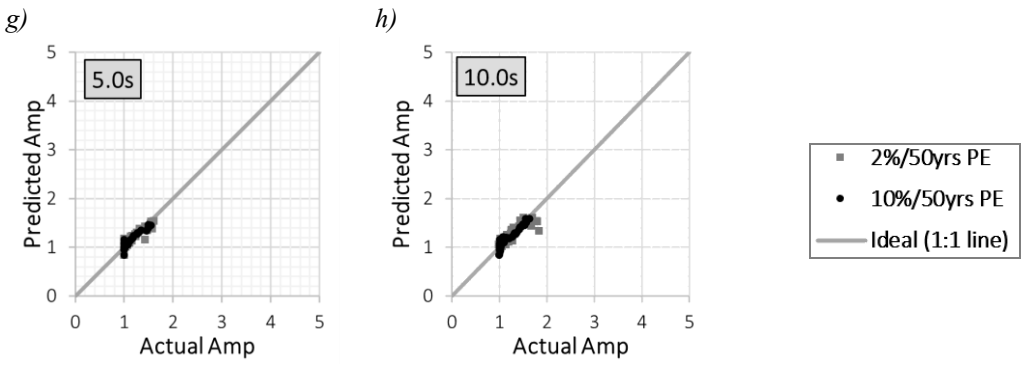

Figure 65. Residual plots (actual vs predicted site amplification) for 2%/50yrs PE and 10%/50yrs PE: a) 0.01s, b) 0.1s, c) 0.2s, d) 0.5s, e) 1.0s, f) 2.0s, g) 5.0s and h) 10.0s.

5.7 Comparison of site amplification predictions

In this section, the predicted site amplifications are compared against the NBCC SA and SA obtained from nonlinear site response analyses. The first comparison with NBCC SAs involves a 20-km cross-section and response periods, T = 0.2s and 1.0s for 2%/50yrs PE hazard. The second comparison involves 300 data points where four typical 1D site profiles were extracted from, and the predicted SA was compared with both NBCC and site amplification from nonlinear site response analyses (Note: these four profiles are independent of the 50 profiles used for model development).

5.7.1 Cross-section

The geology of the study area comprises Precambrian bedrock, stiff glacial till, and soft post-glacial sandy and clayey soils (Salsabili et al., 2021b). The four surficial units exhibit varying V_{s30}, H_{soil}, V_{savg}, and T_{NL}, resulting in distinct site categories according to the employed site categorization methodology. Although the soil thickness approaches zero after ~17.5 km, the computed V_{s30} and V_{savg} values remain slightly lower than the characteristic bedrock velocity. This is due to the presence of a very thin surficial till layer, too small to be shown at the scale of the geological cross-section but still influencing the averages of velocity. To evaluate their efficacy, the resulting site amplification models are compared with the NBCC 2020 SA based on V_{s30} only. The comparison was performed across a representative 20 km cross-section illustrating the geological and geotechnical settings (Figure 66). The best correlation between the proxies: V_{s30}, V_{savg}, T_{NL}, $H_{till,}$ (Equation 5.4) was used to calculate the amplification along the cross-section. The NBCC 2020 site amplification was obtained using the NBCC online tool (https://www.seismescanada.rncan.gc.ca/hazard-alea/interpolat/nbc2020-cnb2020-en.php). By entering soil and rock V_{s30} values, the tool provides corresponding hazard values for different vibration periods, from which the amplification factors

were derived. The empirical amplification factors were subsequently compared with those derived from the NBCC tool. The comparison indicates that very shallow layers within 7km and 17-18km have higher amplification at a short period of 0.2s, where deeper sediments of 7km to 17km have higher amplification at a 1.0s period. NBCC 2020 systematically overestimates amplification at 1.0 s, while at 0.2 s, the bias is not uniform, with NBCC sometimes predicting higher and sometimes lower amplification than the AF-based model. This discrepancy is most evident in areas with thick accumulations of soft sediments—such as clay, sand, and glaciofluvial deposits—between approximately 8 km and 18 km along the profile.

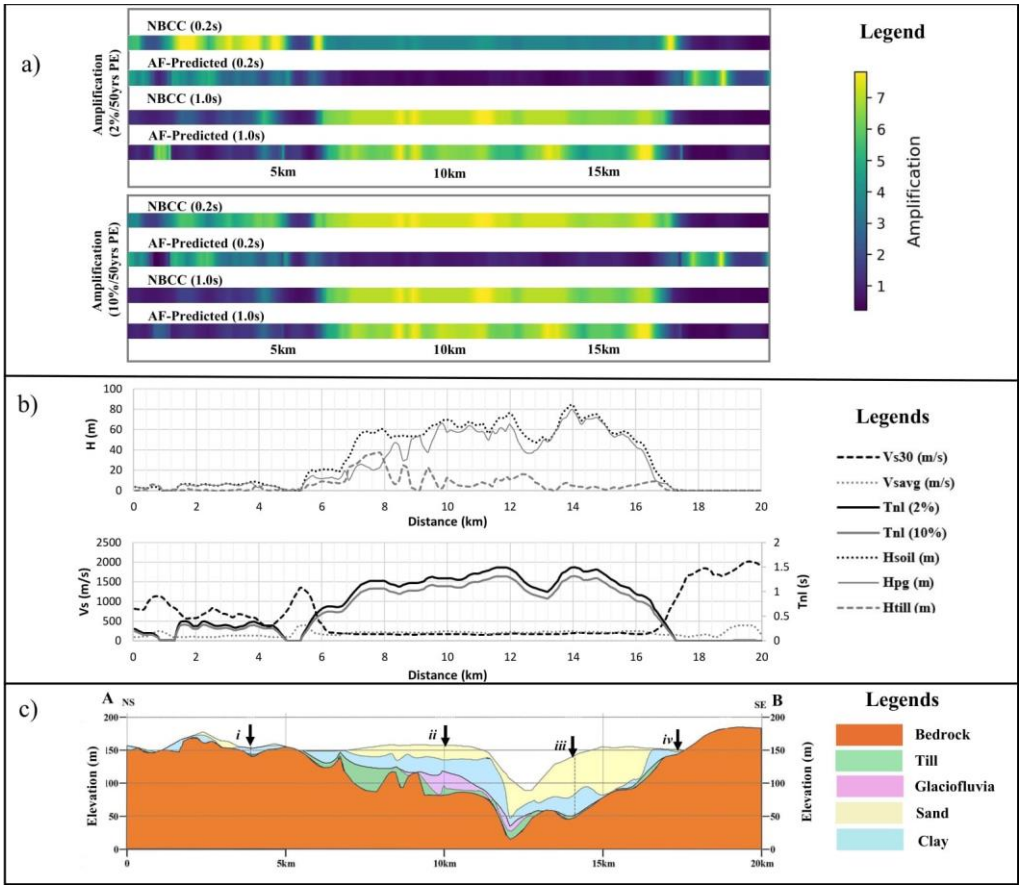

Figure 66. Predicted and NBCC 2020 site amplification and site parameters along a representative cross-section of Saguenay. From top to bottom: (a) site amplification for 0.2 s and 1.0 s periods for 2%/50 yrs PE and 2%/50 yrs PE, (b) site parameters H_{soil}, H_{pg}, and H_{till}, V_{s30}, V_{savg}, V_f, and T_{NL}, and (c) local geology of the cross-section with four stratigraphic columns. Legends are shown on the right side of each figure.

5.7.2 Four soil profiles

The four 1D profiles, indicated by vertical bold arrows in Figure 66, were randomly selected based on different thicknesses for a more detailed comparison of SAs. The profiles vary in terms of total soil thickness, fundamental site period, and other site parameters, as detailed in Table 5. The site amplifications predicted by Equation 5.4 for a range of spectral periods, along with results from GRA, for the 6 input time histories scaled to match the 2%/50 years hazard level, and the SAs according to the NBCC 2020 provisions, are summarized in Figure 67. The uncertainty analysis was performed based on the difference between the upper and lower 95% prediction intervals, as shown in the same Figure.

The amplification comparison of the four selected sites shows that the predicted model aligns well with the numerical GRA results, supporting the validity of the empirical approach. Sites i and iv demonstrate the strongest agreement, reflecting highly consistent representations of site response. In contrast, sites ii and iii show small deviations, particularly within the mid-period range (approximately 0.5–2 s), where site-response predictions are more sensitive to soil-profile thickness and associated uncertainties. Across all profiles, both empirical and GRA models tend to predict lower amplification than the NBCC model beyond 0.5 s, reflecting the NBCC's more conservative estimates. The GRA-derived amplification factors lie within the 95% prediction interval for nearly the entire period range, while the NBCC values show close agreement with the predictions only at periods shorter than 0.5 s.

Table 13. Different site proxies of the selected test soil profiles

Site	**Thickness (m)**					**Shear wave velocity**			**Period (s)**	
	H_{sand}	H_{clay}	H_{pg}	H_{till}	H_{soil}	V_{s30}	V_{savg}	V_f	T_{nat}	T_{nl} (2%)
i	-	32	32	2	34	181	192	9.77	0.71	1.00
ii	32	30	62	8	70	181	232	8.08	1.21	1.56
iii	80	20	100	6	106	182	261	7.18	1.63	1.68
iv	-	10	10	4	14	358	186	10.08	0.30	0.50

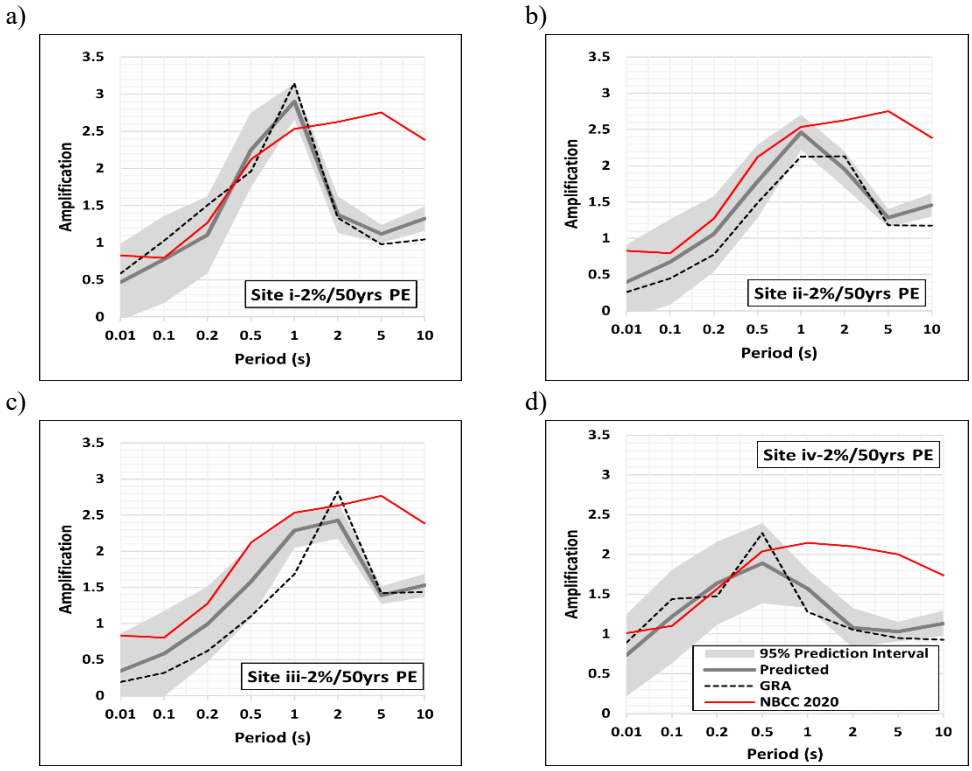

Figure 67. Comparison of site amplification from Ground response analysis (actual), empirical (predicted), and NBCC 2020 for: a) Site i; b) Site ii; c) Site iii and d) Site iv.

An excellent agreement can be observed for sites i, ii, and iii, with R^2 values in the order of 0.8-0.90, indicating a strong correlation and consistent predictive behavior of the developed empirical model. For site iv, the scatter is slightly wider, although the correlation remains reasonably strong ($R^2 \approx 0.72$–0.74), indicating greater variability in shallow and stiffer site conditions. Overall, the high R^2 values reinforce the empirical model's reliability and confirm its ability to capture site-specific amplification trends consistent with analytical predictions.

5.8 Seismic microzonation mapping

A comprehensive seismic microzonation mapping at Level II conducted in the Saguenay region, Eastern Canada, through integration of advanced geological and geotechnical modeling by Salsabili et al. (Salsabili et al., 2023). We conducted detailed seismic microzonation mapping at level III using nonlinear site-response analysis. Based on GRA-based site amplification results, we developed an empirical model to predict site amplification. Combining the empirical site amplification model and previously developed geological and geotechnical models of site parameters, we prepared seismic microzonation maps of site amplification for the Saguenay region.

The spatial distributions of all the site parameters considered in Equation 5.4, V_{s30}, V_{savg}, $H_{till,}$ and T_{NL}, are presented in Figure 68. Figure 68a shows the distribution of V_{s30}, highlighting low-velocity zones (<180 m/s) concentrated in the river valleys and depositional basins around Chicoutimi, La Baie, and parts of Jonquière, while stiffer sediments and rock outcrops dominate the peripheries. Figure 68b illustrates the spatial variability of V_{savg}, which follows a similar pattern, highlighting the contrast between deep, unconsolidated sediments (characterized by low V_{savg}) and the surrounding higher-velocity terrains. Figures 68c and 68d present the computed nonlinear site periods (T_{NL}) at hazard levels of 2%/50 yrs and 10%/50 yrs PE, respectively, showing consistent zones of amplified site response, with dominant periods exceeding 0.54 s in thick sedimentary basins—critical for resonance with mid-rise structures. Finally, Figure 68e illustrates the spatial distribution of till thickness (H_{till}), with localized thick accumulations (up to >7.5 m) underlying key urbanized sectors, particularly near La Baie and parts of Chicoutimi. The presented maps of site parameters in Figure 68 effectively strengthen the foundation for microzonation and seismic risk assessment.

The seismic microzonation map of site amplification was developed by applying the predictive site-amplification model to the spatial distribution of key local site parameters (proxies), namely V_{s30}, T_{NL}, V_{savg}, and H_{till}. The spatial distribution maps for site amplification at 0.2 s and 1.0 s spectral periods are presented in Figures 69 and 70. The amplification distribution derived in this study is generally consistent with the Metro Vancouver Seismic Microzonation Mapping (MVSMMP) national dataset (Assaf et al., 2024d, 2024c, 2024b, 2024a), while reflecting additional local-scale features associated with site-specific geotechnical conditions.

a)

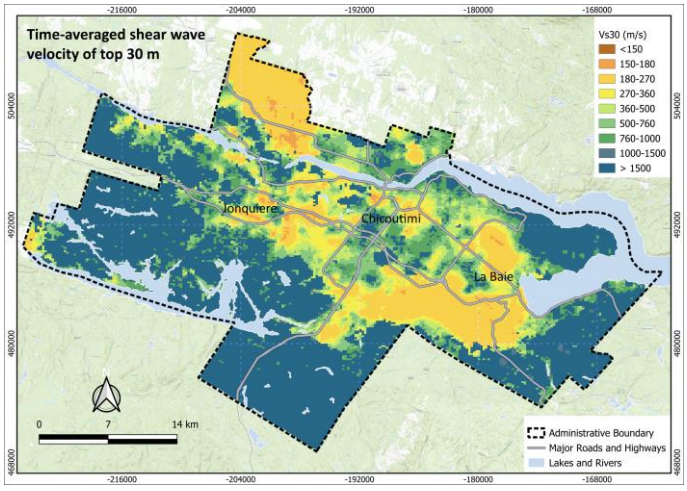

b)

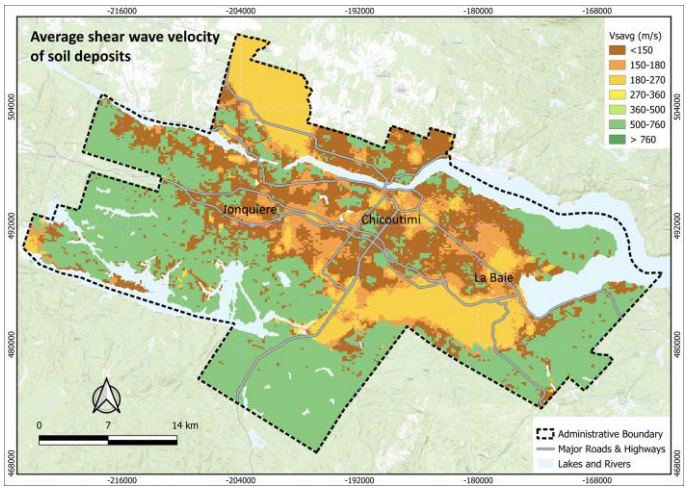
Average shear wave velocity
of soil deposits
Vsavg (m/s)
<150
150-180
180-270
270-360
360-500
500-760
> 760
Jonquiere
Chicoutimi
La Baie
0
7
14 km
Administrative Boundary
Major Roads & Highways
Lakes and Rivers

c)

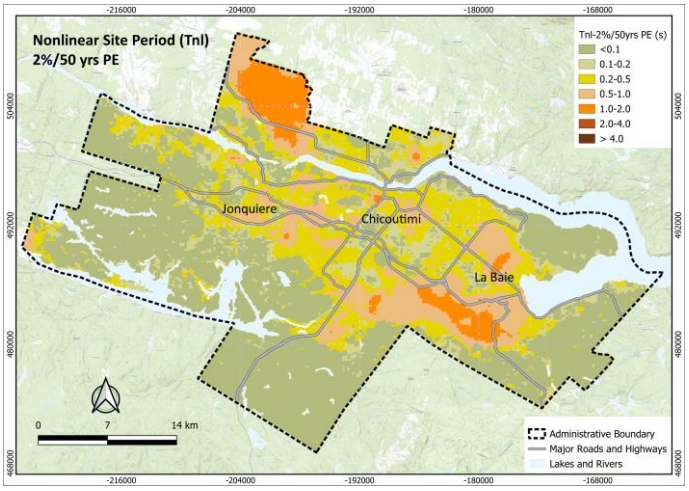
Nonlinear Site Period (Tnl)
2%/50 yrs PE
Tnl-2%/50yrs PE (s)
<0.1
0.1-0.2
0.2-0.5
0.5-1.0
1.0-2.0
2.0-4.0
> 4.0
Jonquiere
Chicoutimi
La Baie
0
7
14 km
Administrative Boundary
Major Roads and Highways
Lakes and Rivers

d)

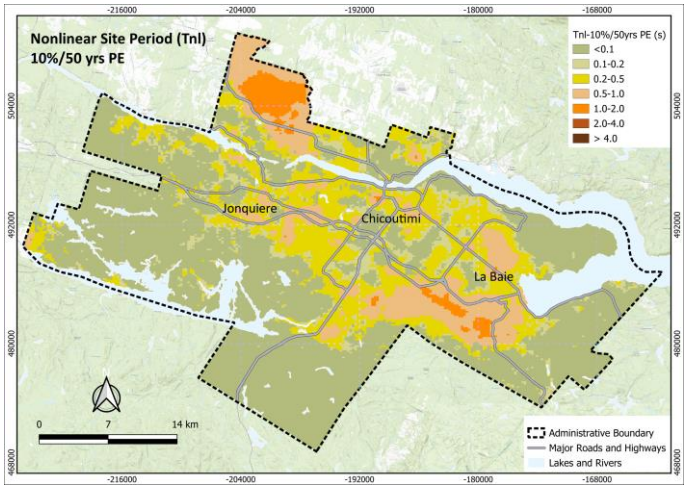
Nonlinear Site Period (Tnl)
10%/50 yrs PE
Tnl-10%/50yrs PE (s)
<0.1
0.1-0.2
0.2-0.5
0.5-1.0
1.0-2.0
2.0-4.0
> 4.0
Jonquiere
Chicoutimi
La Baie
0
7
14 km
Administrative Boundary
Major Roads and Highways
Lakes and Rivers

e)

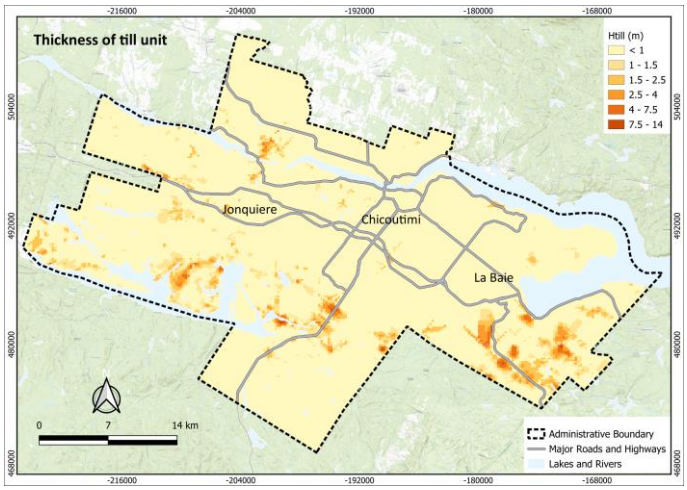

Figure 68. Spatial distribution of a) V_{s30}, b) V_{savg}, c) T_{NL} 2% POE, d) T_{NL} 10% POE, and e) H_{till}

The 0.2-second (2%/50 yrs PE) amplification map (Figure 69a) shows several areas with strong amplification (factors of about 5–8), concentrated in the central Saguenay urban area, the northwestern sector along the Saguenay River, and around Kenogami Lake. These high short-period values are controlled by very soft surficial deposits overlying much stiffer till or bedrock, which create strong shallow impedance contrasts and correspond to the thinner sediment zones in Figure 56a. In comparison, the 1.0-second map (Figure 69b) shows generally lower amplification, with most values between about 1.5 and 3, and the highest responses occurring in areas of thicker Quaternary sediments. A comparison of Figures 56a and 69b shows that long-period amplification increases with total sediment thickness, as the 1-s period is more sensitive to basin depth and geometry. Thus, short-period amplification is dominated by shallow impedance contrasts in the upper deposits, whereas long-period amplification reflects the deeper structure and overall thickness of the sedimentary basin. Similarly, the 10%/50 yrs PE hazard maps for the 0.2-second and 1.0-second spectral periods show higher amplification values than the 2%/50 PE maps (Figure 70). This increase is mainly due to the lower damping associated with weaker input motions, which tends to produce a more linear soil response and therefore greater relative amplification. In the 0.2-second map, several zones—particularly the central and eastern portions of Saguenay exhibit amplification factors approaching or exceeding 8. These high short-period values occur primarily in areas with thin, very soft surficial deposits over stiff till or bedrock, consistent with the shallow sediment zones shown in Figure 56a. The 1.0-second map also shows elevated amplification in parts of the urban core, eastern Saguenay, and northern portions near Saint-Honoré, with values generally between 3 and 5. These long-period

peaks align with the thicker sedimentary regions identified in Figure 56a, reflecting the strong control of total basin depth on the 1-s response and its relevance for taller, more flexible structures.

a)

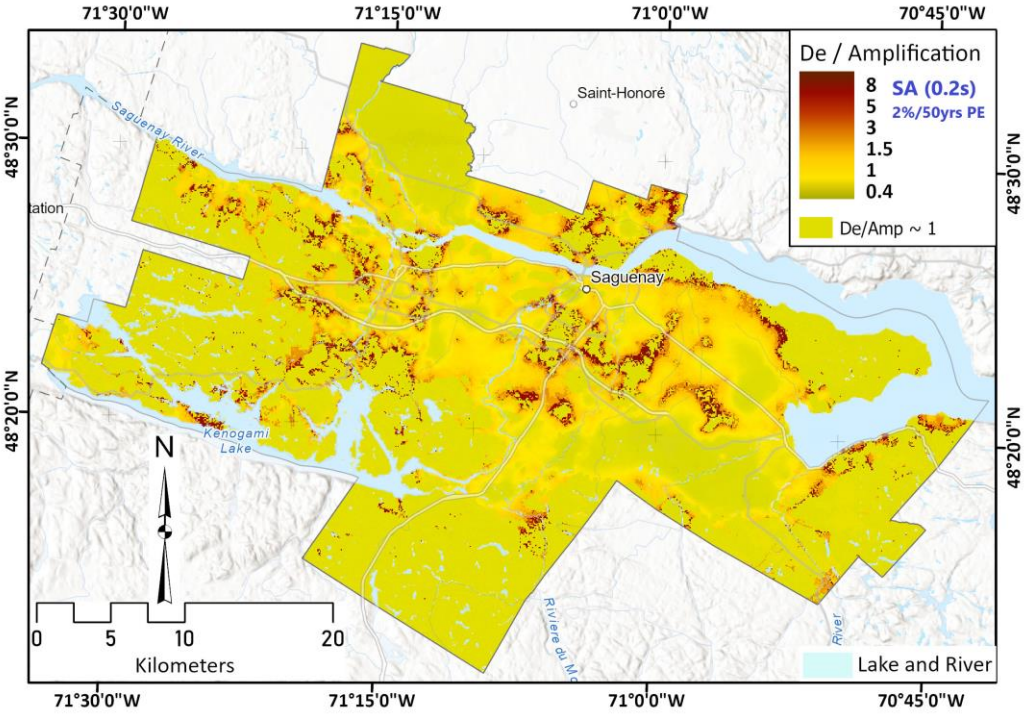

b)

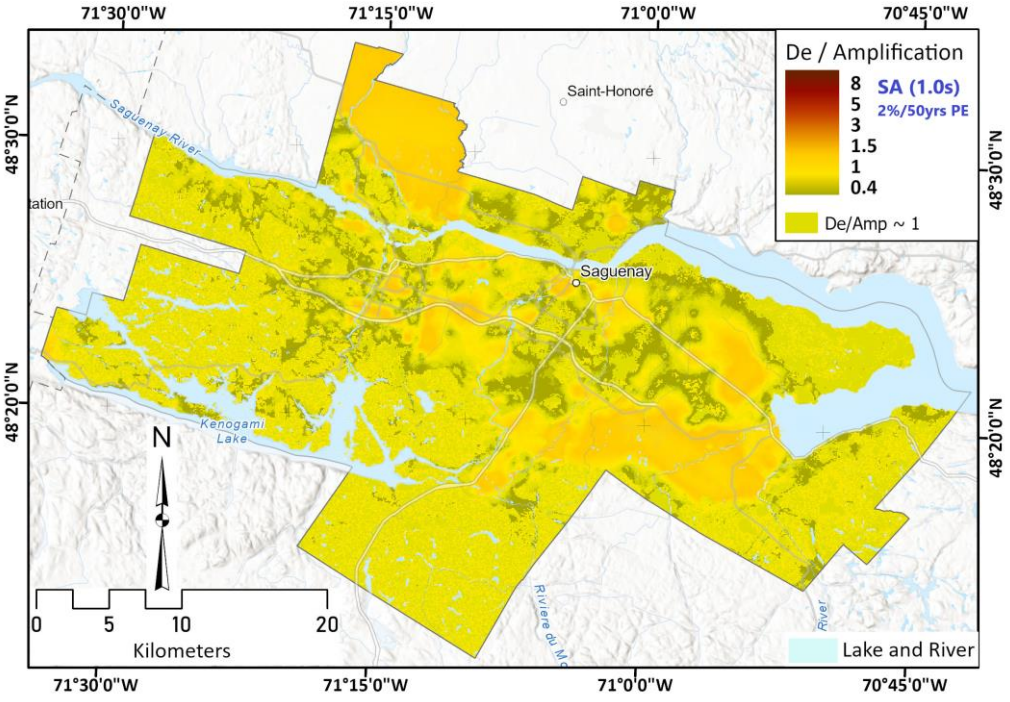

Figure 69. Seismic microzonation maps of site amplification in Saguenay for a 2% probability of exceedance in 50 years: (a) 0.2 s spectral period, (b) 1.0 s spectral period.

a)

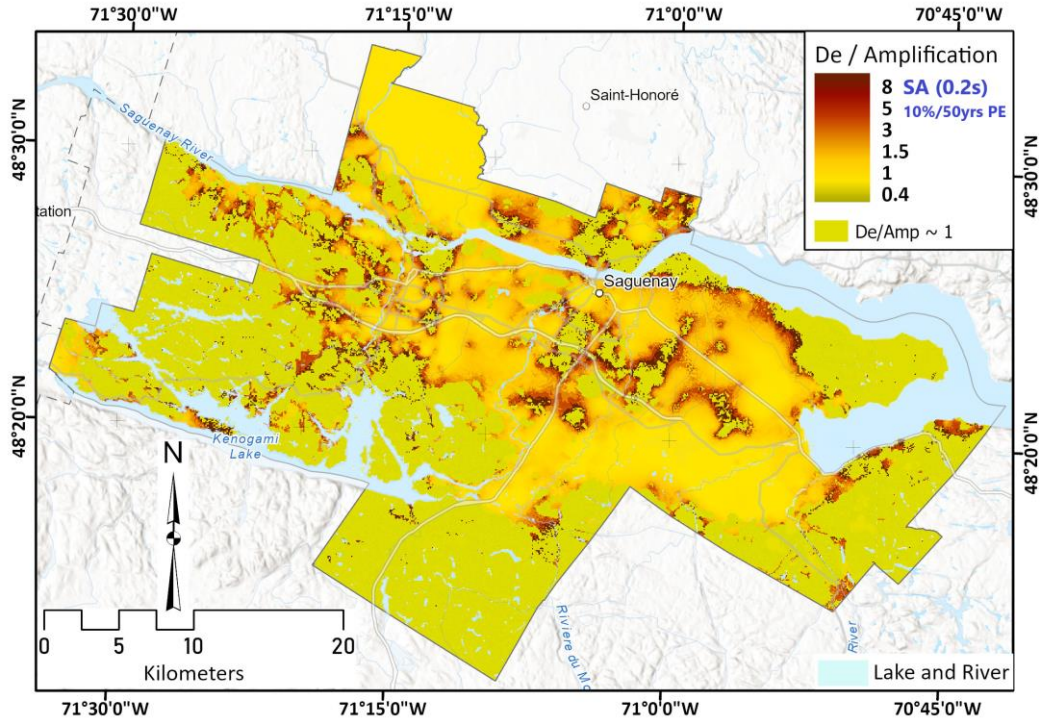

b)

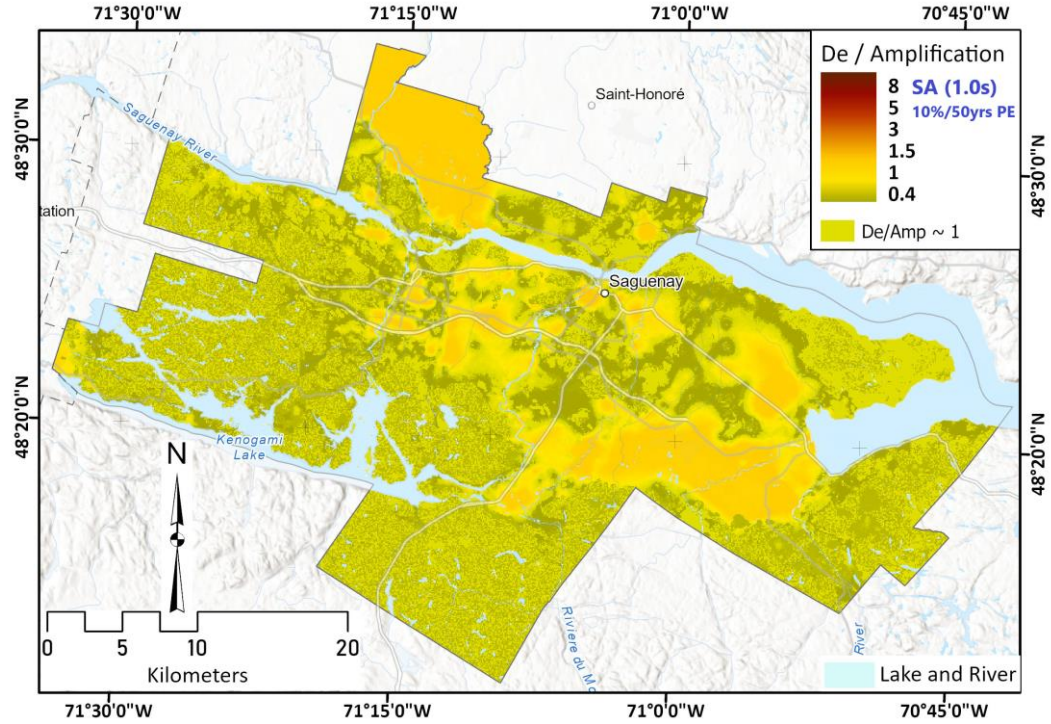

Figure 70. Seismic microzonation maps of site amplification in Saguenay for a 10% probability of exceedance in 50 years: (a) 0.2 s spectral period, (b) 1.0 s spectral period.

5.9 Discussion and conclusion

The original methodology was developed to generate spatial distribution maps of seismic site amplification. It integrates the recently developed geological and geotechnical maps of the Saguenay region with optimized site amplification correlations based on the most efficient combinations of site proxies. To establish this correlation, a comprehensive 1D nonlinear ground response analysis was conducted on representative soil profiles for the study area, one of the most earthquake-prone and vulnerable areas in Eastern Canada. A novel site proxy, the nonlinear site period (T_{NL}), representing the dominant vibration period under nonlinear soil behavior, was introduced. It is determined through numerical simulation from 1D ground response analysis.

Empirical amplification correlations were developed for seismic hazard of 2%/50yrs PE and 10%/50yrs PE. Amplification response was evaluated at various spectral periods with respect to seven site parameters: V_{s30}, V_{savg}, V_f, T_{NL}, H_{soil}, H_{pg}, and H_{till}. Initial analyses showed that no single proxy could adequately predict the amplification across the range of spectral periods of interest, 0.01s to 10.0s. The most efficient combination of site parameters was retained through nonlinear regressions using logarithmic and power functions. It relies on the following four site parameters: shear wave velocity of top 30 m (V_{s30}), average shear wave velocity of Quaternary sediments (V_{savg}), nonlinear vibration period (T_{NL}), and the thickness of the relatively stiff till layer, ubiquitous in the study area at the interface with bedrock (H_{till}). The developed correlation was then used to generate the expected seismic amplification maps across the study area. Because recorded earthquake data are not available for this region, direct validation of the predicted site amplification was not possible. Instead, the predicted amplification from the empirical model was compared with the NBCC 2020 amplification factors along a 20 km-long geological–geotechnical cross-section, as well as with the amplification results obtained from 1D numerical site response analyses of four representative soil profiles. The key findings from the present study are summarized below:

- The nonlinear site amplification of 50 soil profiles shows similar curve shapes for both hazard levels, with higher amplification (up to ~5) at 10%/50-year PE and lower amplification (up to ~4) at 2%/50-year PE due to higher nonlinear damping at higher shaking intensities.
- Considering a single proxy, V_{s30} captures site amplification better at a very short period of 0.01s, whereas T_{NL}, H_{soil}, and H_{pg} better dominant for medium (0.5s) to long periods (>1.0 s).

- Using multiple proxies while keeping V_{s30} and T_{NL} in all correlations, the logarithmic combination of V_{s30}+T_{NL}+V_{savg}+H_{till} shows the best prediction of the potential amplifications and was selected as the site amplification correlation for the Saguenay region.
- Comparison along a 20 km geological/geotechnical cross-section comparison shows that NBCC 2020 generally overestimates the empirical amplifications at medium to longer periods and underestimates them at short periods, with NBCC/empirical median ratios ranging from 0.96–1.29 at 0.2 s and 0.87–1.37 at 1.0 s, respectively. These discrepancies likely arise from NBCC's use of generalized site classes that do not fully capture the effects of locally thick, soft post-glacial sediments and interbedded stiff glacial tills, which modify the impedance contrast and shift the site's resonance characteristics.
- The predicted amplification from the developed model is in good agreement with amplifications from GRA.
- The final seismic amplification (microzonation) maps present the expected amplification at spectral periods of 0.2s and 1.0s for seismic hazard with a 2% and 10%/50yrs PE. The developed empirical correlation, together with such maps, serves as a critical tool in dynamic analyses of soil and structural response, enabling engineers and researchers to obtain spectral accelerations of the surface ground motion with respect to local site conditions. Such an approach supports earthquake-resistant design and improves seismic risk assessment in the region.

Despite the valuable insights gained from this microzonation study, several limitations should be acknowledged. First, the limited availability of strong-motion records in Eastern Canada required the use of both recorded and synthetic input motions. To better capture spectral-shape variability and its influence on nonlinear site response, future work will incorporate larger ensembles of stochastic and catalog-based synthetic ground motions. Second, the analyses relied on one-dimensional ground-response modeling, which, although appropriate for evaluating a large number of soil profiles at the regional scale, cannot fully capture lateral heterogeneity, topographic effects, or basin-geometry influences that may be significant in the Saguenay region. Preliminary two-dimensional simulations conducted for a representative site (Hossain et al., 2025) have already shown how lateral variations can modify amplification patterns. Future studies should therefore integrate 2D and 3D numerical analyses to better represent complex geological structures and quantify their impact on local site amplification and seismic hazard estimates. Additionally, A limitation of this study is the absence of

local cyclic laboratory data to calibrate the MKZ model; future work will incorporate site-specific testing to constrain the nonlinear behavior of Saguenay clays better. Finally, external validation was not feasible due to the absence of site-specific strong-motion recordings or HVSR-derived amplification data, but such observations will be incorporated in future work as they become available.

CHAPTER 6

6.1 Conclusion

This research rigorously evaluated seismic site response characteristics in the Saguenay region of Eastern Canada, combining a critical review, empirical modeling, and numerical site-specific ground response analysis. The collective findings underscore the significant impact of local geological and geotechnical conditions on ground motion amplification, particularly in regions with complex soil stratigraphy and moderate seismic activity, where strong-motion records are scarce.

Key insights reveal that seismic site effects in the Saguenay region are significantly influenced by the thickness of soft soil, impedance contrast, and the nonlinear behavior of soil during intense ground shaking. Introducing intermediate layers, such as till deposits, and a change in bedrock stiffness were shown to modulate amplification and resonance patterns significantly. Furthermore, the study established that nonlinear site response analyses, especially under high-strain conditions, result in decreased amplification but prolonged dominant vibration periods, which is critical for accurate hazard modeling.

The mismatch between standardized code-based amplification values and site-specific results underscores the need for refined micro-zonation maps based on local soil dynamics and nonlinear behavior. The outcomes of this study form the foundation for micro-zonation in the Saguenay region, providing a reliable framework for dynamic soil-structure interaction studies, infrastructure resilience planning, and seismic risk mitigation.

A significant advancement of this work is the development of the seismic microzonation through validated site-specific amplification models that incorporate both conventional proxies (Vs_{30}, Vsavg) and novel resonance-sensitive proxies, such as the nonlinear site period T_{NL} which is more important in strong ground motion, and H_{till}, which is more important in areas like Saguenay.

6.2 Recommendations

In future research extensions, multidimensional modeling approaches—specifically, 2D and 3D nonlinear site response analyses—will be explored to capture better complex subsurface geometries, topographic effects, and lateral variations in soil properties. Such models are particularly valuable for

assessing site amplification in regions characterized by irregular terrain and non-uniform soil deposits, where 1D assumptions may oversimplify reality.

Moreover, expanding the ground motion database to include a broader range of synthetic and recorded seismic events will enhance the reliability and representativeness of site response simulations. A comprehensive motion dataset will allow for more robust hazard-level scaling, period matching, and intensity-based scenario modeling. This is especially important for regions like Saguenay, where recorded strong motions are limited.

The models developed through this research also have significant potential for integration into structural design and seismic risk assessment frameworks. More resilient infrastructure can be designed by incorporating site-specific amplification functions into performance-based engineering practices. This will directly benefit both public safety and the cost-effectiveness of earthquake-resistant construction.

Ultimately, the findings of this thesis provide valuable insights into regional policy and code development. By demonstrating the limitations of generalized code-based amplification factors, such as those in NBCC 2020, and presenting evidence-based alternatives rooted in nonlinear soil dynamics, this research supports the formulation of accurate, region-specific seismic amplification models. Such contributions can inform future revisions of Canadian building codes and enhance seismic resilience on a broader policy level.

REFERENCES

Abdellaziz, M., Karray, M., Chekired, M., Delisle, M.-C., Locat, P., Ledoux, C., & Mompin, R. (2023). New model of shear modulus degradation and damping ratio curves for sensitive Canadian clays. Canadian Geotechnical Journal, 60(6), 784–801. https://doi.org/10.1139/cgj-2021-0475

Abdellaziz, M., Karray, M., Chekired, M., Delisle, M.-C., Locat, P., Ledoux, C., & Mompin, R. (2021). Shear modulus and hysteretic damping of sensitive eastern Canada clays. Canadian Geotechnical Journal, 58, 1118–1134.

Abrahamson, N. A., & Somerville, P. G. (1996). Effects of the hanging wall and footwall on ground motions recorded during the Northridge earthquake. Bulletin of the Seismological Society of America, 86(S1), S93–S99.

Acunzo, G., Falcone, G., Di Lernia, A., Mori, F., Mendicelli, A., & Naso, G. (2024). NC92Soil: A computer code for deterministic and stochastic 1D equivalent linear seismic site response analyses. Computers and Geotechnics, 165, 105857. https://doi.org/10.1016/j.compgeo.2023.105857

Adampira, M., Alielahi, H., Panji, M., & Koohsari, H. (2014). Comparison of equivalent linear and nonlinear methods in seismic analysis of liquefiable site response due to near-fault incident waves: A case study. Arabian Journal of Geosciences, 8, 3103–3118.

Aki, K. (1965). A note on the use of microseisms in determining the shallow structures of the Earth's crust. Geophysics, 30, 665–666.

Aki, K. (1957). Space and time spectra of stationary stochastic waves, with special reference to microtremors. Bulletin of the Earthquake Research Institute, 35, 415–456.

Ambraseys, N. N. (1959). A note on the response of an elastic overburden of varying rigidity to an arbitrary ground motion. Bulletin of the Seismological Society of America, 49, 211–220.

Andrus, R. D., Mohanan, N. P., Piratheepan, P., Ellis, B. S., & Holzer, T. L. (2007). Predicting shear-wave velocity from cone penetration resistance. In Proceedings of the 4th International Conference on Earthquake Geotechnical Engineering (pp. 1–12). Thessaloniki, Greece.

Ansal, A. (2025). Seismic microzonation: Past, present and future. Bulletin of Earthquake Engineering, 23(9), 3483–3506. https://doi.org/10.1007/s10518-025-02182-1

Arslan, H., & Siyahi, B. (2006). A comparative study on linear and nonlinear site response analysis. Environmental Geology, 50, 1193–1200.

Assaf, J., Ghofrani, H., Salsabili, M., Adhikari, S. R., Sirohey, A., & Bilson Darko, A. (2024). MVSMMP Maps 25–27: Long-period amplification hazard (2475-year return period equivalent) (Version 1). Borealis. https://doi.org/10.5683/SP3/ULMSX9

Assaf, J., Ghofrani, H., Salsabili, M., Adhikari, S. R., Sirohey, A., & Bilson Darko, A. (2024). MVSMMP Maps 22–24: Short-period amplification hazard (2475-year return period equivalent) (Version 1). Borealis. https://doi.org/10.5683/SP3/ZIPEZX

Assaf, J., Ghofrani, H., Salsabili, M., Adhikari, S. R., Sirohey, A., & Bilson Darko, A. (2024). MVSMMP Maps 19–21: Long-period amplification hazard (475-year return period equivalent) (Version 1). Borealis. https://doi.org/10.5683/SP3/CBWAIJ

Assaf, J., Ghofrani, H., Salsabili, M., Adhikari, S. R., Sirohey, A., & Bilson Darko, A. (2024). MVSMMP Maps 16–18: Short-period amplification hazard (475-year return period equivalent) (Version 1). Borealis. https://doi.org/10.5683/SP3/VBFCXI

Assaf, J., Molnar, S., El Naggar, M. H., & Sirohey, A. (2022). Seismic site characterization in Fraser River Delta in metropolitan Vancouver. Soil Dynamics and Earthquake Engineering, 161, 107384. https://doi.org/10.1016/j.soildyn.2022.107384

Assimaki, D. (2005). Effects of local soil conditions on the topographic aggravation of seismic motion: Parametric investigation and recorded field evidence from the 1999 Athens earthquake. Bulletin of the Seismological Society of America, 95, 1059–1089.

Assimaki, D., Kausel, E., & Whittle, A. (2000). Model for dynamic shear modulus and damping for granular soils. Journal of Geotechnical and Geoenvironmental Engineering, 126, 859–869.

Assimaki, D., & Li, W. (2012). Site- and ground motion-dependent nonlinear effects in seismological model predictions. Soil Dynamics and Earthquake Engineering, 32, 143–151.

Asten, M. W., & Hayashi, K. (2018). Application of the spatial auto-correlation method for shear-wave velocity studies using ambient noise. Surveys in Geophysics, 39, 633–659.

Atkinson, G. M. (2009). Earthquake time histories compatible with the 2005 National Building Code of Canada uniform hazard spectrum. Canadian Journal of Civil Engineering, 36(6), 991–1000. https://doi.org/10.1139/L09-044

Atkinson, G. M., & Assatourians, K. (2010). Attenuation and source characteristics of the 23 June 2010 M 5.0 Val-des-Bois, Quebec, earthquake. Seismological Research Letters, 81, 849–860. https://doi.org/10.1785/gssrl.81.5.849

Atkinson, G. M., & Adams, J. (2013). Ground motion prediction equations for application to the 2015 Canadian national seismic hazard maps. Canadian Journal of Civil Engineering, 40(10), 988–998. https://doi.org/10.1139/cjce-2012-0544

Aydın, U., Pamuk, E., & Ozer, C. (2022). Investigation of soil dynamic characteristics at seismic stations using H/V spectral ratio method in Marmara Region, Turkey. Natural Hazards, 110(1), 587–606. https://doi.org/10.1007/s11069-021-04959-4

Baghbani, A., Choudhury, T., Samui, P., & Costa, S. (2023). Prediction of secant shear modulus and damping ratio for an extremely dilative silica sand based on machine learning techniques. Soil Dynamics and Earthquake Engineering, 165, 107708.

Baker, J. (2005). Vector-valued ground motion intensity measures for probabilistic seismic demand analysis (Technical Report No. 150). Stanford University.

Baker, J. W., & Cornell, C. A. (2006). Spectral shape, epsilon and record selection. Earthquake Engineering & Structural Dynamics, 35, 1077–1095.

Baker, J. W., & Lee, C. (2018). An improved algorithm for selecting ground motions to match a conditional spectrum. Journal of Earthquake Engineering, 22, 708–723.

Bararpour, M., Janalizade, A., & Tavakoli, H. R. (2016). The effect of 2D slope and valley on seismic site response. Arabian Journal of Geosciences, 9, 93.

Bard, P.-Y., & Bouchon, M. (1985). The two-dimensional resonance of sediment-filled valleys. Bulletin of the Seismological Society of America, 75, 519–541.

Bard, P.-Y., & Riepl-Thomas, J. (2000). Wave propagation in complex geological structures and their effects on strong ground motion. In E. Kausel & G. Manolis (Eds.), Wave motion in earthquake engineering (pp. 1–45). WIT Press.

Basu, D., & Dey, A. (2016). Comparative 1D ground response analysis of homogeneous sandy stratum using linear, equivalent linear and nonlinear Masing approaches. In Geotechnics for Infrastructure Development. Indian Geotechnical Society.

Bayat, M., & Ghalandarzadeh, A. (2018). Stiffness degradation and damping ratio of sand–gravel mixtures under saturated state. International Journal of Civil Engineering, 16, 1261–1277.

Bommer, J. J., & Acevedo, A. B. (2004). The use of real earthquake accelerograms as input to dynamic analysis. Journal of Earthquake Engineering, 8, 43–91.

Boore, D. M. (2003). Simulation of ground motion using the stochastic method. Pure and Applied Geophysics, 160, 635–676.

Boore, D. M., & Atkinson, G. M. (2008). Ground-motion prediction equations for the average horizontal component of PGA, PGV, and 5%-damped PSA at spectral periods between 0.01 s and 10.0 s. Earthquake Spectra, 24(1), 99–138. https://doi.org/10.1193/1.2830434

Borcherdt, R. D. (1970). Effects of local geology on ground motion near San Francisco Bay. Bulletin of the Seismological Society of America, 60(1), 29–61.

Borcherdt, R. D. (1994). Estimates of site-dependent response spectra for design (methodology and justification). Earthquake Spectra, 10(4), 617–653. https://doi.org/10.1193/1.1585791

Bouchon, M., & Barker, J. S. (1996). Seismic response of a hill: The example of Tarzana, California. Bulletin of the Seismological Society of America, 86, 66–72.

Boudghene Stambouli, A., Zendagui, D., Bard, P.-Y., & Derras, B. (2017). Deriving amplification factors from simple site parameters using generalized regression neural networks: Implications for relevant site proxies. Earth, Planets and Space, 69(1), Article 99. https://doi.org/10.1186/s40623-017-0686-3

Bozorgnia, Y., Abrahamson, N. A., Al Atik, L., Ancheta, T. D., Atkinson, G. M., Baker, J. W., Baltay, A., Chiou, B. S.-J., Darragh, R., Gregor, N., Hanks, T., Idriss, I. M., Kamai, R., Kishida, T., Kottke, A., Mahin, S. A., Rezaeian, S., Rowshandel, B., Seyhan, E., Shahi, S., Stewart, J. P., Watson-Lamprey, J., Wooddell, K., & Youngs, R. (2014). NGA-West2 research project. Earthquake Spectra, 30(3), 973–987. https://doi.org/10.1193/072113EQS209M

Bozyigit, I., & Altun, S. (2023). Small-strain behavior and post-cyclic characteristics of low plasticity silts. Bulletin of Earthquake Engineering, 21, 791–810.

Braganza, S., Atkinson, G. M., Ghofrani, H., Hassani, B., Chouinard, L., Rosset, P., Motazedian, D., & Hunter, J. (2016). Modeling site amplification in eastern Canada on a regional scale. Seismological Research Letters, 87(4), 1008–1021. https://doi.org/10.1785/0220160009

Building Center of Japan. (2005). Building standard law. Tokyo, Japan.

Building Seismic Safety Council. (2015). NEHRP recommended seismic provisions for new buildings and other structures. Washington, DC, USA.

Capon, J. (1969). High-resolution frequency–wavenumber spectrum analysis. Proceedings of the IEEE, 57, 1408–1418.

CERM-PACES. (2013). Résultats du programme d'acquisition de connaissances sur les eaux souterraines de la région Saguenay–Lac-Saint-Jean.

Cheng, F., Xia, J., Luo, Y., Xu, Z., Wang, L., Shen, C., Liu, R., Pan, Y., Mi, B., & Hu, Y. (2016). Multichannel analysis of passive surface waves based on cross-correlations. Geophysics, 81, EN57–EN66.

Cheng, F., Xia, J., Xu, Z., Hu, Y., & Mi, B. (2018). Frequency–wavenumber (FK)-based data selection in high-frequency passive surface wave survey. Surveys in Geophysics, 39, 661–682.

Civelekler, E., Afacan, K. B., & Okur, D. V. (2024). Effect of site-specific soil characteristics on nonlinear ground response analysis and comparison with equivalent linear analysis. Journal of Applied Geophysics, 220, 105250.

Clayton, C. (2011). Stiffness at small strain: Research and practice. Géotechnique, 61, 5–37.

Costanzo, A., & Caserta, A. (2019). Seismic response across the Tronto Valley based on geophysical monitoring of the 2016 Central Italy seismic sequence. Bulletin of Engineering Geology and the Environment, 78, 5599–5616.

Darendeli, M. B. (2001). Development of a new family of normalized modulus reduction and material damping curves (Doctoral dissertation). University of Texas at Austin.

Darragh, R. B., & Shakal, A. F. (1991). The site response of two rock and soil station pairs to strong and weak ground motion. Bulletin of the Seismological Society of America, 81, 1885–1899.

Derras, B., Bard, P.-Y., & Cotton, F. (2017). Vs30, slope, H800 and f0: Performance of various site-condition proxies in reducing ground-motion aleatory variability and predicting nonlinear site response. Earth, Planets and Space, 69(1), Article 133. https://doi.org/10.1186/s40623-017-0718-z

Dobry, R. (1987). Dynamic properties and seismic response of soft clay deposits. In Proceedings of the International Symposium on Geotechnical Engineering of Soft Soils (Vol. 2, pp. 51–87).

Dobry, R., Oweis, I., & Urzua, A. (1976). Simplified procedures for estimating the fundamental period of a soil profile. Bulletin of the Seismological Society of America, 66, 1293–1321.

Du Berger, R., Roy, D. W., Lamontagne, M., Woussen, G., North, R. G., & Wetmiller, R. J. (1991). The Saguenay (Quebec) earthquake of November 25, 1988: Seismologic data and geologic setting. Tectonophysics, 186(1–2), 59–74. https://doi.org/10.1016/0040-1951(91)90385-6

Electric Power Research Institute. (1993). Guidelines for determining design basis ground motions (Vol. 2). Palo Alto, CA, USA.

Fahey, M., & Carter, J. P. (1993). A finite element study of the pressuremeter test in sand using a nonlinear elastic–plastic model. Canadian Geotechnical Journal, 30, 348–362.

Falcone, G., Boldini, D., Martelli, L., & Amorosi, A. (2020). Quantifying local seismic amplification from regional charts and site-specific numerical analyses: A case study. Bulletin of Earthquake Engineering, 18(1), 77–107. https://doi.org/10.1007/s10518-019-00719-9

Fernandes, J. B., Rocha, B. P., & Giacheti, H. L. (2023). Maximum shear modulus and modulus degradation curves of an unsaturated tropical soil. Soils and Rocks, 46, e2023013122.

Field, E. H., Zeng, Y., Johnson, P. A., & Beresnev, I. A. (1998). Nonlinear sediment response during the 1994 Northridge earthquake: Observations and finite-source simulations. Journal of Geophysical Research, 103, 26869–26883.

Foulon, T., Saeidi, A., Chesnaux, R., Nastev, M., & Rouleau, A. (2018). Spatial distribution of soil shear-wave velocity and the fundamental period of vibration: A case study of the Saguenay region, Canada. Georisk, 12(1), 74–86. https://doi.org/10.1080/17499518.2017.1376253

Gallipoli, M. R., & Mucciarelli, M. (2009). Comparison of site classification from VS30, VS10, and HVSR in Italy. Bulletin of the Seismological Society of America, 99, 340–351.

Gasparini, D. A., & Vanmarcke, E. H. (1976). SIMQKE: A program for artificial motion generation. Massachusetts Institute of Technology.

Ghofrani, H., & Atkinson, G. M. (2014). Site condition evaluation using horizontal-to-vertical response spectral ratios of earthquakes in the NGA-West2 and Japanese databases. Soil Dynamics and Earthquake Engineering, 67, 30–43. https://doi.org/10.1016/j.soildyn.2014.08.015

Ghofrani, H., Atkinson, G. M., & Goda, K. (2013). Implications of the 2011 M9.0 Tohoku Japan earthquake for the treatment of site effects in large earthquakes. Bulletin of Earthquake Engineering, 11(1), 171–203. https://doi.org/10.1007/s10518-012-9413-4

Goto, H., & Morikawa, H. (2012). Ground motion characteristics during the 2011 off the Pacific Coast of Tohoku earthquake. Soils and Foundations, 52(5), 769–779. https://doi.org/10.1016/j.sandf.2012.11.002

Goulet, C. A., Bozorgnia, Y., Kuehn, N., Al Atik, L., Youngs, R. R., Graves, R. W., & Atkinson, G. M. (2017). NGA-East ground-motion models for the U.S. Geological Survey national seismic hazard maps (PEER Report No. 2017/03). Pacific Earthquake Engineering Research Center.

Graves, R. W., Pitarka, A., & Somerville, P. G. (1998). Ground-motion amplification in the Santa Monica area: Effects of shallow basin-edge structure. Bulletin of the Seismological Society of America, 88, 1224–1242.

Guorui, H., & Tao, L. (2015). Review on baseline correction of strong-motion accelerograms. International Journal of Science and Technology, 3, 309.

Hadjian, A. H. (2002). Fundamental period and mode shape of layered soil profiles. Soil Dynamics and Earthquake Engineering, 22(9–12), 885–891. https://doi.org/10.1016/S0267-7261(02)00111-2

Harmon, J., Hashash, Y. M. A., Stewart, J. P., Rathje, E. M., Campbell, K. W., Silva, W. J., Xu, B., Musgrove, M., & Ilhan, O. (2019). Site amplification functions for central and eastern North America – Part I: Simulation data set development. Earthquake Spectra, 35(2), 787–814. https://doi.org/10.1193/091017EQS178M

Hashash, Y. M. A., Harmon, J., Ilhan, O., Stewart, J. P., Rathje, E. M., Campbell, K. W., & Silva, W. J. (2018). Modelling of site amplification via large-scale nonlinear simulations. In Geotechnical Earthquake Engineering and Soil Dynamics V (pp. 523–537). American Society of Civil Engineers. https://doi.org/10.1061/9780784481462.051

Hashash, Y. M. A., Musgrove, M. I., Harmon, J. A., Ilhan, O., Xing, G., & Numanoglu, O. (2020). DEEPSOIL 7.0: User manual. University of Illinois at Urbana–Champaign.

Hashash, Y. M. A., & Park, D. (2001). Nonlinear one-dimensional seismic ground motion propagation in the Mississippi Embayment. Engineering Geology, 62, 185–206. https://doi.org/10.1016/S0013-7952(01)00061-8

Hashash, Y. M. A., Phillips, C. A., & Groholski, D. R. (2010). Recent advances in non-linear site response analysis. In Proceedings of the Fifth International Conference on Recent Advances in Geotechnical Earthquake Engineering and Soil Dynamics (Paper No. OSP 4).

Hashash, Y. M. A., Dashti, S., Romero, M. I., Ghayoomi, M., & Musgrove, M. (2015). Evaluation of 1-D seismic site response modeling of sand using centrifuge experiments. Soil Dynamics and Earthquake Engineering, 78, 19–31. https://doi.org/10.1016/j.soildyn.2015.07.003

Hashash, Y. M. A., Harmon, J., Ilhan, O., Stewart, J. P., Rathje, E. M., Campbell, K. W., Silva, W. J., & Goulet, C. A. (2018). Modelling of site amplification via large-scale nonlinear simulations. In Geotechnical Earthquake Engineering and Soil Dynamics V (pp. 523–537). American Society of Civil Engineers. https://doi.org/10.1061/9780784481462.051

Hashash, Y. M. A., Musgrove, M. I., Harmon, J. A., Ilhan, O., Xing, G., Numanoglu, O., Groholski, D. R., Phillips, C. A., & Park, D. (2020). DEEPSOIL 7.0: User manual. University of Illinois at Urbana–Champaign.

Hashimoto, T., & Miyajima, M. (2002). Relation between building damage and ground conditions in the 1999 Quindio earthquake in Colombia. Journal of Earthquake Engineering, 6(3), 315–330. https://doi.org/10.1080/13632460209350419

Hassani, B., & Atkinson, G. M. (2016). Site-effects model for central and eastern North America based on peak frequency. Bulletin of the Seismological Society of America, 106(5), 2197–2213. https://doi.org/10.1785/0120160049

Hassani, B., Yong, A., Atkinson, G. M., Feng, T., & Meng, L. (2019). Comparison of site dominant frequency from earthquake and microseismic data in California. Bulletin of the Seismological Society of America, 109(3), 1034–1040. https://doi.org/10.1785/0120180267

Hegazy, Y. A., & Mayne, P. W. (2006). A global statistical correlation between shear-wave velocity and cone penetration data. In Proceedings of the GeoShanghai International Conference (pp. 243–248).

Hossain, A. S. M. F., Saeidi, A., Salsabili, M., Nastev, M., & Suescun, J. R. (2025). Analytical and numerical investigation of the site response period in the Saguenay region, eastern Canada. In Proceedings of the 3rd Croatian Conference on Earthquake Engineering (pp. 118–127). https://doi.org/10.5592/CO/3CroCEE.2025.94

Hossain, A. S. M. F., Saeidi, A., Salsabili, M., Nastev, M., & Suescun, J. R. (2024). Soil dynamic response and site amplification parameters for Saguenay, eastern Canada. Japanese Geotechnical Society Special Publication, 10(52), v10.OS-41-03. https://doi.org/10.3208/jgssp.v10.OS-41-03

Hossain, A. S. M. F., Saeidi, A., Salsabili, M., Nastev, M., Suescun, J. R., & Bayati, Z. (2025). A review of parameters and methods for seismic site response. Geosciences, 15(4), 128. https://doi.org/10.3390/geosciences15040128

Hossain, A. S. M. F., Salsabili, M., Saeidi, A., Nastev, M., & Suescun, J. R. (2025). Effects of complex surficial geology on seismic amplification in Quebec, Canada. Georisk: Assessment and Management of Risk for Engineered Systems and Geohazards, 1–21. https://doi.org/10.1080/17499518.2025.2591757

Hossain, A. S. M. F., Salsabili, M., Saeidi, A., Suescun, J. R., & Nastev, M. (2023). Effects of shear wave velocity and thickness of soil layers on 1D dynamic response in the Saguenay region, Quebec. In Rocscience International Conference (RIC 2023) (pp. 165–173). Atlantis Press. https://doi.org/10.2991/978-94-6463-258-3_17

Hossain, A. S. M. F., Adhikari, T. L., Ansary, M. A., & Bari, Q. H. (2015). Characteristics and consequence of Nepal earthquake 2015: A review. Geotechnical Engineering Journal of SEAGS & AGSSEA, 46, 114–120.

Hossain, A. S. M. F., & Ansary, M. A. (2017). PS logging for site response analysis in Dhaka City. Australian Journal of Science and Technology, 6, 83–99.

Hosseini, S. M. M. M., & Pajouh, M. A. (2012). Comparative study on the equivalent linear and the fully nonlinear site response analysis approaches. Arabian Journal of Geosciences, 5, 587–597.

Hosseinpour, V., Saeidi, A., Salsabili, M., Nastev, M., & Nollet, M.-J. (2024). Development of a probabilistic seismic microzonation software. Georisk. https://doi.org/10.1080/17499518.2024.2302183

Huang, H.-C., Huang, S.-W., & Chiu, H.-C. (2005). Observed evolution of linear and nonlinear effects at the Dahan downhole array, Taiwan. Pure and Applied Geophysics, 162, 1–20.

Hunter, J. A. M., & Crow, H. L. (2015). Shear-wave velocity measurement guidelines for Canadian seismic site characterization in soil and rock. Natural Resources Canada.

Idriss, I. M., & Seed, H. B. (1968). Seismic response of horizontal soil layers. Journal of the Soil Mechanics and Foundations Division, ASCE, 94, 1003–1031.

Idriss, I. M., & Sun, J. I. (1992). User's manual for SHAKE91: A computer program for conducting equivalent linear seismic response analyses of horizontally layered soil deposits. University of California, Berkeley.

Iervolino, I., Galasso, C., & Cosenza, E. (2010). REXEL: Computer-aided record selection for code-based seismic structural analysis. Bulletin of Earthquake Engineering, 8, 339–362.

Ilhan, O., Hashash, Y. M. A., Stewart, J. P., Rathje, E. M., Nikolaou, S., & Campbell, K. W. (2024). Simulated site amplification for central and eastern North America. Earthquake Spectra, 40(1), 200–229. https://doi.org/10.1177/87552930231215723

Iñarritu, P. G. d. Q., Šipčić, N., Alvarez-Sanchez, L., Kohrangi, M., & Bazzurro, P. (2023). A closer look at hazard-consistent ground motion record selection for building-specific risk assessment. Earthquake Spectra, 39, 1683–1720.

Ishihara, K. (1996). Soil behaviour in earthquake geotechnics. Oxford University Press.

ISSMGE Technical Committee for Earthquake Geotechnical Engineering. (1993). Manual for zonation on seismic geotechnical hazards. Japanese Society of Soil Mechanics and Foundation Engineering.

ISSMGE. (1999). Manual for zonation on seismic geotechnical hazards. The Japanese Geotechnical Society.

Jackson, F., Molnar, S., Ghofrani, H., Atkinson, G. M., Cassidy, J. F., & Assatourians, K. (2017). Ground motions of the December 2015 M 4.7 Vancouver Island earthquake: Attenuation and site response. Bulletin of the Seismological Society of America, 107, 2903–2916.

Johari, A., & Heidari, A. (2020). Comparison of equivalent linear and nonlinear ground response analysis methods in the time domain. In Proceedings of the 3rd National & 1st International Conference on Applied Research in Civil Engineering, Architecture and Urban Planning (pp. 1–7).

John, A., Stephen, H., Trevor, A., & Garry, R. (2015). Canada's 6th generation seismic hazard model for the 2020 National Building Code of Canada. In Proceedings of the 12th Canadian Conference on Earthquake Engineering.

Kakoty, P., Dyaga, S. M., & Hutt, C. M. (2021). Impacts of simulated M9 Cascadia subduction zone earthquakes considering amplification due to the Georgia sedimentary basin. Earthquake Engineering & Structural Dynamics, 50, 237–256.

Kakoty, P., Hutt, C. M., Ghofrani, H., & Molnar, S. (2023). Spectral acceleration basin amplification factors for interface Cascadia subduction zone earthquakes in Canada's 2020 national seismic hazard model. Earthquake Spectra, 39, 1166–1188.

Kamalb, D. E. H. A. M., & Alama, A. W. U. M. B. (2013). Comparison of shear wave velocity derived from PS logging and MASW. Bangladesh Journal of Geology, 26, 84–97.

Karray, M., & Hussien, M. N. (2017). Shear wave velocity as a function of cone penetration resistance and grain size for Holocene-age uncemented soils. Acta Geotechnica, 12, 1129–1158.

Kiani, J., & Khanmohammadi, M. (2015). New approach for selection of real input ground motion records for incremental dynamic analysis (IDA). Journal of Earthquake Engineering, 19, 592–623.

Kim, B., & Hashash, Y. M. A. (2013). Site response analysis using downhole array recordings during the March 2011 Tohoku-Oki earthquake and the effect of long-duration ground motions. Earthquake Spectra, 29, 37–54.

Klin, P., Laurenzano, G., Barnaba, C., Priolo, E., & Parolai, S. (2021). Site amplification at permanent stations in northeastern Italy. Bulletin of the Seismological Society of America, 111, 1885–1904.

Kobayashi, K. (1980). A method for presuming deep ground soil structures by means of longer period microtremors. In Proceedings of the Seventh World Conference on Earthquake Engineering (pp. 237–240). Istanbul, Turkey.

Kocaoğlu, A. H., & Fırtana, K. (2011). Estimation of shear wave velocity profiles by the inversion of spatial autocorrelation coefficients. Journal of Seismology, 15, 613–624.

Kolaj, M., Allen, T., Mayfield, R., Adams, J., & Halchuk, S. (2019). Ground-motion models for the 6th generation seismic hazard model of Canada. In Proceedings of the 12th Canadian Conference on Earthquake Engineering. Quebec City, Canada.

Konder, R. L., & Zelasko, J. S. (1963). A hyperbolic stress–strain formulation of sands. In Proceedings of the 2nd Pan-American Conference on Soil Mechanics and Foundation Engineering (pp. 289–324). São Paulo, Brazil.

Kottke, A., & Rathje, E. M. (2008). A semi-automated procedure for selecting and scaling recorded earthquake motions for dynamic analysis. Earthquake Spectra, 24, 911–932.

Kramer, S. L. (1996). Geotechnical earthquake engineering. Pearson Education.

Krinitzsky, E. L., & Marcuson, W. F. (1983). Principles for selecting earthquake motions in engineering design. Environmental Engineering Geoscience, 20, 253–265.

Kumar, S. S., Dey, A., & Krishna, M. (2014). Equivalent linear and nonlinear ground response analysis of two typical sites at Guwahati city. In Proceedings of the Indian Geotechnical Conference (IGC 2014). Kakinada, India.

Kuo, C.-H., Chen, C.-T., Lin, C.-M., Wen, K.-L., Huang, J.-Y., & Chang, S.-C. (2016). S-wave velocity structure and site effect parameters derived from microtremor arrays in the western plain of Taiwan. Journal of Asian Earth Sciences, 128, 27–41.

Kwon, O.-S., & Elnashai, A. S. (2017). Distributed analysis of interacting soil and structural systems under dynamic loading. Innovative Infrastructure Solutions, 2, 30.

L'Heureux, J.-S., & Long, M. (2017). Relationship between shear-wave velocity and geotechnical parameters for Norwegian clays. Journal of Geotechnical and Geoenvironmental Engineering, 143, 04017013.

Lacoss, R. T., Kelly, E. J., & Toksöz, M. N. (1969). S-wave velocity structure and site effect parameters derived from microtremor arrays. Geophysics, 34, 21–38.

Ladak, S., Molnar, S., & Palmer, S. (2021). Multi-method site characterization to verify the hard rock (Site Class A) assumption at 25 seismograph stations across eastern Canada. Earthquake Spectra, 37, 1487–1515. https://doi.org/10.1177/87552930211001076

Lamontagne, M. (2002). An overview of some significant eastern Canadian earthquakes and their impacts on the geological environment. Natural Hazards, 26(1), 55–68. https://doi.org/10.1023/A:1015268710302

Lanzo, G., Vucetic, M., & Doroudian, M. (1997). Reduction of shear modulus at small strains in simple shear. Journal of Geotechnical and Geoenvironmental Engineering, 123, 1035–1042.

Leboeuf, D., Perret, D., Nollet, M.-J., Lamarche, L., Nastev, M. N., & Parent, M. P. (2013). Microzonage sismique des villes de Québec–Ancienne-Lorette et réserve indienne de Wendake (catégories d'emplacement).

Lee, C.-J., Wang, C.-R., Wei, Y.-C., & Hung, W.-Y. (2012). Evolution of the shear wave velocity during shaking modeled in centrifuge shaking table tests. Bulletin of Earthquake Engineering, 10, 401–420.

Lefebvre, G., Leboeuf, D., Hornych, P., & Tanguay, L. (1992). Slope failures associated with the 1988 Saguenay earthquake, Quebec, Canada. Canadian Geotechnical Journal, 29, 117–130. https://doi.org/10.1139/t92-013

Likitlersuang, S., Teachavorasinskun, S., Surarak, C., Oh, E., & Balasubramaniam, A. (2013). Small strain stiffness and stiffness degradation curve of Bangkok clays. Soils and Foundations, 53, 498–509.

Lin, T. (2012). Advancement of hazard-consistent ground motion selection methodology (Doctoral dissertation). Stanford University.

Lin, T., Harmsen, S. C., Baker, J. W., & Luco, N. (2013). Conditional spectrum computation incorporating multiple causal earthquakes and ground-motion prediction models. Bulletin of the Seismological Society of America, 103, 1103–1116.

Ling, S., & Okada, H. (1993). An extended use of the spatial autocorrelation method for the estimation of structure using microtremors. In Proceedings of the 89th SEGJ Conference. Nagoya, Japan.

Livaoğlu, H., Şentürk, E., & Sertçelik, F. (2021). A comparative study of response and Fourier spectral ratios on classifying sites. Pure and Applied Geophysics, 178(5), 1745–1759. https://doi.org/10.1007/s00024-021-02722-1

Locat, J., & Beauséjour, N. (1987). Corrélations entre des propriétés mécaniques dynamiques et statiques de sols argileux intacts et traités à la chaux. Canadian Geotechnical Journal, 24, 327–334.

Long, M., & Donohue, S. (2010). Characterization of Norwegian marine clays with combined shear wave velocity and piezocone cone penetration test data. Canadian Geotechnical Journal, 47, 709–718.

Louie, J. N. (2001). Faster, better: Shear-wave velocity to 100 meters depth from refraction microtremor arrays. Bulletin of the Seismological Society of America, 91, 347–364.

Luna, R., & Jadi, H. (2000). Determination of dynamic soil properties using geophysical methods. In Proceedings of the First International Conference on the Application of Geophysical and NDT Methodologies to Transportation Facilities and Infrastructure (pp. 1–15). St. Louis, MO.

Luzi, L., Puglia, R., Pacor, F., Gallipoli, M. R., Bindi, D., & Mucciarelli, M. (2011). Proposal for a soil classification based on parameters alternative or complementary to Vs30. Bulletin of Earthquake Engineering, 9(6), 1877–1898. https://doi.org/10.1007/s10518-011-9274-2

Madera, G. (1970). Fundamental period and amplification of peak acceleration in layered systems. Massachusetts Institute of Technology.

Madiai, C., & Simoni, G. (2004). Shear wave velocity–penetration resistance correlation for Holocene and Pleistocene soils of an area in central Italy. In V. da Fonseca & P. W. Mayne (Eds.), Proceedings of the 2nd International Conference on Geotechnical and Geophysical Site Characterization (pp. 965–971). Millpress.

Mantovani, A., Abu Zeid, N., Bignardi, S., Tarabusi, G., Santarato, G., & Caputo, R. (2019). Seismic noise-based strategies for emphasizing recent tectonic activity and local site effects. Pure and Applied Geophysics, 176, 2321–2347.

Marafi, N. A., Eberhard, M. O., Berman, J. W., Wirth, E. A., & Frankel, A. D. (2019). Impacts of simulated M9 Cascadia subduction zone motions on idealized systems. Earthquake Spectra, 35, 1261–1287.

Matasović, N., & Vucetic, M. (1993). Cyclic characterization of liquefiable sands. Journal of Geotechnical Engineering, 119, 1805–1822. https://doi.org/10.1061/(ASCE)0733-9410(1993)119:11(1805)

Mayne, P. W. (2001). Stress–strain–strength–flow parameters from enhanced in-situ tests. In Proceedings of the International Conference on In-Situ Measurement of Soil Properties & Case Histories (pp. 27–47). Bali, Indonesia.

Mayne, P. W., & Rix, G. J. (1995). Correlations between shear wave velocity and cone tip resistance in natural clays. Soils and Foundations, 35, 107–110.

Mayoral, J., Assimaki, D., Tepalcapa, S., Wood, C., la Sancha, A. R.-D., Hutchinson, T., Franke, K., & Montalva, G. (2019). Site effects in Mexico City basin: Past and present. Soil Dynamics and Earthquake Engineering, 121, 369–382.

McGann, C. R., Bradley, B. A., Taylor, M. L., Wotherspoon, L. M., & Cubrinovski, M. (2015). Development of an empirical correlation for predicting shear wave velocity of Christchurch soils from cone penetration test data. Soil Dynamics and Earthquake Engineering, 75, 66–75.

Meunier, P., Hovius, N., & Haines, J. A. (2008). Topographic site effects and the location of earthquake-induced landslides. Earth and Planetary Science Letters, 275, 221–232.

Mihalić, S., Oštrić, M., & Krkač, M. (2011). Seismic microzonation: A review of principles and practice. Geofizika, 28, 5–20.

Mihaylov, D. G. (2011). Seismic microzonation of the Greater Toronto Area and influence of building resonances on measured soil responses (Doctoral dissertation). University of Toronto.

Mohammadioun, B. (1997). Nonlinear response of soils to horizontal and vertical bedrock earthquake motion. Journal of Earthquake Engineering, 1, 93–119.

Mohammadioun, B., & Pecker, A. (1984). Low-frequency transfer of seismic energy by superficial soil deposits and soft rocks. Earthquake Engineering & Structural Dynamics, 12, 537–564.

Molnar, S., Assaf, J., Sirohey, A., & Adhikari, S. R. (2020). Overview of local site effects and seismic microzonation mapping in metropolitan Vancouver, British Columbia, Canada. Engineering Geology, 270, 105568. https://doi.org/10.1016/j.enggeo.2020.105568

Molnar, S., & Cassidy, J. F. (2006). A comparison of site response techniques using weak-motion earthquakes and microtremors. Earthquake Spectra, 22, 169–188.

Molnar, S., Cassidy, J. F., Olsen, K. B., Dosso, S. E., & He, J. (2014a). Earthquake ground motion and 3D Georgia Basin amplification in southwest British Columbia: Deep Juan de Fuca plate scenario earthquakes. Bulletin of the Seismological Society of America, 104, 301–320.

Molnar, S., Cassidy, J. F., Olsen, K. B., Dosso, S. E., & He, J. (2014b). Earthquake ground motion and 3D Georgia Basin amplification in southwest British Columbia: Shallow blind-thrust scenario earthquakes. Bulletin of the Seismological Society of America, 104, 321–335.

Molnar, S., Sirohey, A., Assaf, J., Bard, P.-Y., Castellaro, S., Cornou, C., Cox, B., Guillier, B., Hassani, B., Kawase, H., & others. (2022). A review of the microtremor horizontal-to-vertical spectral ratio (MHVSR) method. Journal of Seismology, 26, 653–685.

Moon, S., Hashash, Y. M. A., & Park, D. (2017). USGS hazard map-compatible depth-dependent seismic site coefficients for the Upper Mississippi Embayment. KSCE Journal of Civil Engineering, 21, 220–231.

Moro, G. D. (2019). Effective active and passive seismics for the characterization of urban and remote areas. Pure and Applied Geophysics, 176, 1445–1465.

Moscatelli, M., Albarello, D., Scarascia Mugnozza, G., & Dolce, M. (2020). The Italian approach to seismic microzonation. Bulletin of Earthquake Engineering, 18, 5425–5440. https://doi.org/10.1007/s10518-020-00856-6

Motazedian, D. (2005). Stochastic finite-fault modeling based on a dynamic corner frequency. Bulletin of the Seismological Society of America, 95, 995–1010.

Motazedian, D., Hunter, J. A., Pugin, A., & Crow, H. (2011). Development of a Vs30 map for the city of Ottawa, Ontario. Canadian Geotechnical Journal, 48(3), 458–472. https://doi.org/10.1139/T10-081

Motazedian, D., Khaheshi Banab, K., Hunter, J. A., Sivathayalan, S., Crow, H., & Brooks, G. (2011). Comparison of site periods derived from different evaluation methods. Bulletin of the Seismological Society of America, 101(6), 2942–2954. https://doi.org/10.1785/0120100344

Motazedian, D., Torabi, H., Hunter, J. A., Crow, H. L., & Pyne, M. (2020). Seismic site period studies for nonlinear soil in the city of Ottawa, Canada. Soil Dynamics and Earthquake Engineering, 136, 106205. https://doi.org/10.1016/j.soildyn.2020.106205

Naggar, E. (2010). Geotechnical earthquake engineering. CRC Press.

Nakamura, Y. (1989). A method for dynamic characteristics estimation of subsurface using microtremor on the ground surface. Railway Technical Research Institute.

Nastev, M., Parent, M., Benoit, N., Ross, M., & Howlett, D. (2016). Regional Vs30 model for the St. Lawrence Lowlands, eastern Canada. Georisk: Assessment and Management of Risk for Engineered Systems and Geohazards, 10, 200–212. https://doi.org/10.1080/17499518.2016.1149869

Nastev, M., Parent, M., Ross, M., Howlett, D., & Benoit, N. (2016). Geospatial modelling of shear-wave velocity and fundamental site period of Quaternary marine and glacial sediments in the Ottawa and St. Lawrence Valleys, Canada. Soil Dynamics and Earthquake Engineering, 85, 103–116. https://doi.org/10.1016/j.soildyn.2016.03.006

Nastev, M. (2008). Motions compatible with the NBCC 2005 uniform hazard spectrum for Québec City. In Proceedings of the 36th Annual Conference of the Canadian Society for Civil Engineering (p. 8).

National Cooperative Highway Research Program. (2012). Practices and procedures for site-specific evaluations of earthquake ground motions. National Academies Press.

National Research Council of Canada. (2020). National Building Code of Canada 2020.

Natural Resources Canada. (2020). Seismic hazard calculator for NBCC 2020. https://www.earthquakescanada.nrcan.gc.ca/hazard-alea/interpolat/nbc2020-cnb2020-en.php

Naumoski, N. (2001). Program SYNTH—Generation of artificial accelerograms compatible with a target spectrum. University of Ottawa.

Ohori, M. (2002). A comparison of ESAC and FK methods of estimating phase velocity using arbitrarily shaped microtremor arrays. Bulletin of the Seismological Society of America, 92, 2323–2332.

Pagliaroli, A., & Lanzo, G. (2008). Selection of real accelerograms for the seismic response analysis of the historical town of Nicastro (southern Italy) during the March 1638 Calabria earthquake. Engineering Structures, 30, 2211–2222. https://doi.org/10.1016/j.engstruct.2007.06.002

Pan, Q., Shen, X., Ye, X., & Wang, L. (2024). Fine shear-wave velocity structures beneath the Guangdong–Hong Kong–Macao Greater Bay Area using dense seismic arrays and the SPAC method. Seismological Research Letters, 95, 2894–2909.

Panzera, F., Romagnoli, G., Tortorici, G., D'Amico, S., Rizza, M., & Catalano, S. (2019). Integrated use of ambient vibrations and geological methods for seismic microzonation. Journal of Applied Geophysics, 170, 103820. https://doi.org/10.1016/j.jappgeo.2019.103820

Paolucci, R., Faccioli, E., & Maggio, F. (1999). 3D response analysis of an instrumented hill at Matsuzaki, Japan. Journal of Seismology, 3, 191–209.

Paultre, P., Lefebvre, G., Devic, J.-P., & Côté, G. (1993). Statistical analyses of damages to buildings in the 1988 Saguenay earthquake. Canadian Journal of Civil Engineering, 20(6), 988–998. https://doi.org/10.1139/l93-130

Pelekis, P., & Athanasopoulos, G. (2011). An overview of surface wave methods and a reliability study of a simplified inversion technique. Soil Dynamics and Earthquake Engineering, 31, 1654–1668.

Perret, D., Charrois, E., & Bolduc, M. (2016). Shear wave velocity estimation from piezocone test data for eastern Canada sands. Natural Resources Canada.

Petersen, M. D., Shumway, A. M., Powers, P. M., Mueller, C. S., Moschetti, M. P., Frankel, A. D., Rezaeian, S., McNamara, D. E., Luco, N., Boyd, O. S., & others. (2020). The 2018 update of the U.S. National Seismic Hazard Model. Earthquake Spectra, 36, 5–41.

Pitilakis, K., Riga, E., Anastasiadis, A., Fotopoulou, S., & Karafagka, S. (2019). Proposal for an alternative site classification scheme and associated intensity-dependent spectral amplification factors. Soil Dynamics and Earthquake Engineering, 126, 105137.

Pratt, T. L. (2003). Amplification of seismic waves by the Seattle Basin, Washington State. Bulletin of the Seismological Society of America, 93, 533–545.

Rankka, K., Andersson-Sköld, Y., Hultén, C., Larsson, R., Leroux, V., & Dahlin, T. (2004). Quick clay in Sweden. Swedish Geotechnical Institute.

Regnier, M., Moris, S., Shapira, A., Malitzky, A., & Shorten, G. (2000). Microzonation of expected seismic site effects across Port Vila, Vanuatu. Journal of Earthquake Engineering, 4, 215–231. https://doi.org/10.1080/13632460009350369

Rekoske, J. M., Moschetti, M. P., & Thompson, E. M. (2022). Basin and site effects in the U.S. Pacific Northwest estimated from small-magnitude earthquakes. Bulletin of the Seismological Society of America, 112, 438–456.

Rohilla, S., & Sebastian, R. (2023). Resonant column and cyclic torsional shear tests on Sutlej River sand. Soil Dynamics and Earthquake Engineering, 166, 107766.

Rollins, K. M., Evans, M. D., Diehl, N. B., & Daily, W. D., III. (1998). Shear modulus and damping relationships for gravels. Journal of Geotechnical and Geoenvironmental Engineering, 124, 396–405. https://doi.org/10.1061/(ASCE)1090-0241(1998)124:5(396)

Rosset, P., Bour-Belvaux, M., & Chouinard, L. (2015). Microzonation models for Montreal with respect to Vs30. Bulletin of Earthquake Engineering, 13, 2225–2239. https://doi.org/10.1007/s10518-014-9716-8

Saathoff, J.-E., & Achmus, M. (2023). Excess pore pressure accumulation in sands. Soil Dynamics and Earthquake Engineering, 165, 107721.

Saeidi, A., Heidarzadeh, S., Lalancette, S., & Rouleau, A. (2021). Effects of in situ stress uncertainties on open stope stability. Geomechanics for Energy and the Environment, 25, 100194. https://doi.org/10.1016/j.gete.2020.100194

Salsabili, M., Saeidi, A., Rouleau, A., & Nastev, M. (2021a). 3D probabilistic modelling and uncertainty analysis of glacial and post-glacial deposits of the city of Saguenay, Canada. Geosciences, 11, 204. https://doi.org/10.3390/geosciences11050204

Salsabili, M., Saeidi, A., Rouleau, A., & Nastev, M. (2021b). Seismic microzonation of a region with complex surficial geology based on different site classification approaches. Geoenvironmental Disasters, 8, 27. https://doi.org/10.1186/s40677-021-00198-8

Salsabili, M., Saeidi, A., Rouleau, A., & Nastev, M. (2022). Development of empirical CPTu–Vs correlations for post-glacial sediments in southern Quebec, Canada. Soil Dynamics and Earthquake Engineering, 154, 107131. https://doi.org/10.1016/j.soildyn.2021.107131

Salsabili, M., Saeidi, A., Rouleau, A., & Nastev, M. (2023). Probabilistic approach for seismic microzonation integrating 3D geological and geotechnical uncertainty. Earthquake Spectra, 39, 310–334. https://doi.org/10.1177/87552930221132576

Salsabili, M., Saeidi, A., Rouleau, A., & Nastev, M. (2021a). 3D probabilistic modelling and uncertainty analysis of glacial and post-glacial deposits of the city of Saguenay, Canada. Geosciences, 11(5), 204. https://doi.org/10.3390/geosciences11050204

Salsabili, M., Saeidi, A., Rouleau, A., & Nastev, M. (2021b). Seismic microzonation of a region with complex surficial geology based on different site classification approaches. Geoenvironmental Disasters, 8(1), 27. https://doi.org/10.1186/s40677-021-00198-8

Salsabili, M., Saeidi, A., Rouleau, A., & Nastev, M. (2022). Development of empirical CPTu–Vs correlations for post-glacial sediments in southern Quebec, Canada. Soil Dynamics and Earthquake Engineering, 154, 107131. https://doi.org/10.1016/j.soildyn.2021.107131

Salsabili, M., Saeidi, A., Rouleau, A., & Nastev, M. (2023). Probabilistic approach for seismic microzonation integrating 3D geological and geotechnical uncertainty. Earthquake Spectra, 39(1), 310–334. https://doi.org/10.1177/87552930221132576

Sanou, A.-G., Saeidi, A., Heidarzadeh, S., Chavali, R. V. P., Samti, H. E., & Rouleau, A. (2022). Geotechnical parameters of landslide-prone Laflamme Sea deposits, Canada: Uncertainties and correlations. Geosciences, 12, 297. https://doi.org/10.3390/geosciences12080297

Santucci de Magistris, F., d'Onofrio, A., Penna, A., Puglia, R., & Silvestri, F. (2014). Lessons learned from two case histories of seismic microzonation in Italy. Natural Hazards, 74, 2005–2035. https://doi.org/10.1007/s11069-014-1281-6

Schnabel, P. B., Lysmer, J., & Seed, H. B. (1972). SHAKE: A computer program for earthquake response analysis of horizontally layered sites. University of California, Berkeley.

Seed, H. B. (1970). Soil moduli and damping factors for dynamic response analyses. University of California.

Seed, H. B., & Idriss, I. M. (1982). Ground motions and soil liquefaction during earthquakes. Earthquake Engineering Research Institute.

Seed, H. B., Romo, M. P., Sun, J. I., Jaime, A., & Lysmer, J. (1988). The Mexico earthquake of September 19, 1985: Relationships between soil conditions and earthquake ground motions. Earthquake Spectra, 4, 687–729.

Seed, H. B., Ugas, C., & Lysmer, J. (1976). Site-dependent spectra for earthquake-resistant design. Bulletin of the Seismological Society of America, 66, 221–243.

Seed, H. B., Wong, R. T., Idriss, I. M., & Tokimatsu, K. (1986). Moduli and damping factors for dynamic analyses of cohesionless soils. Journal of Geotechnical Engineering, 112, 1016–1032. https://doi.org/10.1061/(ASCE)0733-9410(1986)112:11(1016)

Seyhan, E., & Stewart, J. P. (2014). Semi-empirical nonlinear site amplification from NGA-West2 data and simulations. Earthquake Spectra, 30, 1241–1256.

Shabani, M. J., & Zakerinejad, M. (2022). Slope topographic impacts on nonlinear seismic analysis of soil–foundation–structure interaction. Soil Dynamics and Earthquake Engineering, 160, 107365.

Shome, N., Cornell, C. A., Bazzurro, P., & Carballo, J. E. (1998). Earthquakes, records, and nonlinear responses. Earthquake Spectra, 14, 469–500.

Silva, W. J., & Lee, K. (1987). WES RASCAL code for synthesizing earthquake ground motions (Report 24). U.S. Army Corps of Engineers.

Sitar, N., & Clough, G. W. (1983). Seismic response of steep slopes in cemented soils. Journal of Geotechnical Engineering, 109, 210–227.

Smerzini, C., Galasso, C., Iervolino, I., & Paolucci, R. (2014). Ground motion record selection based on broadband spectral compatibility. Earthquake Spectra, 30, 1427–1448.

Song, Y. Y., Castagna, J. P., Black, R. A., & Knapp, R. W. (1989). Sensitivity of near-surface shear-wave velocity determination from Rayleigh and Love waves. Society of Exploration Geophysicists.

Spudich, P., Hellweg, M., & Lee, W. H. K. (1996). Directional topographic site response at Tarzana observed in aftershocks of the 1994 Northridge earthquake. Bulletin of the Seismological Society of America, 86, S193–S208.

Steidl, J. H. (2000). Site response in southern California for probabilistic seismic hazard analysis. Bulletin of the Seismological Society of America, 90(6B), S149–S169. https://doi.org/10.1785/0120000504

Stewart, J. P. (2008). Benchmarking of nonlinear geotechnical ground response analysis procedures. Pacific Earthquake Engineering Research Center.

Stone, W. C., Yokel, F. Y., & Celebi, M. (1987). Engineering aspects of the September 19, 1985 Mexico earthquake. Earthquake Engineering Research Institute.

Talhaoui, A., Brahim, A. I., Aberkan, M., Kasmi, M., & Mouraouah, A. E. (2004). Seismic microzonation and site effects at Al Hoceima City, Morocco. Journal of Earthquake Engineering, 8, 585–596. https://doi.org/10.1080/13632460409350502

Talukder, M. K., Rosset, P., & Chouinard, L. (2021). Reduction of bias and uncertainty in regional seismic site amplification factors. GeoHazards, 2, 277–301. https://doi.org/10.3390/geohazards2030015

Tarbali, K., & Bradley, B. A. (2016). The effect of causal parameter bounds in PSHA-based ground motion selection. Earthquake Engineering & Structural Dynamics, 45, 1515–1535.

Tong, L., Che, H., Zhang, M., & Pan, H. (2018). Determination of shear wave velocity of Yangtze Delta sediments using seismic piezocone tests. Transportation Geotechnics, 14, 29–40.

Tonni, L., & Simonini, P. (2013). Shear wave velocity as a function of cone penetration test measurements in sand and silt mixtures. Engineering Geology, 163, 55–67.

Tremblay, R., Atkinson, G. M., Bouaanani, N., Daneshvar, P., Léger, P., & Koboevic, S. (2015). Selection and scaling of ground motion time histories for seismic analysis using NBCC 2015. In Proceedings of the 11th Canadian Conference on Earthquake Engineering (p. 69).

Urgeles, R., Locat, J., Lee, H. J., & Martin, F. (2002). The Saguenay Fjord, Quebec, Canada: Integrating marine geotechnical and geophysical data for spatial seismic slope stability and hazard assessment. Marine Geology, 185, 319–340. https://doi.org/10.1016/S0025-3227(02)00185-8

Urzua, A. (1974). Determinación del período fundamental de vibración del suelo. University of Chile.

Vanmarcke, E. (1979). Representation of earthquake ground motion: Scaled accelerograms and equivalent response spectra. U.S. Army Engineer Waterways Experiment Station.

Vijayendra, K. V., Nayak, S., & Prasad, S. K. (2015). An alternative method to estimate fundamental period of layered soil deposit. Indian Geotechnical Journal, 45, 192–199.

Vucetic, M., & Dobry, R. (1991). Effect of soil plasticity on cyclic response. Journal of Geotechnical Engineering, 117, 89–107.

Wang, S., Shi, Y., Jiang, W., Yao, E., & Miao, Y. (2018). Estimating site fundamental period from shear-wave velocity profile. Bulletin of the Seismological Society of America, 108(6), 3431–3445. https://doi.org/10.1785/0120180103

Xia, J., Miller, R. D., & Park, C. B. (1999). Estimation of near-surface shear-wave velocity by inversion of Rayleigh waves. Geophysics, 64, 691–700.

Yamin, L. E., Reyes, J. C., Rueda, R., Prada, E., Rincon, R., Herrera, C., & others. (2018). Practical seismic microzonation in complex geological environments. Soil Dynamics and Earthquake Engineering, 114, 480–494. https://doi.org/10.1016/j.soildyn.2018.07.030

Zayed, M., Ebeido, A., Prabhakaran, A., Kim, K., Qiu, Z., & Elgamal, A. (2021). Shake table testing: A high-resolution vertical accelerometer array for tracking shear wave velocity. Geotechnical Testing Journal, 44, 1097–1118.

Zhang, Z., Fleurisson, J.-A., & Pellet, F. (2018). Effects of slope topography on acceleration amplification and interaction with seismic input motion. Soil Dynamics and Earthquake Engineering, 113, 420–431.

Zhao, J. X., Irikura, K., Zhang, J., Fukushima, Y., Somerville, P. G., Asano, A., Ohno, Y., Oouchi, T., Takahashi, T., & Ogawa, H. (2006). An empirical site-classification method for strong-motion stations in Japan using H/V response spectral ratio. Bulletin of the Seismological Society of America, 96(3), 914–925. https://doi.org/10.1785/0120050124

Zhu, C., Pilz, M., & Cotton, F. (2020). Which is a better proxy, site period or depth to bedrock, in modelling linear site response in addition to the average shear-wave velocity? Bulletin of Earthquake Engineering, 18(3), 797–820. https://doi.org/10.1007/s10518-019-00738-6

PUBLICATIONS

Journals

1. Hossain, A. F., Saeidi, A., Salsabili, M., Nastev, M., Suescun, J. R., & Bayati, Z. (2025). A Review of Parameters and Methods for Seismic Site Response. Geosciences, 15(4), 128. https://doi.org/10.3390/geosciences15040128 (Published: 1 April 2025).
2. Hossain, A. S. M. F., Salsabili, M., Saeidi, A., Nastev, M., & Suescun, J. R. (2025). Effects of complex surficial geology on seismic amplification in Quebec, Canada. Georisk: Assessment and Management of Risk for Engineered Systems and Geohazards, 1–21. https://doi.org/10.1080/17499518.2025.2591757 (Published: 24 November 2025).
3. Hossain, A. F., Saeidi, A., Salsabili, M., Nastev, M., Suescun, J. R., & Bayati, Z. (2025). Evaluation Of Site Periods Derived from Analytical and Numerical Simulations for Seismic Microzonation in Saguenay, Eastern Canada. (Submitted to Earthquake Spectra on 12 December 2025)
4. Hossain, A. F., Salsabili, M., Saeidi, A., Nastev, M., Suescun, J. R., Seismic Microzonation of a Region with Complex Surficial Geology Based on A Comprehensive Nonlinear Site Amplification Modelling. (First Corrections submitted to Soil Dynamics and Earthquake Engineering on 12 December 2025)

Conferences

1. Hossain, A. F., Salsabili, M., Saeidi, A., Suescun, J. R., & Nastev, M. (2023, November). Effects of shear wave velocity and thickness of soil layers on 1D dynamic response in the Saguenay Region, Quebec. In Rocscience International Conference (RIC, 2023) (pp. 165-173). Atlantis Press.
2. Hossain, A. F., Saeidi, A., Salsabili, M., Nastev, M., & Suescun, J. (2024). Soil Dynamic Response and Site Amplification Parameters for Saguenay, Eastern Canada. Japanese Geotechnical Society Special Publication, 10(52), 1952-1957.
3. Hossain, A. F., Saeidi, A., Salsabili, M., Nastev, M., & Suescun, J. (2025). Analytical and Numerical Investigation of the Site Response Period in The Saguenay Region, Eastern Canada. 3rd Croatian Conference on Earthquake Engineering (3CroCEE) (pp 118-127).

APPENDIX

Appendix A: validation & comparison

The comprehensive ground response analysis in this study was utilized using the DEEPSOIL V7.0 software, where the earlier versions of DEEPSOIL (Hashash et al., 2015) have undergone extensive verification and validation by the broader user community, demonstrating their ability to replicate observed site responses at established soil sites (Hashash et al., 2015; Kim & Hashash, 2013; Régnier et al., 2016; Stewart et al., 2008; Yee & Stewart, 2018). During the 1988 Saguenay earthquake, maximum amplifications ranged from 3.4 to 5, primarily in the short-period range, depending on the epicentral distance (Paultre et al., 1993). Applying the horizontal to vertical response spectral (HVRS) analysis, Braganza et al. (2016) reported maximum linear amplification values of as much as nine at more extended periods in very soft sediments in Eastern Canada. In this study, the maximum linear amplification for the 10%/50-year PE was ~9.5 at around 2.0 s, and 6.5 for nonlinear amplification at around 1.0 s, for soft sediments. At the 2%/50-year PE, the maximum amplification values were 9.5 and 5.5 for the linear and nonlinear analyses, respectively. This indicates that a higher hazard level increases the ground motion amplitude and surface response. However, the relative amplification becomes lower due to the nonlinear behavior of soils with improved damping.

We compared our DEEPSOIL results using the RS2 software by Rocscience. For this purpose, two representative soil models, M35 and M40, were selected from a total of 50 DEEPSOIL models. These two models varied in terms of soil thickness, natural period, V_{s30}, and V_{savg} values, as detailed in Table 1. The Saguenay 1988 earthquake ground motion was chosen and scaled to represent a low-intensity event, approximately equivalent to the NBCC 2020 hazard level of 40% probability of exceedance in 50 years, corresponding to a return period of around 100 years. The time history and response spectrum of the scaled motion are presented in Figure 1.

Table 1: Site parameters of the selected soil models

	H_{soil} (m)	V_{savg} (m/s)	T_0 (s)	V_{s30} (m/s)
Model-1 (M35)	8	166	0.19	500
Model-2 (M40)	48	212	0.94	181

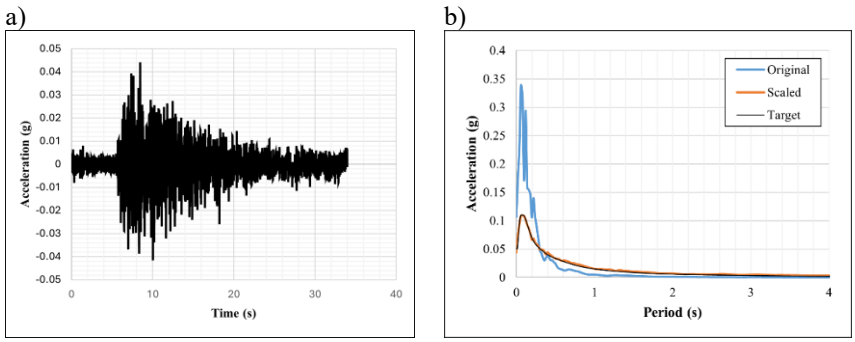

Figure 1. Input earthquake motion for validation: a) time history, b) response spectrum

The 1D soil profiles were modeled by discretizing the total soil depth into 1-meter intervals, with appropriate material properties assigned to each layer, consistent with the DEEPSOIL input. The bottom 1 meter was designated as rock based on its geotechnical properties. A nonlinear site response analysis used the same material models and parameters as in DEEPSOIL. The surface and input response spectra were used to calculate the amplification ratio. As shown in Figure 2, the DEEPSOIL and RS2 results exhibit a similar amplification trend. The comparison is not the primary focus of this study. As shown in Table 2, the maximum amplification and its corresponding period are the two key parameters examined, and they show good agreement. These values are summarized in Table 2. In both software, the thinner soil amplifies the low-period motion, while the deeper soil amplifies the high-period motion. The scatter plot in Figure 3 further illustrates the strong correlation between the two methods, with an R^2 value close to 1, indicating high agreement. Additional validation metrics, including error values, are presented in Table 3, all of which fall within acceptable ranges.

a) b)

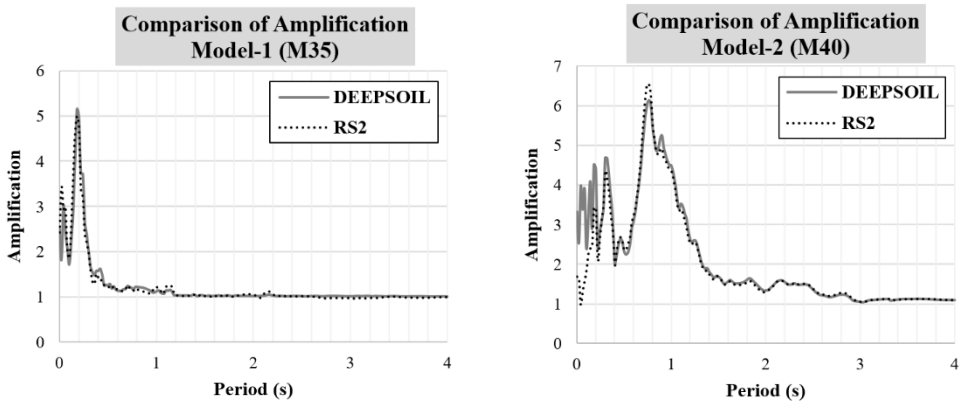

Figure 2. Response spectrum of the soil model: a) model-1 (M35), b) model-2 (M40)

Table 2: maximum amplification and corresponding amplification from the two models from DEEPSOIL and RS2.

	Model-1 (M35)		Model-2 (M40)	
	RS2	**DEEPSOIL**	**RS2**	**DEEPSOIL**
Maximum Amplification	4.99	5.15	6.54	6.14
Corresponding Period	0.18	0.18	0.76	0.76

a) b)

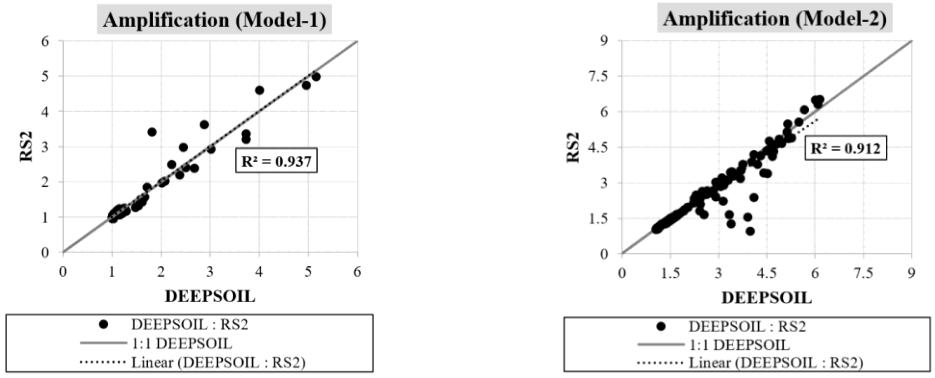

Figure 3. Scattered plot of the Response spectrum of the soil model: a) model-1 (M35), b) model-2 (M40). The orange line is the 1:1 line of the DEEPSOIL simulation.

Table 3: Different amplification errors from the two models between DEEPSOIL and RS2.

	M35	**M40**
Mean Absolute Error (MAE) %	3.46	7.19%
Mean Squared Error (MSE) %	0.34	8.29%
Root Mean Squared Error (RMSE) %	0.58	2.88%
R-squared (R^2)	0.937	0.90

Appendix B: standard errors and p values of the regression parameters

Table 4. Standard Errors and P values of the regression parameters for 2%/50yrs PE

2%/50yrs PE															
Period (s)	R^2	RMSE	Parameters					Std_Errors				P_Values			
			β_0	β_1	β_2	β_3	β_4	β_1	β_2	β_3	β_4	β_1	β_2	β_3	β_4
0.01	0.78	0.26	-0.90	0.12	-0.48	-0.12	0.05	0.28	0.19	0.15	0.02	0.68	0.02	0.44	0.06
0.1	0.63	0.30	0.94	0.32	-0.25	-0.57	0.06	0.32	0.22	0.17	0.03	0.32	0.25	0.00	0.04
0.2	0.53	0.27	0.93	0.67	0.15	-0.81	0.03	0.28	0.19	0.15	0.02	0.02	0.42	0.00	0.25
0.5	0.44	0.26	5.43	-0.64	-0.38	-0.26	-0.01	0.27	0.18	0.15	0.02	0.02	0.05	0.08	0.61
1	0.91	0.12	5.58	-1.42	-0.54	0.52	-0.02	0.13	0.09	0.07	0.01	0.00	0.00	0.00	0.12
2	0.90	0.13	-3.33	0.38	0.69	0.35	-0.02	0.14	0.09	0.07	0.01	0.01	0.00	0.00	0.21
5	0.83	0.06	-1.32	0.16	0.27	0.12	0.00	0.07	0.04	0.04	0.01	0.02	0.00	0.00	0.62
10	0.79	0.08	-0.06	-0.09	0.13	0.16	0.01	0.09	0.06	0.05	0.01	0.30	0.03	0.00	0.46

Table 5. Standard Errors and P values of the regression parameters for 10%/50yrs PE

10%/50yrs PE															
Period (s)	R^2	RMSE	Parameters					Std_Errors				P_Values			
			β_0	β_1	β_2	β_3	β_4	β_1	β_2	β_3	β_4	β_1	β_2	β_3	β_4
0.01	0.74	0.20	-0.18	0.2149	-0.2387	-0.245	0.0467	0.21	0.14	0.11	0.02	0.32	0.09	0.04	0.02
0.1	0.51	0.23	1.42	0.3937	0.0063	-0.6163	0.0459	0.25	0.16	0.13	0.02	0.12	0.97	0.00	0.04
0.2	0.54	0.23	1.97	0.6234	0.2744	-0.8745	0.0217	0.25	0.16	0.13	0.02	0.01	0.09	0.00	0.32
0.5	0.61	0.29	6.76	-1.3005	-0.5416	0.1893	-0.0388	0.31	0.20	0.16	0.03	0.00	0.01	0.25	0.16
1	0.78	0.23	3.57	-1.0991	-0.2235	0.5801	-0.0169	0.25	0.16	0.13	0.02	0.00	0.17	0.00	0.44
2	0.89	0.13	-4.53	0.6546	0.8243	0.3182	-0.0225	0.14	0.09	0.07	0.01	0.00	0.00	0.00	0.07
5	0.87	0.05	-1.60	0.2494	0.2835	0.088	-0.0049	0.05	0.03	0.03	0.00	0.00	0.00	0.00	0.25
10	0.89	0.05	-0.91	0.0741	0.2155	0.1483	-0.0066	0.05	0.03	0.03	0.00	0.18	0.00	0.00	0.17

Appendix C: conference papers

CONFERENCE PAPER-1

Effects of Shear Wave Velocity and Thickness of Soil Layers on 1D Dynamic Response in the Saguenay Region, Quebec

A S M Fahad Hossain[1] Mohammad Salsabili[2] Ali Saeidi[3][0000-0001-6954-5453] Juliana Ruiz Suescun[4] and Miroslav Nastev[5]

[1, 3] Université du Québec à Chicoutimi, Chicoutimi QC

[2]Western University, London ON

[4] Hydro Québec, Montreal QC

[5] Geological Survey of Canada, Quebec City QC

hossain.a-s-m-fahad1@uqac.ca

Abstract

Before reaching the ground surface, the amplitude, duration and frequency content of the vertically propagating seismic waves can be modified by the local stratigraphy and soil physical properties. In this study, we evaluate the impacts of the soil shear wave velocity (V_s) and thickness (H) on the seismic ground response using 1D ground response analysis. Simplified soil profiles typical for the Saguenay Lac-Saint-Jean region (SLSJ) are considered defined with relatively thin glacial sediments overlaid by more than 100m thick marine sequence. Impedance contrasts exist at the bedrock interface and between the fine marine and glacial sediments. Time-domain nonlinear 1D numerical simulations are carried out with Deepsoil®. The seismic input at the bedrock level is defined with synthetic earthquake time histories compatible with eastern Canadian seismo-tectonic settings. It is found that the changes in the Fundamental period of the soil caused by changes in the thickness of the soil deposit and soil V_s have a significant impact on the surficial amplification.

Keywords: 1D nonlinear ground response, response spectrum, fundamental period, soil amplification.

1. Introduction

Several studies have confirmed that seismic shaking during strong earthquakes can be significantly influenced by local soil conditions, as observed in field studies or through numerical modeling. Several numerical approaches for ground response analysis exist in the literature [1]. They can be carried out in 1D, 2D or 3D; with linear, equivalent linear, nonlinear or advanced constitutive models; and in frequency or time domain [2-3].

The soil nonlinear behavior under earthquake loading is defined with soil dynamic stiffness (shear modulus) and damping properties. The maximal acceleration and frequency content of the surface motion are significantly influenced by the level of input ground motion intensity and shear stiffness of the soil deposit [4]. The response of ground during an earthquake motion is related to some soil parameters, such as V_{s30}, the fundamental frequency of vibration of the soil column (F_0), and seismic impedance contrast (I_w) where F_0 which is dependent on the Vs and thickness of the soil deposit is the most helpful parameter for the prediction of seismic amplification function [5]. The majority of seismic site response studies have concentrated on the impacts of the shear wave velocity (V_s) on the peak ground acceleration (PGA), spectral accelerations of interest (S_a), and site-specific amplification factors (AF) [6-9].

The objective of the present study is to investigate the potential effects of the local site conditions on the surface ground motion in the SLSJ region, Quebec. Several representative soil profiles for the study area is considered with glacial and fine marine sediments overlying bedrock formations. 1D nonlinear response analyses are carried out with Deepsoil v7.0 software with generic shear modulus reduction and damping curves. The seismic input consists of a series of synthetic time histories compatible with eastern Canadian seism tectonic settings. The simulations are run for varying thickness of the soil units assigned with respective V_s.

2. Study Area

The SLSJ region is located in Eastern Canada, a relatively stable continental region within the North American plate. Nevertheless, strong earthquakes have struck the region in the past, among which

the most recent one was the 1988 Mw 5.9 Saguenay earthquake with a shallow crustal depth of 28km and an epicentral distance of about 35km (https://earthquakescanada.nrcan.gc.ca/). On the regional scale, SLSJ is mainly affected by the Charlevoix–Kamouraska seismic zone, the seismically most active zone in Eastern Canada located about 75 km southward. Glacial sediments (till), consisting of a wide-graded mixture of debris material, compact to semi consolidated are found at the base of the Quaternary stratigraphic column. As a result of the final meltdown and retreat of the ice sheet, marine waters of the successive Laflamme Sea inundated the region. This incursion contributed to the deposition of more than 100m thick fine marine clay and silt sediments, referred herein as clays, on top of the glacial sediments. A particular problem in the study area is the occasional presence of sensitive clays. They are often related to landslides, liquefaction, lateral spread and other ground failures, where they undergo a quick transition from a solid to a fluid state. In addition, the strong impedance contrast between the unconsolidated deposits and the bedrock formations can have a significant impact on the soil dynamic response.

3. Methodology

The applied methodology can be divided into three main steps: selection of soil input parameters, selection of input ground motions, and 1D nonlinear ground response analyses. The simulations are carried out with Deepsoil® assuming that the soil layers are horizontal and infinite and that the seismic excitation consists of vertically propagating horizontal shear waves. The soil behavior is analyzed using numerical integration of the equation of motion in time domain which allows for rigorous nonlinear analyses. The strength based general quadratic/hyperbolic (GQ/H) soil model proposed by [10] is used as it has a better shear modulus and damping curve fitting method at the larger strains. The input soil parameters and earthquake ground motion are described in detail in the following section.

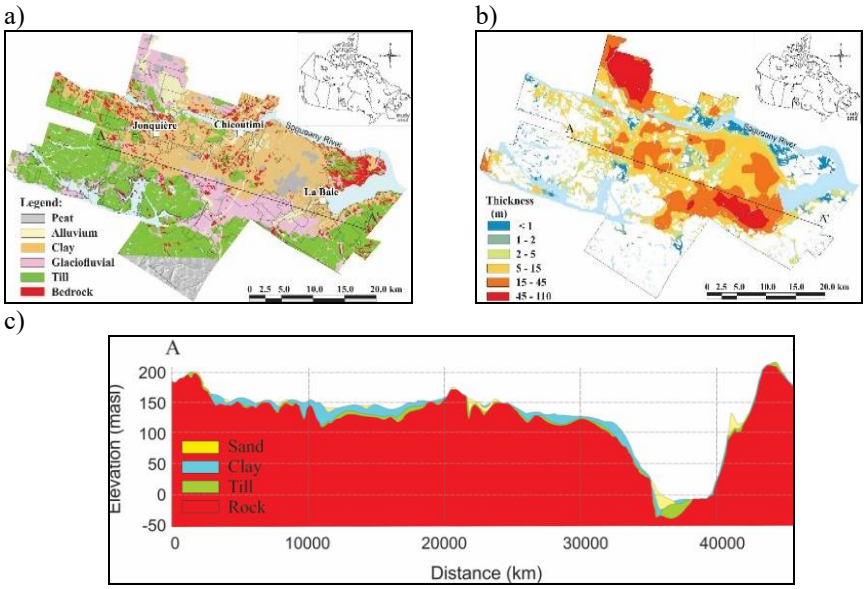

Fig. 1. Saguenay Lac St. Jean study area a) simplified surficial geology, b) thickness of surficial sediments and c) geological cross section [modified from 11 and 12].

3.1 Input soil parameters

Two typical stratigraphic soil columns are considered: (1) a single clay layer, and (2) a combination of clay and till layers on top of the bedrock. The first stratigraphic column has a strong impedance contrast at the bedrock interface. In contrast, the impedance contrast is more gradual in the second column: first between the clay and till layers, and then at the bedrock interface. Three series of simulations are run by varying the thickness of the surficial units and the respective *Vs*.

For clayey soil, the nonlinear dynamic behavior between shear strength and strain is defined with the shear modulus reduction and damping curves adopted from [13], considering a plasticity index of 18. The shear strength is determined by correlating it with the Vs value developed for eastern Quebec [14]. The V_s, shear modulus reduction and damping curves for glacial Laflamme sea sediments are taken from Hydro Quebec. Based on the 3D geological model developed by [15], the thickness of the LaFlamme clay unit varies between a few meters to about 100 m. In the analyses, discrete clay thickness of 10, 20, 30, 50 and 100 m was considered. The thickness of the glacial sediments at the

base of the second soil column was fixed at 10 m. Based on the V_s -depth regression analysis conducted over more than 1000 field measurements by [16], three average shear wave velocities for the clay layer were assumed as V_s =150, 200 to 250 m/s. The bedrock V_s are assumed with fixed value, $V_{s\ rock}$=1875m/s [16]. A total of 30 simulations are conducted, 15 for the clay-rock soil column #1 and additional 15 for the clay-till-rock column #2.

3.2 Input ground motions

In the present analysis, a series of six synthetic ground motions for rock site conditions defined with $V_{s,30}$≥1500 m/s are selected as representative for eastern Canada [https://www.seismotoolbox.ca/index.html] [17]. Three of the input motions correspond to earthquakes with moment magnitude M6.0 and the other three to M7.0. All the input motions are scaled with respect to peak ground acceleration at PGA=0.3g, 0.4g and 0.5g. In this way, they are matching approximately the latest NBCC 2020 hazard for SLSJ region with a return period of 475 years, or 10%/50-year probability of exceedance. The time histories and their acceleration response spectra of the selected ground motions are given in Fig. 2 and Fig. 3, respectively.

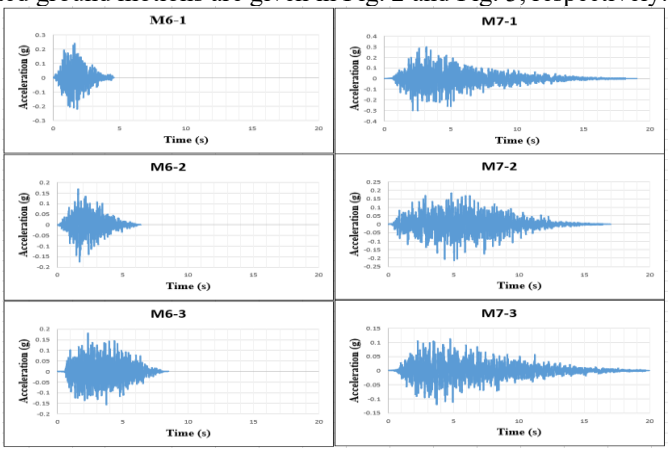

Fig. 2. Time histories of the input ground motions.

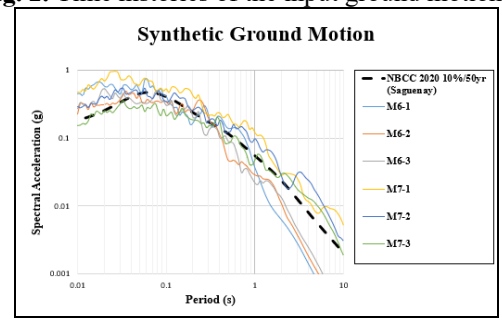

Fig. 3. Spectral acceleration of the selected motions with respect to the NBCC 2020 10%/50year response spectra.

4. Results

A total of 30 nonlinear 1D ground response simulations are performed with Deepsoil® each using the 18 input ground motions (6 synthetic ground motions scaled at PGA=0.2, 0.3 and 0.4g). From the obtained 540 resulting response time histories, the average spectral acceleration values for each model are taken as measures of the model predictive capability. The respective amplification functions are computed as the ratio between the response spectra at the ground surface and at the bedrock level, where the input motions are assigned to the model. The corresponding nonlinear analysis was compared to the equivalent linear analysis results recommended by the Deepsoil manual, and they were found to be a good match.

4.1 Response spectra at ground surface

Impact of clay thickness: In this set of simulations, the response spectra at the ground surface are compared for 5 different thicknesses of the clay unit, separately for each of the 3 assumed average clay V_s. Fig. 4 illustrates the response spectra at the ground surface for soil column #1. The average response spectrum of the input motion is also represented and indicates that the seismic energy content is concentrated in the medium period range (≤1.0s). It can be observed that the increase of the clay layer thickness results in decrease the spectral acceleration values and this result can be

explained by the gradual increase in the overall stiffness of the soil layer with thickness increase. The same observations are valid for soil column #2.

Impacts of clay V_s: Fig. 5 illustrates the response spectra at ground surface for soil column #1 for variation of the clay layer thickness from 10 to 100m and of V_s from 150 to 250 m/s. Provided that the thickness remains the same, the increase of V_s is reflected in the increase of the overall stiffness of the soil columns. This contributes to a shift of the predominant response period towards shorter values. At the same time, the spectral acceleration values increase in the medium period range (around 0.1s), where as they appear to be practically the same with those of the input motions at longer periods. The same observations are valid for soil column #2.

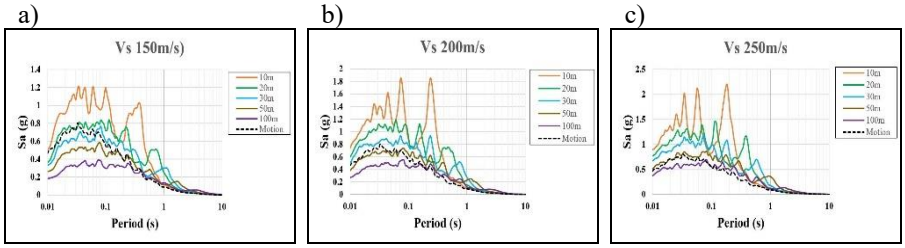

Fig. 4. Response spectra at ground surface for soil column #1 (clay on top of bedrock) with variable thickness and average V_s of: a) 150m/s b) 200m/s and c) 250m/s. The average spectral accelerations of the input motions are indicated with dashed line.

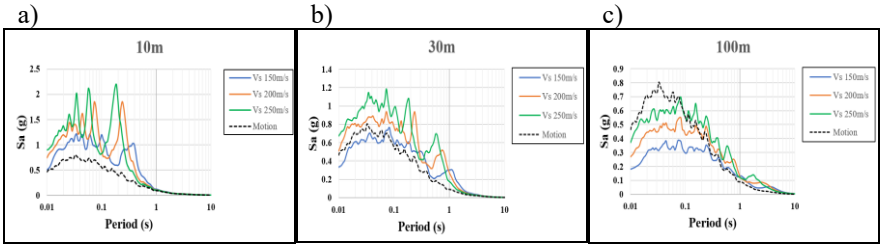

Fig. 5. Response spectra at ground surface for soil column #1 whereas the clay thickness varied as a) 10m, b) 30m and c) 100m. The average spectral accelerations of the input motions are indicated with dashed line.

4.2 Amplification at surface

Impacts of clay thickness: Fig. 6 shows the amplification functions for soil column #1 and #2 with varying thickness and V_s of 200m/s. It can be observed that the predominant period of amplification shifts to ward longer value with the increase of the thickness as the fundamental period is increasing both for two soil columns. Also, amplification of soil column #2 has lower value compared to the soil column #1 as the presence of till layer lower the impedance contrast ratio.

Impacts of clay V_s: The amplification functions results for soil having 30m thickness are presented for both soil columns in Fig. 7. As expected, a gradual shift of the dominant vibration period toward shorter values occurs with the increase of V_s, due to the increase of the stiffness of the both soil columns and the decrease of the fundamental period of soil columns and the shift is less in soil column #2 compared to soil column #1 for the presence of 10m glacial sediment. Also, the presence of glacial sediments results lower amplification in soil column #2 as compared to soil column #1.

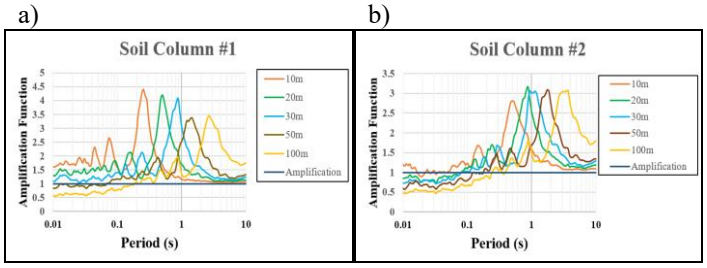

Fig. 6. a) Amplification functions for soil column with varying thickness and V_s of 200m/s: a) soil column #1 and b) soil column #2.

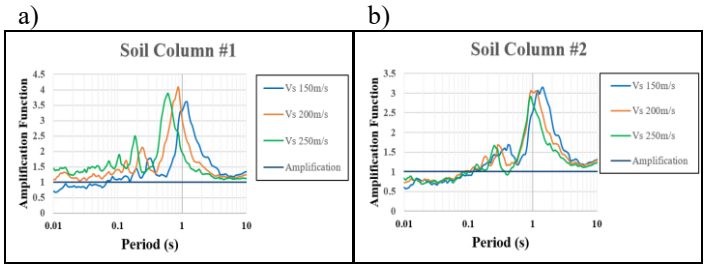

Fig. 7. Amplification function for the variation for V_s for 30m soil deposit a) soil column #1 and b) soil column #2.

5.0 Conclusion

A site-specific numerical simulation of the effects the V_s and thickness of surficial soil sediments exert on the seismic ground response is evaluated for the SLSJ region of Quebec, Canada. It was observed that, due to the gradual increase in the overall stiffness of the soil column with the increase of the clay layer thickness, the spectral acceleration values decrease. The stiffer soil columns with assigned higher clay V_s in case of the same clay layer thickness generated higher dynamic responses with dominant response periods shifted toward the shorter period range. At the same time, de-amplification was observed at shorter period ranges depending on the soil thickness. The amplification of the input ground motions is higher in soil column #1 than the soil column #2 and there is a gradual shift in the predominant period of amplification due to the change of Fundamental period by the soil thickness or V_s. This result demonstrates that the presence of till layer between the clay and rock in the eastern Canada, reduced the impedance contrast that reduce the amplification and hazard potentials. These preliminary results will help to plan the next series of numerical simulations of the dynamic soil response considering more complex soil models with gradually increasing V_s with depth and 2D analyses of the dynamic slope stability.

References

1. Eskandarinejad, Alireza, Mojtaba Jahanandish, and Hamid Zafarani: Divergence between nonlinear and equivalent-linear 1D site response analyses for different VS realizations of typical clay sites. Pure and Applied Geophysics 174 (2017): 3955-3978.
2. Schnabel, P., H. Bolton Seed, and John Lysmer: Modification of seismograph records for effects of local soil conditions. Bulletin of the seismological Society of America 62.6 (1972): 1649-1664.
3. Hashash, Y.M.A., Musgrove, M.I., Harmon, J.A., Ilhan, O., Xing, G., Numanoglu, O., Groholski, D.R., Phillips, C.A., and Park, D. “DEEPSOIL 7.0, User Manual”. Urbana, IL, Board of Trustees of University of Illinois at Urbana-Champaign (2020).
4. Dhakal, R. P., Lin, S. L., Loye, A. K., & Evans, S. J.: Seismic design spectra for different soil classes. Bulletin of the New Zealand Society for Earthquake Engineering, 46(2), 79-87 (2013).
5. Barani, S., De Ferrari, R., Ferretti, G., & Eva, C.: Assessing the effectiveness of soil parameters for ground response characterization and soil classification. Earthquake Spectra, 24(3), 565-597 (2008).
6. Kwok, Annie OL, Jonathan P. Stewart, and Youssef MA Hashash.: "Nonlinear ground-response analysis of Turkey Flat shallow stiff-soil site to strong ground motion." Bulletin of the Seismological Society of America 98.1 (2008): 331-343.
7. Rodriguez-Marek, A., Rathje, E. M., Bommer, J. J., Scherbaum, F., & Stafford, P. J.: Application of single-station sigma and site-response characterization in a probabilistic seismic-hazard analysis for a new nuclear site. Bulletin of the Seismological Society of America, 104(4), 1601-1619 (2014).
8. Griffiths, S. C., Cox, B. R., Rathje, E. M., & Teague, D. P.: Mapping dispersion misfit and uncertainty in V s profiles to variability in site response estimates. Journal of Geotechnical and Geoenvironmental Engineering, 142(11), 04016062 (2016).
9. Barani, S., De Ferrari, R., & Ferretti, G. : Influence of soil modeling uncertainties on site response. Earthquake Spectra, 29(3), 705-732 (2013).
10. Groholski, D. R., Hashash, Y. M., Kim, B., Musgrove, M., Harmon, J., & Stewart, J. P.: Simplified model for small-strain nonlinearity and strength in 1D seismic site response analysis. Journal of Geotechnical and Geoenvironmental Engineering, 142(9), 04016042 (2016).

11. Salsabili, M., Saeidi, A., Rouleau, A., & Nastev, M.: Seismic microzonation of a region with complex surficial geology based on different site classification approaches. Geoenvironmental Disasters, 8(1), 1-13 (2021).
12. Foulon, T., Saeidi, A., Chesnaux, R., Nastev, M., & Rouleau, A.: Spatial distribution of soil shear-wave velocity and the fundamental period of vibration–a case study of the Saguenay region, Canada. Georisk: Assessment and Management of Risk for Engineered Systems and Geohazards, 12(1), 74-86 (2018).
13. Abdellaziz, M., Karray, M., Chekired, M., Delisle, M. C., Locat, P., Ledoux, C., & Mompin, R.: New Model of Shear Modulus Degradation and Damping Ratio curves for Sensitive Canadian Clays. Canadian Geotechnical Journal, (ja).
14. Locat, J., Beauséjour, N., & Bérubé, MA.: Use of the ultrasonic accelerometer on cohesive soils. Canadian Geotechnical Journal, 23 (2), 247-250 (1986) (2022).
15. Salsabili, M., Saeidi, A., Rouleau, A., & Nastev, M.: Probabilistic approach for seismic microzonation integrating 3D geological and geotechnical uncertainty. Earthquake Spectra, 39(1), 310-334 (2023).
16. Ladak, Sameer, Sheri Molnar, and Samantha Palmer.: "Multi-method site characterization to verify the hard rock (Site Class A) assumption at 25 seismograph stations across Eastern Canada." Earthquake Spectra 37.1_suppl (2021): 1487-1515.
17. Atkinson, Gail M.: Earthquake time histories compatible with the 2005 National building code of Canada uniform hazard spectrum. Canadian Journal of Civil Engineering 36.6 (2009): 991-1000.

Soil Dynamic Response and Site Amplification Parameters for Saguenay, Eastern Canada

A S M Fahad Hossain[i)] Ali Saeidi[ii)] Mohammad Salsabili[iii)] Miroslav Nastev[iv)] and Juliana Ruiz Suescun[v)]

i, ii) Université du Québec à Chicoutimi, 555 Bd de l'Université, Chicoutimi, QC G7H 2B1, Canada
iii) University of Western Ontario, 1151 Richmond St, London, ON N6A 3K7, Canada
iv) Geological Survey of Canada, 490 R. de la Couronne, Québec, QC G1K 9A9, Canada
v) Hydro Québec, 75 Boul. René-Lévesque O, Montréal, QC H2Z 1A4, Canada

ABSTRACT

Site effect is an important topic in earthquake engineering and seismic risk analyses. It is widely acknowledged that during the vertical propagation of the seismic waves, this phenomenon generally contributes to amplification of the resulting surface ground motion with respect to the local stratigraphy, surface topography, impedance contrast, and the mechanical properties of the surficial sediments This may lead to significant variation of the seismic shaking and structural damage at short distances. The standard procedure in the site-specific seismic hazard analysis is to evaluate the site effects using local amplification factors (AFs) or dynamic site response simulations. The common indicator of the variety of site conditions is the time-averaged shear wave velocity of the en first 30 m (Vs_{30}). However, Vs_{30} alone may often not be sufficient to adequately assess the site effects and it is often combined with the fundamental vibration period (T_{nat}). The Saguenay Lac-Saint-Jean region (SLSJ) is characterized with moderate seismic activity and a typical Quaternary stratigraphy consisting of stiff glacial sediments at the base, soft post-glacial Laflamme Sea sediments and more recent alluvial planes. Important impedance contrast exists between the crystalline bedrock and the overlying surficial deposits. In this study, we analyse the site dynamic response through 1D linear and nonlinear simulations using representative soil profiles and earthquake motions. Typical parameters are evaluated to develop amplification functions for the region.

Keywords: Site Amplification, Ground Response Analysis, Average Shear Wave velocity for 30m and Fundamental soil period.

1. INTRODUCTION

The assessment of seismic hazard and risks to manmade structures involves characterization of the potential impacts the local site conditions exert on the ground motions. Consequently, the local seismic response can result in considerable variations on short distances with respect to the ground motion amplitudes, duration, and frequency content (Seed (1982)). It is well accepted that the local stratigraphy, geotechnical soil properties, surface topography, impedance contrast, etc., are behind the seismic site effects (Semblat et al (2005)). These effects can properly be determined by applying nonlinear soil response analysis and evaluating the potential amplification of the bedrock motion.

Site amplification factors in the national building codes are commonly defined as function of the time-averaged shear wave velocity of the top 30 m (Vs_{30}) and/or respective site classes A through E (Talukder et al (2021)). Numerous studies have confirmed Vs_{30} as an indicator of the diverse site conditions effectively capturing the local site amplification effects (Gobbi et al (2020)). However, the surficial stratigraphy, stiffness differences between the soil units and bedrock, and material nonlinearity should also be considered when analyzing the seismic response, as pointed out by studies that questioned the capacity of Vs_{30} to capture the complex site amplification phenomenon (Ciancimino et al (2018)). Parameterization of the site effects as combination of the soil natural period T_{nat} and Vs_{30} has shown better overall performance than Vs_{30} alone (Boudghene et al (2017), Hashash et al (2018) and Harmon et al (2019)).

In modern site amplification models, the natural logarithm of site amplification, FS, is frequently taken as a sum of linear and nonlinear amplification components, equation 1. In case of low intensity ground motions, low shear strains and essentially linear viscoelastic material response occur, referred to as “linear” material response for brevity, constituting the linear component. On the other hand, higher intensity ground motions result in nonlinear soil response characterized with increased material stresses combined with decreased shear modulus and increased material damping. Therefore, the nonlinear component in equation 1 represents the difference between the linear site amplification and the amplification that occurs when nonlinear site effects are present (Harmon et al (2019)).

$$F_s = \ln(amp) = F_{lin} + F_{nl} \qquad (1)$$

Generally, the local site parameters Vs_{30}, T_{nat} and soil depth Z_{soil} are considered to determine the linear term for the amplification model. On the contrary, nonlinear amplification is modelled rather as a function of the ground motion intensity parameters, such as the peak ground acceleration (PGA) or spectral accelerations (SA) at the bedrock level (Hashash et al (2018)).

Due to the variation in bedrock and soil geology, respective geotechnical properties and seismic input motions, applying amplification factors of a given region to another may generate unwanted bias in seismic hazard calculations. It is therefore necessary to characterize the local dynamic response and evaluate the parameters necessary for the development of the amplification model. The objective of the present study is to determine the dynamic response and necessary parameters affecting the site amplification for the SLSJ region, Eastern Canada. Simulation of the ground motion is conducted for a series of soil profiles considering typical stratigraphy and soil properties.

2. STUDY AREA

The SLSJ is an intraplate continental region within the North American plate. Nevertheless, strong earthquakes have struck the region in the past. The most recent was the 1988 Mw 5.9 Saguenay earthquake with a shallow crustal depth of 28km and an epicentral distance of about 35km (https://earthquakescanada.nrcan.gc.ca/). On the regional scale, SLSJ is mainly affected by the Charlevoix–Kamouraska seismic zone, the seismically most active zone in Eastern Canada located about 75 km southward.

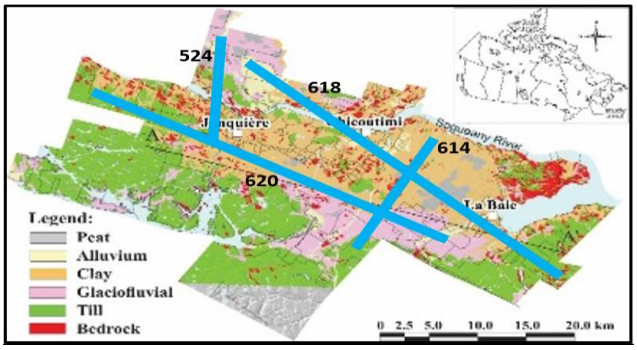

Figure 1. Simplified surficial geology in the Saguenay Lac St. Jean study area. modified from [Salsabili et al (2023)) & PACES (http://paces.uqac.ca/)].

3. METHODOLOGY

The applied methodology can be divided into three main steps: selection of input ground motions, selection of input parameters for each soil type and 1D ground response analyses.

3.1 Soil Profiles

For the selection of the soil profiles four cross-sections were selected as indicated in Figure 1. About twenty 1D soil profiles were extracted from each section considering all stratigraphic combinations. Next, 40 randomized soil profiles were selected considering the percentage of soil types and the minimum, maximum and mean thicknesses for each formation. The ranges of Vs_{30} and T_{nat} were 181m/s to 1531m/s and 0.02s to 1.62s, respectively. The Vs_{30} map of the study area is given in figure 2.

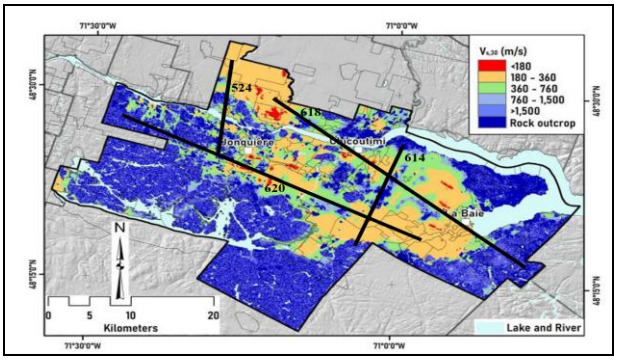

Figure 2. Spetial distribution of Vs30 in SLSJ area (modified from Salsabili et al (2023)).

3.2 Earthquake Ground Motions

Since SLSJ is a stable tectonic crust region characterized with insufficient number of recorded ground motions, a series of four synthetic ground motions for rock site conditions defined with $Vs_{30} \geq 1500$ m/s was selected as representative for moment magnitudes of M6 and M7 (https://www.seismotoolbox.ca/index.html). In addition, two records of eastern Canadian earthquakes were included: the 1988 M5.9 Saguenay earthquake and 2010 M5.1 Val des Bois Earthquake 2010, as shown in Figures 3. These ground motions were scaled using SeismoSoft (2023) according to the 2020 National Building Code of Canada guidelines (NBCC 2020) .

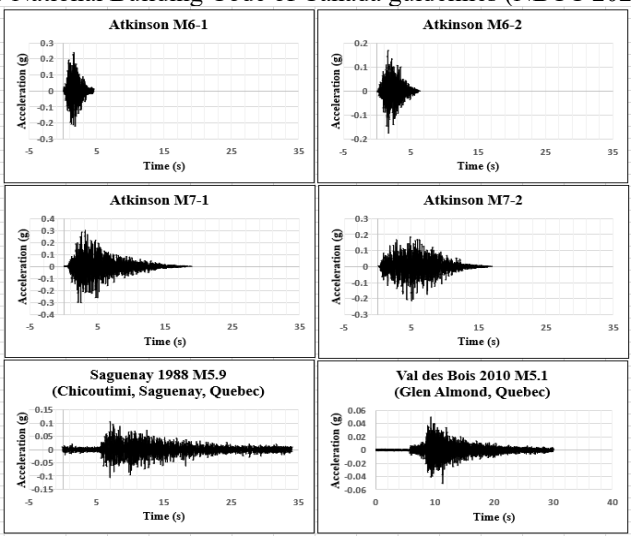

Fig 3. Time histories of the input ground motions.

3.3 Soil Dynamic Properties

The soil behavior under strong dynamic loading varies non-linearly and has significant impact on the site amplification. Proper shear modulus reduction (SM) and damping ratio (DR) curves are therefore required for dynamic analysis. Herein, SM and DM curves for gravel, sand and clay soil were selected from (Seed et al (1986), EPRI (1993) and Abdellaziz et al. (2022)), respectively. Randomized SM and DR curves were developed for sand and clay soil types based on the depth and plasticity index (PI) and assigned across the different soil profiles based on the average shear wave velocity. Empirical relation of shear wave velocity vs depth was developed based on field tests in the study area, whereas soil density values were assigned from studies in eastern Canada. The shear wave velocity of till and rock layer were taken from previous studies that were developed for eastern Canada. The references are shown in table 1.

Table 1. Retained shear wave velocity and density values

	Shear Wave Velocity (m/s)	Density (kN/m^3)
Clay	Vs = 114.5 + 9.4xD$^{0.76}$ (Salsabili et al (2023))	18.17 (Sanou et al (2022))
Sand	Vs = 144.9 + 2.55 x D (Salsabili et al (2023))	17.48 (Sanou et al (2022))
Gravel	Vs = 46.861 + 61.55 x D$^{0.5}$ (Salsabili et al (2023))	18.33 (Rollins et al (1998))
Till	582 ±174 (Motazedian et al 2011))	21 (Urgeles et al (2002))
Rock	1875 ± 781 (Ladak et al (2021))	28 (Saeidi et al (2021))

3.3 Linear and Nonlinear 1D Ground Response Analysis

The simulations were carried out with Deepsoil (Hashhash et al (2020)) assuming vertically propagating horizontal shear waves in horizontal and infinite soil layers. The non-linear? soil behavior was analyzed using numerical integration of the equation of motion in time domain allowing for rigorous nonlinear analyses. The linear analyses were conducted in the frequency domain. The pressure-dependent hyperbolic model (MKZ) was used in the analyses. The minimum

damping ration obtained from the MKZ model was used in the linear analysis. Deepsoil calculates the response spectra of the soil model assuming single degree of freedom (SDOF) system response and solving the dynamic equilibrium equation given in equation 2. The frequency domain equivalent linear analysis was also performed to validate the nonlinear results as suggested by the software manual.

$$m\ddot{u} + c\dot{u} + ku = -m\ddot{u}_g \qquad (2)$$

where, m, c, and k stand for the SDOF system's mass, viscous damping, and system stiffness, respectively. The nodal relative accelerations, relative velocities, and relative displacements are denoted by $\ddot{u}$, $\dot{u}$, and u, respectively, while the excitation acceleration at the base of the SDOF is given with $\ddot{u}g$.

4.1 Dynamic Response

The dynamic response spectra at the soil surface for profile M4 with 30m clay over 3m till are shown in Figure 5 for four hazard conditions and three types of analyses. It can be observed that the response spectral accelerations are decreasing with the increase of the hazard probability. The nonlinear and equivalent linear analyses give similar response spectra. The linear analysis yields higher response at low to medium period range since it considers minimum damping compared to NL and EL analysis.

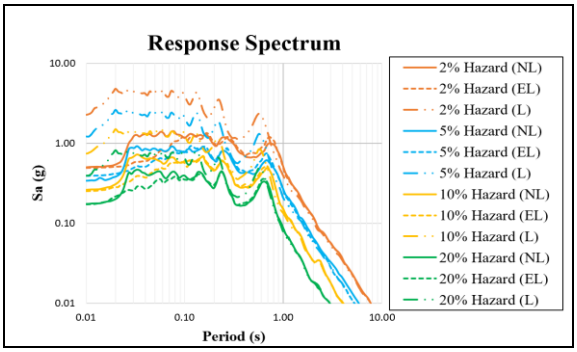

Fig. 5. Response spectra at ground surface for soil profile M-4. The hazard intensity is given as probability of exceedance in percentage in 50 years. Nonlinear (NL), equivalent linear (EL) and linear (L) analyses.

The amplification functions were determined as the ratio between the response spectra of the ground motions at the ground surface and at the bedrock level (Figure 6). In this case, practically opposite observation can be made as opposed to Figure 5. In other words, an increase in the input motion amplitudes (decreased probability) contributes to the decrease the overall amplification. The change is more visible for EL and NL results because of the nonlinear effects due to the increased damping ratios for increased strains. De-amplification was observed at low periods in EL and NL analyses. These trends are similar for practically all considered models.

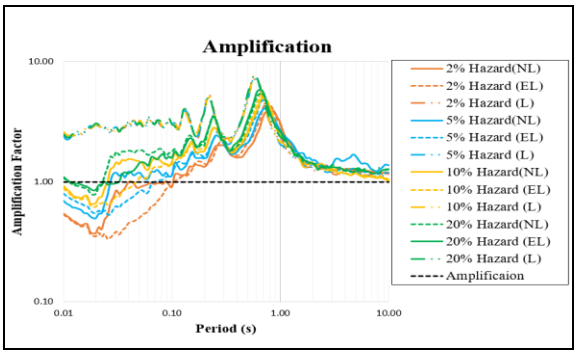

Fig. 6. Amplification factors for 2%, 5%, 10% and 20% probability of exceedance in 50 years for soil profile M-4.

4.2. Amplification Parameters

For the development of an amplification model, it is important to determine the two limiting shear wave velocities: V_L is limiting velocity below which amplification does not scale linearly, and Vc is limiting velocity beyond which site amplification is independent of V_{S30}. In figure 7 are shown the amplification factors for 2%/50yrs hazard for NL and L analyses for two spectral periods: 0.2s and 1.0s. It can be seen that for 0.2s, L amplification is higher than the NL amplification for Vs_{30} up to 500m/s. Following this threshold level, the trend is reversed. For period of 1.0s, both NL and L amplifications are almost similar. The limiting shear wave velocity V_C and V_L values for 0.2s and 1.0s periods are around: 180m/s and 1500m/s, and 180m/s and 500m/s, respectively.

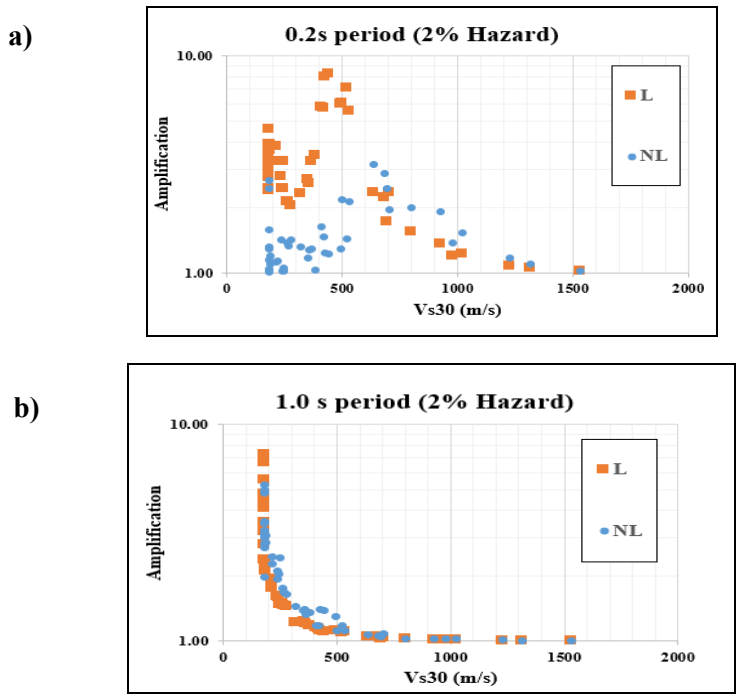

Fig. 7. Amplification factors as a function of Vs30 for soil a column M-4 a) 0.2s Period b) 1.0s period

Another important parameter for modeling the site amplification is the natural vibration period of the soil, T_{nat}. T_{nat} exerts a high impact on the soil dynamic response and the amplification is high at periods close to T_{nat}. This effect is referred to as the resonance (Hossain et al (2023)). To identify the resonance amplification effect, linear amplification for 2%/50yrs hazard was plotted at different periods as a function of the ratio of the oscillation period divided by T_{nat} for each soil profile. Figure 8 shows such plots for 20 soil models with different natural periods, where the resonance is clearly noticed for almost all models. The peak is within the period range ratio of 0.8 to 1.0, which denotes a resonance amplification that follows the Ricker wavelet pattern.

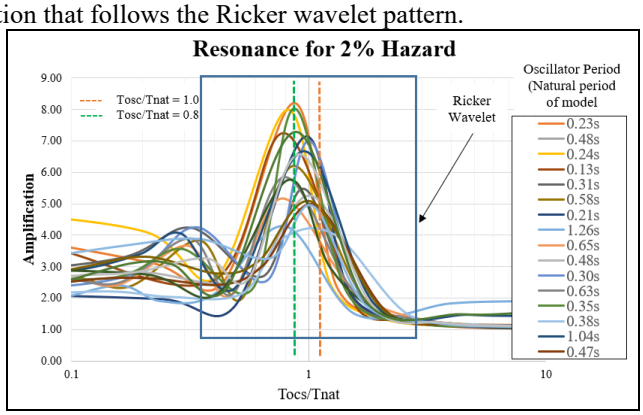

Fig. 8. Amplification as a function of T_{osc}/T_{nat} for periods 0.1s to 10.0s for soil a column M4.

4.3 Comparison with NBCC 2020

NBCC 2020 provides the seismic hazard values based on different site class or Vs_{30} values for different probably of exceedance (%). The amplification for four models with different Vs_{30} and T_{nat} values were compared to the amplifications calculated from NBCC 2020 based on the Vs_{30} values and are given in Figure 9. The NBCC 2020 curves are almost linear for all soil models and the difference between the two hazards are reduced by increasing the Vs_{30} values. The L and NL analyses gave higher amplification at lower period and lower amplification at higher period compared to NBCC curves. For the NL analyses, the amplification is higher at low to medium period for 10% hazard where it is reversed at medium to high period. The predominant periods also shift to longer period for the decrease in the hazard probability. The L analysis gives near values for both hazard probabilities but compared to NL the predominant period for the L analyses is at shorter period and the amplification for the predominant period is higher than NL analyses. It is because of using the minimum damping values in the L analyses where in the NL analyses the damping increases at higher strain at high frequencies or lower periods. Also, it was observed that high amplification happens in short to medium period ranges, but the NBCC presents lower amplification factors.

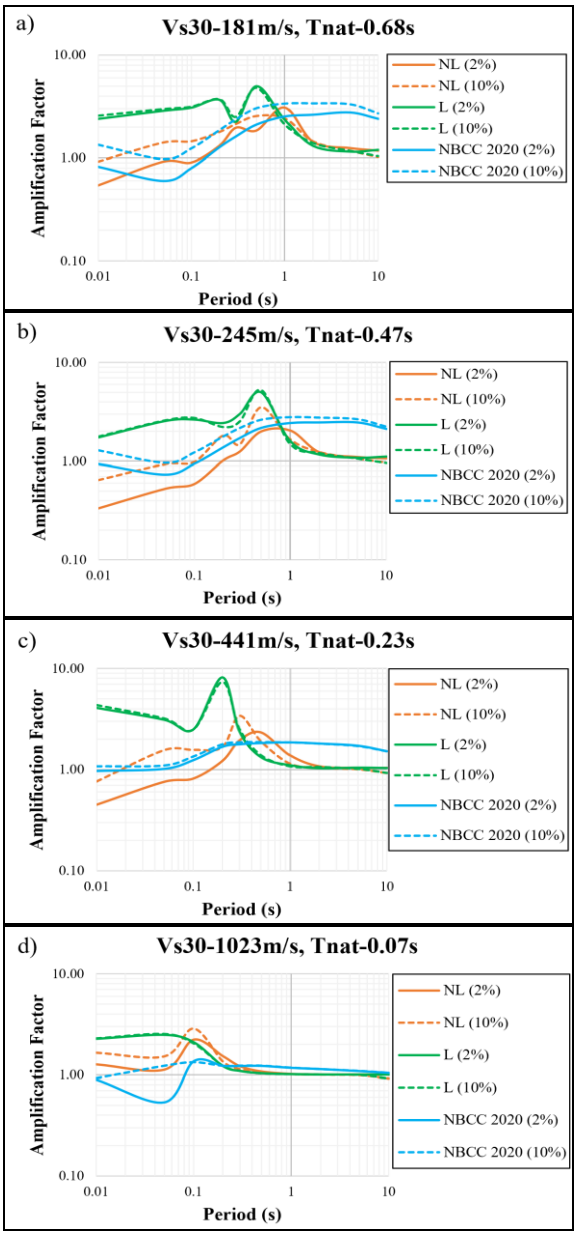

Fig. 9. Amplification factors for L and NL analyses compared to NBCC 2020 for different soil columns based on Vs30 values: a) M-4 (Vs30 181 m/s), b) M-3 (Vs30 245 m/s) c) M-2 ((Vs30 441 m/s)) and d) M-1 ((Vs30 1023m/s))

5. CONCLUSION

Site-specific nonlinear 1D dynamic analyses were carried out to investigate the soil response and site amplification parameters for the SLSJ, eastern Canada. As expected, the ground response is increasing with the increased intensity of the input ground motion. The nonlinear effects contribute to a decreasing trend of ground motion amplification. In general, the observed amplifications correlate to the Vs_{30} values. At the same time, large amplification variations with Vs_{30} were observed because of the variety of natural periods for the same Vs_{30}. As well, resonance amplification was clearly identified for the geological and geotechnical settings in the study region. This contributes to considerable differences in the amplification at the predominant period range when compared to the NBCC 2020 amplification. It can be concluded that it is crucial to consider T_{nat} in combination with Vs_{30} to simulate accurately the soil amplification considering the resonance effect.

As a recommendation for future work, regional site amplification model for SLSJ should be developed based on the regression analysis of the amplification values obtained from linear and nonlinear soil response simulations considering Vs_{30} and T_{nat} parameters conditioned to the PGA and spectral periods of the input ground motions scaled to different return periods. A regional site amplification map can also be developed using the 1D regression analysis and including also 2D and 3D analyses.

REFERENCES

1. Abdellaziz, M., Karray, M., Chekired, M., Delisle, M. C., Locat, P., Ledoux, C., & Mompin, R. (2022). New model of shear modulus degradation and damping ratio curves for sensitive Canadian clays. *Canadian Geotechnical Journal*, *60*(6), 784-801.
2. Boudghene Stambouli, A., Zendagui, D., Bard, P. Y., & Derras, B. (2017). Deriving amplification factors from simple site parameters using generalized regression neural networks: implications for relevant site proxies. *Earth, Planets and Space*, *69*(1), 1-26.
3. Ciancimino, A., Foti, S., & Lanzo, G. (2018). Stochastic analysis of seismic ground response for site classification methods verification. *Soil Dynamics and Earthquake Engineering*, *111*, 169-183.
4. Electric Power Research Institute (EPRI), 1993. Guidelines for Determining Design BasisGround Motions. Palo Alto, CA: Electric Power Research Institute, vol. 1—5, EPRI TR-102293
5. García de Quevedo Iñarritu, P., Šipčić, N., Alvarez-Sanchez, L., Kohrangi, M., & Bazzurro, P. (2023). A closer look at hazard-consistent ground motion record selection for building-specific risk assessment: Effect of soil characteristics and accelerograms' scaling. *Earthquake Spectra*, 87552930231173713.
6. Gobbi, S., Lenti, L., d'Avila, M. P. S., Semblat, J. F., & Reiffsteck, P. (2020). Influence of the variability of soil profile properties on weak and strong seismic response. *Soil Dynamics and Earthquake Engineering*, *135*, 106200.
7. Harmon, J., Hashash, Y. M., Stewart, J. P., Rathje, E. M., Campbell, K. W., Silva, W. J., ... & Ilhan, O. (2019). Site amplification functions for central and eastern North America–Part I: Simulation data set development. *Earthquake Spectra*, *35*(2), 787-814.
8. Hashash, Y. M., Harmon, J., Ilhan, O., Stewart, J. P., Rathje, E. M., Campbell, K. W., ... & Goulet, C. A. (2018). Modelling of site amplification via large scale nonlinear simulations with applications to North America. In *Geotechnical Earthquake Engineering and Soil Dynamics V* (pp. 523-537). Reston, VA: American Society of Civil Engineers.
9. Hashash, Y.M.A., Musgrove, M.I., Harmon, J.A., Ilhan, O., Xing, G., Numanoglu, O., Groholski, D.R., Phillips, C.A., and Park, D. (2020) "DEEPSOIL 7.0, User Manual". Urbana, IL, Board of Trustees of University of Illinois at Urbana-Champaign.
10. Hossain, A S M F.; Salsabili M.; Saeidi A.; Suescun J. R. and Nastev M; (2023). Effects of Shear Wave Velocity and Thickness of Soil Layers on 1D Dynamic Response in the Saguenay Region, Quebec (Canada). Rocscience International Conference April 24-26, 2023.
11. Kolaj, M., Allen, T., Mayfield, R., Adams, J., & Halchuk, S. (2019). Ground-motion models for the 6th Generation Seismic Hazard Model of Canada. In *12th Canadian Conference on Earthquake Engineering*.
12. Ladak, Sameer, Sheri Molnar, and Samantha Palmer.: "Multi-method site characterization to verify the hard rock (Site Class A) assumption at 25 seismograph stations across Eastern Canada." Earthquake Spectra 37.1_suppl (2021): 1487-1515.
13. Motazedian, D., Hunter, J. A., Pugin, A., & Crow, H. (2011). Development of a VS30 (NEHRP) map for the city of Ottawa, Ontario, Canada. *Canadian Geotechnical Journal*, *48*(3), 458-472.

14. Rollins, K. M., Evans, M. D., Diehl, N. B., & III, W. D. D. (1998). Shear modulus and damping relationships for gravels. *Journal of geotechnical and Geoenvironmental Engineering*, *124*(5), 396-405.
15. Saeidi, A., Heidarzadeh, S., Lalancette, S., & Rouleau, A. (2021). The effects of in situ stress uncertainties on the assessment of open stope stability: Case study at the Niobec Mine, Quebec (Canada). *Geomechanics for Energy and the Environment*, *25*, 100194.
16. Salsabili, M., Saeidi, A., Rouleau, A., & Nastev, M. (2023). Probabilistic approach for seismic microzonation integrating 3D geological and geotechnical uncertainty. *Earthquake Spectra*, *39*(1), 310-334.
17. Salsabili, M., Saeidi, A., Rouleau, A., & Nastev, M. (2023). Probabilistic approach for seismic microzonation integrating 3D geological and geotechnical uncertainty. *Earthquake Spectra*, *39*(1), 310-334.
18. Sanou, A. G., Saeidi, A., Heidarzadeh, S., Chavali, R. V. P., Samti, H. E., & Rouleau, A. (2022). Geotechnical Parameters of Landslide-Prone Laflamme Sea Deposits, Canada: Uncertainties and Correlations. *Geosciences*, *12*(8), 297.
19. Seed, H. B. (1982). Ground motions and soil liquefaction during earthquakes. *Earthquake engineering research insititue*.
20. Seed, H. B., Wong, R. T., Idriss, I. M., & Tokimatsu, K. (1986). Moduli and damping factors for dynamic analyses of cohesionless soils. *Journal of geotechnical engineering*, *112*(11), 1016-1032.
21. SeismoSoft (2023) SeismMatch Software applications for analysis of structures subjected to seismic actions (online). Available from URL:http://www.seismosoft.com
22. Semblat, J. F., Kham, M., Parara, E., Bard, P. Y., Pitilakis, K., Makra, K., & Raptakis, D. (2005). Seismic wave amplification: Basin geometry vs soil layering. *Soil dynamics and earthquake engineering*, *25*(7-10), 529-538.
23. Talukder, M. K., Rosset, P., & Chouinard, L. (2021). Reduction of bias and uncertainty in regional seismic site amplification factors for seismic hazard and risk analysis. *GeoHazards*, *2*(3), 277-301.
24. Tremblay, R., Atkinson, G. M., Bouaanani, N., Daneshvar, P., Léger, P., & Koboevic, S. (2015, July). Selection and scaling of ground motion time histories for seismic analysis using NBCC 2015. In *11th Canadian Conference on Earthquake Engineering (11CCEE), Victoria, BC, Canada* (Vol. 99060, p. 69).
25. Urgeles, R., Locat, J., Lee, H. J., & Martin, F. (2002). The Saguenay Fjord, Quebec, Canada: integrating marine geotechnical and geophysical data for spatial seismic slope stability and hazard assessment. *Marine Geology*, *185*(3-4), 319-340.

Conference paper-3

Analytical and numerical investigation of the site response period in the Saguenay region, Eastern Canada

A S M Fahad Hossain[(1)], Ali Saeidi[(2)], Mohammad Salsabili[(3)], Miroslav Nastev[(4)] and Juliana Ruiz Suescun[(5)]

[(1,2)] Université du Québec à Chicoutimi, 555 Bd de l'Université, Chicoutimi, QC G7H 2B1, Canada

[(3)] University of Western Ontario, 1151 Richmond St, London, ON N6A 3K7, Canada

[(4)] Geological Survey of Canada, 490 R. de la Couronne, Québec, QC G1K 9A9, Canada

[(5)] Hydro Québec, 75 Boul. René-Lévesque O, Montréal, QC H2Z 1A4, Canada

Abstract

The fundamental vibration period T_0 is often applied with the standard V_{S30} approach to improve the prediction of the seismic site effects. The commonly used equivalent single-layer method ($4H/V_{Savg}$) usually overestimates T_0. The present study applies a multi-layered method to develop empirical correlations for T_0 prediction. Numerical analyses examine the effects of the soil nonlinearity on T_0 shift and reduction of peak amplitude, establishing correlations for different hazard levels. The Saguenay Lac-Saint-Jean region (SLSJ), characterised by moderate seismicity and a strong impedance contrast at the bedrock interface, was selected as the study area. Results indicate that the analytical approach using the multiple soil layer method considerably reduces the T_0 overestimation. Empirical models were developed for site period evaluation using the multiple soil layer method for elastic strain and nonlinear dynamic response.

Keywords: Fundamental site period, Nonlinear site period, nonlinear analysis.

1. Introduction

The local geological and geotechnical properties of soils may lead to rapid variations of the seismic shaking in terms of duration and amplitudes at certain period ranges. In response to cyclic loading during the strong earthquake motion, the shear strains in soil increase, accompanied by a damping increase causing softening of the soil while reducing the amplitude of the ground motion amplification. This phenomenon contributes to a shift of the fundamental site period (T_0) to longer values, referred to as the nonlinear site period. These so-called seismic site effects were well observed during the 1985 Michoacan and 1989 Loma Prieta earthquakes. [1]. In seismic hazard evaluations, site effects are commonly accounted for with simple site conditions proxies, where the time-averaged shear-wave velocity of the top 30 m (V_{S30}), related to soil stiffness, is considered as the primary site parameter [2]. T_0 is also applied as an indicator of the resonance frequency to help improve surface ground motion prediction. It represents a soil column's most extended natural vibration period and can be determined through field measurements, analytical and empirical solutions, and numerical analysis.

[3] and [4], demonstrated the benefits of using dominant periods from H/V spectral ratios (HVSR) for consistent site classification across diverse geologies. [5] refined this approach with H/V response spectra, creating new site categories. Studies by [6] and [7] confirmed HVSR's reliability, revealing sediment thickness effects missed by geology-based methods. [8] expanded HVSR analysis with Spanish data, while recent research employs Fourier and response spectra to calculate dominant periods (e.g., [9]; [10]). [11], [12] used nonlinear site response methods to evaluate the role of soil nonlinearity in shifting site periods. These findings underline the importance of considering nonlinear site periods for accurate seismic site classification.

[13] analyzed the existing methods to calculate T_0 from shear-wave velocity V_S using various analytical approaches. The simple characteristic site period approximation $T_0=(4H/V_{Savg})$ is mainly applied when the time-averaged shear-wave velocity (V_{Savg}) and the thickness of the soil column (H) are known [14]. However, it tends to overestimate T_0 as the nonlinear soil behavior during earthquakes, where stiffness degradation increases the site period, is not accounted for. Also, the equivalent single layer (ESL) assumption with uniform V_S across thick soil deposits, instead of the common increasing velocity depth gradient, shifts the evaluated T_0 to longer periods [11], [12]. To improve accuracy, [15] proposed the multilayer soil Layer (MSL) approach, building on the work of [16] and [17] to account for variations across layers. Therefore, comparing T_0 across different methods is essential, as ESL is frequently used as a secondary proxy in ground motion equations.

The present study is part of the ongoing site categorization in the Saguenay region, eastern Canada. Located near the Charlevoix-Kamouraska seismic zone, the Saguenay region is exposed to strong earthquakes with a predicted magnitude of up to M7.0 and a 2%/50yrs probability of exceedance (PE). The 1988 M5.9 Saguenay earthquake was the strongest recorded earthquake in eastern North America in more than 50 years, highlighting the need to assess the site response during intense seismic events. The study's objective is to investigate the dynamic site response, focusing on the fundamental site period (T_0). Site responses of 52 typical soil profiles in the study area, exposed to synthetic and recorded strong ground motions, are analyzed and compared to existing analytical models. Predictive T_0 models are developed with ESL and MSL approaches using equivalent linear and nonlinear analyses.

2. Materials and Methods

Saguenay, situated 200 km north of Québec City with a population of 147,100, serves as a central hub for commerce and administration. Positioned within the seismically active Saguenay graben, part of the Charlevoix-Kamouraska seismic zone, the city has experienced significant earthquakes, such as those in 1663 and 1988 with magnitudes of 6.0. The region's bedrock is composed of Precambrian rocks from the Grenville Province. At the same time, the lowlands are layered with glacial and postglacial deposits, including till, glaciofluvial gravel, glaciomarine clay, and deltaic sands, creating a geologically diverse landscape. The selection of 52 soil profiles in this area was based on the vertical and geographic distribution of four surface components: sand, gravel, clay, and till, distributed over four cross-sections shown in Figure 1(a), with thickness details for surface soils in Saguenay. 10 to 15 profiles were retrieved for each cross-section, with 52 stratigraphic soil profiles analyzed. The bedrock was modeled as an elastic half-space with specific density and shear-wave velocity parameters. Two earthquake scenarios, with moment magnitudes of M6 and M7 and exceedance probabilities of 1/975 and 1/2475 years, represented Saguenay's seismic hazard (www.seismotoolbox.ca). Four artificial ground movements were selected based on source-to-site distances of 40–60 km, and two accurate earthquake records from eastern Canada were incorporated: the 1988 M5.9 Saguenay earthquake (35 km from the epicenter) and the 2010 M5.1 Val-des-Bois earthquake (22 km from the epicenter). Figure 1(b) illustrates initial acceleration time histories for each ground movement, scaled to target spectra using the SeismoMatch software (www.seismosoft.com/). All site-specific soil properties used in the analysis are shown in Table 1.

The site response analysis was carried out on 52 soil profiles, using six input ground motions, each scaled to five earthquake hazard levels: 2%/50yrs, 3.5%/50yrs, 5%/50yrs, 10%/50yrs and 20%/50yrs PE from NBCC 2020. This analysis employed nonlinear methods in the time domain and equivalent linear methods in the frequency domain. The open-source software DEEPSOIL v7.0 was used and recognized for its reliability in site response analysis. Earlier versions of DEEPSOIL have been extensively validated and shown to replicate observed responses in well-documented soil sites accurately. In DEEPSOIL, the MKZ hyperbolic model, which accounts for pressure dependency, was applied to simulate modulus reduction and shear stress characteristics. The software technical guidelines provide an overview of the methods used for calculating the site response of a soil column discretized into individual layers using a single- or multi-degree-of-freedom system and solving the dynamic equilibrium equations. Seismic amplification is the ratio of calculated surface to bedrock response spectral accelerations in time domain solution or Fourier amplitude spectrum ratio from frequency domain solution. The final amplification factor for each model was determined by taking the geometric mean of six responses obtained from different earthquake motions at the surface.

a) b)

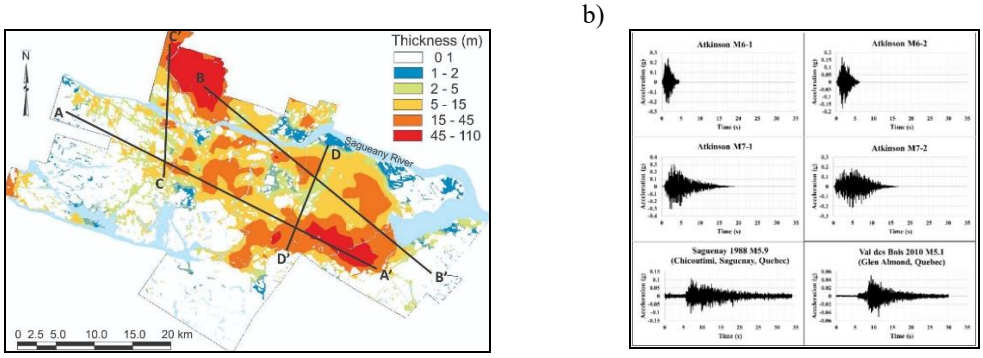

Figure 1. a) Thickness of surficial deposits with four cross-sections for selection of the 52 soil profiles used in the site response analyses (modified from [18] and b) unscaled input time histories.

Table 1. Adopted geotechnical and dynamic properties of soils and rock in the Saguenay region.

	Shear-Wave Velocity vs. Depth (m/s)	Density (kN/m^3)	Shear Modulus Reduction and Damping Ratio curves
Clay	Vs = 114.5 + 9.4 x D$^{0.76}$ [19]	18.7 [20]	[21]
Sand	Vs = 144.9 + 2.55 x D [19]	17.5 [20]	[22]*
Gravel	Vs = 46.861 + 61.55 x D$^{0.5}$ [19]	18.3 [23]*	[24]*
Till	V_{Still} = 582, σ=±174 (Motazedian et al., 2011)	21.0 [26]	Hydro Quebec (internal communication)
Rock	V_{Srock} = 1875, σ=±781 [27]	28.0 [28]	N/A

* Studies conducted in other regions

3. Analytical approach

The fundamental site period of 52 typical vertical profiles was calculated using both the equivalent single layer (ESL; T_0=4H/Vs) and multiple soil layers (MSL) approaches as described in Hadjian (2002). The procedure for calculating the T_0 in MSL profiles is described with equations 1 to 3. The process starts by considering the top two layers with respective fundamental periods T_1 and T_2. The combined fundamental period $T_{i=1}$ of these two layers is determined. In the next step, these two layers are treated as a single layer, and the third layer underneath is incorporated to calculate the combined $T_{i=2}$. This process is repeated iteratively across all the layers until the final T_0 is calculated for each of the 52 soil profiles. The number of iterations equals the number of assumed layers minus 1.

$$\frac{T}{T_1} = \sqrt{\frac{\pi^2}{8}\left[0.75 + \left(\frac{T_2}{T_1}\right)^2\left(1 + 2\frac{H_1}{H_2}\right)\right]} \quad ; \quad \left[\text{For } \frac{T_2}{T_1} > 0.1, H_1 > H_2\right] \tag{1}$$

$$\frac{T}{T_1} = \left[1 + \beta\left(\frac{T_2}{T_1}\right)^n\left(1 + 2\frac{H_1}{H_2}\right)^n\right]^{\frac{1}{n}} \quad ; \quad \left[\text{For } \frac{T_2}{T_1} > 0.1, H_1 \le H_2\right] \tag{2}$$

$$\frac{T}{T_1} = \left[1 + \frac{H_1}{H_2}\left(\frac{T_2}{T_1}\right)^2\right] \quad ; \quad \left[\text{For } \frac{T_2}{T_1} \le 0.1\right] \tag{3}$$

where, $\beta = 1\text{-}0.2\left(\frac{H_1}{H_2}\right)^2$; and $n = 4 - 1.8\frac{H_1}{H_2}$

An empirical correlation was developed at the end of the process to convert the fundamental site period from TESL to TMSL, as shown in equation 4.

$$T_{MSL} = 0.87 * T_{ESL}^{0.93}\ ; \quad R^2 = 1.00\ ; \quad \sigma = 0.018 \tag{4}$$

The calculated and empirical fundamental site period in multiple soil layered methods is plotted against the computed site fundamental period in equivalent single-layer methods, as shown in Figure 2. It can be seen in Figure 2 that the fundamental site period calculated using MSL is lower than that using ESL and that the difference increases for soil columns with higher fundamental periods.

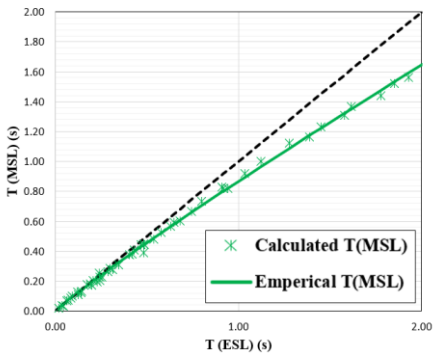

Figure 2. Correlation between the fundamental site periods obtained using the equivalent single layer, T_{ESL}, and the multiple TMSL approaches of soil layering. The black dashed line indicates the 1:1 correlation, where T_{MSL}=T_{ESL}.

4. Nonlinear numerical modelling

In response to cyclic loading during the strong earthquake motion, the shear strains in soil increase, accompanied by a damping increase causing softening of the soil and reducing the amplitude of the ground motion amplification. This phenomenon contributes to a shift of the fundamental site period (T_0) to longer values, which becomes more significant for stronger earthquake motions. Nonlinear site response simulations were carried out with the DEEPSOIL software to evaluate the magnitude of the period shift. The results are compared to the standard T_{ESL}. Two sets of 6 ground motions (Figure 1b) were scaled according to the NBCC 2020 hazard for the Saguenay region with a probability of exceedance (PE in the further text) of 2%/50yrs, which corresponds to a return period of 2475yr, and 10%/50yrs PE (475yr; NBCC2020). The nonlinear site period, T_{NL}, was determined from the acceleration response spectra at the ground surface for the period with maximum spectral amplification. The results are shown in Figure 3.

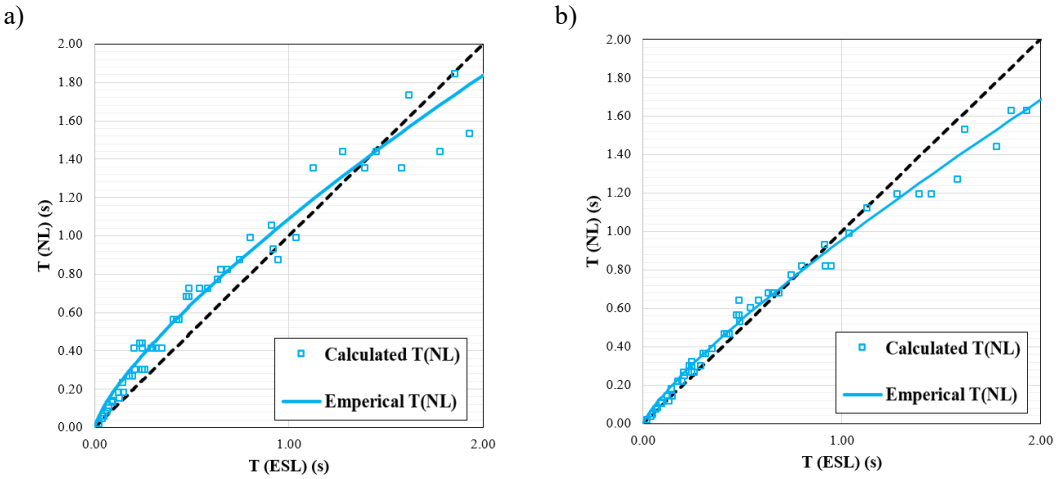

Figure 3. Nonlinear site period of soil for ground motion with a) 2%/50yrs PE and b) 10%/50yrs PE. The black dashed line indicates 1:1 correlation, where T_{NL}=T_{ESL}.

Figure 3 indicates that in the short period range, T_{NL} is higher than T_{ESL} for both hazard levels and shifts toward longer periods. In the longer period ranges, it becomes lower than T_{ESL}. The shift below the 1:1 line first occurs for ground motions scaled to 10%/50yrs PE, at approximately T=0.7s, and then for the ground motions scaled to 2%/50yrs PE, at approximately T=2.0s. Such performance can be explained by the conventional ESL method, which tends to overestimate T_0 values, especially for thicker soil columns. On the other hand, the MSL method provides better T_0 estimates. Also, soil columns with higher V_{Savg} display higher stiffness, resulting in a smaller T_0 shift due to earthquake loading compared to softer soil columns. For both sets of input motions, empirical correlations were developed as described with equations 5 and 6 for 2%/50yrs and 10%/50yrs PE, respectively. Additionally, a relationship between the nonlinear site period T_{NL}, on one hand side, and the peak ground acceleration (PGA) and the fundamental site period (T_0), on the other, was developed considering all five hazard levels with PE of 2%, 3.5%, 5%/, 10% and 20% in 50yrs, equation 7.

$$T_{NL\text{-}2\%/50yrs\ PE} = 1.09 * T_{ESL}^{0.76};\quad R^2 = 0.97;\quad \sigma = 0.093 \qquad (5)$$

$$T_{NL\text{-}10\%/50yrs\ PE} = 0.96 * T_{ESL}^{0.82};\quad R^2 = 0.99;\quad \sigma = 0.047 \qquad (6)$$

$$T_{NL} = 1.28 * PGA^{0.14} * T_{ESL}^{0.92};\quad R^2 = 0.98;\quad \sigma = 0.086 \qquad (7)$$

Figure 4 shows the scatter of nonlinear site period results from all five hazards with the fundamental site periods T(ESL) and T(MSL). In all empirical correlations, the R^2 value is close to 1, indicating low errors in the regression analysis.

In the numerical site response modeling process, it is important to conduct an equivalent linear analysis to compare and validate the results of the nonlinear analysis. To this end, the amplification values were calculated as the ratio between the ground surface acceleration response spectra and Fourier amplitude spectra and their analogs of the input ground motions. In both cases, the site periods were determined to correspond to the maximum amplification. The site period in the frequency domain analysis was defined as the reciprocal value of the frequency. Figures 5 and 6 compare maximum amplification values and the corresponding site periods from the response

spectrum using a time-domain nonlinear approach (NL) and frequency-domain equivalent linear analysis (EL) corresponding to 2%/50-year and 10%/50-year PE hazard scenarios.

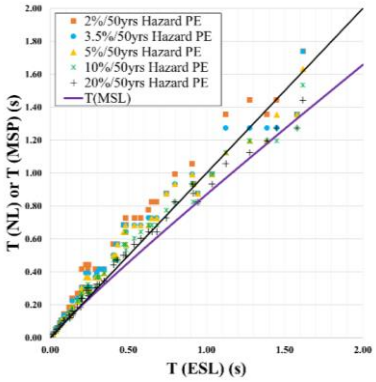

Figure 4. The scatter of nonlinear site periods T(NL) from different soil models for all five hazard levels and T(MSL) against the fundamental site periods T(ESL). The black dashed line indicates a 1:1 correlation, where T_{NL} or T_{MSL}=T_{ESL}.

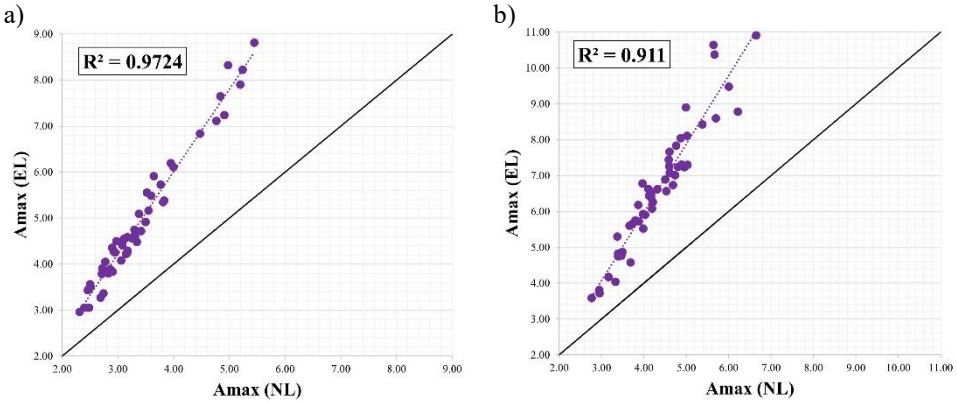

Figure 5. Comparison of the maximum amplifications from nonlinear, Amax (NL), and equivalent linear, Amax (EL), analyses for: a) 2%/50yrs PE and b) 10%/50yrs PE. (Black straight line is the 1:1 line where Amax (EL)=Amax (NL))

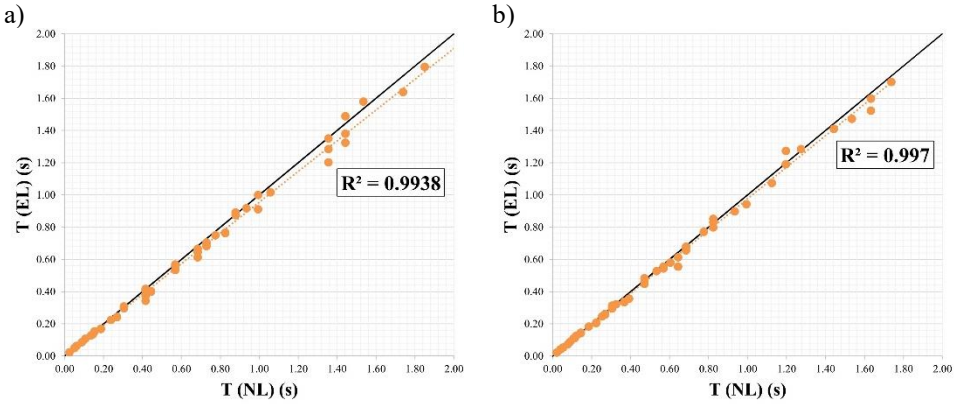

Figure 6. Comparison of the maximum amplification and corresponding site periods from nonlinear, T_{NL}, and equivalent linear, T_{EL}, analyses for a) 2%/50yrs PE and b) 10%/50yrs PE. (Black straight line is the 1:1 line where Amax (EL)=Amax (NL))

The results in Figures 4 and 5 demonstrate high correlations between the maximum amplifications and fundamental site periods, with R2 values ranging from 0.91 to 0.99 for both hazard levels. Slightly higher deviations among the data points can be observed for higher amplifications and longer periods. These results suggest a stable and predictable relationship between nonlinear and equivalent linear analyses across both hazard scenarios.

5. Resonance Effect

In soil dynamics, the resonance effect occurs when the dominant period range of the incoming seismic waves, where most of the earthquake energy is concentrated, aligns with the fundamental site

period or the natural frequency of the soil column. This alignment contributes to amplified seismic shaking at the ground surface. The buildup in the soil vibrations amplitude can potentially lead to permanent soil deformations, such as subsidence, lateral spread, landslide, etc. Site response analyses indicate that maximum amplification occurs when the ratio between the dominant input vibration period and the site response period becomes close or equal to 1 [29]. Here, most of the earthquake energy content is concentrated in the dominant input vibration period. The site response period refers to the maximum period at which the soil vibrates, with T_0 indicating low (elastic) strain conditions and T_{NL} indicating nonlinear soil behavior under earthquake loading. The nonlinear amplification values were plotted with respect to the ratio of the oscillation period and site period, as shown in Figure 7.

The nonlinear analysis correlated against the vibration period to fundamental site period ratio in Figure 7a indicates that a shift in the resonance period occurs due to the considered nonlinearity. However, when nonlinear amplification is compared against the ratio of the oscillation period (T_{osc}) to the nonlinear site period (T_{NL}) derived from the empirical models discussed in section 4, resonance occurs steadily near the ratio of 1 (Figure 7b).

a) b)

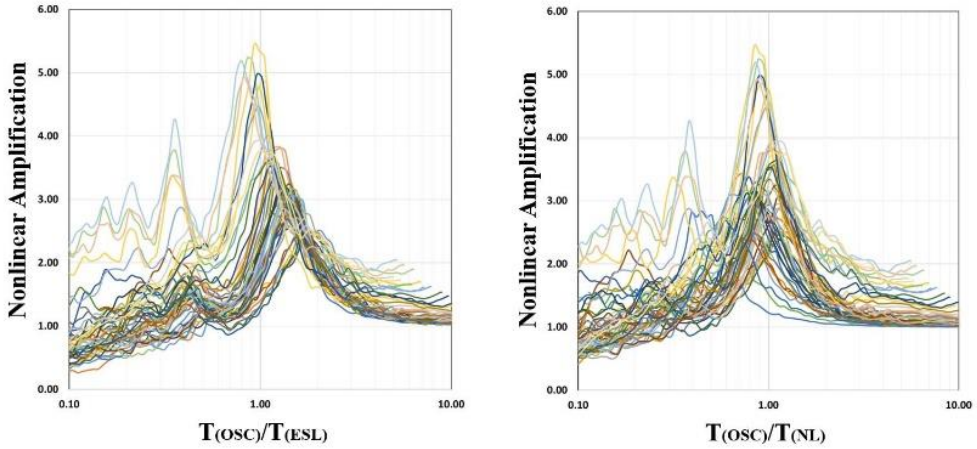

Figure 7. Amplification Values vs. Ratio of Vibration Period to Site Natural Period for 2%/50yrs PE: a) a) Nonlinear amplification vs T_{osc}/T_{ESL} b) Nonlinear amplification vs T_{osc}/T_{NL}.

6. Conclusion

A comprehensive 1D site response analysis was conducted in the Saguenay region on 52 soil profiles with site-specific properties. Both the nonlinear time-domain and the equivalent linear frequency-domain methods were used. This analysis employed hazard levels of 2%, 3.5%, 5%, 10% and 20% probability of exceedance in 50 years as specified in NBCC2020. Results from both time-domain and frequency-domain methods align well, validating the findings.

Each soil column's fundamental site period was calculated using the widely used equivalent single-layer method and a multiple-soil-layer profile method. The multiple-layer method was observed to be more effective, resulting in less overestimation of the fundamental site period. We developed an empirical correlation for the multiple-layer method, enabling precise calculation of the fundamental site period from the commonly used single-layer method.

Additionally, we calculated the nonlinear site period from the site response analysis by identifying the maximum amplification and developing empirical models for different hazard levels. We highlighted the resonance effect in the Saguenay region, which is critical as it may amplify the amplitudes of the ground motion and cause site-induced damage due to resonance. An amplification model incorporating nonlinear site response and accounts for the resonance effect using the nonlinear site period is essential for accurate assessment in this region.

References

[1] J. H. Steidl, “Site Response in Southern California for Probabilistic Seismic Hazard Analysis,” Bulletin of the Seismological Society of America, vol. 90, no. 6B, pp. S149–S169, Dec. 2000, doi: 10.1785/0120000504.

[2] A. F. Hossain, A. Saeidi, M. Salsabili, M. Nastev, and J. Suescun, “Soil Dynamic Response and Site Amplification Parameters for Saguenay, Eastern Canada,” Japanese Geotechnical Society Special Publication, vol. 10, no. 52, p. v10.OS-41-03, 2024, doi: 10.3208/jgssp.v10.OS-41-03.

[3] J. X. Zhao et al., “An empirical site-classification method for strong-motion stations in Japan using H/V response spectral ratio,” Bulletin of the Seismological Society of America, vol. 96, no. 3, pp. 914–925, Jun. 2006, doi: 10.1785/0120050124.

[4] Y. Fukushima, L. F. Bonilla, O. Scotti, and J. Douglas, “Site Classification Using Horizontal-to-vertical Response Spectral Ratios and its Impact when Deriving Empirical Ground-motion Prediction Equations,” Journal of Earthquake Engineering, vol. 11, no. 5, pp. 712–724, Oct. 2007, doi: 10.1080/13632460701457116.

[5] C. Di Alessandro, L. F. Bonilla, D. M. Boore, A. Rovelli, and O. Scotti, “Predominant-Period Site Classification for Response Spectra Prediction Equations in Italy,” Bulletin of the Seismological Society of America, vol. 102, no. 2, pp. 680–695, Apr. 2012, doi: 10.1785/0120110084.

[6] N. Harinarayan and A. Kumar, “Seismic Site Classification of Recording Stations in Tarai Region of Uttarakhand, from Multiple Approaches,” Geotechnical and Geological Engineering, vol. 36, no. 3, pp. 1431–1446, Jun. 2018, doi: 10.1007/s10706-017-0399-1.

[7] S. Chopra, V. Kumar, P. Choudhury, and R. B. S. Yadav, “Site classification of Indian strong motion network using response spectra ratios,” J Seismol, vol. 22, no. 2, pp. 419–438, Mar. 2018, doi: 10.1007/s10950-017-9714-9.

[8] L. A. Pinzón, L. G. Pujades, A. Macau, E. Carreño, and J. M. Alcalde, “Seismic Site Classification from the Horizontal-to-Vertical Response Spectral Ratios: Use of the Spanish Strong-Motion Database,” Geosciences (Basel), vol. 9, no. 7, p. 294, Jul. 2019, doi: 10.3390/geosciences9070294.

[9] H. Ghofrani, G. M. Atkinson, and K. Goda, “Implications of the 2011 M9.0 Tohoku Japan earthquake for the treatment of site effects in large earthquakes,” Bulletin of Earthquake Engineering, vol. 11, no. 1, pp. 171–203, Feb. 2013, doi: 10.1007/s10518-012-9413-4.

[10] H. Livaoğlu, E. Şentürk, and F. Sertçelik, “A Comparative Study of Response and Fourier Spectral Ratios on Classifying Sites,” Pure Appl Geophys, vol. 178, no. 5, pp. 1745–1759, May 2021, doi: 10.1007/s00024-021-02722-1.

[11] D. Motazedian, K. Khaheshi Banab, J. A. Hunter, S. Sivathayalan, H. Crow, and G. Brooks, “Comparison of Site Periods Derived from Different Evaluation Methods,” Bulletin of the Seismological Society of America, vol. 101, no. 6, pp. 2942–2954, Dec. 2011, doi: 10.1785/0120100344.

[12] D. Motazedian, H. Torabi, J. A. Hunter, H. L. Crow, and M. Pyne, “Seismic site period studies for nonlinear soil in the city of Ottawa, Canada,” Soil Dynamics and Earthquake Engineering, vol. 136, p. 106205, Sep. 2020, doi: 10.1016/j.soildyn.2020.106205.

[13] S. Wang, Y. Shi, W. Jiang, E. Yao, and Y. Miao, “Estimating Site Fundamental Period from Shear-Wave Velocity Profile,” Bulletin of the Seismological Society of America, vol. 108, no. 6, pp. 3431–3445, Dec. 2018, doi: 10.1785/0120180103.

[14] A. F. Hossain, M. Salsabili, A. Saeidi, J. R. Suescun, and M. Nastev, “Effects of Shear Wave Velocity and Thickness of Soil Layers on 1D Dynamic Response in the Saguenay Region, Quebec,” in Rocscience International Conference (RIC 2023), Toronto: Atlantis Press, 2023, pp. 165–173. doi: 10.2991/978-94-6463-258-3_17.

[15] A. H. Hadjian, “Fundamental period and mode shape of layered soil profiles,” Soil Dynamics and Earthquake Engineering, vol. 22, no. 9–12, pp. 885–891, Oct. 2002, doi: 10.1016/S0267-7261(02)00111-2.

[16] Madera G., “Fundamental period and amplification of peak acceleration in layered systems,” 1970.

[17] Dobry, R., Oweis, I., & Urzua, A. (1976). Simplified procedures for estimating the fundamental period of a soil profile. Bulletin of the Seismological Society of America, 66(4), 1293-1321.

[18] M. Salsabili, A. Saeidi, A. Rouleau, and M. Nastev, “Development of empirical CPTu-V correlations for post-glacial sediments in Southern Quebec, Canada, in consideration of soil type and geological setting,” Soil Dynamics and Earthquake Engineering, vol. 154, p. 107131, Mar. 2022, doi: 10.1016/j.soildyn.2021.107131.

[19] M. Salsabili, A. Saeidi, A. Rouleau, and M. Nastev, “Probabilistic approach for seismic microzonation integrating 3D geological and geotechnical uncertainty,” Earthquake Spectra, vol. 39, no. 1, pp. 310–334, Feb. 2023, doi: 10.1177/87552930221132576.

[20] A.-G. Sanou, A. Saeidi, S. Heidarzadeh, R. V. P. Chavali, H. E. Samti, and A. Rouleau, “Geotechnical Parameters of Landslide-Prone Laflamme Sea Deposits, Canada: Uncertainties and Correlations,” Geosciences (Basel), vol. 12, no. 8, p. 297, Jul. 2022, doi: 10.3390/geosciences12080297.
[21] M. Abdellaziz et al., “New model of shear modulus degradation and damping ratio curves for sensitive Canadian clays,” Canadian Geotechnical Journal, vol. 60, no. 6, pp. 784–801, Jun. 2023, doi: 10.1139/cgj-2021-0475.
[22] EPRI, “Guidelines for Site Specific Ground Motions,” 1993.
[23] K. M. Rollins, M. D. Evans, N. B. Diehl, and W. D. D. III, “Shear Modulus and Damping Relationships for Gravels,” Journal of Geotechnical and Geoenvironmental Engineering, vol. 124, no. 5, pp. 396–405, May 1998, doi: 10.1061/(ASCE)1090-0241(1998)124:5(396).
[24] H. B. Seed, R. T. Wong, I. M. Idriss, and K. Tokimatsu, “Moduli and Damping Factors for Dynamic Analyses of Cohesionless Soils,” Journal of Geotechnical Engineering, vol. 112, no. 11, pp. 1016–1032, Nov. 1986, doi: 10.1061/(ASCE)0733-9410(1986)112:11(1016).
[25] D. Motazedian, J. A. Hunter, A. Pugin, and H. Crow, “Development of a Vs 30 (NEHRP) map for the city of Ottawa, Ontario, Canada,” Canadian Geotechnical Journal, vol. 48, no. 3, pp. 458–472, Mar. 2011, doi: 10.1139/T10-081.
[26] R. Urgeles, J. Locat, H. J. Lee, and F. Martin, “The Saguenay Fjord, Quebec, Canada: integrating marine geotechnical and geophysical data for spatial seismic slope stability and hazard assessment,” Mar Geol, vol. 185, no. 3–4, pp. 319–340, Jun. 2002, doi: 10.1016/S0025-3227(02)00185-8.
[27] S. Ladak, S. Molnar, and S. Palmer, “Multi-method site characterization to verify the hard rock (Site Class A) assumption at 25 seismograph stations across Eastern Canada,” Earthquake Spectra, vol. 37, no. 1_suppl, pp. 1487–1515, Jul. 2021, doi: 10.1177/87552930211001076.
[28] A. Saeidi, S. Heidarzadeh, S. Lalancette, and A. Rouleau, “The effects of in situ stress uncertainties on the assessment of open stope stability: Case study at the Niobec Mine, Quebec (Canada),” Geomechanics for Energy and the Environment, vol. 25, p. 100194, Mar. 2021, doi: 10.1016/j.gete.2020.100194.
[29] J. Harmon et al., “Site Amplification Functions for Central and Eastern North America – Part I: Simulation Data Set Development,” Earthquake Spectra, vol. 35, no. 2, pp. 787–814, May 2019, doi: 10.1193/091017EQS178M.